

THE QUETICO FAULT  
IN THE SUPERIOR PROVINCE  
OF THE SOUTHERN CANADIAN SHIELD

by

© MYRA CAROLYN KENNEDY

A THESIS SUBMITTED IN PARTIAL FULFILLMENT OF  
THE REQUIREMENTS FOR THE DEGREE OF  
MASTER OF SCIENCE

LAKEHEAD UNIVERSITY, THUNDER BAY, ONTARIO

MARCH, 1984

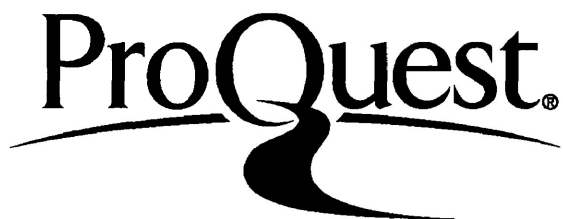
ProQuest Number: 10611704

All rights reserved

INFORMATION TO ALL USERS

The quality of this reproduction is dependent upon the quality of the copy submitted.

In the unlikely event that the author did not send a complete manuscript and there are missing pages, these will be noted. Also, if material had to be removed, a note will indicate the deletion.



ProQuest 10611704

Published by ProQuest LLC (2017). Copyright of the Dissertation is held by the Author.

All rights reserved.

This work is protected against unauthorized copying under Title 17, United States Code  
Microform Edition © ProQuest LLC.

ProQuest LLC.  
789 East Eisenhower Parkway  
P.O. Box 1346  
Ann Arbor, MI 48106 - 1346

## ABSTRACT

The Quetico fault is a major transcurrent fault in the southern Superior Province of the Canadian Shield. Along part of its length the fault forms the boundary between the Quetico and Wabigoon subprovinces. Dextral motion on the fault is indicated by dextral microfaults and appropriately asymmetrical quartz c-axis petrofabrics.

The fault comprises a zone of dynamically metamorphosed rocks - primarily mylonitic rocks with some cataclastic rocks and pseudotachylite. A transition from predominantly ductile deformation to brittle deformation occurred during the time the fault was active.

The ductile deformation of quartz within the fault zone is the result of crystal-plastic processes, predominantly slip on prism planes in the a-direction and slip on rhomb planes in the a-direction, accompanied by dynamic recovery and syntectonic recrystallization. Feldspar grains are commonly deformed in a brittle manner by fracture processes. Particulate flow appears to have made a significant contribution to deformation in the fault zone.

The harmonic mean of deformed grain axial-ratios and strain determinations by the all object-object separations method indicate that flattening strain is predominant within the fault zone. The magnetic susceptibility anisotropy ellipsoid is also flat-shaped and coaxial with the strain ellipsoids. The characteristics of microfaults and folds within the fault zone indicate that flattening may have been accompanied by or followed by shearing. The harmonic mean of deformed quartz grain axial ratios yields a minimum strain estimate of 130% extension in X, 58% extension in Y, and 71% shortening in the Z direction.

## ACKNOWLEDGEMENTS

The author gratefully acknowledges Dr. Graham J. Borradaile who supervised and allotted financial support for this research from NSERC grant #A6861. His perception, careful guidance and encouragement were of great benefit to the author. We thank Dr. D. Tarling of The University of Newcastle upon Tyne, U.K. for performing magnetic susceptibility determinations. Advisor, Dr. Manfred M. Kehlenbeck reviewed much of the manuscript and is thanked for his comments on the manuscript. My husband, Roger, was my able field assistant and helped with this work in many ways. Without his patience and support I would never have finished this thesis. My parents, Shirley and Jim Gerow assisted with many tasks. They also provided, respectively, quiet understanding and persistent "encouragement".

Technical support was provided by Lakehead University Geology Department technicians Ronald Bennett and Diane Crothers. Sam Spivak provided valuable drafting advice. The student advisors of the L.U. computer centre were also very helpful.

John Scott is thanked for his help with photography and moral support. Wendy Bons typed the manuscript. Her skill is here evident. I thank her for her careful work and friendship. Many others, in particular my co-workers at the Geological Branch, Ministry of Natural Resources have contributed in many ways.

Finally, I acknowledge with gratitude the receipt of a NSERC student award during my studies.

## TABLE OF CONTENTS

ABSTRACT . . . . .	i
ACKNOWLEDGEMENTS . . . . .	ii
TABLE OF CONTENTS . . . . .	iii
1-INTRODUCTION . . . . .	1-1
A) Introduction . . . . .	1-1
B) Previous Geological Studies . . . . .	1-5
C) Study Objectives . . . . .	1-16
D) Methods . . . . .	1-16
E) Terminology . . . . .	1-17
2-STRUCTURE AND MICROSTRUCTURES OF THE QUETICO FAULT ZONE . . . . .	11-1
A) Macroscopic Structure . . . . .	11-1
<i>Width of the fault zone</i> . . . . .	11-1
Discussion . . . . .	11-1
<i>Geometry of the fault zone and associated         faults and fractures</i> . . . . .	11-3
Discussion . . . . .	11-3
B) Small Scale Structures . . . . .	11-6
<i>Mylonitic schistosity</i> . . . . .	11-6
<i>Mylonitic banding or layering</i> . . . . .	11-6
<i>Mineral lineations</i> . . . . .	11-9
<i>Slickensides</i> . . . . .	11-13
<i>Microfaults</i> . . . . .	11-13
<i>Ductile shear zones</i> . . . . .	11-20
<i>Brittle shear zones</i> . . . . .	11-22
<i>Folds</i> . . . . .	11-22
<i>Significance of the small scale structures</i> . . . . .	11-31
C) Fault Rocks of the Quetico Fault Zone . . . . .	11-35
<i>Mylonite series rocks</i> . . . . .	11-36
<i>Cataclasite series rocks</i> . . . . .	11-38
<i>Pseudotachylite</i> . . . . .	11-41
Discussion . . . . .	11-41
D) Deformation Mechanisms - Theory . . . . .	11-46
<i>Particulate flow</i> . . . . .	11-47
<i>Fracture or cataclastic processes</i> . . . . .	11-47
<i>Physical conditions for fracture</i> . . . . .	11-48
<i>Crystal plastic processes</i> . . . . .	11-49
<i>Physical conditions for crystal-plasticity</i> . . . . .	11-55
<i>Diffusional processes</i> . . . . .	11-56

E)	Deformation Mechanisms and Microstructures, . . . . .	11-57
	<i>Microstructures associated with fracture and cataclastic flow,</i> . . . . .	11-57
	<i>Microstructures associated with crystal-plasticity,</i> . . . . .	11-58
	<i>Microstructures associated with dynamic recovery and recrystallization,</i> . . . . .	11-60
	<i>Microstructures associated with diffusion processes</i> . . . . .	11-61
F)	Microstructures and Deformation Mechanisms in the Quetico Fault Zone . . . . .	11-62
	<i>Deformation mechanisms determined from microstructural evidence,</i> . . . . .	11-62
	<i>Discussion,</i> . . . . .	11-69
	3-STRAIN STUDY OF THE QUETICO FAULT ZONE . . . . .	111-1
A)	Introduction. . . . .	111-1
B)	Grain Shape Analysis. . . . .	111-3
	<i>Application of the method</i> . . . . .	111-6
C)	Centre to Centre Method . . . . .	111-13
	<i>Limitations</i> . . . . .	111-17
	<i>Application of the method</i> . . . . .	111-18
D)	All Object-Object Separations Method (The Fry Method) . . . . .	111-23
	<i>Assumptions</i> . . . . .	111-24
	<i>Limitations</i> . . . . .	111-25
	<i>Application of the method</i> . . . . .	111-28
	<i>All object-object separations from the Quetico fault zone</i> . . . . .	111-35
E)	Results and Conclusions of the Strain Study . . . . .	111-66
F)	Magnetic Susceptibility Anisotropy. . . . .	111-75
	<i>Method</i> . . . . .	111-77
	<i>Results</i> . . . . .	111-77
	4-QUARTZ <u>C</u> -AXIS PETROFABRICS-THEORY . . . . .	IV-1
A)	Introduction . . . . .	IV-1
B)	Intracrystalline Slip and the Development of Crystallographic Preferred Orientations . . . . .	IV-5
C)	Slip Systems in Quartz . . . . .	IV-8

D) Factors Influencing the Development of Quartz <u>c</u> -axis Preferred Orientations . . . . .	IV-14
i) <i>The Influence of Slip Systems on Quartz <u>c</u>-axis fabrics.</i> . . . . .	IV-14
<i>Numbers of slip systems required for deformation.</i> . . . . .	IV-18
<i>Computer model simulating quartz <u>c</u>-axis petrofabrics resulting from slip on several slip systems</i> . . . . .	IV-19
ii) <i>The Influence of Recovery and Recrystallization on Quartz <u>c</u>-axis Fabrics</i> . . . . .	IV-25
iii) <i>The Influence of the Shape and Orientation of the Finite Strain Ellipsoid on Quartz <u>c</u>-axis Fabrics</i> . . . . .	IV-28
iv) <i>The Influence of Strain History on Quartz <u>c</u>-axis Fabrics: Coaxial versus Non-coaxial Deformation</i> . . . . .	IV-34
E) Sense of Shear Determined from Quartz <u>c</u> -Axis Fabric Asymmetry . . . . .	IV-39
5-QUARTZ <u>C</u> -AXIS PETROFABRICS IN THE QUETICO FAULT ZONE. . . . .	V-1
A) Method . . . . .	V-1
B) Petrofabric Diagrams . . . . .	V-1
C) Data . . . . .	V-2
D) Observations. . . . .	V-39
E) Axial Distribution Analysis . . . . .	V-45
<i>Method</i> . . . . .	V-45
<i>Results</i> . . . . .	V-46
<i>Results of the Axial Distribution Analysis</i> . . . . .	V-46
F) Interpretation of the Quartz <u>c</u> -axis Petrofabric Diagrams . . . . .	V-59
G) Discussion . . . . .	V-63
6-SUMMATION . . . . .	VI-1
REFERENCES . . . . .	vi
APPENDIX I . . . . .	xxiv

## 1-INTRODUCTION

## A) Introduction

In the Superior Province of Northwestern Ontario, the Quetico fault zone forms a pronounced geological structure. The fault zone is traceable along strike for about 400 kilometers extending from near Greenwich Lake east of Highway 527 to Fort Frances, Ontario and west to the Canada-United States border (Figure 1-4).

The present known extent of the fault zone is based primarily on topographic lineaments as well as on detailed geological mapping by various workers (see next section). Figure 1-1 shows the topographic expression of the Quetico fault zone as it appears on satellite photographs. Here the continuous fault zone is marked by linear topographic lows commonly occupied by long narrow lakes. On aeromagnetic maps the fault zone is associated with long narrow magnetic "highs".

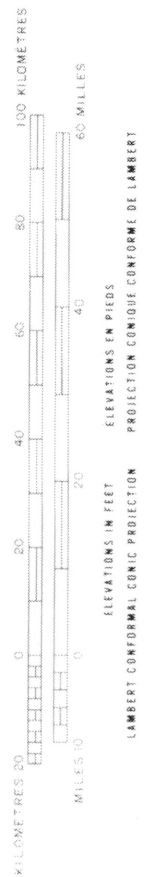
The fault comprises a steeply dipping zone of dynamically metamorphosed rock. Thus the structure is generally referred to as a "fault zone" in this thesis rather than simply a fault. The rocks in the fault zone are variable in composition and texture exhibiting evidence of both brittle and ductile deformation. Individual fault rock types can be identified as members of the cataclasite and mylonite series as described by Sibson (1977).





Fig. 1-1

QUETICO FAULT ZONE



As can be seen in Figure 1-2, the western portion of the Quetico fault zone lies well within the boundaries of the Wabigoon belt whereas the eastern segment of the fault zone is situated within the Quetico belt (Stockwell, 1964). Along the central portion which extends for about 160 kilometers, the Quetico fault zone forms the boundary between these two belts.

It has been suggested that the Quetico fault and other similar structures in the Superior Province represent late features resulting from tectonic overprinting produced by transcurrent movement along zones of inherent structural weakness (Mackasey et al (1974), Schwerdtner et al (1979)). In the case of the Quetico fault they suggest that the fault occurs along a lithological discontinuity at the Quetico-Wabigoon subprovince interface. Schwerdtner et al (1979) note that the faulting postdates major episodes of folding of supracrustal rocks and diapirism because the faults are oblique to many major fold axial traces (also Borradaile 1982, fig. 3) and cut massive plutons. They also propose that regional shortening in a northwesterly direction was responsible for the Quetico fault and other faults in the Archean of Northwestern Ontario.

The lack of stratigraphic markers makes determination of the sense of motion on the Quetico fault difficult by conventional methods. There is no irrefutable evidence of the sense of motion on the fault. A dextral displacement has been suggested most commonly for the Quetico fault (Hawley (1929), Shklanka (1972),

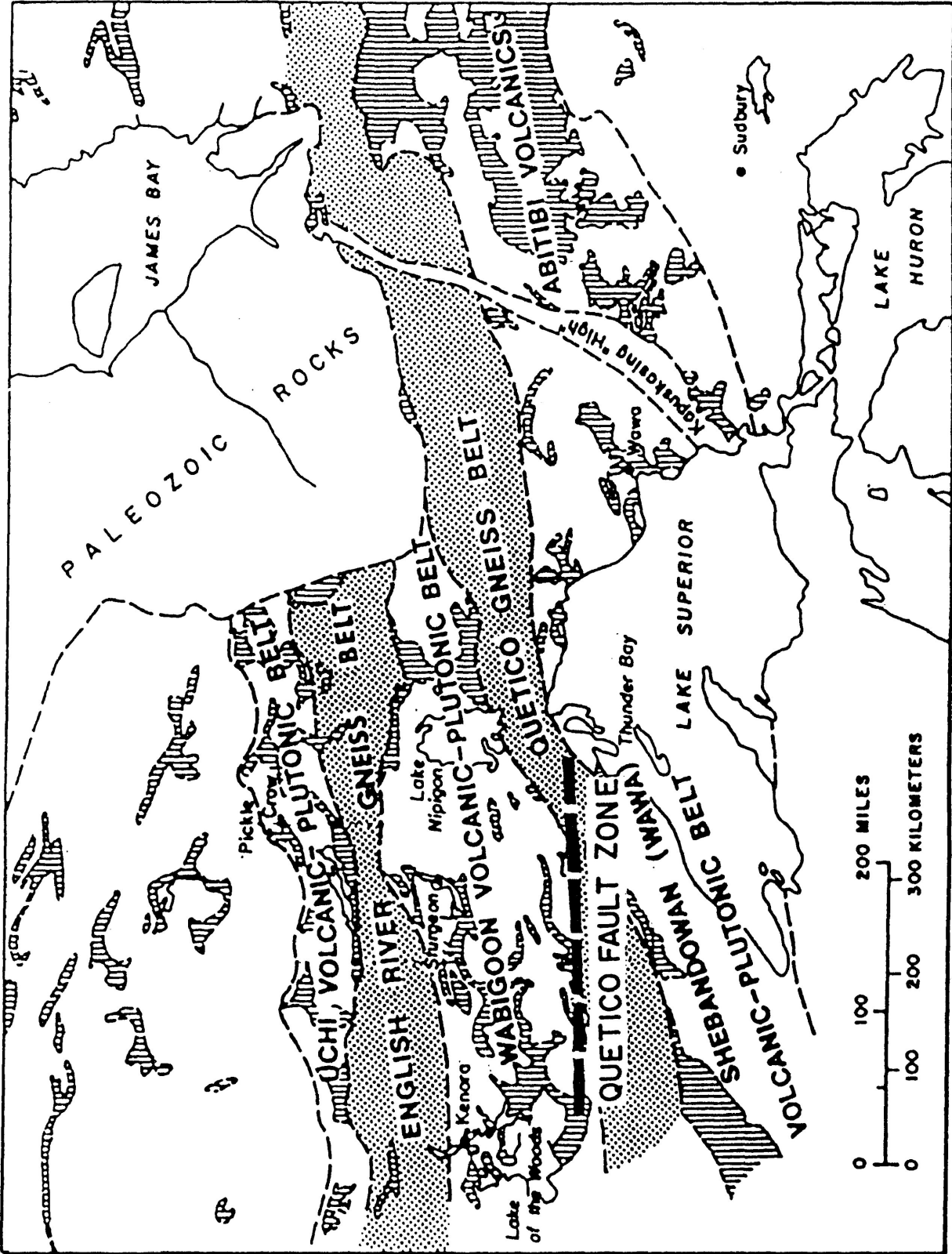


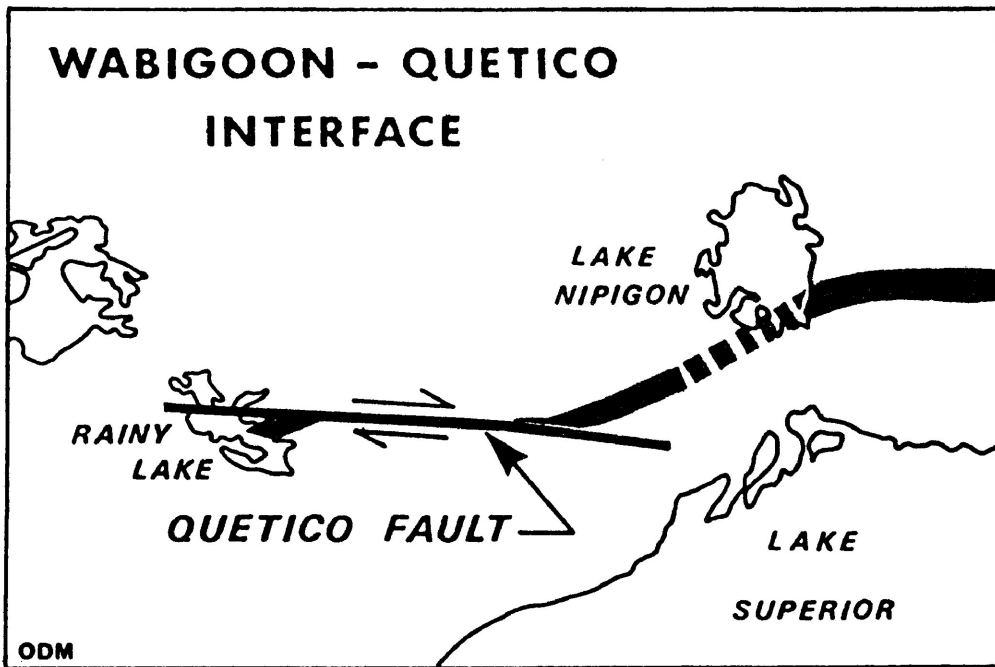
FIG. 1-2 Regional geological setting of the Quetico Fault Zone

Davies (1973), Harris (1974), Mackasey et al (1974), Pirie (1978) and Schwerdtner et al (1979)). Kaye (1967), however, suggested that sinistral motion on the fault occurred in the Lac des Mille Lacs area. Minor vertical motion on the fault has been described by several workers (Hawley (1929), Mackasey et al (1974) and Pirie (1978)). Mackasey et al suggest that the boundary between the Quetico and Wabigoon belts is stratigraphic and that the original lithostratigraphic continuity was dislocated by large scale, right lateral, horizontal displacement along the Quetico fault between Lac des Mille Lacs and Mine Centre (Figure 1-3).

#### B) Previous Geological Studies

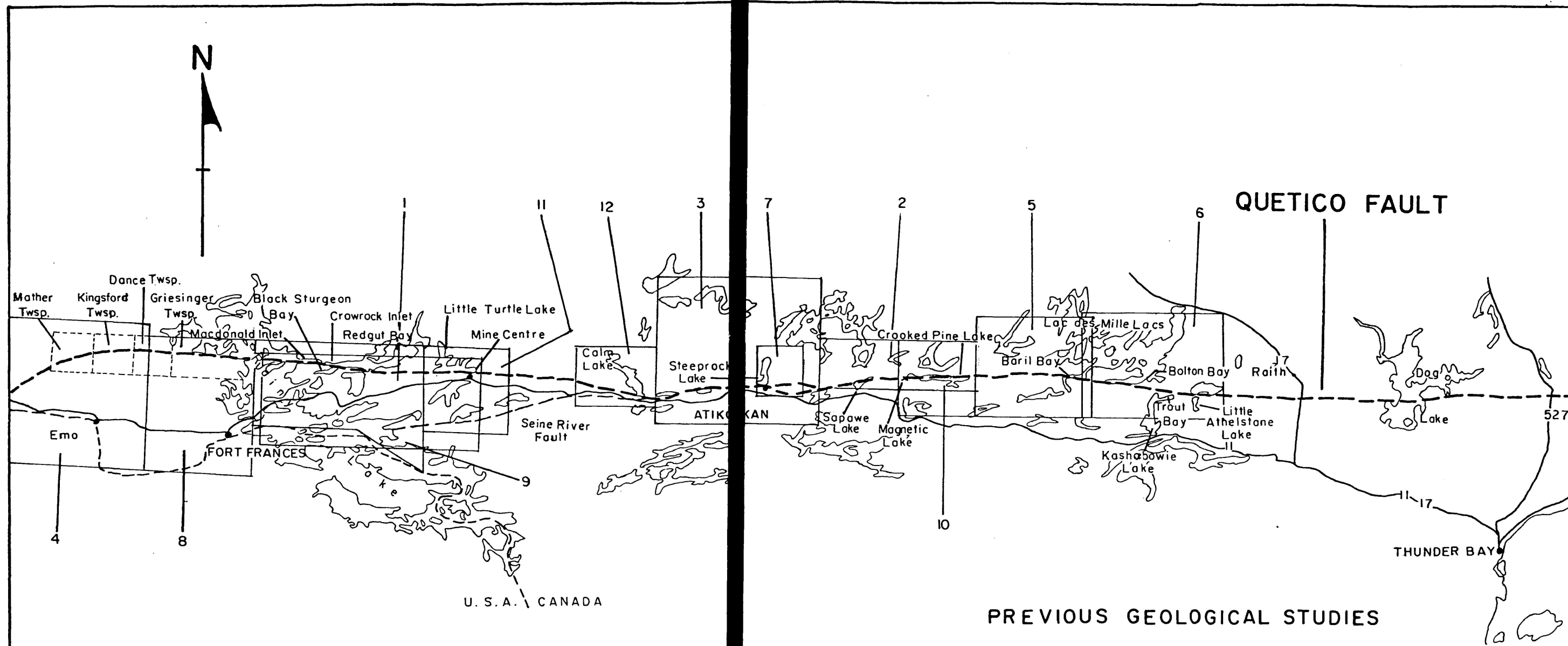
The Quetico fault zone and associated rocks have been described in many publications and reports, although few have dealt specifically with the Quetico fault zone. This section reviews studies which have dealt with various aspects of the fault zone and contributed to its delineation. The location of these studies and localities pertinent to this discussion are indicated in Figure 1-4.

The Quetico fault as described in this thesis was identified based on air photograph interpretation by Parkinson (1962) as a continuous fault zone extending from Fort Frances to the Lac des Mille Lacs-Kashabowie Lake area. Ayres et al (1970) recognized that the fault continues eastward through Dog Lake. Kehlenbeck (1976) noted that the fault zone extends still further east to Highway 527. The author notes that the lineament defining the fault zone can be

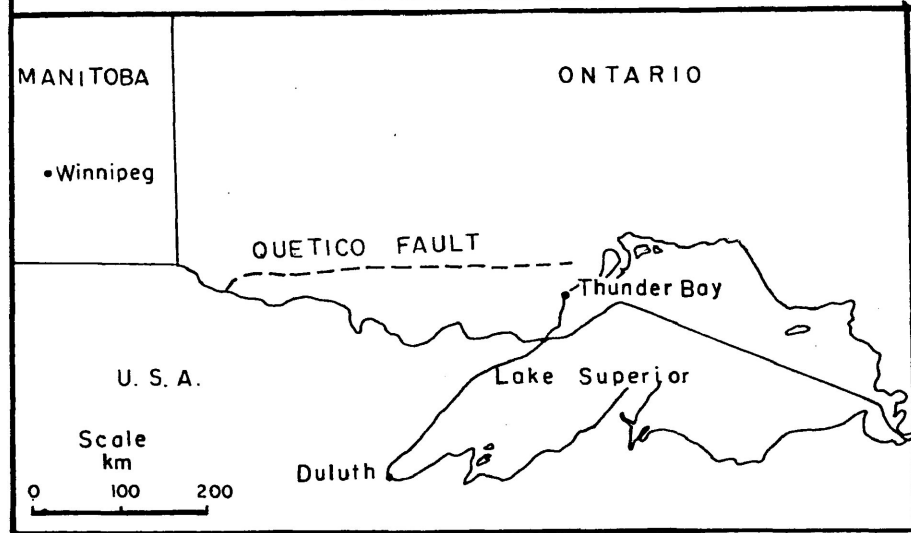


from Mackasey et al (1974)

FIG. 1-3: Sketch map illustrates the displacement of the Wabigoon-Quetico interface (heavy line) by right lateral movement on the Quetico Fault as suggested by Mackasey et al (1974).



**LOCATION MAP**



**PREVIOUS GEOLOGICAL STUDIES**

- |                               |                                   |
|-------------------------------|-----------------------------------|
| 1) LAWSON (1888, 1913)        | 7) SHKLANKA (1972)                |
| 2) HAWLEY (1929)              | 8) DAVIES (1973)                  |
| 3) MOORE (1939)               | 9) HARRIS (1974)                  |
| 4) FLETCHER AND IRVINE (1954) | 10) PIRIE (1978)                  |
| 5) IRVINE (1963)              | 11) WOOD ET AL (1980)             |
| 6) KAYE (1967)                | 12) FUMERTON AND BUMGARNER (1980) |

**FIG. 1-4**

**SCALE**

kilometers



drawn by M. Kenne

traced east of Highway 527, through the south part of Greenwich Lake until it disappears beneath the overlying Proterozoic diabase sills.

Deformed rocks which are now recognized as part of this major fault zone were first described by Lawson (1888, 1913) in the Rainy Lake area. He described a rock unit which he called "Porphyroid Gneiss" as a remarkably linear and persistent belt of sheared granitic rock. He traced the unit in nearly continuous exposure for a distance of 34 kilometers from the eastern end of Little Turtle Lake westward to Black Sturgeon Bay and suggested that the unit most likely extended eastward beyond Little Turtle Lake. He noted a similar unit exposed for a distance of 6.5 kilometers on islands in Rainy Lake, west of the first exposure. Lawson, however, did not identify a western boundary for the unit. He regarded the unit as a marginal facies to the great batholithic area of banded gneisses lying north of the unit. He observed that the "porphyroid gneiss" had no definite boundary with the layered gneisses but graded into them across and along strike. Lawson noted that red or flesh coloured rocks graded into grey coloured rocks and that porphyritic textures were almost always present. Feldspar phenocrysts occurred as augen in a foliation which he attributed to shearing. He observed the presence of cataclastic textures and described them as such from thin sections of the porphyroid gneiss.

Portions of the Quetico fault zone have been described in a number of reports of the Ontario Department of Mines, Ontario

Division of Mines, and Ontario Geological Survey since Lawson first described the fault rocks. These reports are reviewed below in chronological order.

Hawley (1929) postulated a fault of some magnitude forms the boundary between sedimentary rocks to the south and greenstones to the north in the Sapawe Lake area. He noted that the straight line contact between the two units is marked by a band of highly schistose rocks across the eastern part of the map area. He believed that the fault continued westward and was there marked by a topographic depression but added that it was mostly obscured by glacial drift, swamps and lakes. He noted that the fault is near vertical in dip as indicated by the steeply dipping schistosity. Despite the lack of stratigraphic markers Hawley proposed that horizontal movement on the fault was predominantly dextral. This suggestion was based on the orientation of a prominent "fracture cleavage" (sic) which he believed to be related to the major fault movement. Vertical motion indicated by "drag" folds suggests both up and down movements of the north side of the fault with respect to the south in different locations although Hawley noted more evidence to suggest that the south side moved up with respect to the north side in an area east of Steeprock Lake fault.

Moore (1939) worked west of the Sapawe Lake area. He noted that the fault defined by Hawley extends into the Atikokan area and believed that the fault is gradational into a zone of intense shearing just east of Atikokan.



In the Emo map area, west of Fort Frances, Fletcher and Irvine (1954) relied extensively on topographic lineaments to fix the position of the fault because of the thick cover of Quaternary deposits in this area. An east-west trending gully occurring in quartz monzonite in eastern Kingsford Township was described as a fault. A second fault, trending N80W, was located in Mather Township, 6.5 to 8 kilometers west of the Kingsford Township fault. Both of these faults are now recognized as part of the western extension of the Quetico fault. They occur directly along strike from excellent isolated exposures of fault rock in Dance Township.

In the Western Lac des Mille Lacs area, Irvine (1963) described a zone of chlorite schist which marks the contact between basic volcanic rocks to the north and paragneiss and granite to the south. Irvine concluded that this contact was probably a fault. From exposures near Baril Bay he described rocks which appeared to be silicified in or near the contact zone. In thin section the rocks showed textures which were produced by cataclasis and mylonitization.

Kaye (1967) described the Quetico fault in the Eastern Lac des Mille Lacs map area. He noted that the sharp contact between metavolcanic and metasedimentary rocks is marked by the occurrence of silicified and brecciated metabasalt. Kaye suggested a displacement of 16 kilometers in a sinistral sense occurred on the fault. This observation was based on the occurrence of an isolated layer of metabasalt, approximately 300 meters wide enclosed by metasedimentary rocks and extending from Trout Bay on

Kashabowie Lake to Little Athelstane Lake. He suggested that the layer of metabasalt represents a wedge of the metabasalt occurring on the south shore of Bolton Bay, Lac des Mille Lacs and that this wedge was caught up in a zone of dislocation along the Quetico fault and moved eastward to its present location. The author notes that this unit may or may not be a wedge of metabasalt. The fault rocks in this area may merely resemble metavolcanics.

Shklanka (1972) described the fault zone in the Steep-rock Lake area as comprising the Quetico fault and the North Branch of the Quetico fault. He described the North Branch as an earlier offset which became locally in-folded and in-faulted. He supposed that reactivation of the Quetico fault system did not occur on the North Branch and displacement occurred only on the fault to the south. Because of the steep dip and straight trace of the fault Shklanka suggested that motion on the fault was predominantly strike-slip. He proposed dextral motion on the fault based on the disruption of major structural features. He suggested that the fault had a complex history involving numerous episodes of motion along different directions spread over a long period of time (pre-Kenoran to Paleozoic).

Davies (1973) described the Quetico fault zone in the Fort Frances area as a major east-west trending zone extending through Dance and Griesinger Townships. From Dance Township to Little Turtle Lake he described the fault zone as 500-1000 meters

wide and vertical or steeply dipping to the north. He stated that aeromagnetic patterns, rock-type distribution and small scale structures suggest dextral movement on the fault. Davies referred to the rocks of the fault zone as "fault zone gneiss" which included layered biotite granite gneisses gradational with mylonites in the zone. These rocks, Lawson's porphyroid gneiss, commonly show porphyroclastic textures with large feldspar grains in a finer grained matrix. Davies noted that recrystallization in these rocks is common.

Harris (1974) reported on the rocks of the Quetico fault zone in the Rainy Lake area. He described an east-west zone of dynamically deformed granitic rocks. The zone which is 350-1000 meters in width is well exposed on islands in Rainy Lake, on the south sides of Macdonald Inlet and Crowrock Inlet and in Redgut Bay. Rocks of the fault zone include crushed granite, augen gneiss and mylonite. East of Black Sturgeon Bay, Harris noted that the fault rocks are confined between two well defined lineaments. Migmatite exposed north and south of these lineaments shows an increase in deformation with decreasing distance from the fault zone. There is also an abrupt change from migmatites to the fault rocks across the lineaments. Harris noted that west of Black Sturgeon Bay the fault zone is narrower and here the migmatite is gradational into fault rocks. He further observed that dextral movement occurred on the fault. He based this conclusion on changes in the attitude of

rocks near the fault as shown on the Kenora-Fort Frances Map 2115 (Davies and Pryslak (1967)) and on the presence of joints which he thought might be feather joints as well as on "drag" folds. Lineations measured by Harris in fault zone rocks trend east-west and have shallow plunges to the east or west suggesting predominant strike-slip motion on the fault.

Pirie (1978) described the fault zone in the Crooked Pine Lake map area. Here the fault forms the contact between meta-volcanic and metasedimentary rocks of the Wabigoon and Quetico subprovinces, respectively. Based on exposures along the south shore of Magnetic Lake and the north shore of Crooked Pine Lake, the fault comprises a highly deformed, vertically dipping zone up to 100 meters wide. Mafic metavolcanics were dynamically metamorphosed to chloritic phyllite. Felsic to intermediate meta-volcanics and greywacke have altered to sericite phyllite. Less micaceous rocks are mylonites. Pirie observed that movement on the fault is indicated by a change in metamorphic grade across the fault. He supposed that because the foliation is oblique to the fault zone it suggests dextral displacement. However, minor structures that he observed indicate dextral, sinistral and vertical motions.

The Mine Centre area was mapped by Wood et al (1980). Their maps show the fault extending east and west of Little Turtle Lake. They noted a red-feldspar mafic porphyry unit which is found

only in proximity to the Quetico fault, in this map area. "Drag" folds indicate dextral and sinistral motion to Wood et al but they noted that regional trends suggest that motion was dextral.

Fumerton (1980, 1982) and Fumerton and Bumgarner (1980) worked in the Calm Lake area. They found no direct connection between the Quetico fault as previously described east and west of this area. They described the Quetico fault to the east of Calm Lake as being continuous with the Seine River fault to the west (Figure 1-4) and proposed that these two faults together be named the Quetico fault. They suggested the name "Little Turtle Fault" be given to the fault extending west of Calm Lake which has hitherto been called the Quetico fault. However in this thesis the continuous east-west trending lineament from Rainy Lake to Thunder Bay area (as shown on Figure 1-4) is still called the Quetico fault, which is in agreement with publications prior to those of Fumerton.

Carter (1983) noted the presence of "cataclastic" textures in rocks in the south part of Greenwich Lake but did not identify them as belonging to the eastern extension of the Quetico Fault Zone.

Some other recent studies have also described some features of the Quetico fault zone. Bau (1979) described the fault zone in the Kashabowie - Lac des Mille Lacs area\*, Kennedy (1980) examined the rocks of the fault zone near Raith and Borradaile (1982) described microfaults in the rocks of the Quetico fault zone at

---

\*The author attempted to obtain a copy of this thesis from the University of Toronto but was unable to do so.

Dog Lake. Further, Borradaile and Kennedy (1982) described flow-banding in pseudotachylite from the fault zone at Crowrock Inlet.

## C) Study Objectives

The objectives of this thesis are outlined below:

- 1) To examine the fault zone and fault rocks to:
  - (a) examine the brittle/ductile nature of deformation in the fault zone
  - (b) determine, if possible, the mechanisms responsible for deformation in the fault zone.
- 2) To determine the sense of motion on the fault in the absence of stratigraphic markers.
- 3) To investigate the nature of strain within the fault zone and obtain strain estimates.
- 4) To determine the original structural level of the presently exposed fault rocks at times when the fault was active.

## D) Methods

The objectives will be attained by:

- a) examining field structures and microstructures in the fault zone.
- b) strain analysis
- c) the investigation of quartz c-axis petrofabrics.

Field study comprising collection of data and collection of oriented specimens was carried out at various localities along the fault zone. These localities, which will be referred to throughout this paper, are indicated on Figure 1-4. They are Dance Township, Macdonald Inlet, Crowrock Inlet, Turtle River Road (West of Little Turtle Lake), Little Turtle Lake, Calm Lake, Bolton Bay of Lac des

Mille Lacs, Kashabowie Lake, Little Athelstane Lake, Raith, Dog Lake and Highway 527.

#### E) Terminology

Classification of the dynamically metamorphosed rocks studied in this thesis follows Sibson (1977) (Table 1-1). He proposed the use of the term "fault rocks" as "a collective term for the distinctive rock types found in zones of shear dislocation at both high and low crustal levels, whose textures are thought to arise, at least in part, from the shearing process". The fault rocks are classified on textural criteria. Incohesive fault rocks exhibit random fabrics and include fault breccia and fault gouge. Cohesive fault rocks are subdivided into the cataclasite series (random-fabric fault rocks) and the mylonite series (foliated fault rocks). Polymineralic rocks are classified according to the texture of the matrix. The mylonite and cataclasite series are subdivided based on the proportion of matrix in the rock, into protomylonite, mylonite and ultramylonite and protocataclasite, cataclasite and ultracataclasite respectively. Phyllonite varieties of mylonites are mica-rich mylonites and ultramylonites which have the silky appearance of phyllites. Blastomylonites are mylonites in which significant grain growth has occurred. Pseudotachylite is glassy material which is commonly found associated with random-fabric cohesive fault rocks in fault zones.



Table 1-1

# Textural Classification of Fault Rocks

(Sibson, 1977)

		RANDOM-FABRIC	FOLIATED		
INCOHESIVE		<b>FAULT BRECCIA</b> visible fragments > 30% of rock mass	?		
		<b>FAULT GOUGE</b> visible fragments < 30% of rock mass	?		
COHESIVE	Glass/ Devitirified Glass	<b>PSEUDOTACHYLITE</b>	?		
	NATURE OF MATRIX Tectonic reduction in grain size dominates grain growth by recrystallization & neomineralization	<b>CRUSH BRECCIA</b> <b>FINE CRUSH BRECCIA</b> <b>CRUSH MICROBRECCIA</b>	fragments > 0.5 cm 0.1cm < frags. < 0.5cm fragments < 0.1cm	0-10%	
		<b>PROTO-CATACLASITE</b>	PHYLLO- NITE VARIETIES	<b>PROTO-MYLONITE</b>	10-50%
		<b>CATACLASITE</b>		<b>MYLONITE</b>	50-90%
		<b>ULTRA-CATACLASITE</b>		<b>ULTRA-MYLONITE</b>	90-100%
Grain Growth Pronounced	?	<b>BLASTOMYLONITE</b>			

Lapworth (1885) first used the term mylonite to describe fine grained, laminated rocks of the Moine Thrust whose textures he believed developed from brittle processes (crushing and milling). Dynamically metamorphosed rocks have also been classified and described in more recent studies by Christie (1963), Higgins (1971) and Zeck (1974). These authors describe the rocks in terms of brittle processes with recrystallized textures being the result of post-tectonic recrystallization in accordance with Lapworth's original concept. Bell and Etheridge (1973) recognized that ductile processes were more important than brittle processes in the formation of mylonites. They established that recrystallization was syntectonic.

Sibson's classification avoids genetic inferences and therefore provides useful descriptive terminology. However, it is now generally accepted that mylonites result from ductile deformation processes and cataclasites from brittle processes. The term ductile infers the capacity of a material for substantial shape change (strain) without gross fracturing (Paterson, 1978, p. 161). Ductile deformation processes include crystal plasticity accompanied by syntectonic recovery and recrystallization as well as diffusive processes. Brittle behaviour involves penetrative fracturing after very low permanent strain (Handin, 1966). Brittle deformation processes include fracturing with variable amounts of grain boundary sliding and grain rotation. (Deformation mechanisms are discussed

in greater detail in the next chapter.) The transition from brittle to ductile behaviour is temperature and pressure dependent. Brittle behaviour predominates at low temperatures and confining pressures while ductile behaviour predominates at higher temperatures and pressures.

## 2 - STRUCTURE AND MICROSTRUCTURES OF THE QUETICO FAULT ZONE

## A) Macroscopic Structure

*Width of the fault zone:* The Quetico fault comprises a zone of highly deformed rocks which is variable in width (Table 2-1). The differences in width along the length of the fault zone appear to be related to the local lithology. This study concentrates on the quartzo-feldspathic mylonitic fault rocks in the eastern and western parts of the fault zone where it is quite wide (300 m. to 1200 m.). The fault zone is generally more narrow in the central portion (Calm Lake to Lac des Milles Lacs) (10 m. to 300 m.) where it occurs within metasedimentary rocks and metavolcanic rocks.

*Discussion:* Mylonitic microstructures are very evident in quartzo-feldspathic rocks due to the quartz-feldspar ductility contrast and a wide fault zone develops. The mica-rich metavolcanic and metasedimentary rocks generally comprise phyllonitic rocks. The narrower zone of deformation in these rocks may be due to their smaller internal ductility contrasts. Also, high water content, which has been reported in phyllonites (Sibson, 1977), could result in enhanced ductility (hydrolytic weakening of minerals) allowing the deformation to be concentrated in a narrow zone. The presence of fluids in the fault zone rocks could also

Table 2-1: The Width of the Quetico Fault Zone from West to East in descending order.

	Locality	Approximate Width	Reference
(Western-most)	Dance Township	400 m	
	Macdonald Inlet	600 m	
	Crowrock Inlet	800 m	
	*Pearson's Road	600 m	(Harris, 1974)
	Turtle River Road	800 m	
	Little Turtle Lake	700 m	
	Calm Lake	<10 m	
	*Crooked Pine Lake	100 m	(Pirie, 1978)
	*Sapawe Lake	100-300 m	(Hawley, 1929)
	*Atikokan	300	(Shklanka, 1972)
	*Lac des Milles Lacs	(W)400-600 m	(Irvine, 1963)
	*	(E)200-400 m	(Kaye, 1967)
	Kashabowie Lake	700 m	
	Athelstane Lake	200-300 m	
Raith	1000 m		
Dog Lake	1000-1200 m		
(Eastern-most)	Hwy. 527	1000 m	

Width of the fault zone as determined by the author. The width was defined by the zone comprising macroscopically visible mylonitic and/or cataclastic textures.

\*At these localities the width was inferred from observations by previous authors (noted).

promote diffusive deformation processes possibly resulting in volume change across the fault zone which would not occur in the 'dry' quartzo-feldspathic rocks. The author offers no evidence of volume change in the phyllonitic rocks as they were not studied in detail. No evidence of diffusive deformation processes was observed in the quartzo-feldspathic fault rocks as will be discussed later in this chapter.

*Geometry of the fault zone and associated faults and fractures:*

Fig. 2-1 illustrates the geometry of the Quetico fault zone and associated faults and lineaments compiled from various geological maps and reports (as indicated on the figure). In general the lineaments near the fault zone are oriented northeast, northwest or parallel to the fault zone (approximately east-west). These structures may or may not be related to motion or activity on the main fault. Only a few lineaments cross the fault zone suggesting they post-date movement on the fault. Most of the lineaments and faults occurring in the vicinity of the fault terminate at the fault suggesting they may be related to motion on the fault or pre-date motion on the fault.

Discussion: Fractures and faults parallel to and branching from a main fault are commonly associated with wrench faults (Hobbs et al, 1976, p. 384). Lineaments clearly identified as faults such

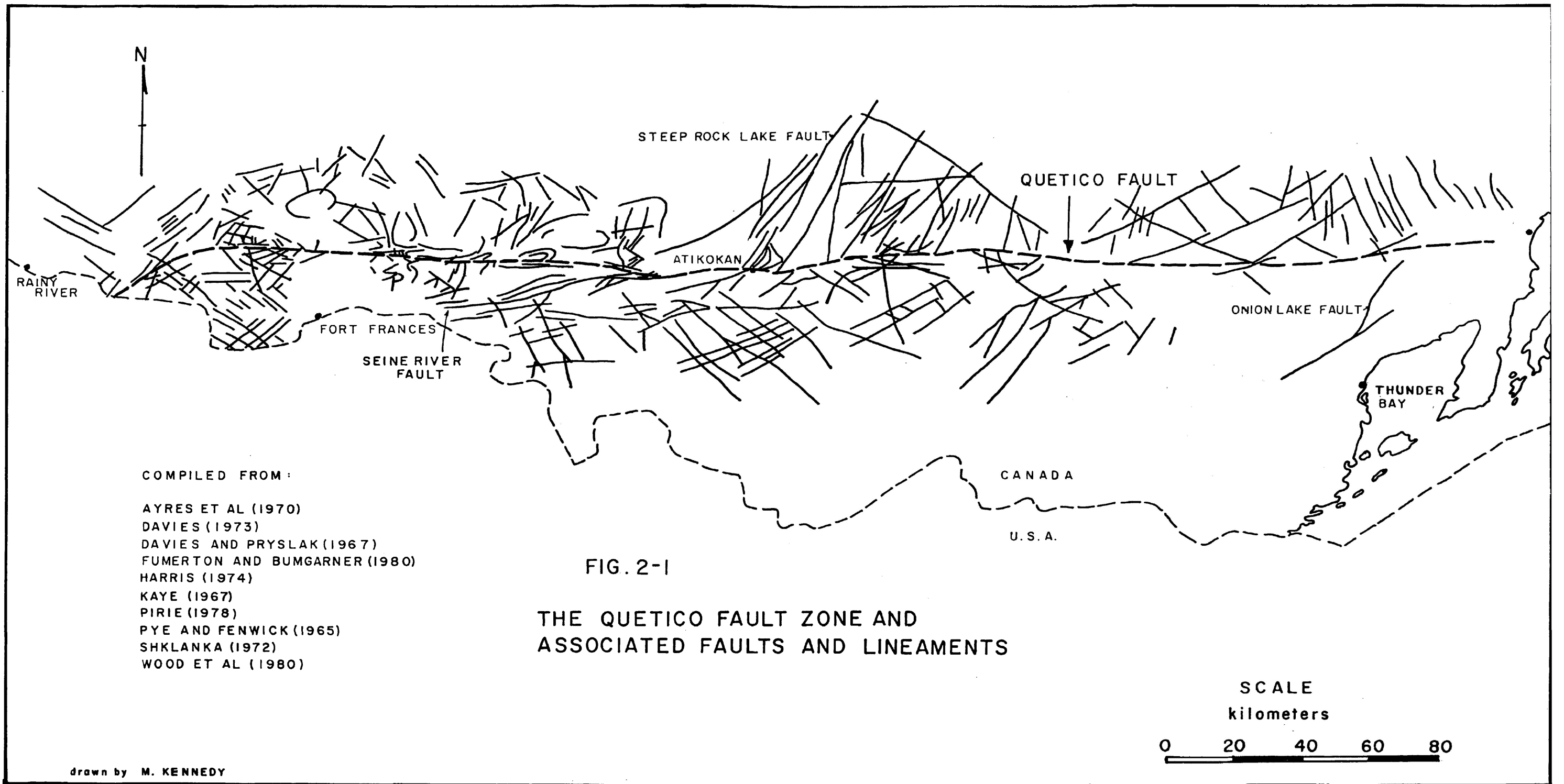


FIG. 2-1

THE QUETICO FAULT ZONE AND  
ASSOCIATED FAULTS AND LINEAMENTS

as the Seine River fault, Steep Rock Lake fault and the Onion Lake fault (Fig. 2-1) may represent splay faults or second-order faults. Second-order faults form when the principal stress directions are reoriented with the onset of faulting (McKinstry, 1953, Moody and Hill, 1956). They occur oblique to the first order fault. Splay faults develop at the ends of the first order faults. Stress conditions build up around the ends of the fault and the axes of principal stresses swing around and tend to become approximately normal and parallel to the fault plane (Price, 1966).

The author suggests that the regional pattern of northeast and northwest trending joints or faults associated with the Quetico fault zone may represent conjugate shear fractures. Shear fractures form at an angle less than 45 degrees to the principal stress direction (about 30 degrees is common). The Quetico fault zone, the main mylonite zone, would thus possibly represent the primary flattening plane. This does not preclude shear motion on the fault as flattening normal to the fault zone could have occurred prior to, associated with, or later than the shearing. Alternatively, the northeast and northwest trending structures may be feather joints (also known as pinnate fractures). These fractures may form prior to or synchronously with the fault zone development. Such fractures are common, intersecting the main fault zone in an acute angle (Hobbs et al, 1976, p. 294). The acute angle between the fracture and the main fault zone points in



the direction of relative motion of the block in which the fracture is contained. The development of two sets of pinnate fractures may indicate that motion in both dextral and sinistral senses occurred.

#### B) Small Scale Structures

*Mylonitic schistosity:* The most widespread feature associated with the fault zone is the steeply-dipping mylonitic schistosity. The mylonitic fabric trends east-west or north of east in most localities; roughly parallel to the fault zone (Fig. 2-2). It is a penetrative fabric developed due to ductile deformation within the fault zone. The mylonitic schistosity is best developed in quartz and mica rich rocks and poorly developed in quartz poor rocks. It is defined by the preferred dimensional orientation of minerals in the fault rocks. In quartzo-feldspathic rocks the mylonitic schistosity is defined by very strained, flattened quartz grains (see Chapter 3) and by the preferred dimensional orientation of feldspar grains as shown in Fig. 2-3. The feldspar grains commonly comprise ovoid porphyroclasts. In mica-rich rocks the mylonitic schistosity is defined by the preferred crystallographic orientation of micaceous minerals. Feldspar-rich (quartz poor) rocks tend to lack schistosity.

*Mylonitic banding or layering:* Mylonites in the Quetico fault

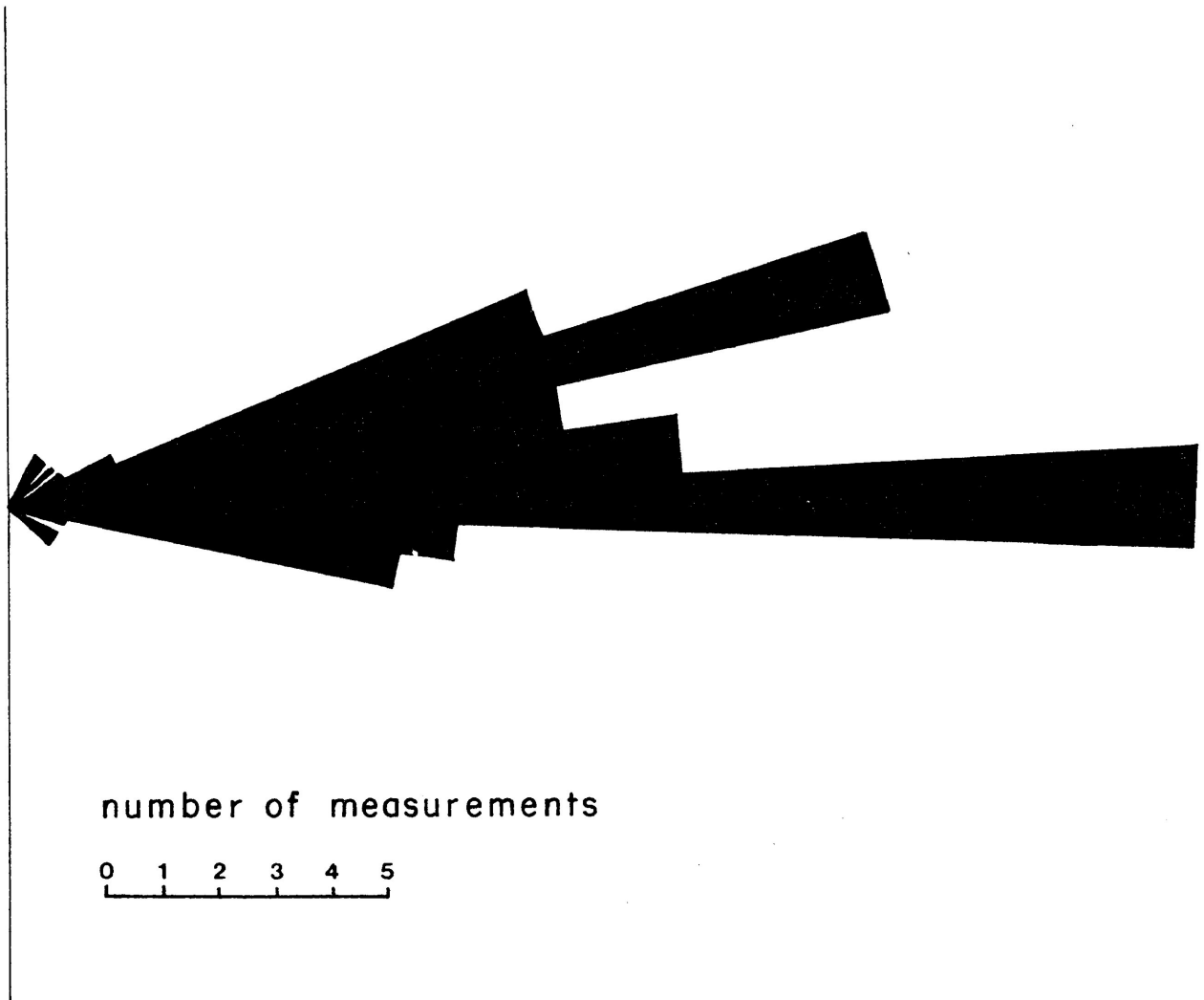


Fig. 2-2: Rose diagram  
Orientation of mylonitic schistosity planes.

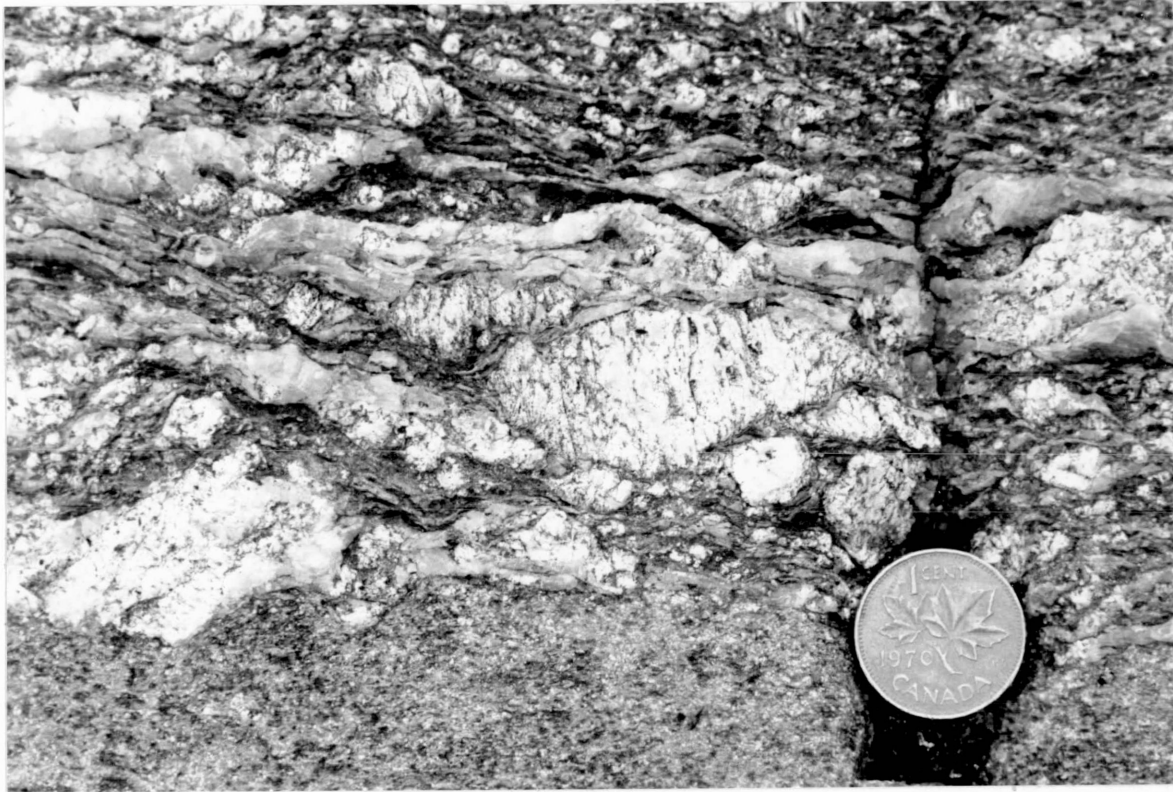


Fig. 2-3: Mylonitic Schistosity

The mylonitic schistosity is defined by highly strained quartz grains and ovoid porphyroclasts of feldspar. Note the tension fractures in the feldspar grains roughly normal to the schistosity.

Locality - Stirrett Bay, Dog Lake

zone are commonly banded. The banding strikes east-west and north of east (Fig. 2-4) roughly parallel to the fault zone and similar in orientation to the mylonitic schistosity. It is difficult to determine to what extent the banding reflects earlier, possibly gneissic, layering or if it formed due to the deformation process. The layering tends to be somewhat discontinuous. In general the layering is parallel to primary layering emphasizing the banded appearance of the rocks (see Fig. 2-5). In some localities rocks which may have been fairly coarse grained (large remnant feldspar grains are observed in thin section) comprise finely laminated mylonites (Fig. 2-6). The fine layers are composed of different minerals. In this situation, the layering may be due to the deformation and recrystallization of former large grains into thin lenses which appear as discontinuous bands or layers as described by Vernon (1974).

*Mineral lineations:* Mineral lineations were noted within the fault zone. Most grains within the mylonitic rocks are strongly flattened (see Chapter 3). Thus the mineral lineations are often poorly developed. Quartz, feldspar and amphibole grains were observed to comprise the lineations. Where observed the mineral lineations lay parallel to the mylonitic schistosity, dipping shallowly to the east or west.

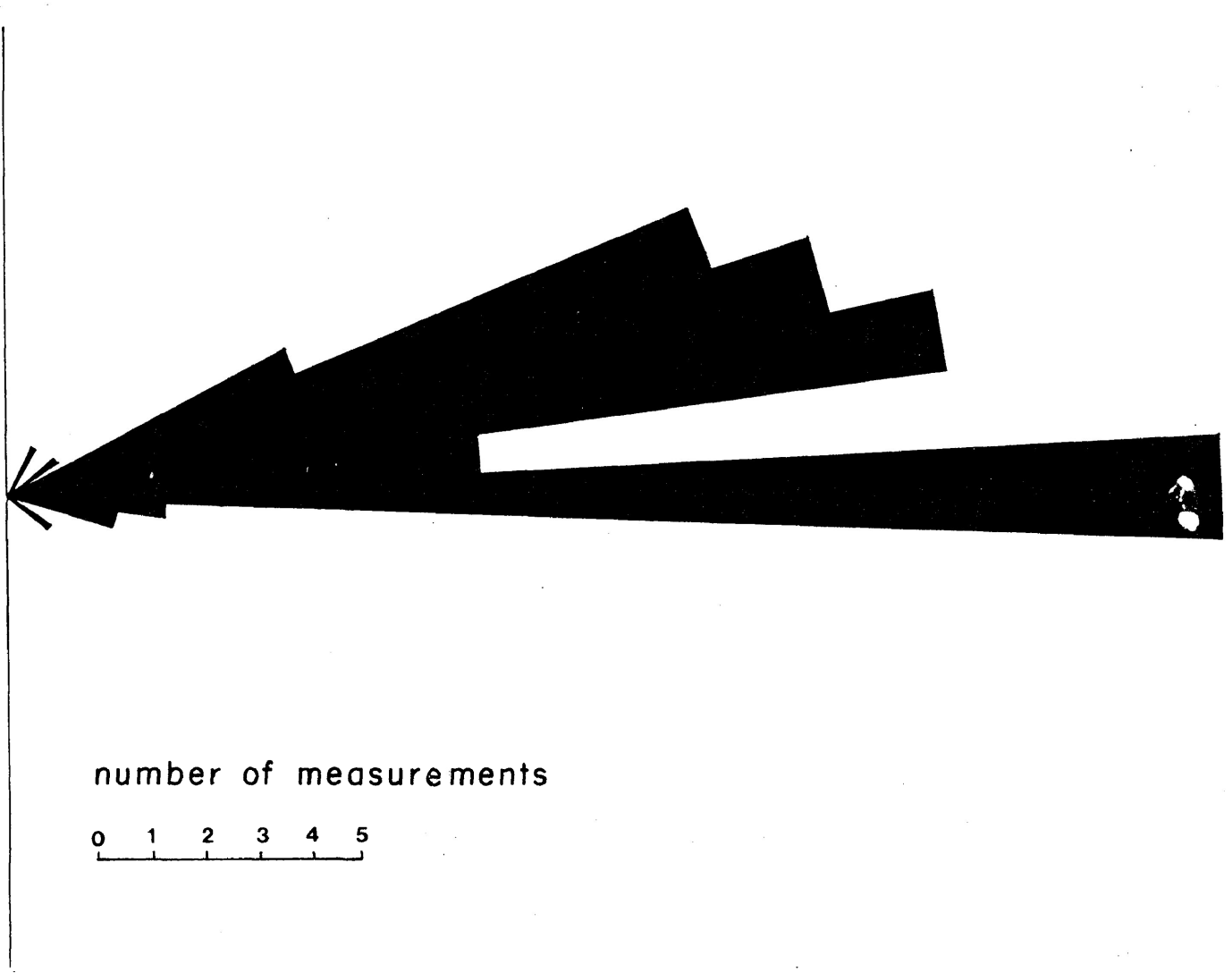


Fig. 2-4: Rose diagram  
Orientation of mylonitic layering or banding.

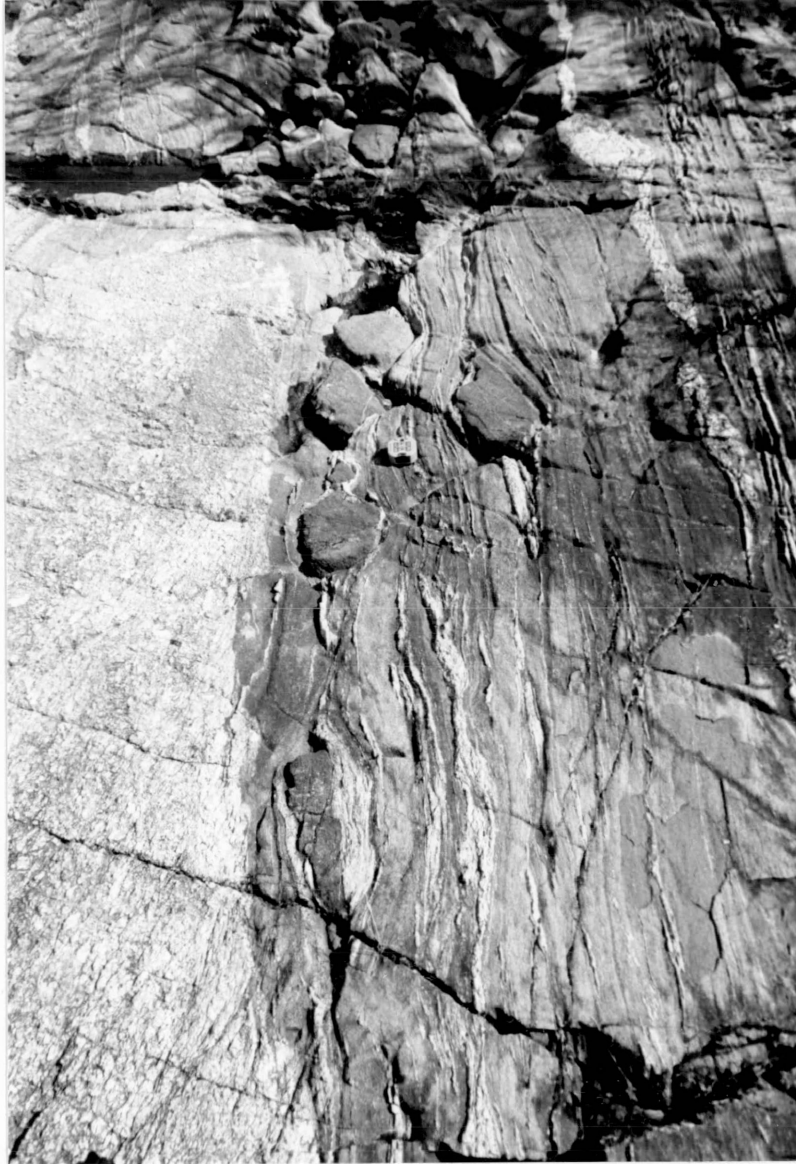


Fig. 2-5: Deformation within the fault zone has resulted in the gneissic layering developing a discontinuous appearance and boudinage of more competent layers.

Locality; Stirrett Bay, Dog Lake

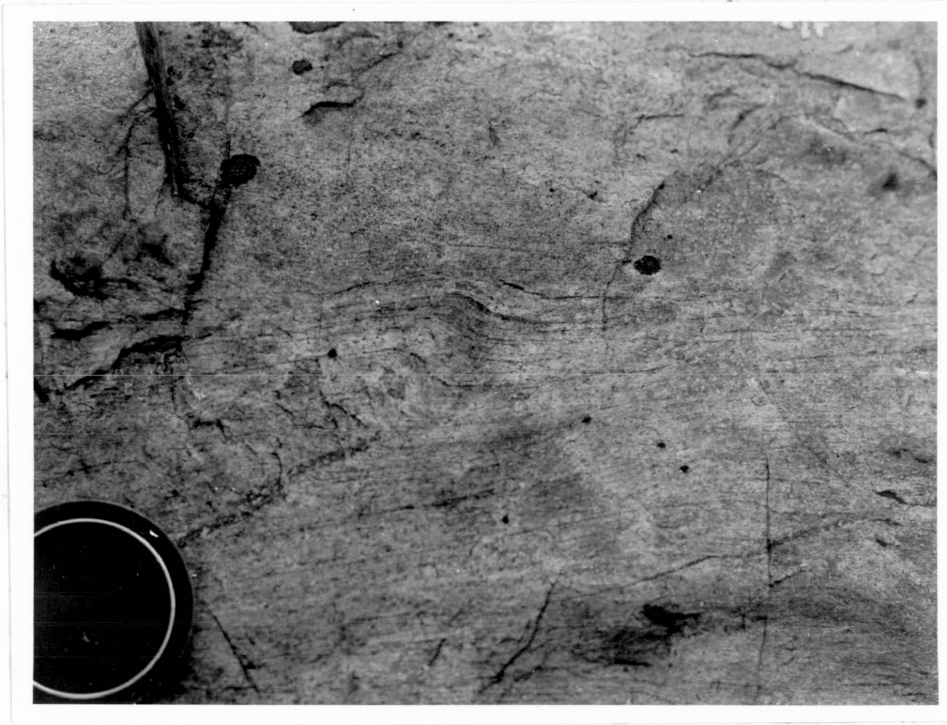


Fig. 2-6: Finely laminated mylonite. The fine, discontinuous layers may have been former large grains.

Locality: Dance Twp.

*Slickensides:* Slickenside surfaces were commonly observed in the field study of the Quetico fault zone (Fig. 2-7). The slickensides occur both parallel to the mylonitic schistosity and small fault and microfault surfaces which occur at an angle to the mylonitic schistosity. The smooth, polished surfaces are commonly rich in phyllosilicate minerals. Slickenside striations or ribbing composed of resistant minerals were observed in some localities. These lineations are near horizontal on the slickenside surfaces suggesting horizontal movement on the above surfaces. Steps in the striations on the slickenside surfaces may or may not be an indication of the slip direction on the surface (Hobbs et al, 1976, p. 303). These steps on slickenside surfaces within the Quetico fault zone indicate dextral motion commonly and, very rarely, sinistral motion.

*Microfaults:* Microfaults or small scale faults are a distinctive feature which can be observed within the Quetico fault zone. Microfaults are surfaces on which small scale slip occurs. Along the length of the fault zone microfaults commonly offset the fault zone rocks. Microfaults associated with the Quetico fault zone at Dog Lake have been described by Borradaile (1982). At this locality the rocks of the fault zone are well exposed. On the north side of the fault zone the gneissic layering which is parallel to the fault zone is displaced in a dextral sense by microfaults which





Fig. 2-7: Slickenside surfaces are commonly rich in phyllosilicate minerals (here green chlorite). Note the horizontal striations on the slickenside surfaces.

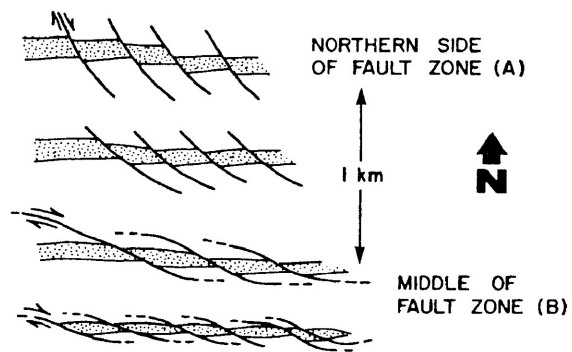
Locality: Highway 527.

cut obliquely across the layering at a fairly high angle (Fig. 2-8). Within the fault zone Borradaile noted that the microfaults form a significant component of the fabric together with the mylonitic schistosity parallel to the layering. The microfaults cut across the bands and curve parallel to the layering where they appear to disappear into grain boundaries. The dextral slip on the microfaults is presumably taken up along the grain boundaries parallel to the banding and the fault zone. Fig. 2-9 illustrates the appearance of the microfaults within the fault zone. When the microfaults offset layers, the layers tend to develop a lenticular appearance. A texture resembling boudinage commonly develops.

Figures 2-10 and 2-11 demonstrate the orientation of various structures, including microfaults, from localities along the length of the fault zone. The rose diagrams of Fig. 2-10 serve to indicate the variation in orientation of the microfaults observed but do not indicate the frequency with which these structures occur. Microfaults seem to be more prominent at some localities and within some lithologies than others. Microfaults are more commonly observed in quartzo-feldspathic rocks than in phyllonitic rocks.

Microfaults were observed on which slip had occurred in a dextral sense and in a sinistral sense. Often the sense of slip could not be determined. Dextral microfaults are the most common (see, for instance, the rose diagrams from Dog Lake Fig. 2-11)

Fig. 2-8:



Occurrence of microfaults within the Quetico fault zone at Dog Lake.

from Borradaile, 1982.

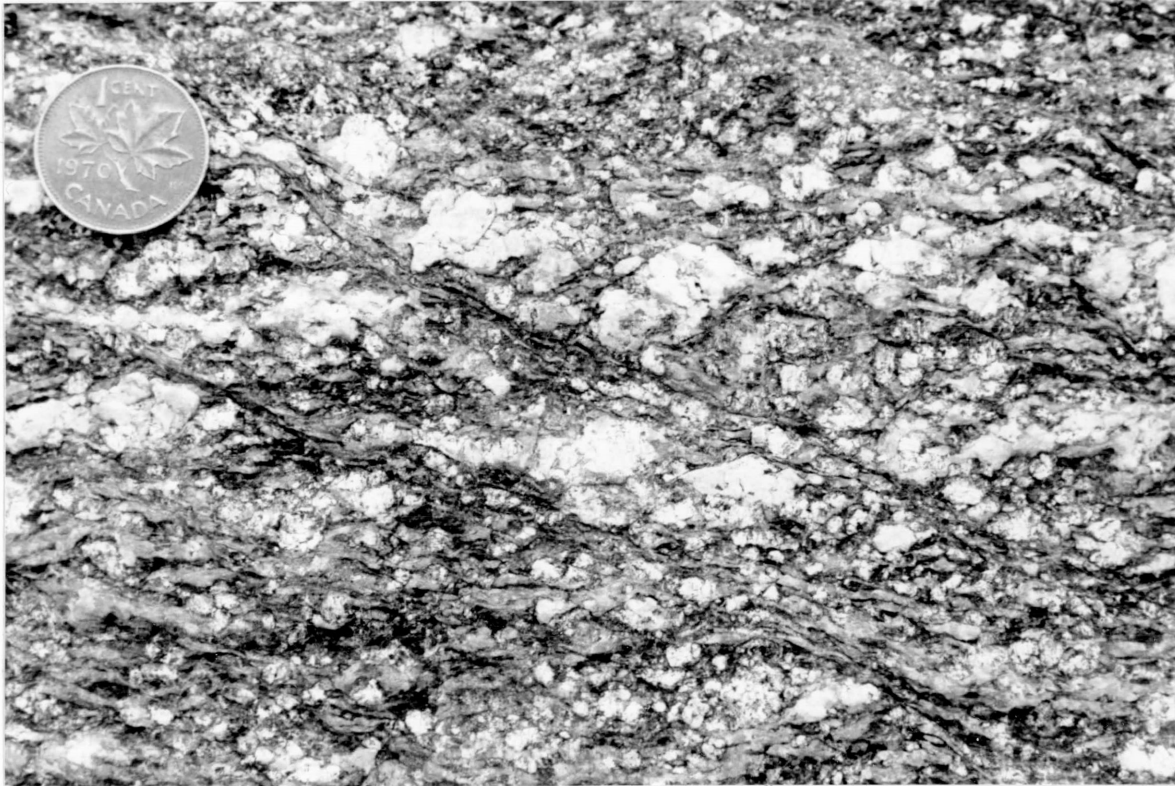
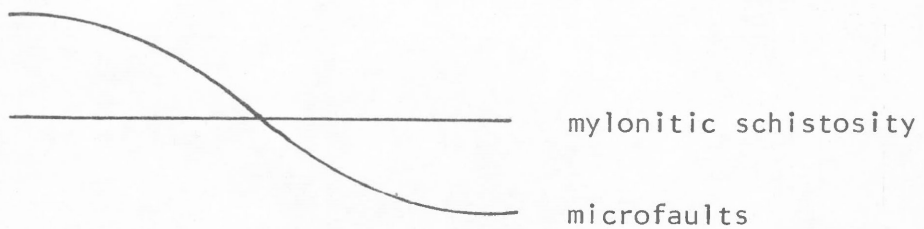


Fig. 2-9; Microfaults in quartzofeldspathic mylonite at Dog Lake. Note the orientation of the microfaults with respect to the mylonitic schistosity.



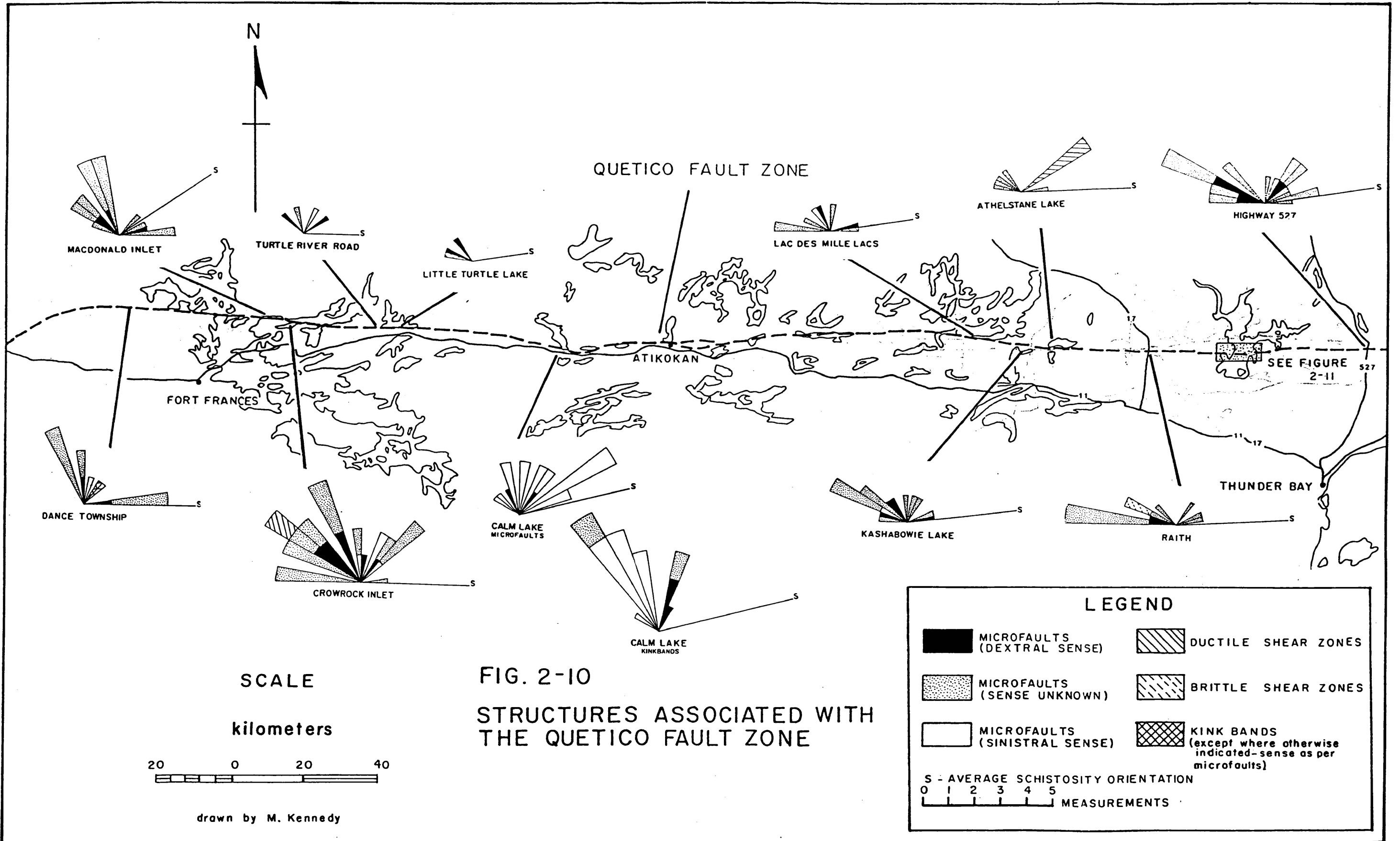


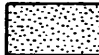





FIG. 2-10  
STRUCTURES ASSOCIATED WITH  
THE QUETICO FAULT ZONE

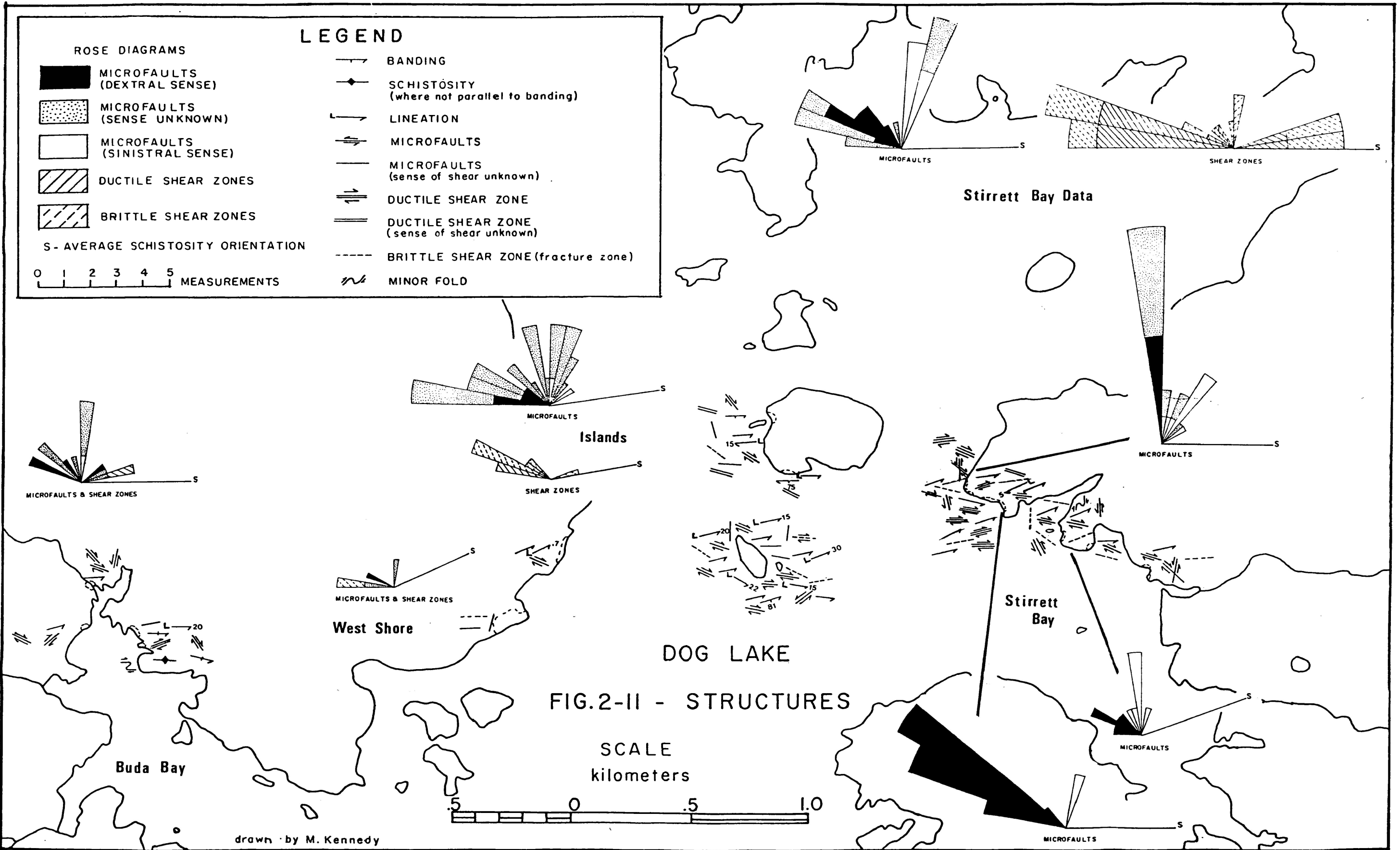
SCALE  
kilometers  
20 0 20 40

drawn by M. Kennedy

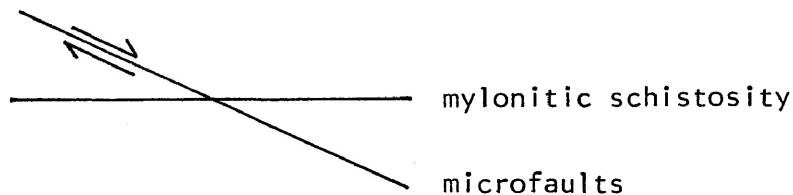
**LEGEND**

	MICROFAULTS (DEXTRAL SENSE)		DUCTILE SHEAR ZONES
	MICROFAULTS (SENSE UNKNOWN)		BRITTLE SHEAR ZONES
	MICROFAULTS (SINISTRAL SENSE)		KINK BANDS (except where otherwise indicated - sense as per microfaults)

S - AVERAGE SCHISTOSITY ORIENTATION  
0 1 2 3 4 5 MEASUREMENTS



although both dextral and sinistral microfaults were observed at most localities. The only exception to this is Calm Lake where many sinistral microfaults were observed. The dextral microfaults commonly lie clockwise from the mylonitic schistosity (as shown below) although the angle the microfaults make with the schistosity is variable and generally less than  $60^\circ$  as in Fig. 2-9.



Note that at Stirrett Bay, Dog Lake (Fig. 2-11) the microfaults are at a higher angle to the mylonitic schistosity than the microfaults further south in the more strongly deformed rocks in the fault zone as described by Borradaile (1982). Sinistral microfaults commonly occur at a higher angle to the schistosity.

*Ductile shear zones:* Small scale ductile shear zones were observed within the fault zone at many localities. The shear zones are commonly oblique to the mylonitic fabric. The layering and the mylonitic schistosity bend into the shear zones across which displacement has occurred. Fig. 2-12 is a typical example of the ductile shear zones observed. The shear zones are variable in orientation (Fig. 2-10 and 2-11) and most exhibit a dextral sense of shear.

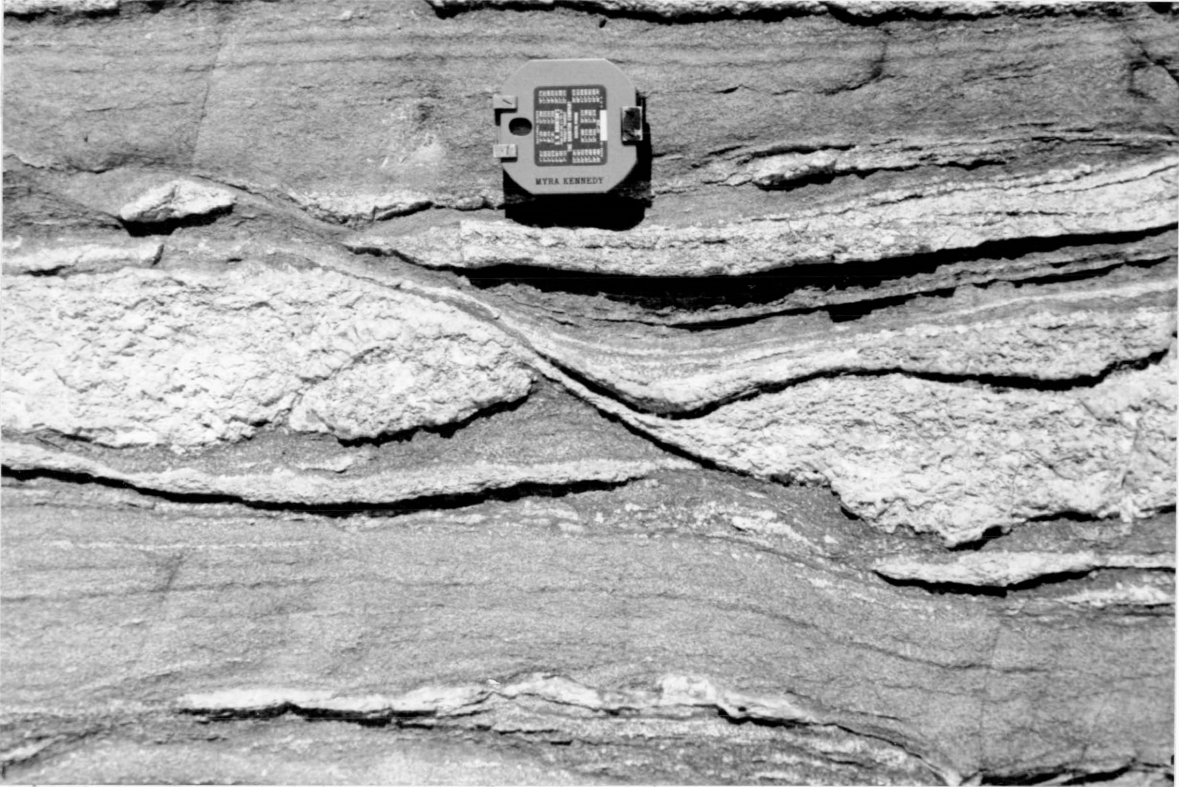


Fig. 2-12: Ductile shear zone in layered mylonitic rocks. Note that the layers and the mylonitic schistosity bend into the shear zone. The shear zone itself bends and disappears parallel to the mylonitic fabric in a manner similar to the microfaults.



*Brittle shear zones:* These structures appear to be zones in which intense fracturing has occurred (Fig. 2-13). They were most commonly observed at Dog Lake. The brittle shear zones are variable in orientation (Fig. 2-11) commonly at small angles to the mylonitic schistosity although some occur at high angles to the mylonitic fabric as in Fig. 2-13. Displacement was observed across some brittle shear zones although displacement could not be determined across others, in particular those close in orientation to the mylonitic fabric.

*Folds:* Folds of the mylonitic banding were not commonly observed within the fault zone. A few folds were seen at Dog Lake and Athelstane Lake. A relatively large number of folds occur at Little Turtle Lake. Fig. 2-14 is typical of the folds observed at Little Turtle Lake. The author was particularly interested in the timing of the folding i.e. whether the folds formed pre, syn or post mylonite formation. Figures 2-15 to 2-20 comprise sketches of a number of folds (in profile) from thin sections. The microstructures associated with each fold are described briefly accompanying the figures.

The sketches illustrate that the folds are variable in form. However, to some extent, in each example the mylonitic foliation cross-cuts the fold hinge and is parallel to the axial plane of the fold. Some of the folds may predate the mylonitic



Fig. 2-13: Brittle shear zone cross-cuts the layered mylonitic rocks.



Fig. 2-14: Fold in the Quetico fault zone, Little Turtle Lake.

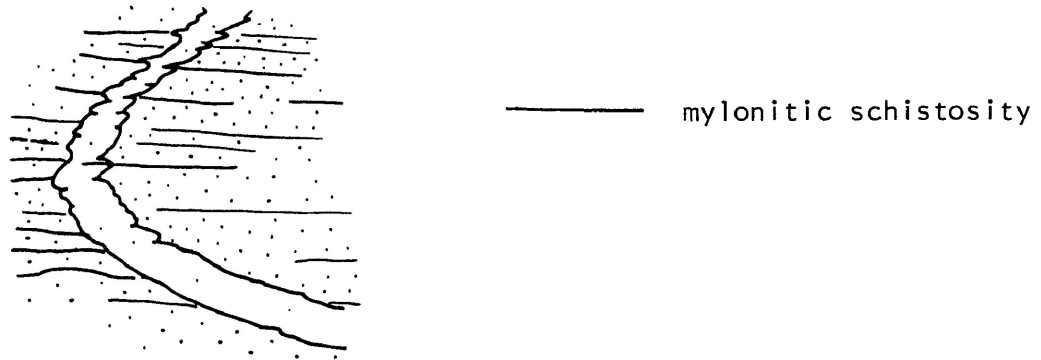


Fig. 2-15

## #1 - Dog Lake

The folded specimen comprises a narrow quartzo-feldspathic layer in biotite schist. In thin section the mylonitic schistosity, defined by quartz ribbons, elongate feldspar grains and deformed biotite grains, is constant in orientation cross-cutting the fold hinge and limbs. Mica-rich surfaces also cross-cut the fold as indicated in the sketch. These surfaces may represent slip surfaces and may, in fact, have been responsible for the formation of the fold.

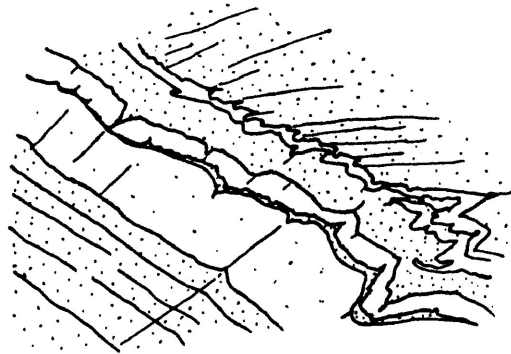


Fig. 2-16

## #2 - Little Turtle Lake

The sample comprises small folds on the limb of a larger fold. The alternating dark, fine grained, schistose layers and light coloured feldspar-rich layers are disrupted by the cross-cutting non-penetrative foliation. Fine dark wisps define the foliation surfaces parallel to the fold axial plane. Displacement is apparent on some of the surfaces. In thin section it can be seen that the mica-rich layers (in particular the thin, central layer) have been drawn out along these surfaces in a ductile manner. Shearing parallel to the foliation and displacement along the foliation may have been responsible for the formation of the folds.

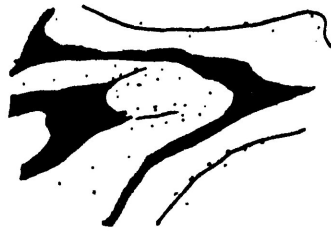


Fig. 2-17

## #3 - Little Turtle Lake

The sample comprises folded amphibole-epidote-magnetite rich layers and quartzo-feldspathic layers. In thin section, at the fold hinge, fine grained chlorite in both layers is oriented parallel to the fold axial plane. The amphibole-rich layers appear to be drawn out at the fold hinge parallel to the axial plane, possibly due to shearing.

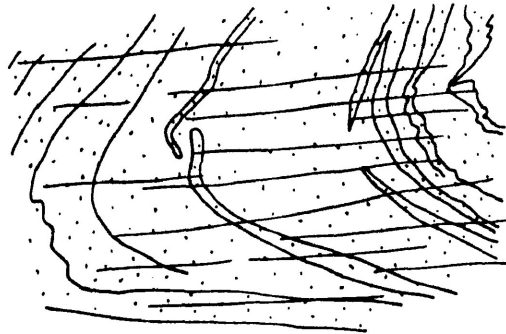


Fig. 2-18

## #4 - Little Turtle Lake

Rather diffuse layers of chlorite-epidote rich rock are folded in this example. A non-penetrative foliation is defined by thin wispy layers parallel to the fold axial plane. In thin section chlorite and muscovite are strongly oriented parallel to the fold axial planes.



Fig. 2-19

## #5 - Little Turtle Lake

The folded layers are alternate amphibole-epidote-magnetite rich layers and quartzo-feldspathic layers. No preferred dimension orientations were observed in the quartzo-feldspathic layers which appeared to be recrystallized. In the amphibole rich layers the amphiboles were oriented parallel to the fold axial surface.



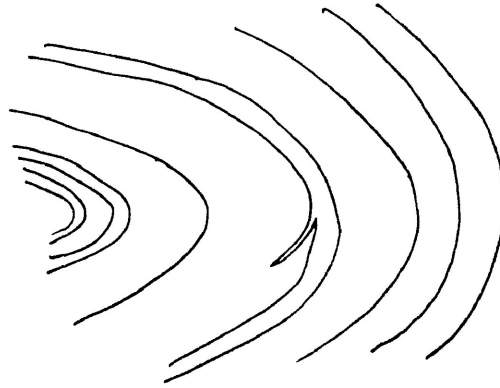


Fig. 2-20

## #6 - Little Turtle Lake

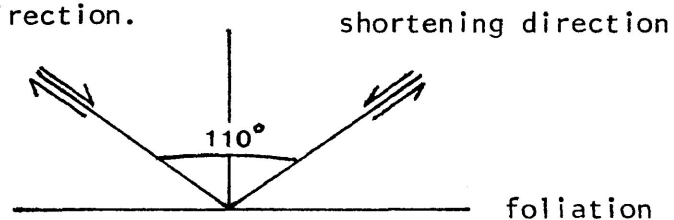
The sample comprises folded layers of recrystallized quartz and quartzo-feldspathic layers. The quartzo-feldspathic layers contain fine micas which tend to be oriented parallel to the axial plane.

schistosity. However, most appear to have been formed at least in part from the shearing process and may have formed synchronously with the mylonite structures.

*Significance of the small scale structures:* The mylonitic schistosity is thought to correspond to the XY plane of the finite strain ellipsoid and mineral lineations to the X-direction (Ramsay and Graham, 1970). In the Quetico fault zone mineral grains which define the schistosity and presumably reflect the shape of the finite strain ellipsoid are most commonly flattened (see Chapter 3). The grains' shortest dimensions lie normal to the mylonitic schistosity which, thus, may have formed by bulk flattening across the fault zone. The sub-horizontal mineral lineation, which may correspond to the X-direction of the finite strain ellipsoid, suggests a component of strike-slip movement associated with the ductile deformation. Slickensides also suggest slip parallel to the mylonitic foliation. The mylonitic layering is similar in orientation to the mylonitic schistosity and may, therefore, be similar in origin forming as a result of flattening across the fault zone. The banding and mylonitic schistosity would thus comprise surfaces of tensile strain. Tensional fractures, normal to the mylonitic fabric, in large feldspar grains are common (Fig. 2-3). Folds within the fault zone may be the result of flattening across the fault zone although they exhibit microstructural

evidence of having been affected by shear parallel to the mylonitic foliation.

The microfaults observed in the fault zone closely resemble structures described by Platt and Vissers (1980). They describe fractures which they suggest are extensional structures which appear when the principal extension direction lies close to a plane of anisotropy. They propose that the strong planar anisotropy of the foliation limits the ductile extension parallel to the foliation resulting in fracture. They call the structure "foliation boudinage" because the foliation is pinched in at extension fractures. Symmetric foliation boudinage comprises small scale extension fractures normal to the foliation. Asymmetric foliation boudinage comprises shear fractures oblique to the foliation on which dextral and sinistral slip occurs such that displacement along the fractures in both senses causes extension along the foliation. The fractures curve at their ends toward the foliation. The microfaults in the Quetico fault zone most clearly resemble asymmetric foliation boudinage. Platt and Vissers note that the dextral and sinistral fractures develop at  $110^\circ$  about the shortening direction.



Their model predicts that with continued shortening this angle

will increase. This resembles the occurrence of the microfaults at Dog Lake documented by Borradaile (1982). The microfaults become closer in orientation to the schistosity as the centre of the fault zone is approached. However, the microfaults at Dog Lake commonly form at high angles to the schistosity in the north part of the fault zone. The author suggests that the microfaults may originate as extension fractures (symmetric foliation boudinage) on which slip occurs as they become progressively rotated towards the schistosity.

In some cases the microfaults appear to be somewhat more ductile in nature than foliation boudinage which comprises brittle fractures (Fig. 2-9). The microfaults also resemble a late penetrative foliation described by White et al (1980). The foliation occurs at a low angle (commonly  $35^\circ$ ) to the mylonitic schistosity. They compare the structures to shear bands in metals. White et al note that two sets of surfaces may develop but usually only one develops which reflects the sense of shear - the acute angle between the bands and the schistosity points in the shear direction. These structures are also thought to be the result of a pre-existing anisotropy. The ductile shear zones observed in the Quetico fault zone have this geometry.

Microfaults of both sinistral and dextral senses occur within the fault zone which is somewhat confusing. The microfaults may serve to reflect the overall sense of displacement on the fault

but this is not a clear-cut determination. The somewhat variable nature which the microfaults display may indicate that deformation within the fault zone was complex. The author suggests that in the case of the Quetico fault zone that microfaults of both senses developed as a result of extension parallel to the mylonitic schistosity. Shear motion accompanying flattening normal to the schistosity (responsible for the extension parallel to the schistosity) resulted in the prominent development of microfaults with the same sense of shear as the overall motion. Thus, the prominent dextral microfaults observed in the fault zone may reflect the overall sense of motion on the fault. The sinistral microfaults comprise conjugate shear fractures. The flattening and shearing responsible for the microfault development may have been synchronous or the flattening may have been earlier than the shearing. This is not to suggest that the microfaults are the result of a distinct deformation phase later than the mylonite formation but possibly represent a late stage in the deformation producing the mylonites. White et al (1980) note that in metals shear bands mark the breakdown of homogeneous deformation. The microfaults may indicate the initiation of a more brittle phase of deformation in the fault zone. They may have formed when ductile mylonite formation became unstable. Their formation would allow the rocks of the fault zone to continue to accommodate large strains.

The microfaults are clearly associated with the early ductile deformation as they curve into the foliation where slip on the microfaults is presumably taken up along grain boundaries without dilation. This would not be possible if ductile deformation were not continuing allowing the grain boundary sliding to be accommodated (dependent or controlled particulate flow (Borradaile, 1981)). The microfaults also appear to have rotated towards the mylonitic schistosity as ductile deformation continued. The brittle shear zones provide evidence of late stage brittle deformation as they clearly post-date the mylonite formation.

#### C) Fault Rocks of the Quetico Fault Zone

The fault rocks observed in the Quetico fault zone are variable in type, texture and composition. They exhibit a variety of microstructures which will be described later in this chapter. Fault rocks of the mylonite series and the cataclasite series and pseudotachylite are found within the fault zone. The author observed no fault rocks in which grain-growth was pronounced (ie.) no blastomylonites. The mylonites are foliated fault rocks exhibiting ductile deformation textures. They comprise the majority of the fault rocks in the fault zone. The cataclasites are locally developed. These random-fabric fault rocks exhibit brittle deformation textures. Pseudotachylite, a fault rock with a glassy matrix, was observed at almost every locality examined.

This study focuses on quartzo-feldspathic fault rocks. The fault rocks comprising former granitic rocks, gneisses and migmatites of quartzo-feldspathic composition exhibit distinctive textures associated with deformation in the fault zone. In former metavolcanic and metasedimentary rocks rich in phyllosilicates, textures are more subtle.

*Mylonite series rocks:* Many of the rocks in the fault zone are protomylonites and mylonites. A few are ultramylonites. The foliated fault rocks are characterized by mineral preferred dimension and preferred crystallographic orientations. It appears that the presence of quartz is essential for the development of the mylonitic fabric as it is the ductile deformation of this mineral which is responsible for the mylonitic foliation in most of the fault rocks. In general the mylonites which contain larger amounts of quartz appear to have exhibited greater ductility than those containing relatively less quartz. The textures within the mylonites commonly reflect the ductility contrast between quartz and feldspar. Porphyroclastic texture comprises "porphyroclasts" of more resistant feldspar which are ovoid in shape in a matrix of highly strained quartz (Fig. 2-21).

The rocks of the series protomylonite-mylonite-ultramylonite exhibit progressive deformation of mineral grains and progressive reduction in grain size. The quartz grains in pro-

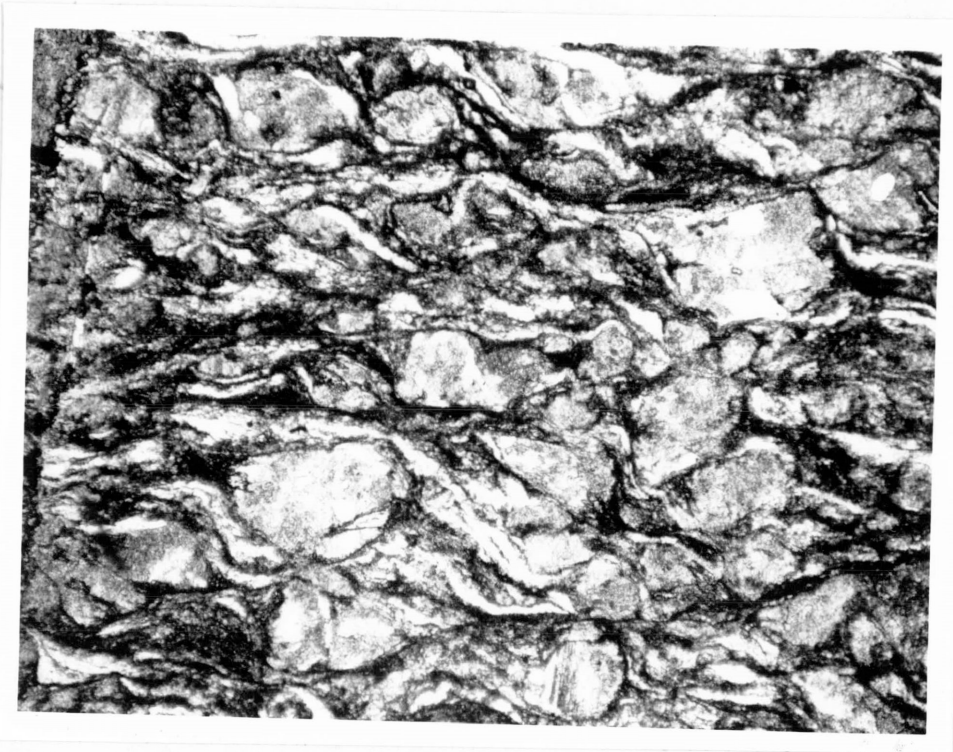


Fig. 2-21: Mylonite

A mylonite exhibiting porphyroclastic texture. The ovoid feldspar grains occur in a matrix of elongate quartz grains and fine grained micaceous material. The feldspar grains are clearly less ductile than their matrix.

Field of view 5 mm PPL



tomylonites are somewhat elongate, exhibiting a small amount of strain. The quartz grains become progressively strained and within the ultramylonites comprise "ribbon grains" having a very high aspect ratio (length/width) (Fig. 2-22). In protomylonites the feldspar grains are fractured. They become progressively finer grained as the rocks become ultramylonites. In ultramylonites a few remnant, rounded feldspars "float" in a very fine grained matrix (Fig. 2-22).

Some of the mylonites observed were phyllonites. The phyllonites are strongly foliated. The foliation is defined by the preferred crystallographic orientation of the phyllosilicate minerals. The phyllonites are commonly rich in chlorite and sericite and may contain quartz and feldspar porphyroclasts as in Fig. 2-23.

*Cataclasite series rocks:* Random-fabric fault rocks were observed at many localities. Most were protocataclasites and cataclasites. Within the Quetico fault zone there are apparently two types of cataclasites. The first appears to be lithologically controlled, occurring in quartz-poor, feldspar-rich rocks. The rocks comprise angular fragments of feldspar grains. The feldspars are fractured and broken and appear to become progressively more diminutive. The second type of cataclasite occurs in localized zones and comprises fragments of fault rocks - in some cases mylonites, in

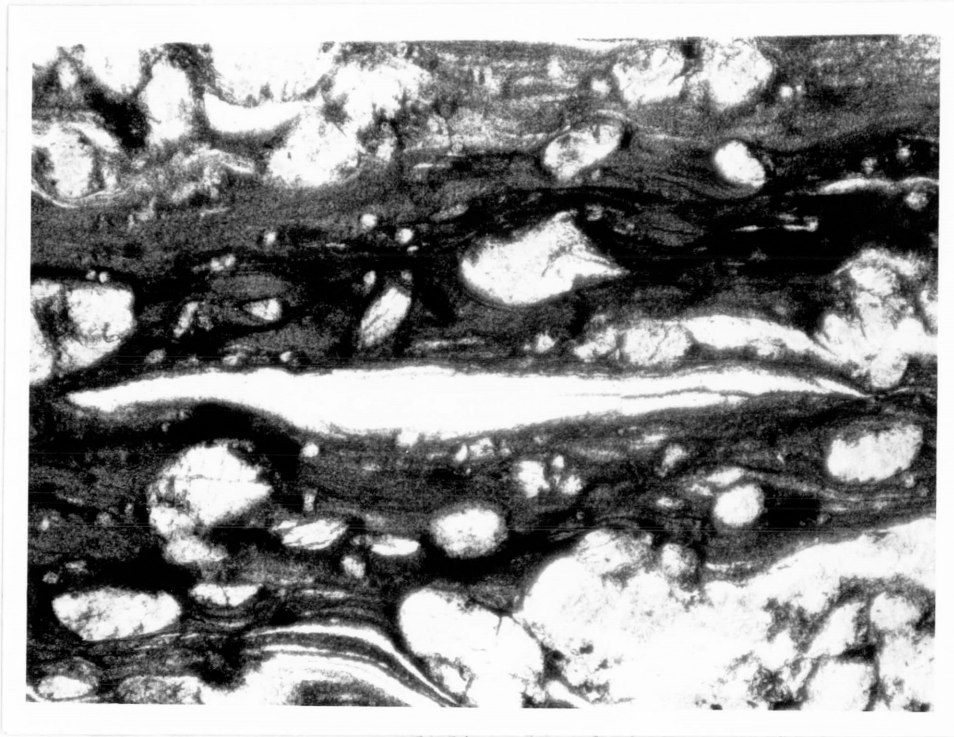


Fig. 2-22: Ultramylonite

Note that the fine grained matrix of this ultramylonite contains rounded remnant grains of feldspar and very elongate quartz "ribbon" grains.

Field of view 2 mm PPL

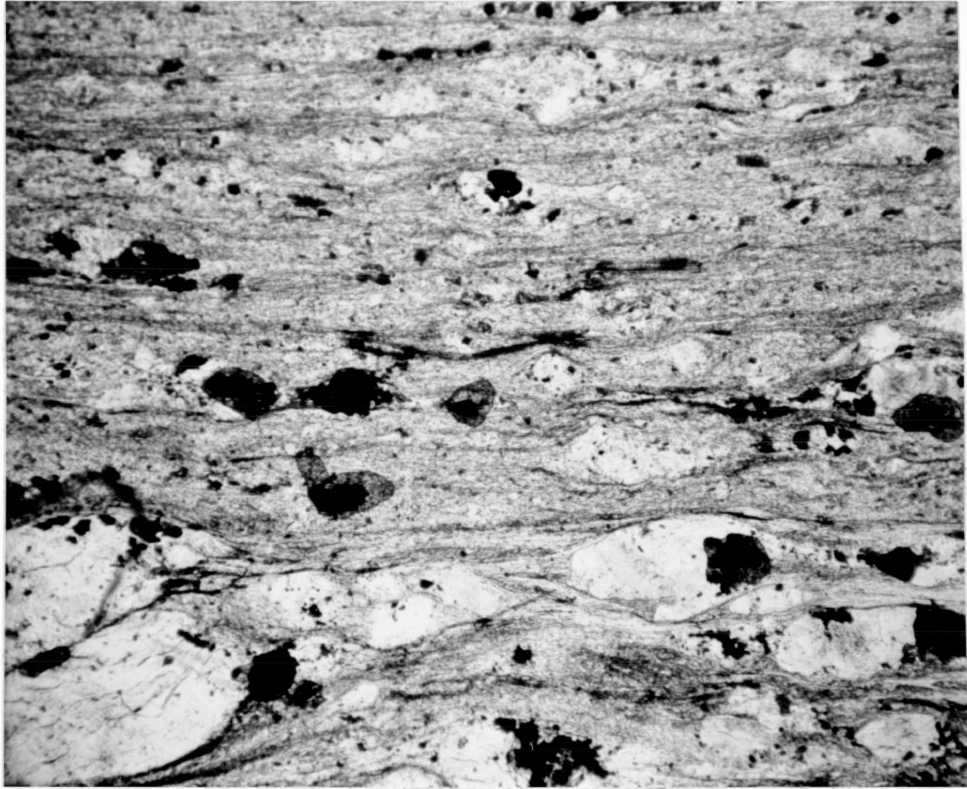


Fig. 2-23: Phyllonite

The fine grained, foliated matrix of this rock is rich in phyllosilicate minerals. The sample contains ovoid porphyroclasts of quartz and feldspar.

Field of view 5 mm PPL

others fragments of cataclasites of the first type (Fig. 2-24). These fragments also become smaller as the rocks become more deformed.

*Pseudotachylite:* Much of the pseudotachylite observed within the Quetico fault zone is black and glass-like. It is often devitrified however, altering to fine grained sericite and chlorite. Pseudotachylite commonly contains fragments of host rock. It sometimes occurs associated with the second type of cataclasite (above) as a thin film along the fracture surfaces. More commonly, pseudotachylite occurs along surfaces parallel to the pre-existing mylonitic schistosity and along fractures at high angles to the surfaces. The pseudotachylite in these fractures is commonly banded and occasionally shows internal flow folds (Borradaile and Kennedy, 1982), as in Fig. 2-25.

*Discussion:* The occurrence of the various types of fault rocks in the Quetico fault zone suggests that significant ductile deformation within the fault zone was followed by brittle deformation.

The mylonitic rocks appear to have been the earliest formed fault rocks. The cataclasites formed in feldspar-rich rocks may have developed at the same time as the mylonitic rocks. These are both "overprinted" by cataclastic textures and pseudotachylite.

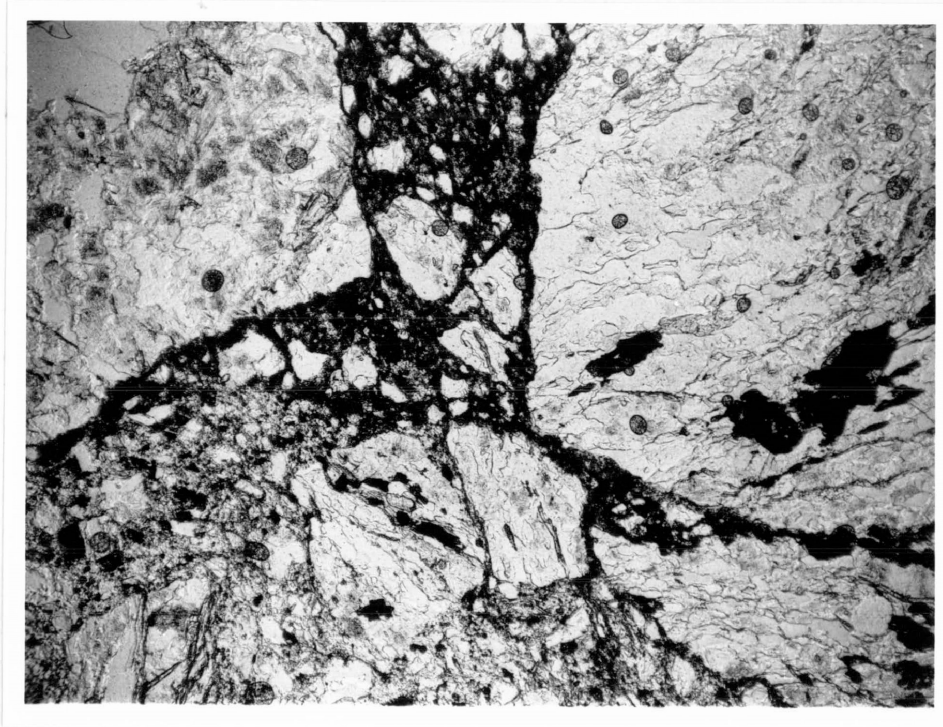


Fig. 2-24: Cataclasite

This cataclasite is composed of angular fragments of mylonite.

Field of view 5 mm PPL



Fig. 2-25: Pseudotachylite

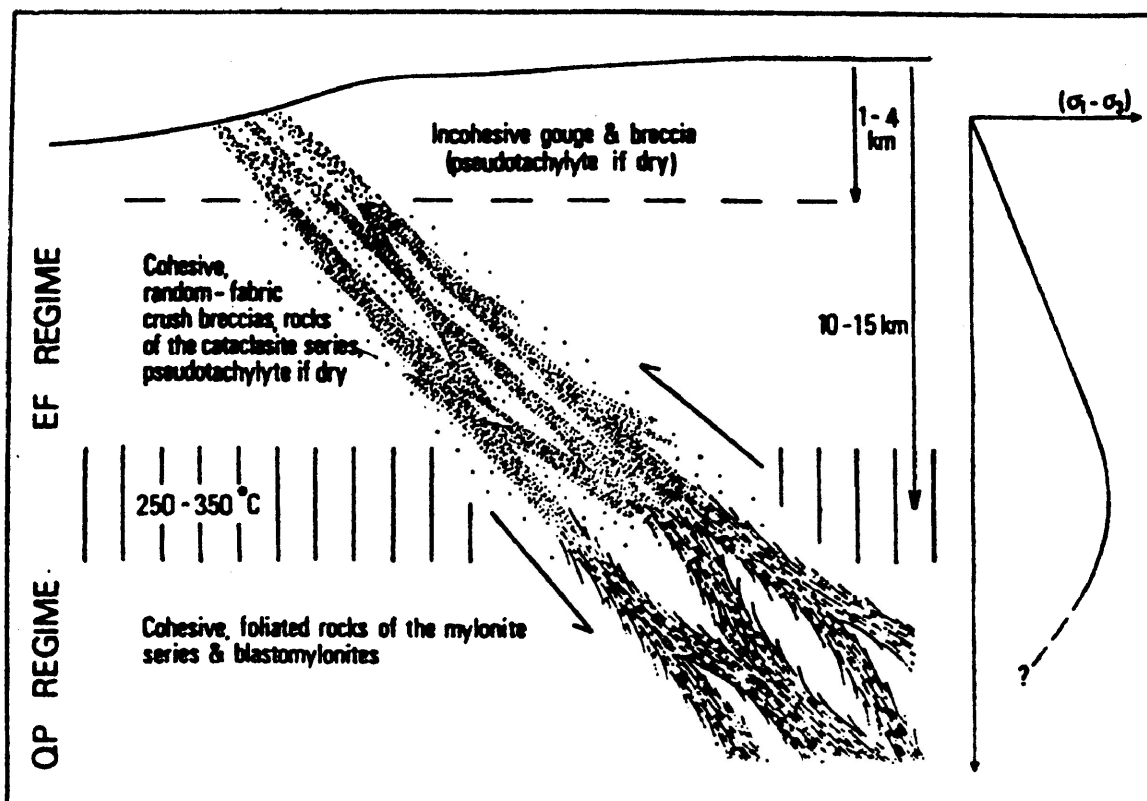
Flow fold of banded pseudotachylite occurring in fractures cross-cutting the mylonitic schistosity. Note the fragments of host rock which occur within the pseudotachylite.

Field of view 1 cm PPL

Cataclasites were observed composed of the earlier formed mylonites and cataclasites. Pseudotachylite is thought to be glass formed by frictional melting as a result of transient, rapid slip on discrete planes (Sibson, 1975, 1977, 1980). In the Quetico fault zone it occurs associated with the cataclasite series rocks but commonly appears to have been generated by slip on surfaces parallel to the pre-existing mylonitic foliation. The pseudotachylite appears to have been injected into fractures cross-cutting the mylonitic foliation. The flow folding observed in the pseudotachylite may be the result of the injection of the frictional melt into the fractures in pulses.

Fig. 2-26 is a conceptual model of a major fault zone in quartzo-feldspathic crust developed by Sibson, 1977. It is a two-layer model comprising the elasto-frictional (EF) regime at high crustal levels and the quasi-plastic (QP) regime at lower crustal levels. Random fabric fault rocks occur above greenschist facies metamorphic conditions. Deformation in the EF regime is dominated by elastic behaviour (rocks are unable to accommodate large continuous strains) and deformation is friction-dominated. Within the QP regime the mylonite series rocks develop when a major rock constituent deforms in a plastic manner to remain a continuum.

The early formed rocks in the Quetico fault zone appear to have formed in the QP regime. Quartz in the mylonites has deformed in a ductile manner resulting in the foliated fault



from Sibson, 1977.

Fig. 2-26: Sibson's Conceptual Model of a Major Fault Zone.



rock textures common to this regime. The feldspar-rich rocks exhibiting cataclastic textures were probably also formed in this regime as they appear to be early formed. The author suggests that the textures observed are the result of the lack of minerals in the rock which could deform in a plastic manner under the conditions of deformation.

Later deformation in the fault zone took place under conditions resembling those in the EF regime resulting in the formation of rocks of the cataclasite series. The presence of pseudotachylite indicates that seismic slip must have occurred periodically in the fault zone and that the deformation, at least at this stage, took place under dry conditions.

#### D) Deformation Mechanisms - Theory

Three groups of crystal deformation mechanisms described by Paterson (1976) encompass a number of well known deformation mechanisms. The three groups are:

- 1 - fracture or cataclastic processes
- 2 - crystal-plastic processes
- 3 - diffusional processes

Within fault zone rocks fracture and crystal-plastic processes accompanied by dynamic recovery and dynamic recrystallization are the most important deformation mechanisms. However, intragranular and intergranular deformation processes may contribute to the

total strain of a rock. Intragranular deformation processes are responsible for the deformation which takes place within the grains of a rock resulting in grain shape changes. Deformation which takes place between grains (intergranular deformation) by slip on grain boundaries or multigranular surfaces and by rotation of grains has been termed particulate flow (Borradaile, 1981). The contribution of particulate flow to the deformation of rocks in fault zones can be of great importance accompanying any of the intragranular deformation mechanisms described by Paterson.

*Particulate flow:* During deformation of the grains of an aggregate by fracture, crystal-plastic processes, or diffusional processes, some sliding of grains may be required to minimise the dilation of the aggregate. When particulate flow is limited by the incompatible deformation of the grains it has been termed dependent particulate flow by Borradaile. More commonly, Borradaile suggests grain sliding would be more than that dependent on grain deformation. Controlled particulate flow occurs when grains slide past one another at a rate controlled by grain deformation but may be encouraged by other factors such as modest pore fluid pressure.

*Fracture or cataclastic processes:* Cracks and pores are found within and between the grains of most rocks. The cracks and pores will generally close when the rock is first stressed. Some cracks,

however, are oriented such that stress is concentrated at their tips and they start to grow (Tullis, 1978). Fracture results from the extensive or catastrophic growth of these cracks forming an intersecting en echelon network leading to the formation of a macroscopic penetrative fracture (Tullis, 1978, Nicolas and Poirier, 1976). Fracture results in dilatancy (an increase in volume).

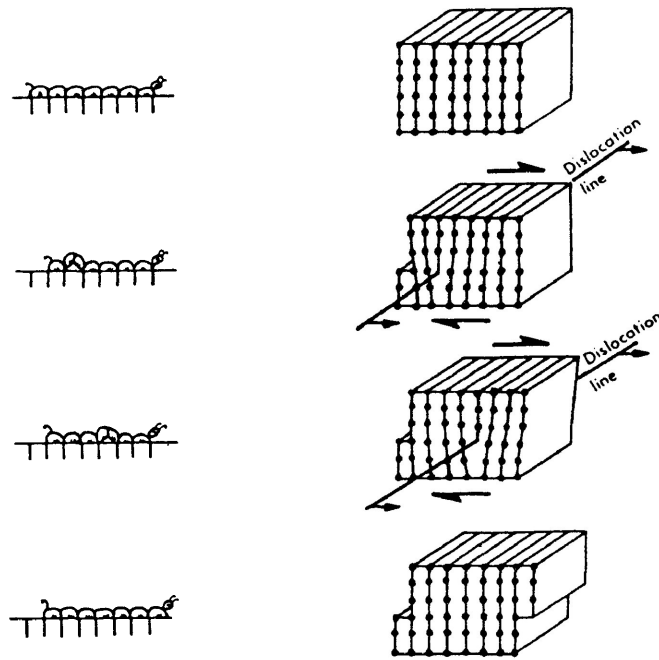
As deformation proceeds, fracturing may continue resulting in the formation of smaller and smaller fragments or rock fragments may slide past and roll over each other on old and new grain surfaces. The latter may also involve grain rotation (Ashby and Verrall, 1977) and has been termed cataclastic flow (Borg et al, 1960). Cataclastic flow thus involves extensive fracture and particulate flow.

*Physical conditions for fracture:* Fracture is important at low temperatures, low confining pressures and at high strain rates. Fracture is not temperature dependent, but other deformation mechanisms which are ineffective at lower temperatures, such as crystal-plastic processes, become more efficient at higher temperatures and tend to replace fracture as the predominant deformation mechanisms. Hydrostatic pressure opposes dilatancy. Thus high pressure conditions inhibit fracture. Sliding and rolling of grains, however, are more pressure-sensitive than

fracture. Therefore, deformation may occur by progressive fracturing rather than cataclastic flow at higher pressure when sliding and rolling of grains are suppressed (Ashby and Verrall, 1977).

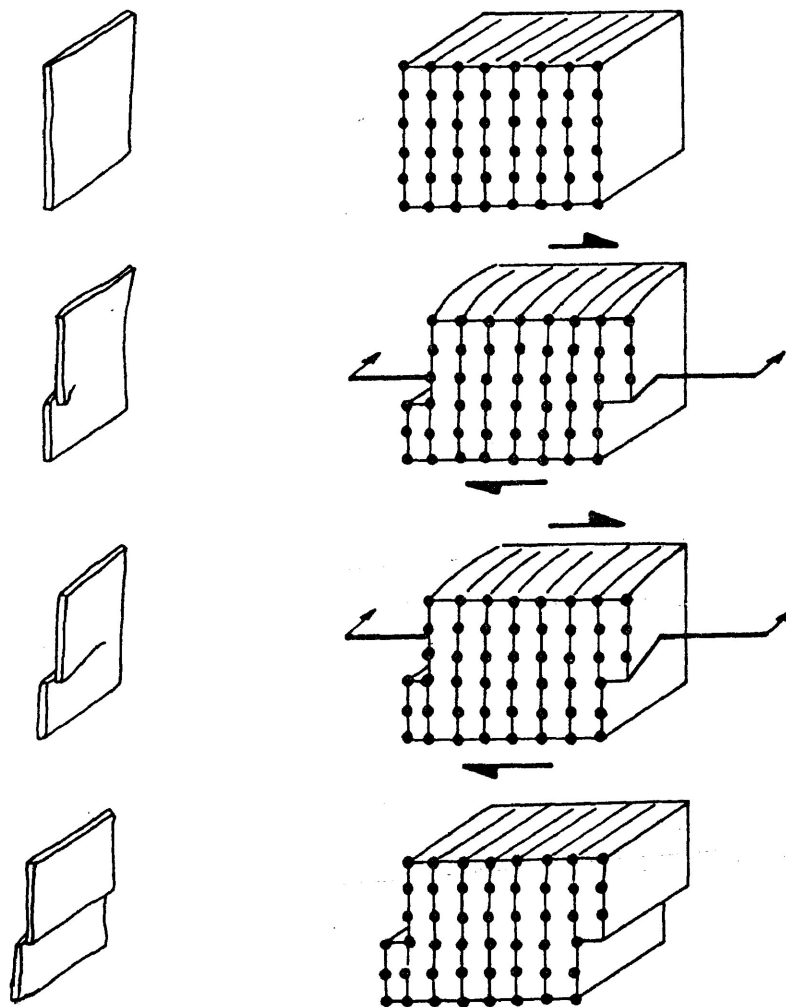
*Crystal-plastic processes:* Crystal-plastic deformation mechanisms involve the plastic deformation of crystals in a rock by dislocation glide. Dislocations are line defects in a crystal lattice which are grown in when the crystal forms. New dislocations form in the crystal when it is stressed. When an external stress is applied dislocations move through the crystal producing small displacements of the lattice. The glide of dislocations, or slip, usually occurs on planes with the highest atomic-densities.

Edge dislocations occur perpendicular to the slip direction. An edge dislocation may be envisaged as an extra half plane of atoms in a cubic lattice as shown in Fig. 2-27. The edge of the extra half-plane represents the dislocation. Tullis (1978) notes that in silicates the extra half-plane is larger and much more complex than in the simple cubic lattice. Screw dislocations occur parallel to the slip direction. A screw dislocation may be compared in form to the tearing of a sheet of paper (Fig. 2-28). The tip of the tear represents the dislocation. Many dislocations are of mixed character, comprising components of both edge and screw dislocations (Nicolas and Poirier, 1976, p. 77).



From Nicolas and Poirier  
(1976) p. 75.

Fig. 2-27: Nicolas and Poirier compare slip by movement of an edge dislocation through the crystal lattice to the progression of a caterpillar. The extra-half plane corresponds to the ruck in the caterpillar. Note that the dislocation (the edge of the extra half-plane) is perpendicular to the slip direction.



from Nicolas and Poirier (1976)  
p. 76

Fig. 2-28: The movement of a screw dislocation through the lattice is compared to the tearing of a sheet of paper. The tip of the tear represents the dislocation. Note that a screw dislocation occurs parallel to the slip direction.

Slip occurs by the movement of dislocations along the slip plane or by the outward spreading of the boundary of the slipped area the plane (Nicolas and Poirier, 1976, p. 74). A dislocation may thus be described as the boundary between the slipped and the unslipped crystal. The glide of dislocations through the lattice involves the breaking of atomic bonds and the formation of new bonds along the length of the dislocation. The process is progressive as only a few bonds are broken at a time rather than all the bonds along the length of the dislocation being broken simultaneously.

Dislocation slip is inhibited by resistance within the crystal lattice associated with the breaking of bonds and by other dislocations, grain boundaries and obstacles such as point defects, impurities and precipitates. Dislocation density increases with increasing strain due to the continuous formation of dislocations and the pinning of dislocations at obstacles, dislocation-tangles and grain boundaries. Thus as strain increases the obstructions to dislocation glide increase. Greater stresses are required by dislocations to overcome these obstructions than to glide unhindered. Therefore, more and more stress is required to produce successive increments of strain as total strain increases. This process is called strain hardening or work hardening. At higher temperatures, where diffusion rates are higher, recovery processes become active. Recovery is the process by which dis-

locations are annihilated or rearranged into low energy configurations allowing plastic deformation to continue. Thus recovery opposes work hardening. When recovery balances work hardening, steady state deformation known as dislocation creep takes place.

Recovery processes involve the diffusion of vacancies and thus are thermally activated. The main recovery process is climb. Dislocations may shorten or lengthen their half-planes when atoms exchange with vacancies by diffusion. During climb, a line of atoms along the edge of the extra half-plane is removed or added. This occurs progressively and the half-plane becomes jogged as atoms are removed or added. Climb allows dislocations to surmount obstacles permitting glide to continue in a parallel plane. Dislocations which are creating slip in opposing senses, in parallel glide planes, may climb toward each other and annihilate. Climb may also permit dislocations to arrange themselves in low energy stable walls. This process, called climb polygonization, results in the formation of slightly misoriented subgrains which contain fewer dislocations than the rest of the grain. At higher temperatures cross slip of screw dislocations from one slip plane to another may occur. In this manner screw dislocations may annihilate or climb over obstacles.

Dynamic recrystallization may also take place at higher temperatures. Gillope and Poirier (1979) define dynamic recrystallization as a solid state process leading to the creation of a new



grain structure in the course of plastic deformation of crystalline solids. They found, at the lower temperatures and stresses where recrystallization occurred, that "new grains" formed by the progressive rotation of sub grains and that at higher temperatures and stresses that the new grains were the result of migration of the high angle grain boundaries of the rotated subgrains. Dynamic recrystallization is actually another recovery process since the production of strain free grains opposes work hardening and permits dislocation glide to continue. Dynamically recrystallized grains themselves become strained as a result of the ongoing dislocation processes.

Although not themselves responsible for the strain, dynamic recovery and recrystallization make an important contribution to deformation by crystal-plastic processes by allowing the movement of dislocations to continue. Other deformation mechanisms such as diffusional processes may however become favourable as a result of grain refinement by dynamic recovery and recrystallization.

Some particulate flow may be required to maintain the fit between grains of an aggregate deforming by crystal-plastic processes. The grains of an aggregate are constrained during deformation by their neighbours and by the geometry of the deforming body. Compatible deformation by dislocation glide alone or by glide and climb is restricted if insufficient slip systems are available in a crystal to permit homogeneous

deformation of the whole rock. This is common in silicate rocks (see Chapter 4 - part D for further discussion). Dependent or controlled particulate flow as described by Borradaile (1981) may accompany crystal-plasticity.

*Physical conditions for crystal-plasticity:* Dislocation glide occurs at relatively low temperatures ( $<0.5 T_m$  where  $T_m$  is the mineral's absolute melting temperature (Tullis, 1978) and high strain rates. At the lower temperatures, however, the mobility of the dislocations is limited and they quickly become obstructed or tangled and result in limited amounts of strain. At low temperatures fracture may follow dislocation glide. At higher temperatures (0.75  $T_m$  (Tullis, 1978)) recovery processes become effective enhancing the mobility of dislocations. At higher temperatures dynamic recrystallization is also an important process. Thus crystal-plasticity is temperature-sensitive. Increasing temperature makes bonds easier to break and thus facilitates dislocation glide. Increasing temperature allows the diffusion of vacancies necessary for climb to occur. Dislocation glide may be inhibited by increased confining pressure. Climb is affected by confining pressure as increased pressure slows diffusion (Ashby and Verall, 1977). Increased pressure may inhibit particulate flow accompanying crystal-plasticity.

*Diffusional processes:* Grain shape change may be accomplished by the diffusion of atoms from sites of high stress to sites of low stress within a material by various paths. Diffusion of atoms may take place through grains (Nabarro-Herring creep), along grain boundaries (Coble creep) and along grain boundaries in the presence of a fluid phase (pressure solution or solution-re-deposition). Diffusional processes are generally considered small strain deformation mechanisms. Nabarro-Herring creep and Coble creep are important under low strain rate conditions and at high temperatures where diffusion rates are high. Raj and Ashby (1971) have shown that grain boundary sliding is required accompanying diffusional creep (dependent particulate flow (Borradaile, 1981)). However, Tullis et al (1982) note that diffusional creep which is well documented in metals has not been observed in silicates and thus cannot be considered an important deformation mechanism in fault zones. Pressure solution, which operates at lower temperatures, may occur in fault rocks at shallow crustal levels when water is present between grains of the rock (Tullis, et al, 1982). Structural superplasticity is a related process. It involves significant amounts of intercrystalline slip (controlled particulate flow (Borradaile, 1981)). Grains slide past each other and their shape is altered by diffusion when necessary (Ashby and Verall, 1973). Diffusive processes remove asperities which would inhibit sliding. Superplasticity results in large strains in fine

grained rocks deformed at temperatures greater than  $0.5 T_m$  and at fast strain rates. The shape and size of the grains is not significantly changed. Boullier and Gueguen (1974) and White (1977) have suggested that some mylonitic rocks may have undergone super-plastic flow.

#### E) Deformation Mechanisms and Microstructures

The mechanisms responsible for deformation of a rock may be recognized microstructurally as some microstructures are characteristic of particular deformation processes. The identification of the deformation mechanisms operative in the rocks of the fault zone may be useful in determining, broadly, the physical conditions at the time of deformation.

##### *Microstructures associated with fracture and cataclastic flow:*

Rocks deformed by fracture processes are characterized by the presence of through-going fractures or faults. Grains may be fractured or broken and are angular. Fracture thus produces textures which we term "brittle", and poor preferred orientation fabrics on the microscopic and macroscopic scales. Cataclastic flow, on the other hand, may result in an apparent foliation and thus a macroscopically ductile appearance as individual surfaces of fracture/faulting are not apparent. Microscopically, however, the fragments are angular and their origin is discernable. Very

fine grained material (as fine as 1  $\mu\text{m}$ ) produced by progressive fracturing is called fault gouge. If fault gouge contains phyllosilicates it may have a foliation. Again, microscopic angular fragments may be identified. (Tullis et al, 1982).

*Microstructures associated with crystal-plasticity:* Crystal-plasticity produces ductile textures and crystallographic preferred orientations. A number of optical features have been related to dislocation processes including undulatory extinction, deformation lamellae, deformation bands and mechanical twinning. White (1973) notes that the optical effects are not due to the presence of the dislocations but due to lattice misorientation across dislocation walls.

Undulatory extinction may develop at low strains due to lattice bending. The lattice bending is accommodated by almost parallel walls of dislocations. The lattice misorientation across these dislocation walls results in the wavy extinction observed under the optical microscope (White, 1973). With increasing strain undulatory extinction may become more distinct and a banded appearance develops due to greater misorientation across the dislocation walls.

Deformation lamellae are thin (0.5-5  $\mu\text{m}$ ) roughly planar features with slightly different refractive index than their host grain (Hobbs et al, 1976). Deformation lamellae are the result

of long, almost parallel dislocation walls across which misorientation is slight but detectable (White, 1973). Some deformation lamellae comprise dislocation arrays in slip planes and others may be due to twinning (in quartz at least) (Nicolas and Poirier, 1976, pg. 202).

Deformation bands are sharply bounded planar regions of a grain which have undergone deformation different to that experienced by adjacent parts of the grain (Hobbs et al, 1976, pg. 98). Kink bands are one type of deformation band in which the lattice is sharply bent. Other deformation bands may differ from adjacent parts of the grain by the amount of slip which has occurred on a particular slip plane or different slip systems may operate to different degrees in adjacent bands. Deformation bands may contain undulatory extinction. Adjacent deformation bands have different optical features and sharp boundaries.

Mechanical twinning is thought to provide some ductility for minerals with few slip systems (Nicolas and Poirier (1976) p. 45). Mechanical or deformation twins are commonly lenticular in shape. Mechanical twinning occurs by the displacement of successively higher layers of atoms of a crystal resulting in a structure in which it appears that one part of the crystal has undergone a homogeneous shear with respect to another part across the twin boundary (Kelly and Groves, 1970, p. 291, Hobbs et al, 1976 p. 107). The process involves the movement of partial dis-

locations.

*Microstructures associated with dynamic recovery and recrystallization:* Subgrains and dynamically recrystallized grains in deformed rocks indicate that recovery processes have been active. A subgrain is a slightly misoriented part of a grain resulting from polygonization. Subgrains exhibit slightly different optical extinction from the rest of the grain due to the misorientation across the subgrain walls. They commonly develop around the edges of grains. Subgrains may form by dynamic processes or by annealing or static recovery. Subgrains resulting from dynamic processes are formed by climb polygonization and slip polygonization (subgrain formation by interference of dislocations gliding on neighbouring slip planes) whereas subgrains resulting from static processes form by climb polygonization alone (White, 1977). The subgrains formed in these two ways are difficult to discern but they may be distinguished by some characteristics as described by White. Subgrains formed by climb alone are distinctly polygonal reflecting evenly spaced dislocation walls. Subgrains formed by slip polygonization develop unevenly as the dislocation walls are uneven "hedges" of dislocations. Thus, dynamically formed subgrains may develop unevenly when slip polygonization has occurred. The dynamic subgrains will also show evidence of deformation which continued after their formation in the form of internal deformation

features such as undulatory extinction (White, 1977).

Dynamic recrystallization results in the development of new small grains. These may be distinguished from crushed grains by their regular size, shape and distinct grain boundaries. Gillope and Poirier (1979) describe the characteristics of new grains formed by rotation recrystallization and migration recrystallization. The former preserve the spatial arrangement of subgrains. They are generally small, equant and homogeneous in size with straight grain boundaries. These grains will have a strong preferred crystallographic orientation. The latter may vary in size. Some grains may be large having bulging, scalloped or corrugated grain boundaries. These new grains may exhibit no obvious preferred crystallographic orientation. Dynamically recrystallized grains may be deformed, elongate and contain optical strain features distinguishing them from grains formed by annealing recrystallization. Dynamically formed subgrains and recrystallized grains often form around the edges of grains resulting in a texture known as core-and-mantle texture. The subgrains and new grains form a mantle about the original grain.

*Microstructures associated with diffusion processes:* Since pressure solution and superplasticity are the diffusion related processes considered likely to occur in fault rocks only the microstructures associated with these two deformation mechanisms will be considered



here. Evidence for the operation of pressure solution may comprise the penetration of one grain into another with an insoluble residue along the boundary between the grains where material has been removed. Material may be deposited in extension fractures (forming veins) or in the "pressure shadows" of rigid, insoluble grains. Planar markers which are oriented obliquely to zones of pressure solution may appear to be displaced across these zones due to volume loss.

Evidence for superplasticity may consist of an aggregate of very fine, equant grains which show little evidence of dislocation related microstructures and which lack crystallographic preferred orientations (Boullier and Gueguen (1974)) in a rock which is known to have undergone large strains (Tullis et al, 1982).

#### F) Microstructures and Deformation Mechanisms in the Quetico Fault Zone

##### *Deformation mechanisms determined from microstructural evidence:*

The rocks of the Quetico fault zone contain abundant evidence of crystal-plastic deformation processes. Quartz grains commonly exhibit undulatory extinction (Fig. 2-29). The ribbon-like quartz grain in Fig. 2-30 exhibits deformation bands which are also commonly observed in the fault rocks. Feldspar grains may be kinked (Fig. 2-31). They also commonly contain lenticular

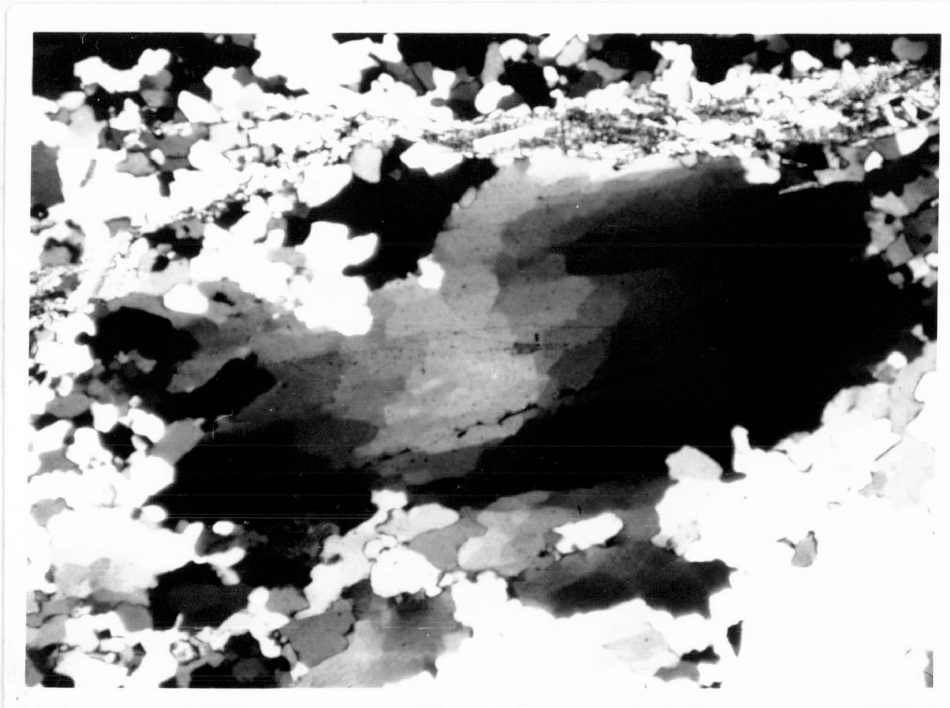


Fig. 2-29: Quartz grain exhibits undulatory extinction and the formation of subgrains. Polygonal subgrains occur in the core of the crystal. Subgrains become progressively rotated until they become distinct grains. The rim of grains around the large grain have recrystallized in this manner. The texture is known as core and mantle texture.

F.O.V. - 5 mm XN



Fig. 2-30: Quartz grain comprising deformation bands. The sharply bounded regions of the crystal exhibit different optical features.

F.O.V. - 5 mm XN

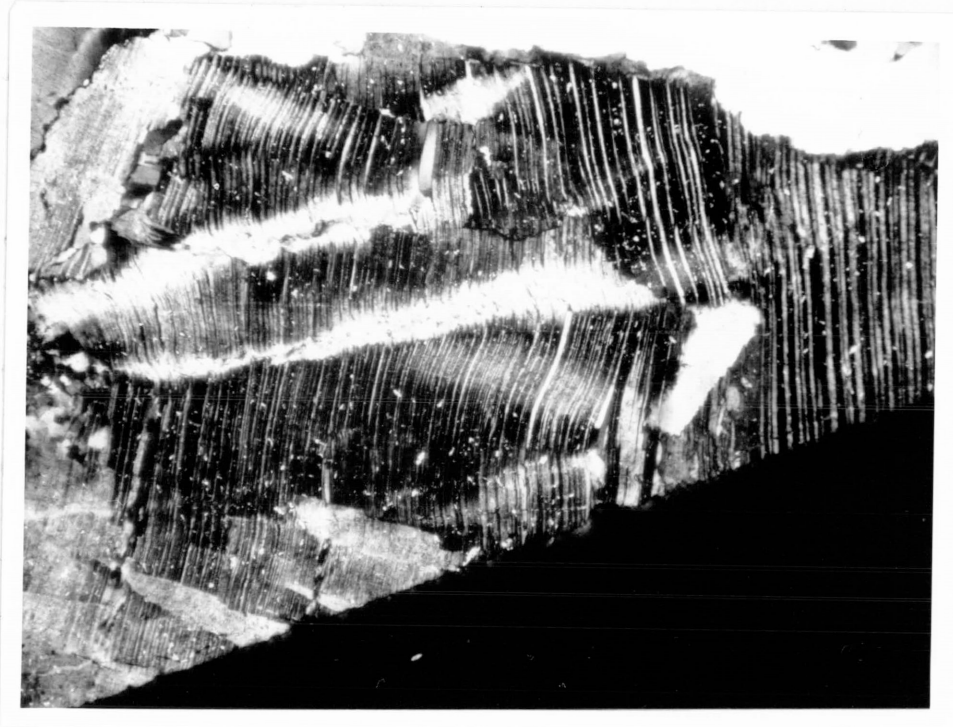


Fig. 2-31: Kinked feldspar grain.

Kinks are one type of deformation band.

F.O.V. - 5 mm XN

mechanical twins (Fig. 2-32). In a few samples undulatory extinction was observed in feldspar grains.

Much evidence of dynamic recovery and dynamic recrystallization processes accompanying the crystal-plastic processes is also found in the fault zone rocks. Fig. 2-29 exhibits a texture known as core and mantle texture in which a mantle of small grains surrounds a large deformed grain. The core grain exhibits undulatory extinction indicating deformation by crystal-plastic processes. However, within the grain polygonal subgrains are developing. Progressive rotation of the subgrains results in the formation of "new grains" (rotation recrystallization) which surround the parent grain. The new grains are somewhat elongate and exhibit undulatory extinction as a result of the continuous deformation by crystal-plastic processes. This is typical of the syntectonically recrystallized grains. Fig. 2-33 contains elongate quartz grains which are composed of recrystallized grains which also contain evidence of internal deformation and which possibly formed by migration recrystallization. Other quartz grains comprise aggregates of very fine grained recrystallized grains. Evidence of dynamic recovery and recrystallization was uncommon in feldspar grains but in a few samples subgrains and recrystallized grains were observed.

Evidence of fracture processes and cataclastic processes was less commonly observed. Most commonly feldspar grains are

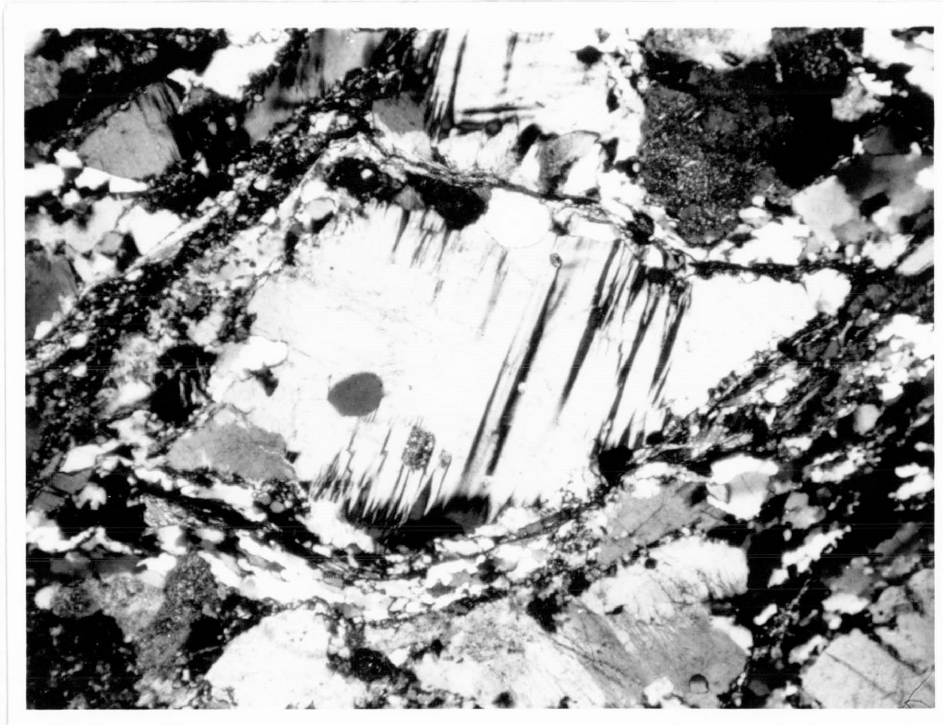


Fig. 2-32: Lenticular mechanical twins in feldspar grain.

F.O.V. - 3 mm XN

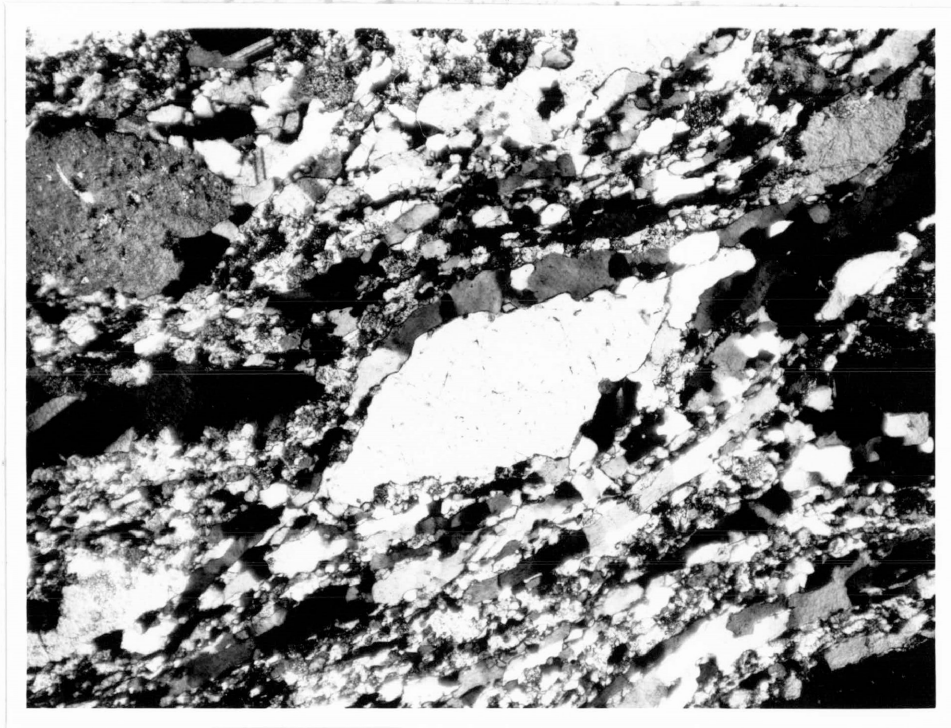


Fig. 2-33: Elongate recrystallized quartz grains around deformed feldspar grain.

F.O.V. - 5 mm XN

deformed by fracture. In feldspar-rich rocks the feldspars undergo progressive fracturation into smaller and smaller fragments. Feldspar grains in a rock in which the matrix is deforming by ductile processes are commonly fractured normal to the foliation (Fig. 2-3). The angular fragments of feldspar are separated as deformation of the ductile matrix continues and the original grains may not be identifiable. Rocks comprising angular fragments, sometimes in a fine grained matrix, which appears to consist of angular fragments as in Fig. 2-24, are clearly formed by cataclastic processes. Cataclastic flow may be the deformation mechanism responsible for textures such as in Fig. 2-34. The fine grained band through the middle of the photo comprises angular fragments of the host rock in a very fine grained matrix and may represent crush-microbreccia.

The author observed no evidence of diffusive processes. The absence of pressure shadows suggests that pressure solution was not an important deformation mechanism. It is possible that superplastic flow could have occurred in some of the fine grained samples but this could not be determined.

*Discussion:* Crystal-plastic deformation processes and dynamic recovery and dynamic recrystallization are responsible for the ductile textures and foliated nature of the rocks of the mylonite series in the Quetico fault zone. Quartz grains in the mylonitic



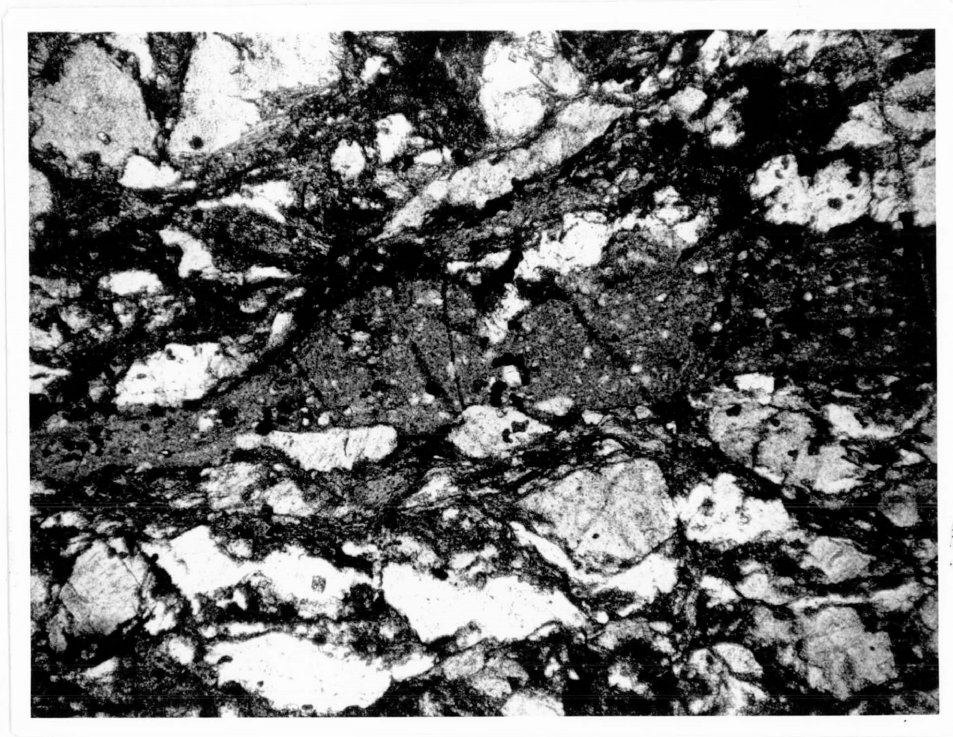


Fig. 2-34: Crush micro-breccia

Fine grained band in mylonite may have formed by cataclastic flow. Angular fragments of the matrix occur in the band.

F.O.V.- 5 mm PPL

rocks have deformed only by the above processes. Within the mylonites feldspar porphyroclasts sometimes show evidence of crystal-plasticity and dynamic recovery and recrystallization but are commonly fractured, having undergone brittle deformation within the ductile matrix. The brittle textures and random-fabrics of the rocks of the cataclasite series have formed by fracture and cataclastic flow.

Knowledge of the mechanisms which were responsible for deformation in the fault zone allows one to outline broadly the conditions at the time of deformation. Evidence indicating that crystal-plastic processes were important in the formation of the mylonites suggests that deformation took place under higher temperature, higher pressure conditions than in the later formed cataclasites resulting from brittle deformation. The operation of crystal-plastic processes in quartz begins at lower greenschist facies metamorphic conditions and is marked by the development of distinct crystallographic fabrics (Spry, 1969, p. 5). Thus crystal-plasticity in quartz may initiate around 250-300°C and 3-4 kb ( $P_{LOAD} = P_{H_2O}$ ). This led Sibson (1977) to place the EF - QP transition of his model fault zone at 250°-350°C (at 10-15 km depth with normal geothermal gradients of 20°-30°C/km) (Fig. 2-26). This represents the lowest temperature and pressure conditions at which the mylonites of the Quetico fault zone were formed. Most of the mylonitic rocks exhibit some evidence of dynamic recovery

and recrystallization suggesting they formed at higher temperatures. In cases where feldspar grains exhibit evidence of crystal-plasticity and dynamic recovery and recrystallization the rocks have clearly been deformed at higher temperatures. Thus, the cataclasites, in which fabrics are random and there is no evidence of their formation by crystal-plastic processes have formed at temperatures and pressures less than 250°-300°C and 3-4 kb.

The study of microstructures in the Quetico fault zone has revealed much about the intracrystalline deformation mechanisms responsible for deformation in the fault zone. However, the contribution to the total strain within the fault zone of inter-crystalline deformation mechanisms should not be overlooked. In particular, the microfaults described earlier in this chapter demonstrate how movement on multigranular surfaces may be an integral part of the deformation process.

## 3 - STRAIN STUDY OF THE QUETICO FAULT ZONE

## A) Introduction

The analysis of strain in a zone of intense deformation, such as the Quetico fault zone, is a difficult task. When high strains are localized in relatively narrow zones as in the case here, it is difficult to correlate strain measurements across the fault zone as well as along strike. This is especially true where a sufficiently large number of strain determinations cannot be made across the fault zone due to either limited rock exposure or lack of suitable samples for strain analysis.

The Quetico fault zone is a complex structure comprising elements of brittle and ductile deformation observable at most localities. The brittle component of deformation produces strain discontinuities at various scales which cannot be assessed quantitatively. The amount of continuous strain arising from ductile deformation may be determined where regions of homogeneously strained rock can be isolated that are sufficiently large for a given method of strain analysis.

Conventional strain markers such as fossils and pebbles have not been found in the Quetico fault zone. Grain shape analysis of quartz and feldspar grains and strain analysis methods based on the spatial distribution of grains are employed here in an attempt

to study the strain within the fault zone. The methods are applicable to quartzo-feldspathic rocks within the fault zone (protomylonites, mylonites). Mica-rich fault rocks (phyllonites) generally lack strain markers of any kind. Unfortunately strain estimates from rocks in the fault zone which appear the most strained are impossible as these rocks are fine grained, laminated mylonites and ultramylonites in which the original grains can no longer be distinguished. Dynamic recovery and dynamic recrystallization have resulted in textures in which recognition of original grains is difficult.

The method of Ramsay and Graham (1970), which is based on the variation in orientation of the schistosity developed within a ductile shear zone as a measure of shear strain and displacement, cannot be used in the case of the Quetico fault zone. In the present study, no systematic variation in schistosity across the fault zone was observed. Structural and textural elements of the fault zone do not comply with the constraints outlined by Ramsay and Graham for a shear zone formed by ideal simple shear. In general the mylonitic schistosity of the Quetico fault zone is parallel to the fault zone itself and parallel to the regional schistosity outside the fault zone.

It is suspected that particulate flow (Borradaile, 1981) was an important deformation mechanism within the fault zone (see chapter 2). It is difficult to assess the contribution to the

total strain of the rocks in the fault zone by this intergranular deformation because multigranular strain markers have not been observed. Strain determinations derived from multigranular markers would probably serve in delineating the whole rock strain better than the grain scale determinations.

The methods used in this study are:

- 1) The Harmonic Mean of deformed quartz and feldspar grain shapes (Lisle, 1977).
- 2) The Centre to Centre Method in which the centre to centre distances between grains are proportional to the longitudinal strain in the direction of the line joining the two grain centres (Ramsay, 1967).
- 3) The All Object-Object Separations Method which determines the orientation and shape of the strain ellipsoid from the centre to centre distance separating every grain from every other grain (Fry, 1979).

The first method allows determination of the strain affecting the grains alone. The second and third methods provide estimates of the strain affecting the grains and the matrix. The all object-object separations method has the potential to delineate grain strain and intergranular deformation (particulate flow) by observing dispersed particles.

The methods should provide an estimate of the strain resulting from ductile deformation and some information about the shape and orientation of the strain ellipsoid.

#### B) Grain Shape Analysis

The mean axial ratio of deformed, passive, original shape

markers may be used to determine the shape of the finite strain ellipse ( $R_s = \frac{1 + e_1}{1 + e_2}$ ). The arithmetic mean  $\bar{R} = \frac{\sum R_f}{n}$  where  $R_f$  = the final axial ratio of the deformed marker;  $n$  = the number of markers, was used by Cloos (1947) in his study of deformed oörites. The arithmetic mean is considered to be a satisfactory method of estimating  $R_s$  for originally spherical markers (Lisle, 1977). However, markers which are exactly spherical in the unstrained state are considered to be rare. Most markers exhibit some initial eccentricity (Ramsay, 1967, p. 202). Lisle (1977) used computer models of suites of passive elliptical markers deformed by an homogeneous pure shear strain to examine the accuracy of various means of  $R_f$  in determining  $R_s$ . He made use of various initial axial ratios ( $R_i$ ) in his computations. Lisle determined that none of the three simple means he examined gave the shape of the finite strain ellipse ( $R_s$ ) exactly but that the harmonic mean ( $H = \frac{n}{\sum 1/R_f}$ ) gave a closer approximation to  $R_s$  for initially elliptical markers than either the geometric mean ( $G = \sqrt[n]{R_{f_1} \times R_{f_2} \times R_{f_3} \times \dots \times R_{f_n}}$ ) or the arithmetic mean ( $\bar{R}$ ). Generally the means gave values which were larger than  $R_s$  and  $\bar{R} > G > H$  (Fig. 3-1). Lisle found that as  $R_s$  increased the percentage error in the mean values decreased. This was especially notable for H. The percentage error also decreased with decreasing  $R_i$  (Fig. 3-2). In this figure it can be seen that if  $R_s$  is greater than 2 there is generally less than 10 percent error in strain estimates using the harmonic mean. If  $R_s$  is greater

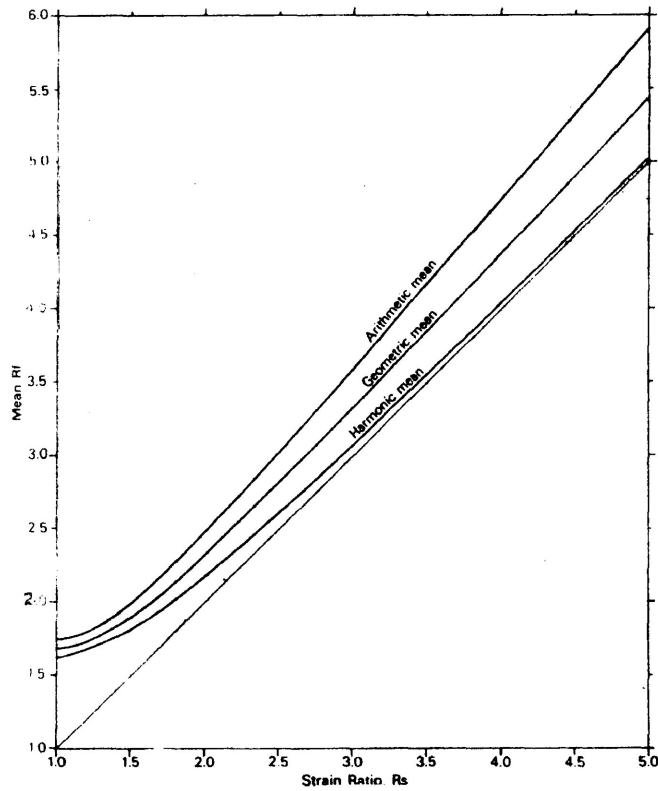


FIG. 3-1: The mean axial ratio of deformed elliptical markers as determined using R, G and H compared to the tectonic strain ratio.

(from Lisle, 1977)

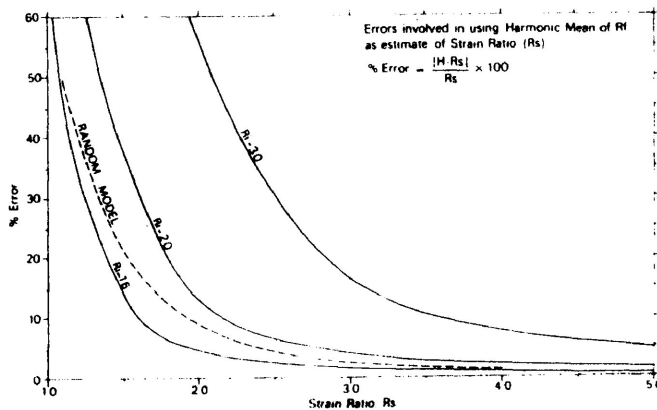


FIG. 3-2: Percentage error in strain ellipse determinations using the harmonic mean decreases with increasing strain ratio. Various initial axial ratios of elliptical markers (1.6, 2.0, 3.0 and random axial ratios) with random initial orientations are shown. The percentage error is small when  $R_i$  is small.

(from Lisle, 1977)



than 3, errors are very small. Thus the harmonic mean should provide good strain estimates where initial axial ratios are small to moderate and where  $R_s$  is reasonably large. The method, however, also requires that strain was homogeneous and that there was no preferred orientation of long axes of markers prior to the deformation.

Lisle applied this method to pebbles in a deformed conglomerate but it is equally applicable to other suitable markers. His results were comparable to those obtained using  $R_f = \phi$  techniques of strain analysis in which the axial ratio and orientation of long axes of markers are measured to compute the strain of initially ellipsoidal particles (Ramsay (1967), Dunnet (1969), Dunnet and Siddans (1971), Lisle (1977)). At high strains, where fluctuation in marker orientation is low, this method would seem to be a more definitive and simpler method of obtaining valuable strain estimates.

*Application of the method:* The method was used to evaluate the strain of grains in a number of quartzo-feldspathic rock samples from the study area. Strained quartz and feldspar grains were measured. Grain-shape measurements were recorded from tracings of grains in thin section or from cut rock surfaces. Where a lineation was visible, two sections were cut; one normal to the lineation, the second parallel to the lineation. Both sections

were also normal to the schistosity. In samples which had no visible lineation, sections were cut normal to the schistosity parallel and perpendicular to the dip direction of the schistosity. Sections prepared in this manner closely approximate the orientation of sections cut from samples where a lineation was present. The results of the grain shape analysis are shown in Table 3-1. Assuming that the above planes correspond to the YZ and XZ planes of the strain ellipsoid ( $X > Y > Z$ ),  $a (=X/Y)$  and  $b (=Y/Z)$  were determined. Assuming constant volume was maintained during deformation the lengths of the principal axes of the strain ellipsoid were determined and are listed in Table 3-2. Figure 3-3 is a Flinn plot of the measurements (Flinn, 1962).

The Flinn diagram demonstrates that in general the grains have been very flattened ( $K \ll 1$ ). The tables and the Flinn plot clearly illustrate that the quartz grains are a great deal more strained than the feldspar. They lie further from the origin of the Flinn plot. Where quartz and feldspar were measured from the same sample they are joined by a line on Figure 3-3. The quartz and feldspar appear, in general, to be flattened by the same amount. In some examples quartz grains are slightly more flattened or slightly more constricted than the feldspar grains. Figure 3-4 is a sketch of a typical sample used in this study. It shows how the various components of the rock have strained by different amounts. The quartz grains may provide a good

Table 3-1: Harmonic Mean of Grain Axial Ratios

Sample (Locality)	$R_f$ Quartz				$R_f$ Feldspar			
	$\perp$ SLL	n	$\perp$ SILL	n	$\perp$ SLL	n	$\perp$ SILL	n
* M95 t.s. (Dance Township)	3.39	70	3.74	70	1.57	65	1.84	65
* M140 t.s.	10.01	70	10.59	70	1.99	70	1.99	70
* M137 t.s. (Macdonald Inlet)	7.42	70	9.02	70	1.98†	70	1.93†	70
M100 sl. (Crowrock Inlet)	-	-	-	-	1.99	70	2.38	70
* M108 t.s.	-	-	-	-	2.45	70	2.81	63
M73 t.s./sl. (Turtle R. Road)	3.51	60	29.63	40	-	-	-	-
* M120 t.s. (Turtle Lake)	6.47	70	8.36	70	-	-	-	-
* M166 t.s. (Calm Lake)	3.04	70	3.41	70	-	-	-	-
* M54 t.s. (Lac des Mille Lacs)	8.48	70	11.02	70	2.33†	70	1.90†	70
M27 t.s. (Kashabowie Lake)	4.99	70	7.04	70	1.98†	70	1.87†	70
26 t.s. (Athelstane Lake)	3.87	70	5.28	70	1.56	70	1.89	50
M11 t.s. (Raith)	4.45	70	6.47	70	1.83	70	1.96	70
M68 t.s.	8.44	70	9.96	70	1.95	70	1.95	70
* M22 t.s.	6.79	70	7.33	70	1.59†	70	1.40†	70
M19 t.s.	3.01	70	4.91	70	1.54	70	1.60	70
M70 t.s.	-	-	-	-	1.88	70	2.18	70
M155 t.s. (Dog Lake)	5.41	70	7.09	70	1.87	70	2.14	70
15 t.s. (Highway 527)	4.63	70	5.52	70	1.83	64	1.94	70

measured from:

t.s. - thin section

sl. - cut slab

\* - measurements made in planes cut parallel and perpendicular to the dip direction of the schistosity and normal to the schistosity

† - these measurements were not used in strain calculations (see text)

n = number of measurements

Table 3-2: Results of Strain Analysis Using Harmonic Mean of Grain Axial Ratios

Sample	Q-quartz F-feldspar	$a = \frac{x}{y}$	$b = \frac{y}{z}$	X : Y : Z	x.y.z	$k = \frac{a-1}{b-1}$
M95	Q	1.10	3.39	1.60 : 1.46 : 0.43	1.00	0.042
	F	1.17	1.57	1.29 : 1.10 : 0.70	0.99	0.298
M140	Q	1.06	10.01	2.24 : 2.11 : 0.21	0.99	0.007
	F	1.00	1.99	1.26 : 1.26 : 0.63	1.00	0
M137	Q	1.22	7.42	2.23 : 1.83 : 0.25	1.02	0.034
M100	F	1.15	1.99	1.38 : 1.20 : 0.60	0.99	0.152
M108	F	1.15	2.45	1.48 : 1.29 : 0.53	1.01	0.103
M73	Q	8.44	3.51	6.30 : 0.75 : 0.21	0.99	2.964
M120	Q	1.29	6.47	2.21 : 1.71 : 0.26	0.98	0.053
M166	Q	1.12	3.04	1.56 : 1.39 : 0.46	1.00	0.059
M54	Q	1.30	8.48	2.43 : 1.87 : 0.22	1.00	0.040
M27	Q	1.41	4.99	2.15 : 1.52 : 0.31	1.01	0.103
26	Q	1.36	3.87	1.93 : 1.42 : 0.37	1.01	0.125
	F	1.21	1.56	1.32 : 1.09 : 0.70	1.01	0.375
M11	Q	1.45	4.45	2.11 : 1.45 : 0.33	1.01	0.130
	F	1.07	1.83	1.28 : 1.20 : 0.65	1.00	0.084
M68	Q	1.18	8.44	2.27 : 1.93 : 0.23	1.01	0.024
	F	1.00	1.95	1.25 : 1.25 : 0.64	1.00	0
M22	Q	1.08	6.79	1.99 : 1.85 : 0.27	0.99	0.014
M19	Q	1.63	3.01	2.00 : 1.23 : 0.41	1.01	0.313
	F	1.04	1.54	1.19 : 1.14 : 0.74	1.00	0.074
M70	F	1.16	1.88	1.36 : 1.17 : 0.62	0.99	0.182
M155	Q	1.31	5.41	2.10 : 1.60 : 0.30	1.01	0.070
	F	1.14	1.87	1.34 : 1.18 : 0.63	1.00	0.161
15	Q	1.19	4.63	1.87 : 1.57 : 0.34	1.00	0.052
	F	1.06	1.83	1.27 : 1.20 : 0.66	1.00	0.072

X, Y, Z - calculated from a and b assuming constant volume

a, b - calculated from Y/Z and X/Z ratios

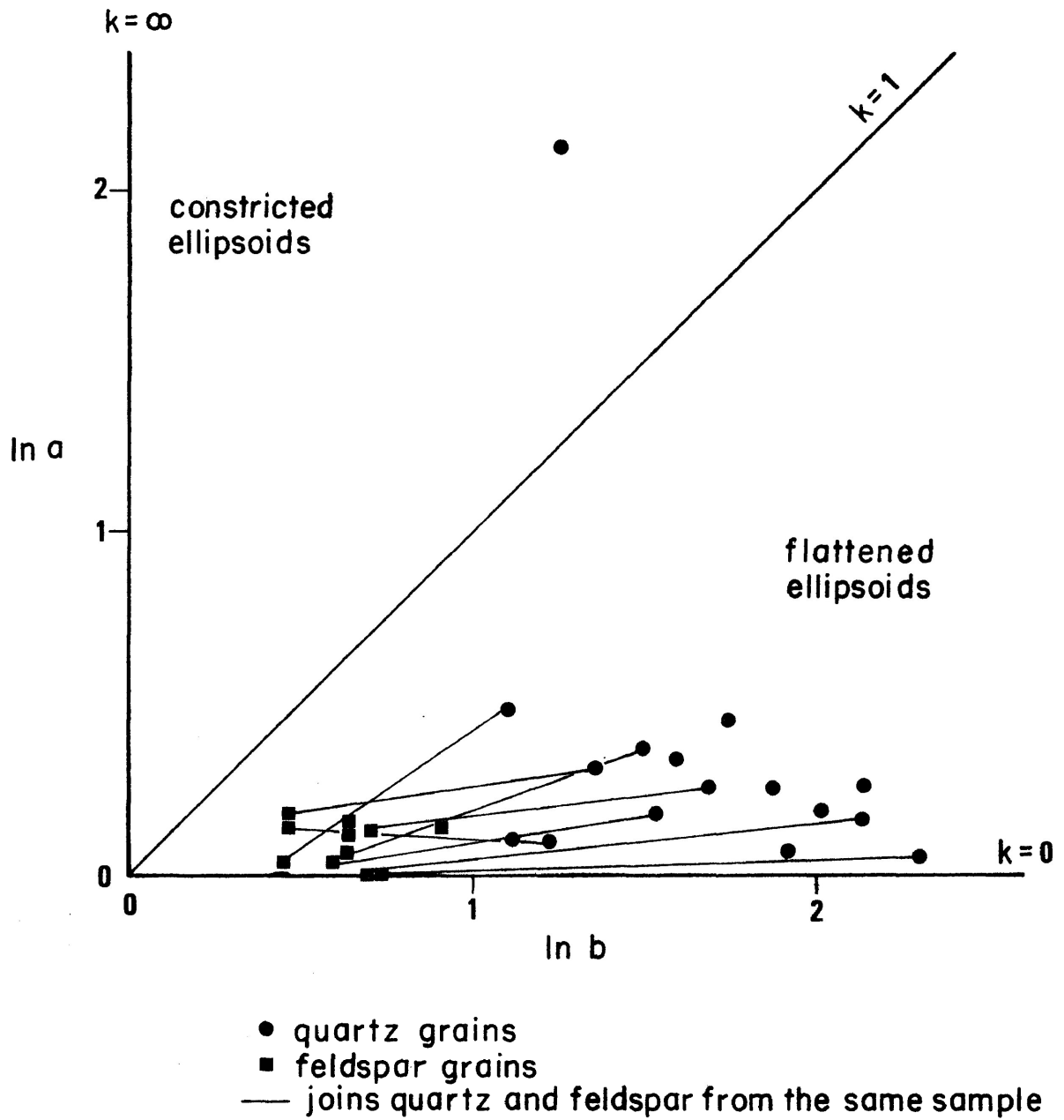


FIG. 3-3: Flinn Plot - Strain determined using the Harmonic Mean of grain axial ratios

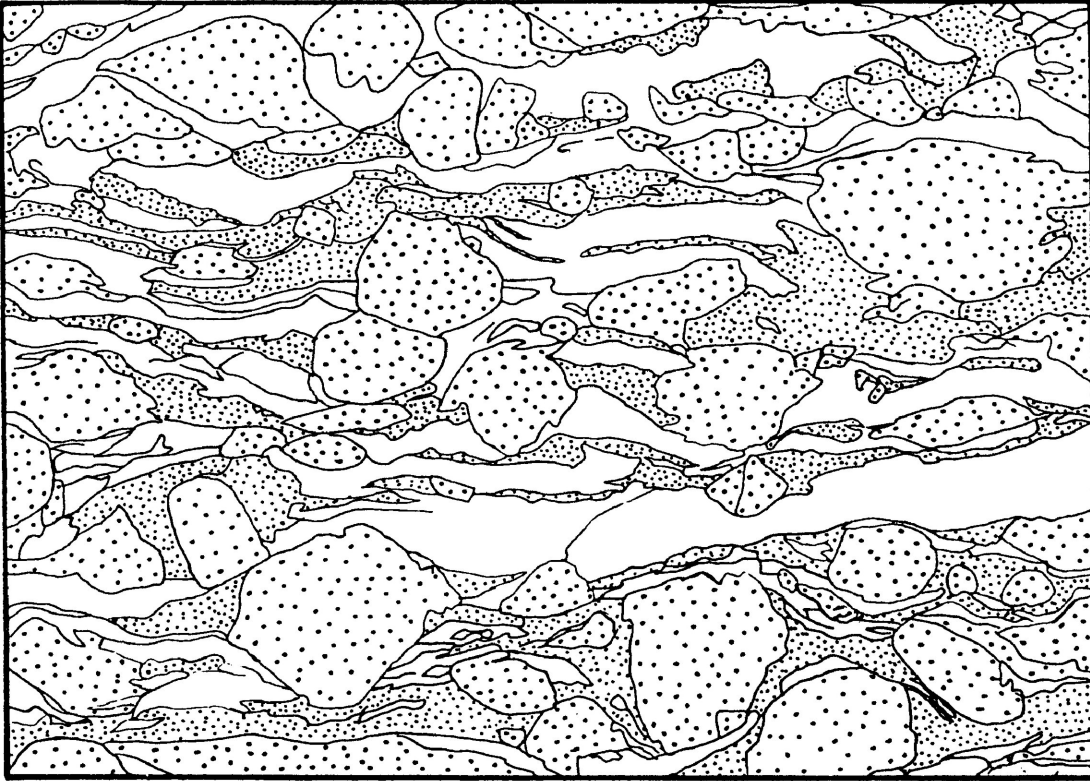


FIG. 3-4: Relatively equant feldspar grains are dispersed in a matrix of highly strained quartz and fine-grained feldspar. Any fluctuation in orientation of grains occurs where quartz grains bend around the more rigid feldspar grains.

approximation of the strain typifying the rocks in the fault zone. They have deformed homogeneously with the matrix and, in fact, generally behave as the matrix for the feldspar grains. The feldspar grains, on the other hand, do not seem to reflect the rock strain as they have not deformed homogeneously with their matrix. The feldspar grains appear to have behaved in a rigid manner and are relatively undeformed when compared to the rest of the rock. In many cases the feldspar grains are fractured or broken.

The harmonic mean should provide a good estimate of the strain in the quartz grains. The grains are elongate ( $R_f > 3.0$ ) in the sections measured as outlined by Lisle. The grains show little fluctuation in orientation. Minor fluctuations are generally due to quartz grains which bend around the feldspar grains (Figure 3-4). This would preclude the use of  $R_f - \phi$  strain analysis techniques. The  $R_s$  values determined for the feldspar grains may be inaccurate as the values (generally  $R_f < 2.0$ ) lie in the range in which the percentage error is quite high. The values, however, still serve to illustrate that the feldspars have not been greatly strained. The feldspar grains show wide variation in orientation. Many are broken and the grain-shape measurements may in some cases be meaningless for strain determinations because only pieces of the deformed grains can be measured. Despite this, measurements of the feldspar grains may indicate the relative

amount of strain of the components of the rock. In Figure 3-3 lines have been drawn between quartz and feldspar grains from the same sample. It can be seen from Fig. 3-3 that the more deformed feldspar grains correspond to the more deformed quartz grains. In samples where quartz is less deformed, feldspar is less deformed also.

As indicated in Table 3-1, several measurements of feldspar grain axial ratios were not used to calculate the shape of the strain ellipsoid. The feldspar grain axial ratios were reversed in these samples compared to the measurements of quartz grains (i.e.  $X/Y > X/Z$ ). The feldspar grains may have changed shape in a different manner than the quartz grains, but the difference could be due to errors resulting from the factors discussed above.

#### C) Centre to Centre Method

When a body of rock containing uniformly distributed particles is strained, the particle centres are displaced relative to one another such that the centres of particles that were adjacent in the undeformed rock come to lie closer together in shortened directions of the deformed rock and farther apart in extended directions.

Ramsay (1967, p. 195-197) utilized this phenomenon to determine the shape and orientation of the finite strain ellipse.



The method, which has become known as the centre to centre method, is applicable to rocks with initially equally distributed particles or particles of a known unequal distribution (Ramsay, 1967, p. 195). The method is applied by measuring the distance between initially adjacent particle centres ( $d$ , Fig. 3-5) and the orientation of a line joining the two centres with respect to a reference azimuth ( $\alpha$ , Fig. 3-5). A graph of  $d$  vs.  $\alpha$  is plotted for many pairs of measurements (Fig. 3-6). In the undeformed rock the points scatter along a distance (average ' $m$ ') which does not vary with orientation (Fig. 3-6). When the rock is deformed, as in Fig. 3-7, the distance between grain centres varies with direction and is proportional to the amount of longitudinal strain in the  $\alpha$  direction. The strain ratio and the orientation of the maximum and minimum principal strains can be determined from the  $d$  vs.  $\alpha$  plot for the deformed rock (Fig. 3-8) as follows.  $m_x/m_y$  is equivalent to  $X/Y$  of the strain ellipse where  $m_x$  is the maximum distance between grain centres and  $m_y$  is the minimum distance. The orientations of  $m_x$  and  $m_y$  correspond to the orientations of  $X$  and  $Y$ , the maximum and minimum principal strains.  $m_x$  and  $m_y$  should lie 90 degrees apart (Ramsay, 1967, p. 197).

Ramsay developed this strain analysis method for rocks in which pressure solution is evident. Grain shape analysis is unsuitable in such rocks due to the dissolution of parts of grains along pressure solution surfaces. His examples comprise initially

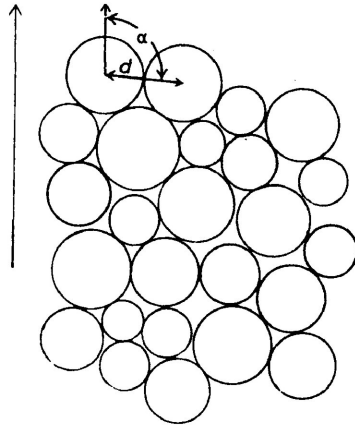


FIG. 3-5: Section through a rock made up of an aggregate of undeformed spheres.

(Ramsay, 1967)

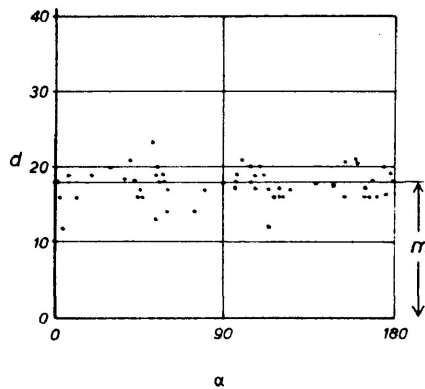


FIG. 3-6: Plot of  $d$  against  $\alpha$  for the material of Fig. 3-5.

(Ramsay, 1967)

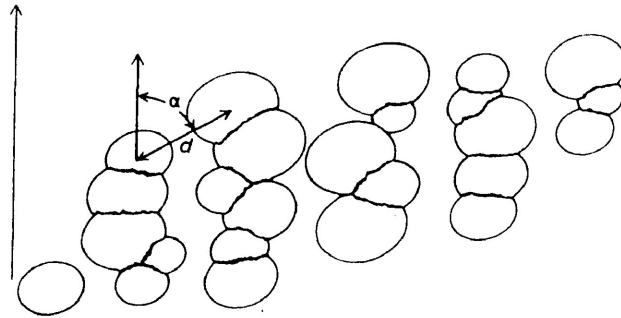


FIG. 3-7: Section through a deformed aggregate. The partially deformed spheres have undergone partial pressure solution along their mutual contacts.

(Ramsay, 1967)

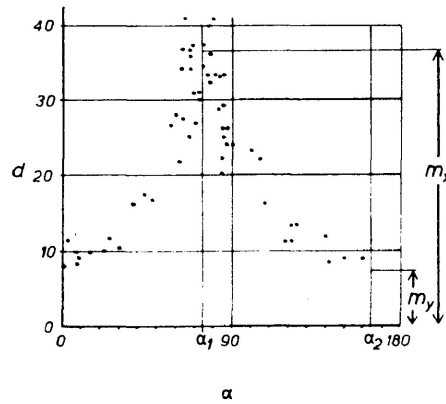


FIG. 3-8: Plot of  $d$  against  $\alpha$  for the material of Fig. 3-7.

(Ramsay, 1967).

close packed spherical grains which have undergone pressure solution (Figures 3-5 and 3-7). He noted that the technique is applicable to any rock in which particles were originally uniformly distributed. The centre to centre method may provide a more realistic estimate of strain than grain shape measurements in situations where dispersed particles in a matrix have not deformed homogeneously with their matrix or, as Ramsay suggests, the method may serve as a check on the assumption that the included particles have deformed homogeneously with their matrix. If, for instance, the particles have deformed less than their matrix, estimates of strain from grain shape measurements of the particles would be less than the strain of the whole rock (particles plus matrix). The method has the potential to overcome this problem. The strain of grains and the matrix between grains is taken into account by the grain centre to centre measurements.

*Limitations:* The main limitation of the method is that one must be able to identify nearest neighbouring grains of the undeformed rock when examining rocks in the deformed state. Nearest neighbours of the undeformed state are hard to identify in the deformed state, especially at high strains. The method is invalid if originally adjacent grains cannot be identified. Another limitation of the method is the assumption that particles were uniformly distributed in the undeformed state. Unless the equivalent undeformed rock

can be observed, the original particle distribution is unknown. If the original distribution varied from a uniform distribution irregularities in the  $d$  vs.  $\alpha$  plot could make interpretation difficult.

*Application of the method:* The method was applied to eight samples from the Quetico fault zone to test its suitability for determination of strain in the fault zone and to compare the results to those of the All Object-Object Separations Method (Section 3-D). Data were collected in the field by recording grain centre locations of dispersed feldspar grains on tracing paper. The data were collected from horizontal surfaces approximately normal to the schistosity and parallel to the weakly defined stretching lineation of the feldspar grains. Portions of the plots were enlarged as indicated on the  $d$  vs.  $\alpha$  plots (Figures 3-9 - 3-16) in order to facilitate measurement of grain centre separations. It was not possible to determine which grains were adjacent to each other in the undeformed state because many grains are now adjacent to one another as recorded on the diagrams of grain centre distribution. The grain centre separation of nearest grains was measured in each of twelve 30 degree sectors around each grain centre. The resulting  $d$  vs.  $\alpha$  plots are shown in Figures 3-9 - 3-16. The orientation of the schistosity is shown on each plot.

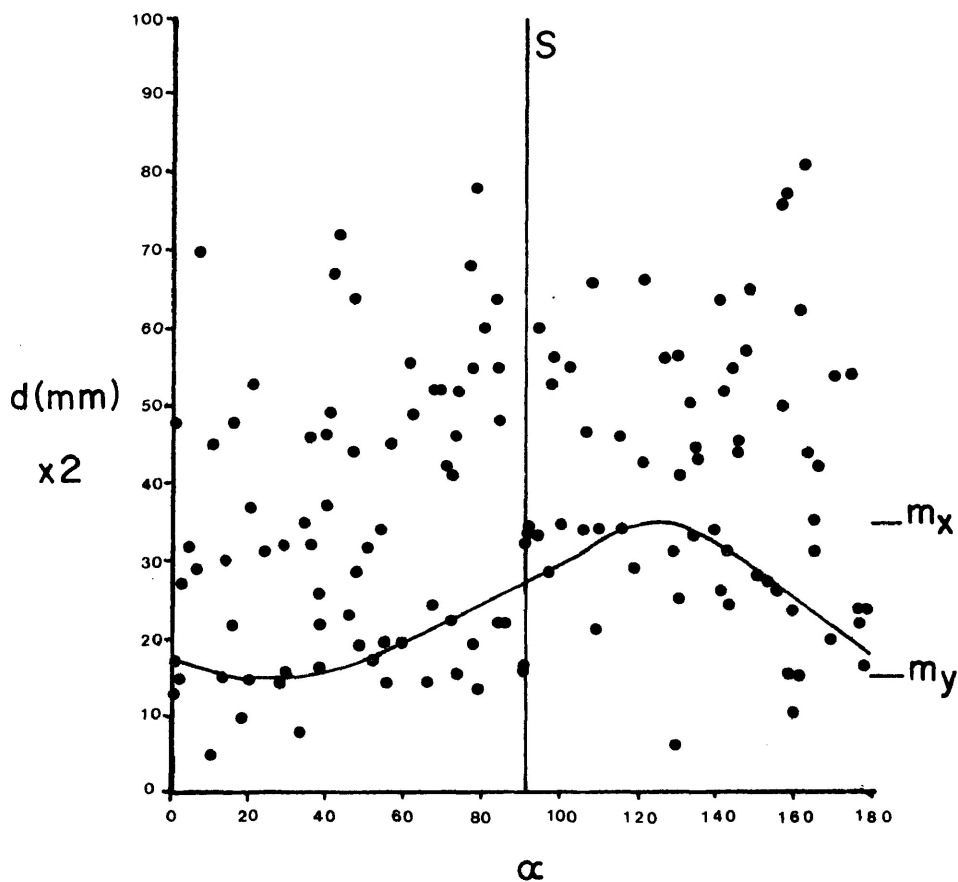


FIG. 3-9

Centre to Centre  
Method

Graph of  $d$  vs.  $\alpha$

#1 Seagull Island,  
Dog Lake

strain ratio  
1:2.33

S - schistosity

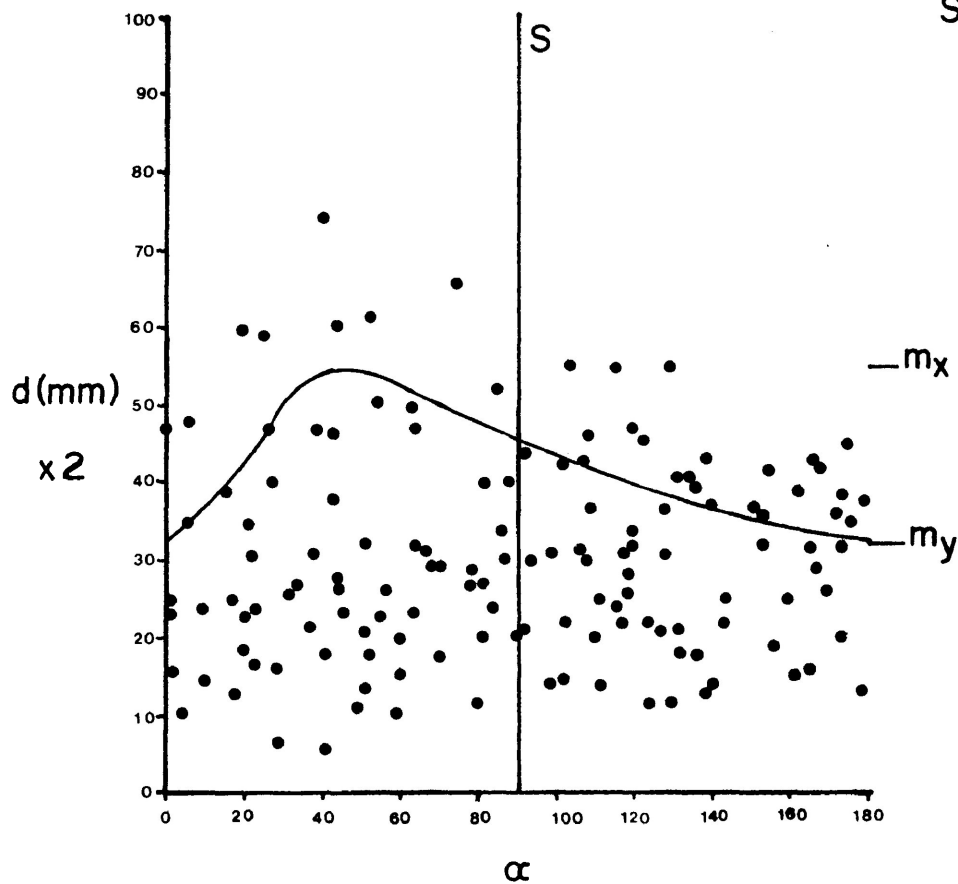


FIG. 3-10

Centre to Centre  
Method

Graph of  $d$  vs.  $\alpha$

#2 Seagull Island,  
Dog Lake

strain ratio  
1:1.69

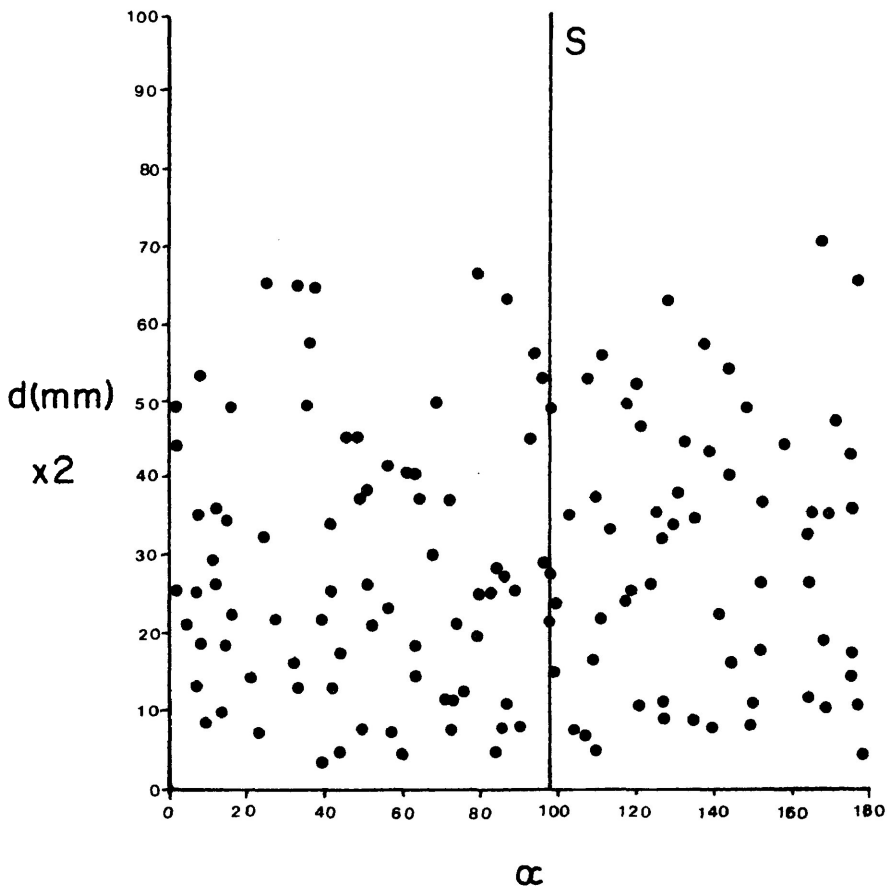
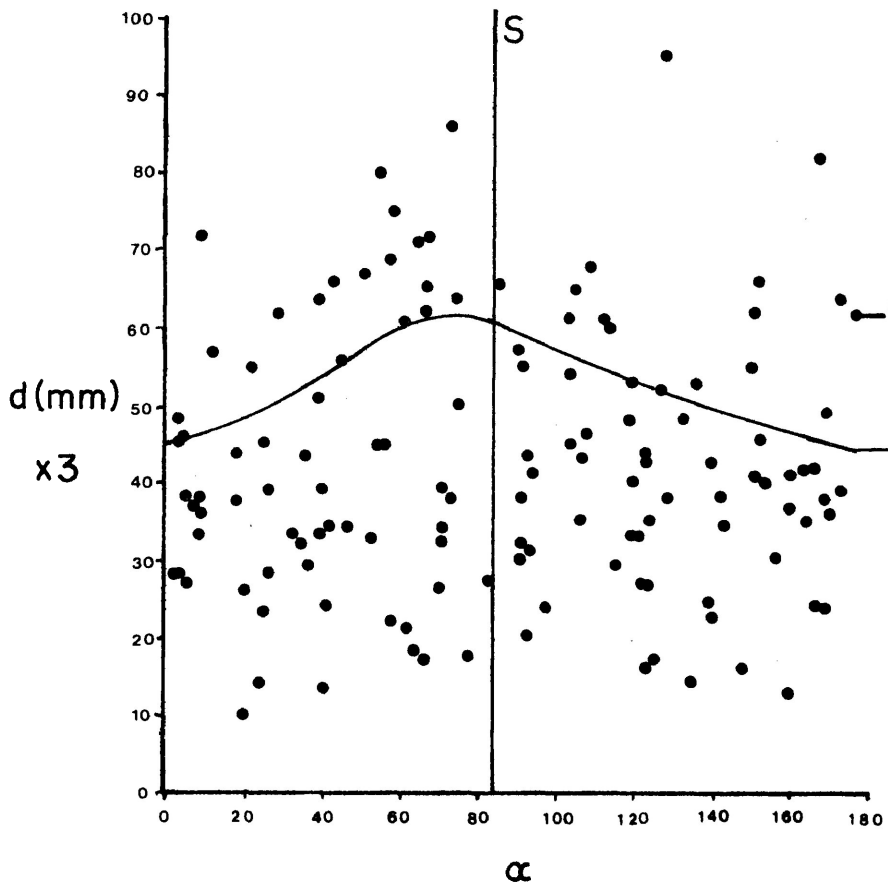


FIG.3-11

Centre to Centre  
Method

Graph of  $d$  vs.  $\alpha$

#3 Dad's Island,  
Dog Lake



S - schistosity

FIG.3-12

Centre to Centre  
Method

Graph of  $d$  vs.  $\alpha$

#4 Dad's Island,  
Dog Lake

strain ratio  
1:1.38

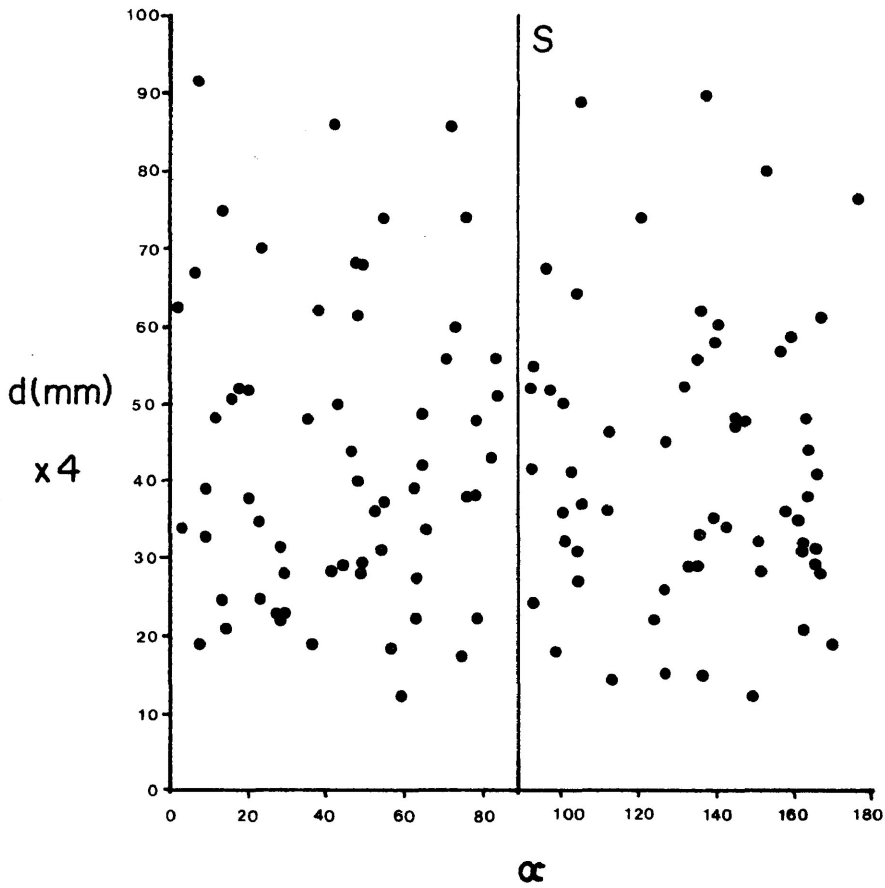
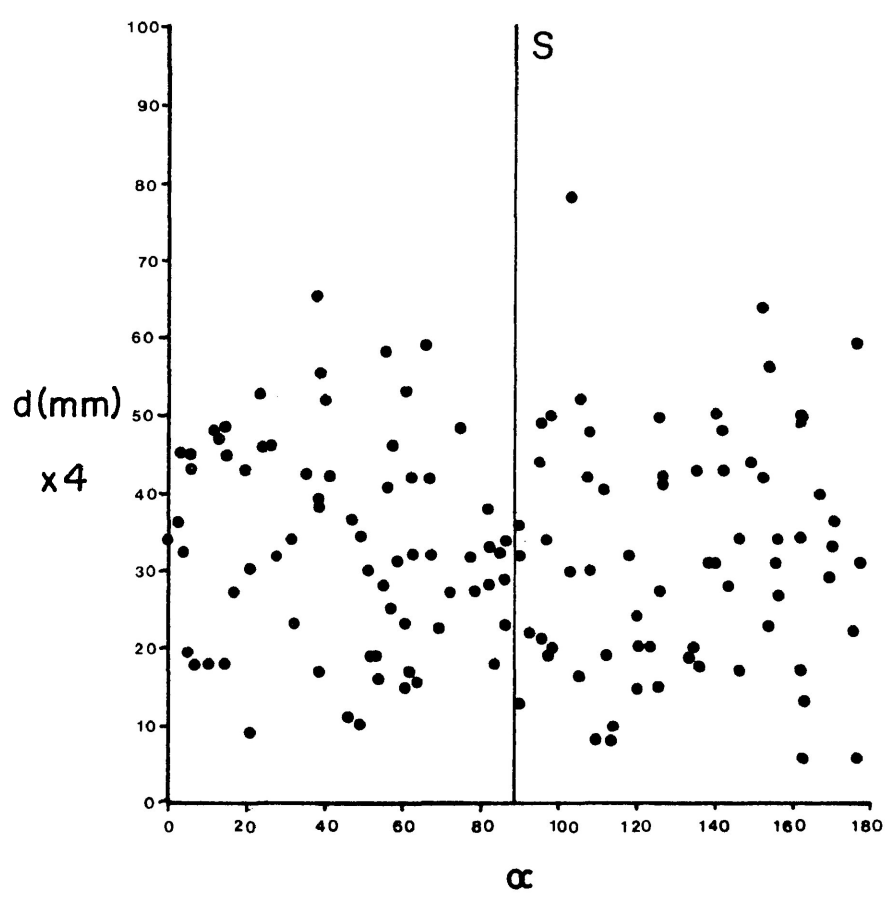


FIG. 3-13  
Centre to Centre  
Method  
Graph of  $d$  vs.  $\alpha$   
#5 Raith



S - schistosity  
FIG. 3-14  
Centre to Centre  
Method  
Graph of  $d$  vs.  $\alpha$   
#6 Raith



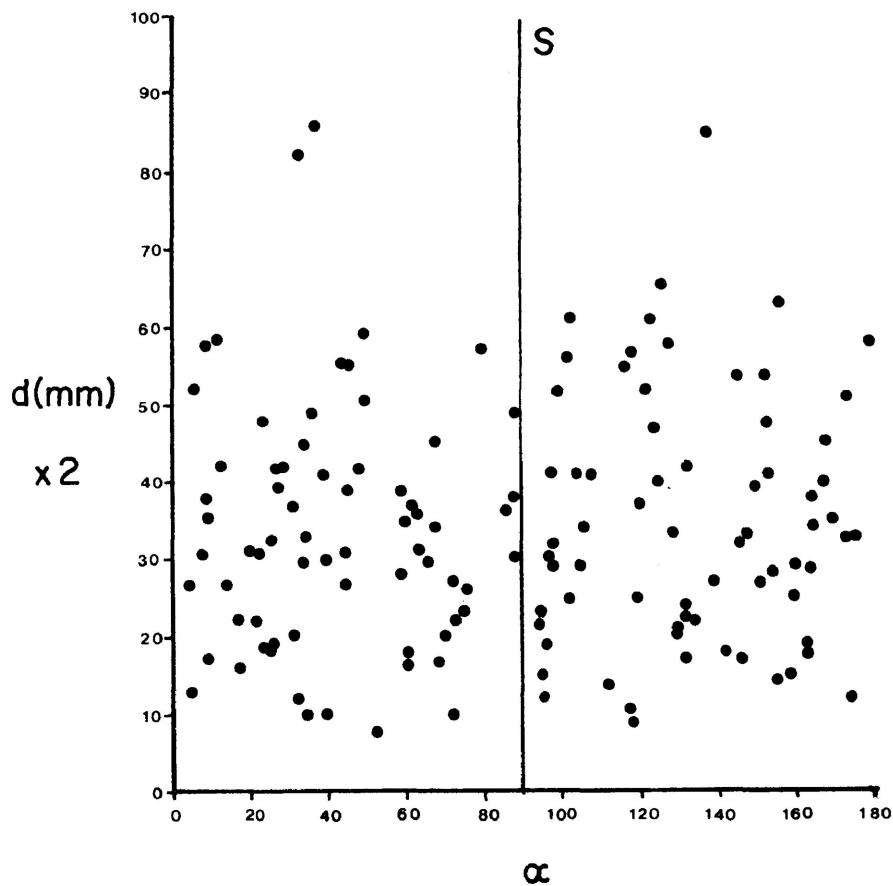


FIG.3-15

Centre to Centre  
Method

Graph of d vs.  $\alpha$

#7 Crowrock Inlet

S - schistosity

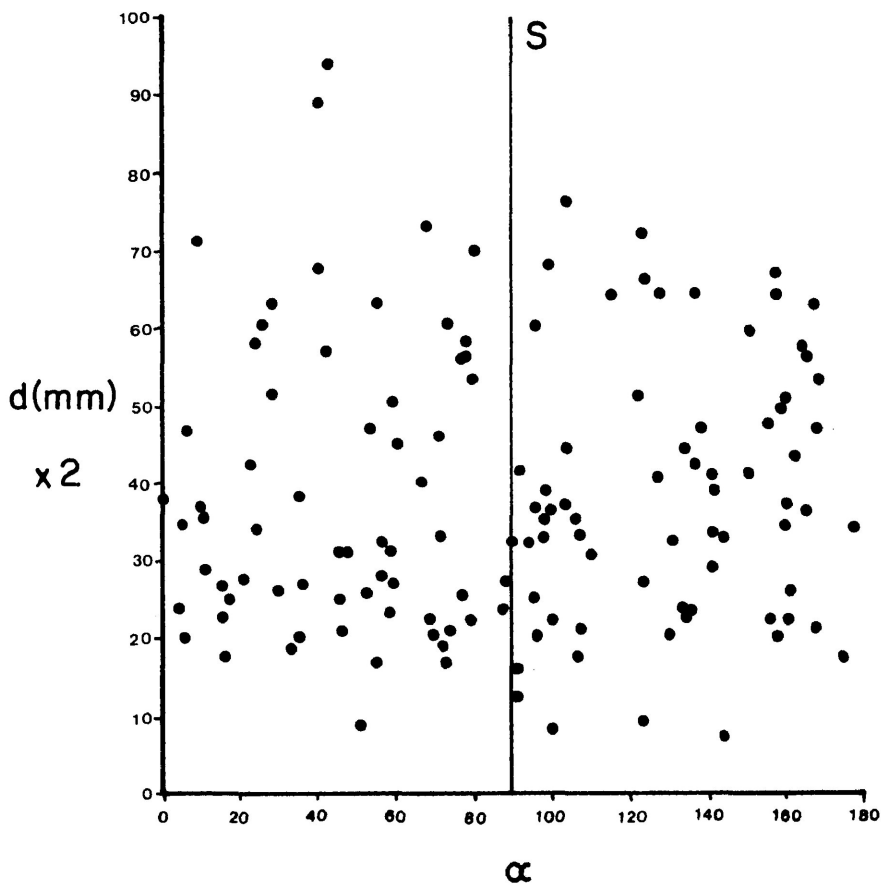


FIG.3-16

Centre to Centre  
Method

Graph of d vs.  $\alpha$

#8 Crowrock Inlet

A wide, constant range of  $d$  values exists for most orientations on the plots. Several plots, however, show some variation in grain centre separation with direction (Figures 3-9, 3-10 and 3-12). This is indicated on the graphs and is a weakly developed feature in each case. The graphs in general, however, do not yield useful strain values. This may be the result of particulate flow (Borradaile, 1981) which makes it impossible to identify predeformation neighbouring grains. Lacking evidence to the contrary it is also necessary to assume that the original distribution of grains was uniform.

#### D) All Object-Object Separations Method (The Fry Method)

Fry (1979) developed this method of strain analysis. It is based on the same principle as the centre to centre method but eliminates the problem of identifying objects which were nearest neighbours before deformation. The centre to centre distances separating every object from every other object define the shape of the finite strain ellipse. The method is performed as follows (after Fry (1979)):

- 1 - A tracing is made which records the positions of the centres of the strain markers. This is called the "original plot".
- 2 - One of the points of the original plot is chosen as the centre of a second plot - the "derived plot".
- 3 - The positions of all other points within the bounds of the derived plot are recorded on the derived plot.

- 4 - A second point of the original pattern is placed at the centre of the derived plot and the positions of all other points are added to the derived plot.
- 5 - This procedure is repeated until all the points of the original plot have been used as the centre of the derived plot.

The final product is a plot which features a point free region or region with low point density at the centre. The shape of this point free zone reflects the shape of the strain ellipse. It delineates the preferred distances separating object centres and the variation in distance with direction.

*Assumptions:* The method requires that strain was homogeneous.

At least the area of the original plot must have been homogeneously strained for the method to be valid.

Objects used for this method must have originally been distributed isotropically and homogeneously. Fry suggested that suitable markers might be objects on sedimentary bedding planes and minerals in homogeneous igneous and metamorphic rocks. Fry demonstrated that the method did not work for random (Poisson type) distributions. He noted that some clustering or anticlustering of objects was necessary for the method to work. Clustering means the probability that a second item exists is greater at smaller distances from a known item than it is farther away. Anticlustering means the probability that a second item exists is less at smaller distances from the known item than farther away. In the Poisson

or random case the probability of existence of a second object is constant at all distances from the known object (Fry, 1979). The assumption that the distribution of objects was not truly random appears to be valid as anticlustering is inherent in a sample comprising a group of objects or markers. This is particularly true of close packed markers. Consider close packed spherical markers. There is a minimum distance which can separate two marker centres. This distance is equal to twice the radius of the markers. Thus the probability of encountering a second object centre at less than this distance is zero making the distribution extremely anticlustered. In a more general case of close packed markers and in the case of dispersed markers the minimum distance which may separate marker centres may vary but a region of low density of marker centres will still surround each marker centre. This region will become more diffuse as markers become more widely dispersed. The all object-object separations method serves to delineate the shape of this region of low density of object centres around each centre by demonstrating the centre to centre distances separating every object from every other object in a sample. The change in shape of this region of low density of object centres from circular to elliptical defines the shape of the strain ellipse.

*Limitations:* Fry described three main constraints on the method.

- 1 - edge effects
- 2 - sample size
- 3 - visual interpretation

The constraints associated with edge effects result from the limited size of the original plot. As each point of the original plot is to be used as the centre of the derived plot a problem may arise whereby apparent point density on the plot falls away with distance. When points near the edge of the original plot are used as centres it is impossible to extrapolate the positions of points (unrecorded) which lie beyond the original plot. Thus, a limit must be put on the size of the derived plot and the area of the original plot containing object centres which may be used as the centre of the derived plot. Figure 3-17 illustrates the area of a rectangular original plot in which the centres may be used in constructing the derived plot so that all edge effects will be eliminated.

Fry determined that to define the strain ellipse would require the use of 1100 centres as origins. To roughly define the ellipse would require 260 origins from the original plot. Less than 300 origins were not considered likely to produce quantitative results.

The evaluation of the final plot of all object-object separations requires visual interpretation of the shape of the strain ellipse. Fry pointed out the problem of the inability of the human eye to identify girdles of differing point density.

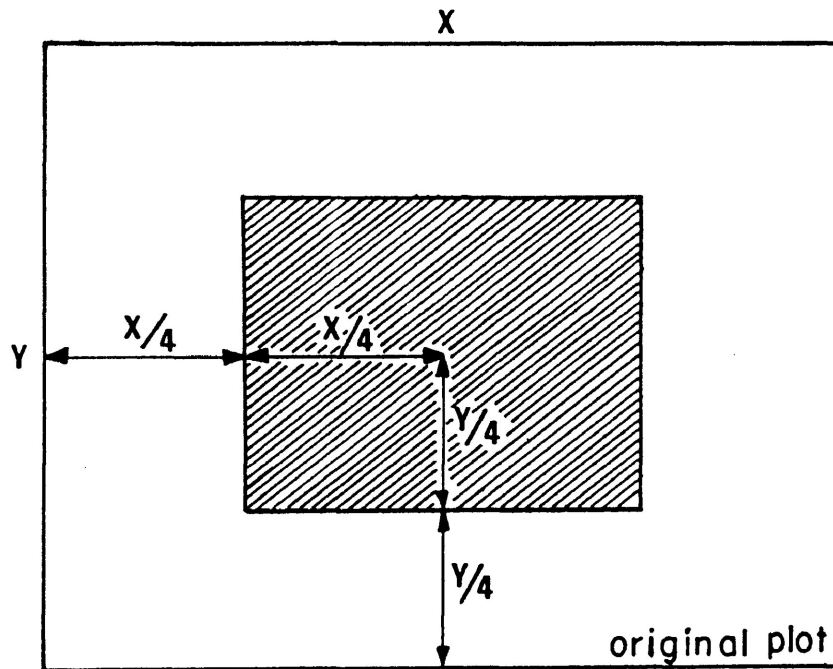


FIG. 3-17: ELIMINATING EDGE EFFECTS ON ALL OBJECT-OBJECT SEPARATIONS PLOTS.

All edge effects will be eliminated if only the points which lie within the shaded area of the rectangular original plot are used as origins of the derived plot.

He also noted that slight variations in strain across the sample field could result in blurring of the pattern of the final plot thus impairing visual interpretation. At high strains (strain ellipse axial ratio 6:1 or greater) the strain ellipse ends are defined by few points. The ellipse ends can become blurred to the point that they cannot be identified if there are small variations in strain within the area of the original plot.

*Application of the method:* A computer program designed by Dr. G.J. Borradaile was adapted by the writer to carry out the steps of all object-object separations method and produce the plots for strain analysis. The Fortran program was run on the IBM 360 computer with graph plotter at Lakehead University. The program is listed in Appendix I.

Data for the program consists of N- the number of data points, a scale factor, and the data set comprising marker centres which have been given X-Y coordinates. The program scales the data so a reasonable size plot will be produced, chooses a centre point, and determines the size of the derived plot. The derived plot in each case is equal in size to the area from which points were used as origins on the original plot (Fig. 3-17). The steps of the method are performed by transforming the array of points so that each point in turn lies at the centre. The locations of all the points within the limits of the derived plot are

recorded by the graph plotter. The centre point is marked by a cross, all other points are represented by triangles. The program allows a maximum of 200 data points (marker centres) to be used. This number was sufficient to define the strain ellipse for most samples. A greater number was not chosen as the graph plotting routine is very time consuming. Using 200 points keeps the computer time to a reasonable value while still providing fairly high definition of the point free zone around the centre point of the plot.

To test the program and demonstrate some aspects of the method, as described by Fry, plots of random and anticlustered point distributions were derived. The pseudo-random number generator of the VAX II computer was used to produce pairs of random X and Y coordinates which represent a random marker centre distribution. An homogeneous strain was then simulated by shortening distances in the Y direction and extending distances in the X direction such that the strain ellipse would have an axial ratio of 4:1. The all object-object separations method was applied to the unstrained and the strained data. Figures 3-18 and 3-19 are the resulting computer plots. The plots demonstrate that the method does not work for random distributions. There is no circular point free zone around the centre of the unstrained plot and no elliptical point free zone around the centre of the strained plot. The method does not work for the random point distribution because there

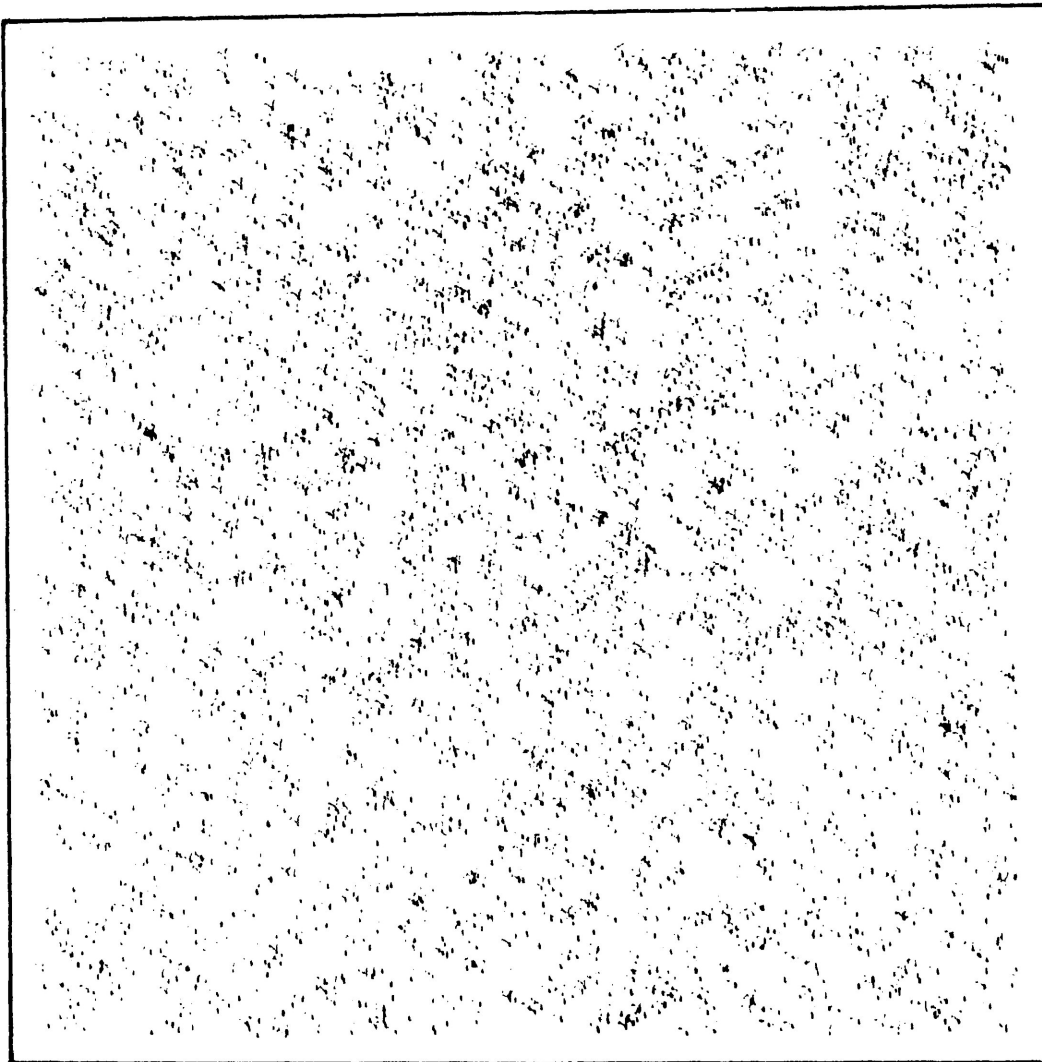


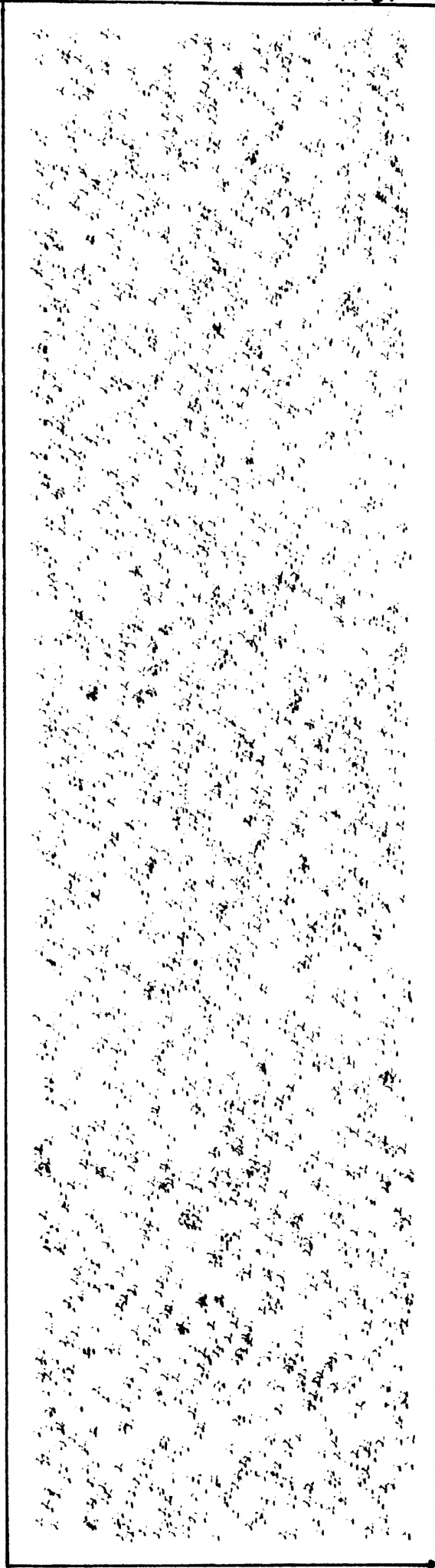
**FIG. 3-18**

All Object-Object Separations Method

Random Point Distribution

Unstrained Plot





**FIG. 3-19**

All Object-Object Separations Method

Random Point Distribution

Strained Plot

is no inherent zone of low point density surrounding each point. Points may lie immediately adjacent to one another.

An anticlustered point distribution was generated using the random number generator and comparing each point to every other point. If a point was less than a specified distance from any other point it was not accepted. If the point was greater than the specified distance from every other point it was retained. The resulting anticlustered point distribution was strained in the same manner as the random example. Figures 3-20 and 3-21 are the unstrained and strained plots for the anticlustered distribution. The point free zone around the centre of the plot is clear in each case and represents the shape of the finite strain ellipse. The unstrained case (Fig. 3-20) has a circular point free region. The strained version (Fig. 3-21) has an elliptical point free zone with axial ratio 4:1. The method works for the anticlustered distribution and thus is applicable to rocks as markers are inherently anticlustered.

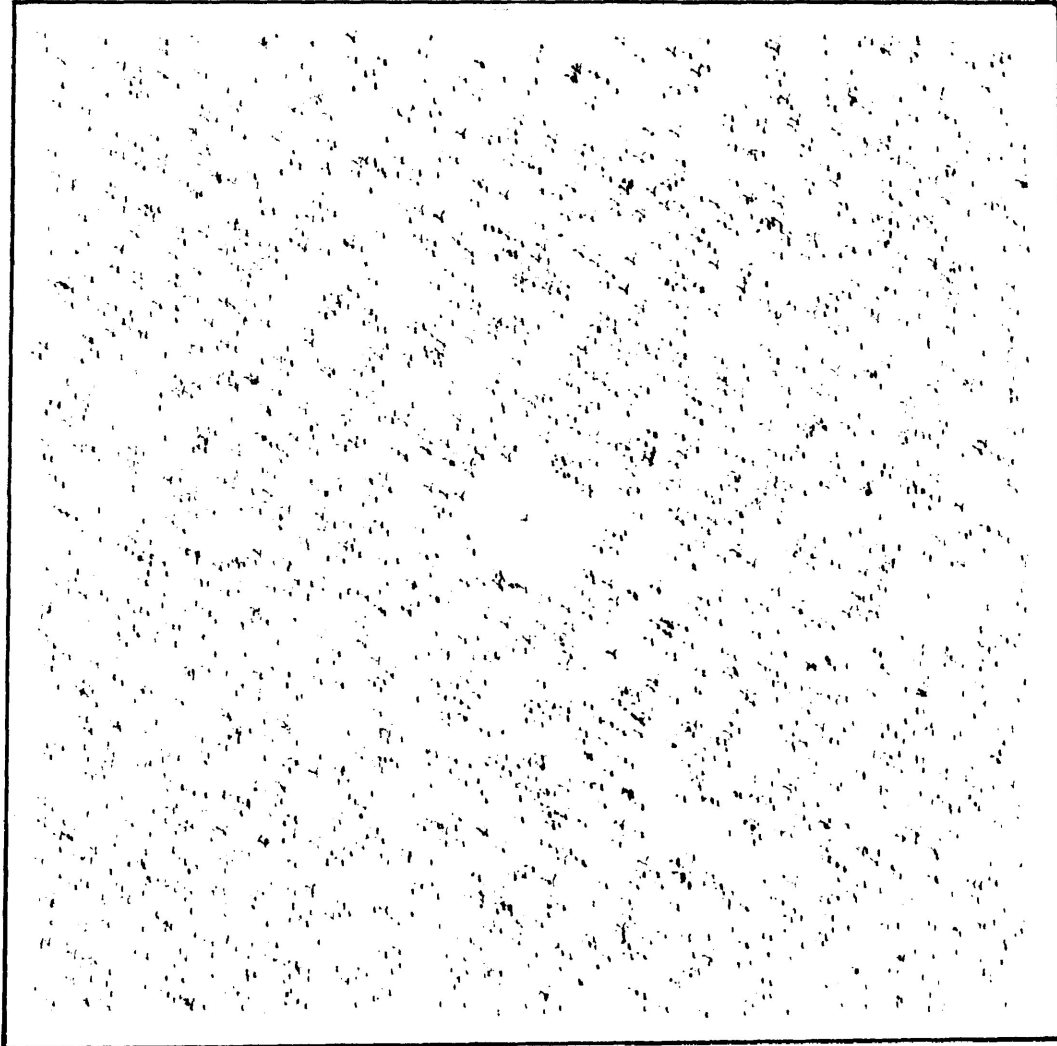
Theoretically the all object-object separations method should provide a good strain estimate in that it records the strain of markers plus matrix. Thus if markers have not deformed homogeneously with their matrix the method will give a strain estimate closer to the true strain than would methods which measure the strain of the grains alone. The method does not require recognition of predeformation nearest neighbours and is

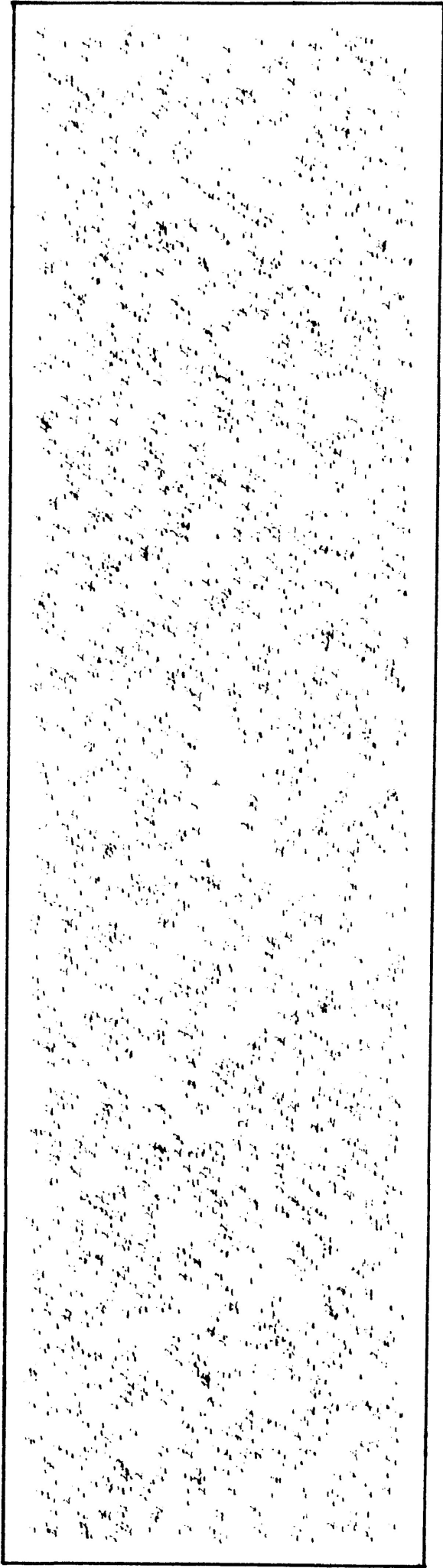
**FIG. 3-20**

All Object-Object Separations Method

Anticlustered Point Distribution

Unstrained Plot





**FIG. 3-21**

All Object-Object Separations Method

Anticlustered Point Distribution

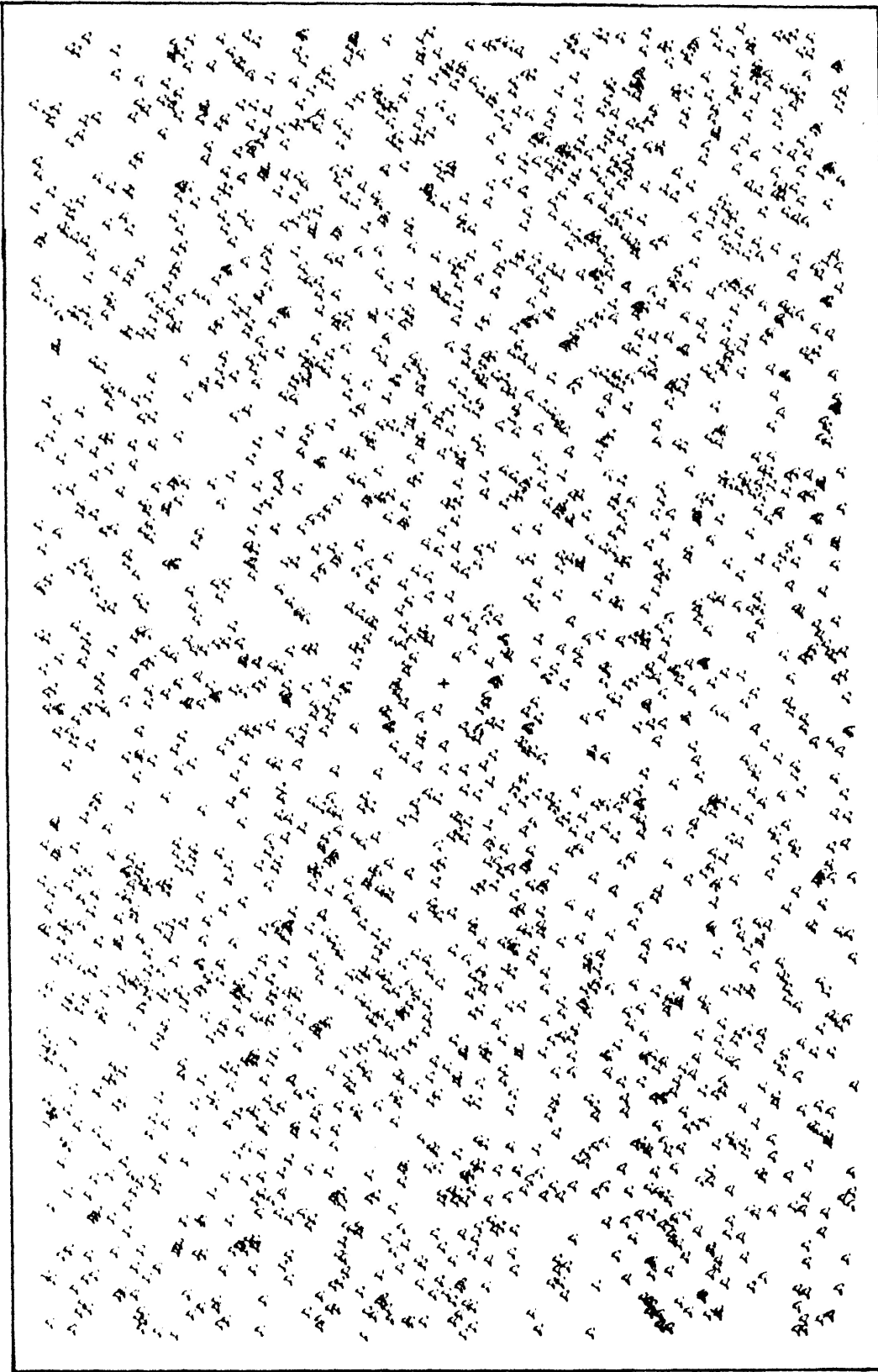
Strained Plot

thus preferable to the centre to centre method. The strain can be measured in samples where markers are dispersed and where particulate flow has made the identification of originally nearest neighbours impossible.

In the case of close packed grains, particulate flow (without grain deformation) would not be recorded by the all object-object separations method if grains remained intact. The point free zone is determined strictly by the grain size and shape. However, with dispersed particles the point free zone comprises the grain volume and matrix between grains. If particulate flow has occurred and distances between grains in matrix have been altered the original shape of the point free zone has been changed. Thus the strain measured by the all object-object separations method for dispersed grain distributions should reflect grain shape changes as well as intergranular deformation by particulate flow.

*All object-object separations from the Quetico fault zone:*

Initially data were collected in the field. Tracings from horizontal rock outcrop surfaces showing the location of feldspar grain centres were made. The plots derived from these data are shown in Figures 3-22 to 3-29. The data provide two dimensional strain estimates approximating  $X/Z$  as the surfaces are normal to the schistosity and parallel to a mineral lineation where this is visible. The



scale x2

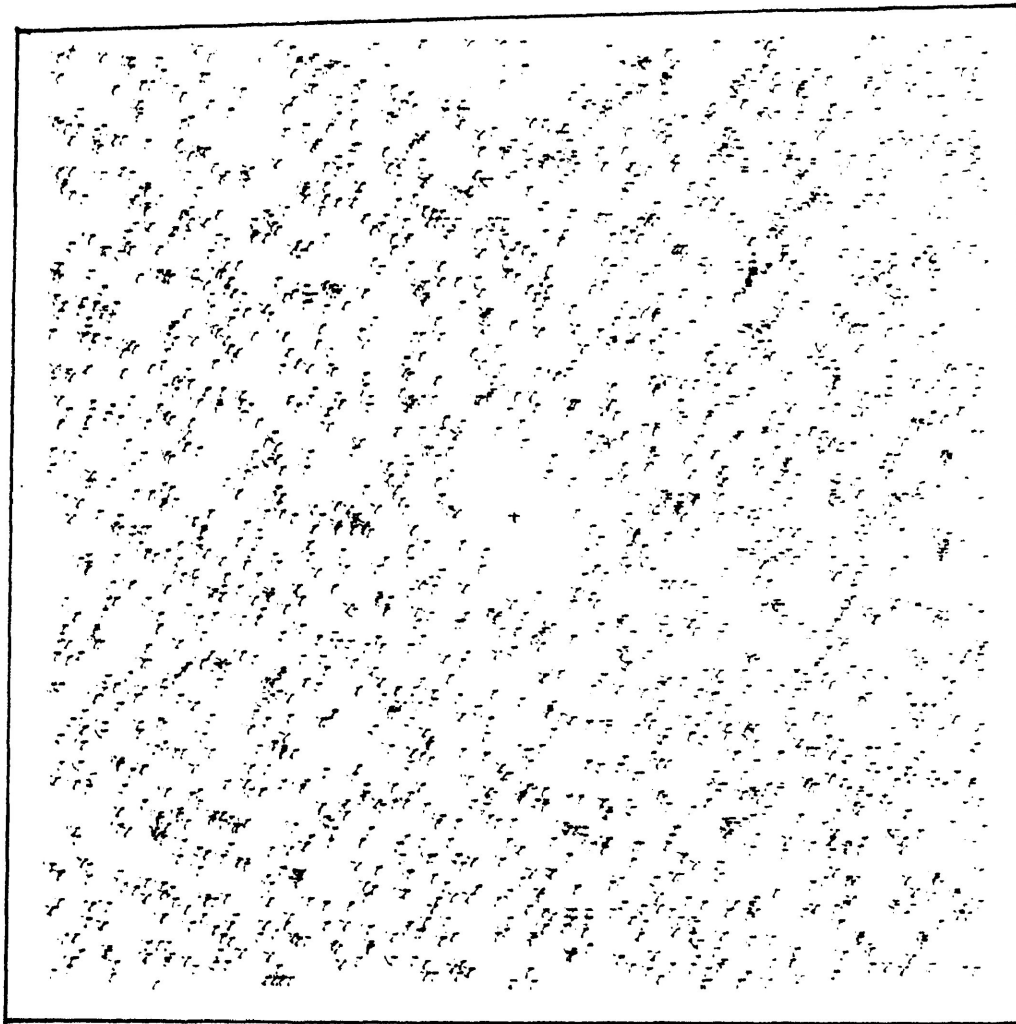
strain ratio 1.6:1

S ————— S

— S, horizontal

#1 SEAGULL ISLAND, DOG LAKE

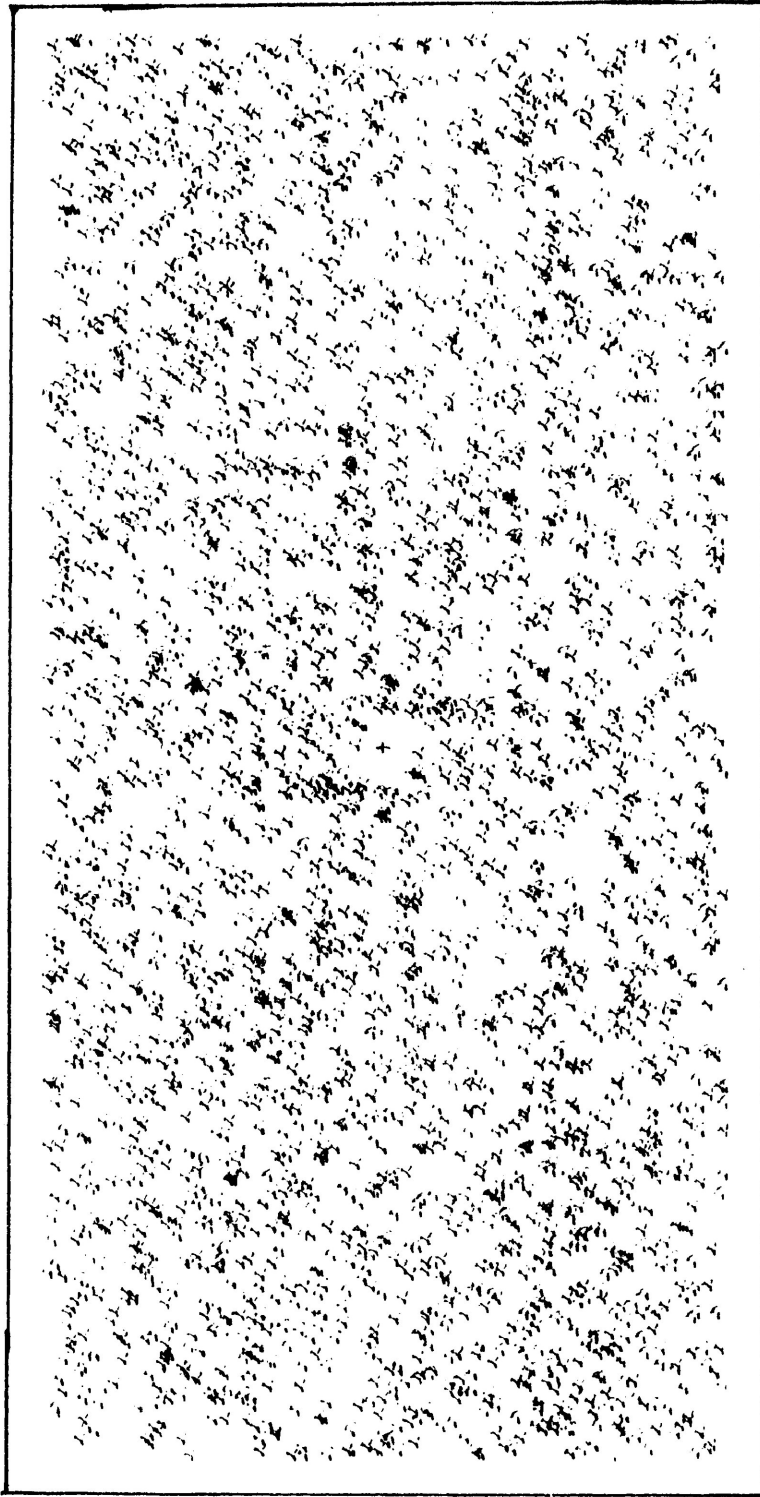
**FIG. 3-22**



⊥ S, horizontal      S ————— S      scale x2  
#2 SEAGULL ISLAND, DOG LAKE      strain ratio 2:1

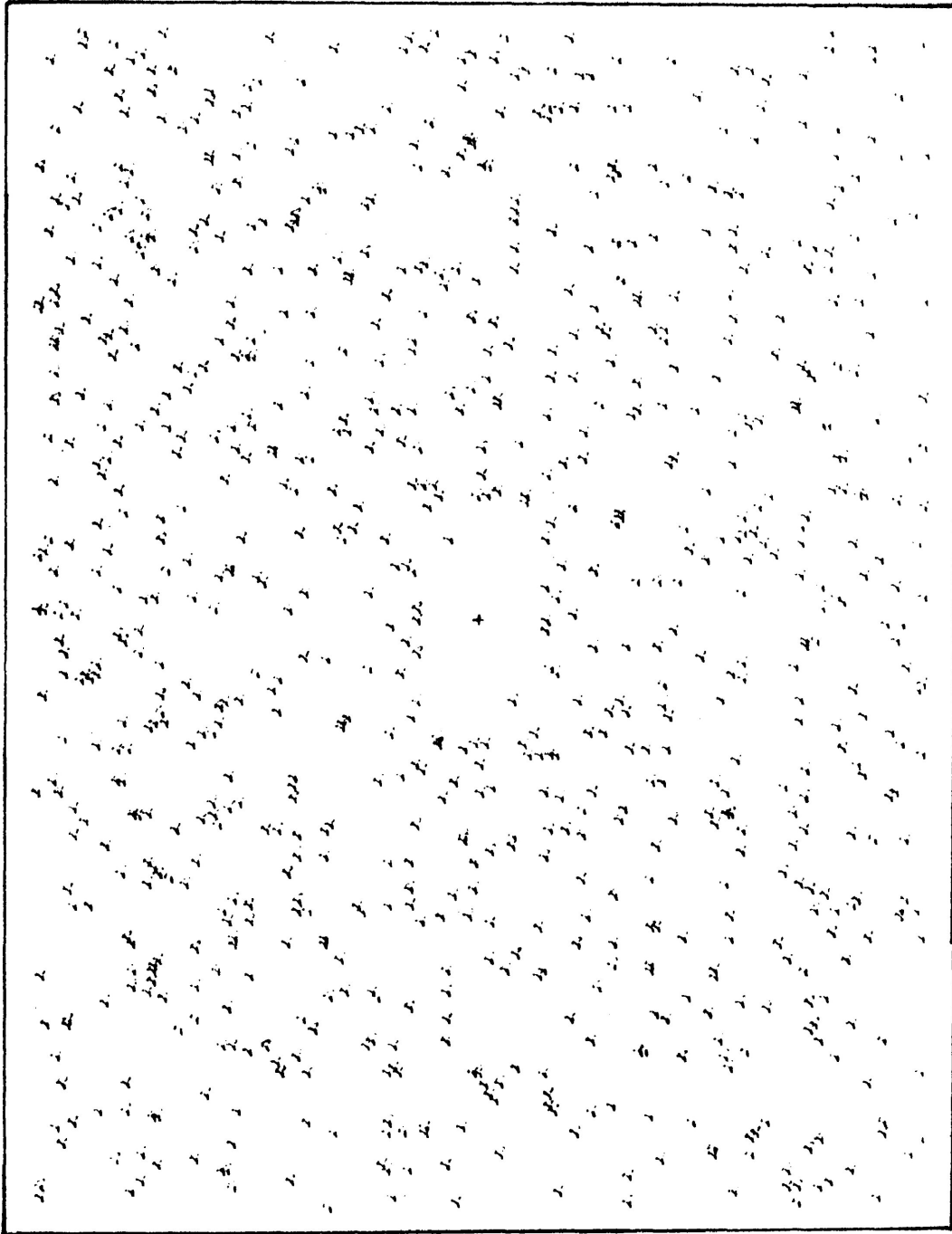
**FIG. 3-23**





— S, horizontal S — scale x2  
#3 DADS ISLAND, DOG LAKE strain ratio 1.5:1

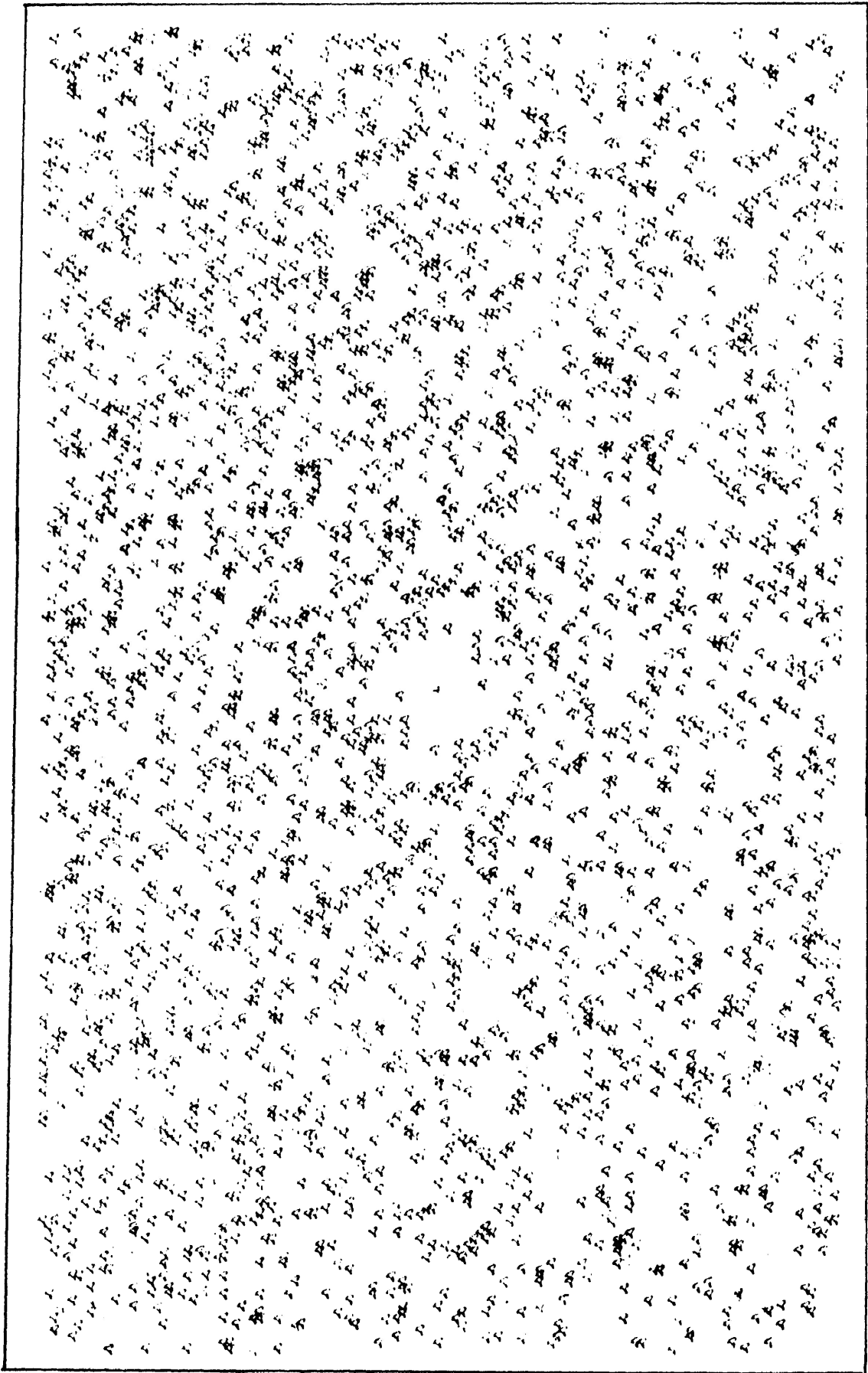
**FIG. 3-24**



— S, horizontal S — scale x3

#4 DADS ISLAND, DOG LAKE strain ratio 2.3:1

**FIG. 3-25**



L-S, horizontal

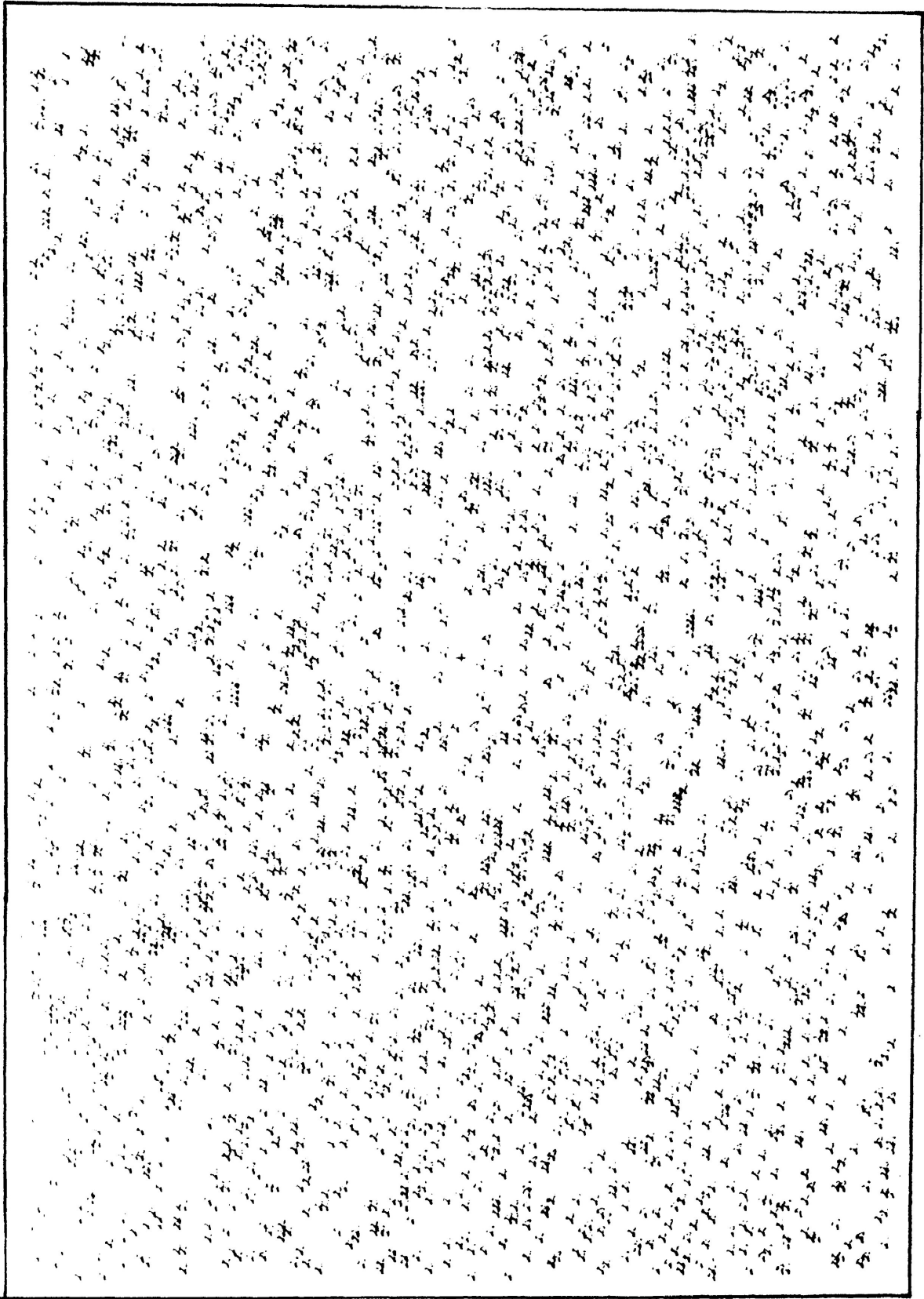
S ——— S

scale x4

#5 RAITH

strain ratio 3.6:1

**FIG. 3-26**

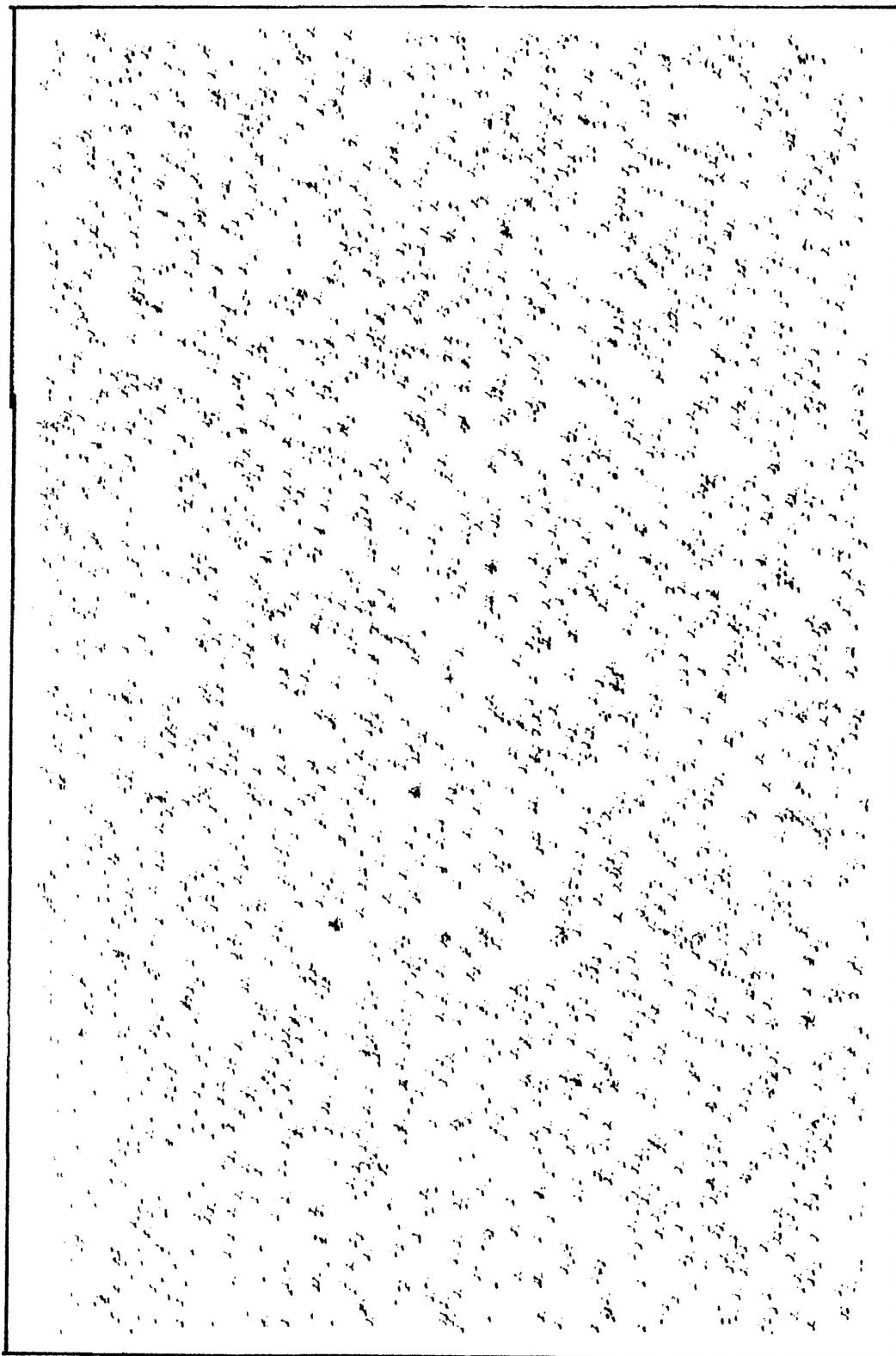


— S, horizontal  
#6 RAITH

S —

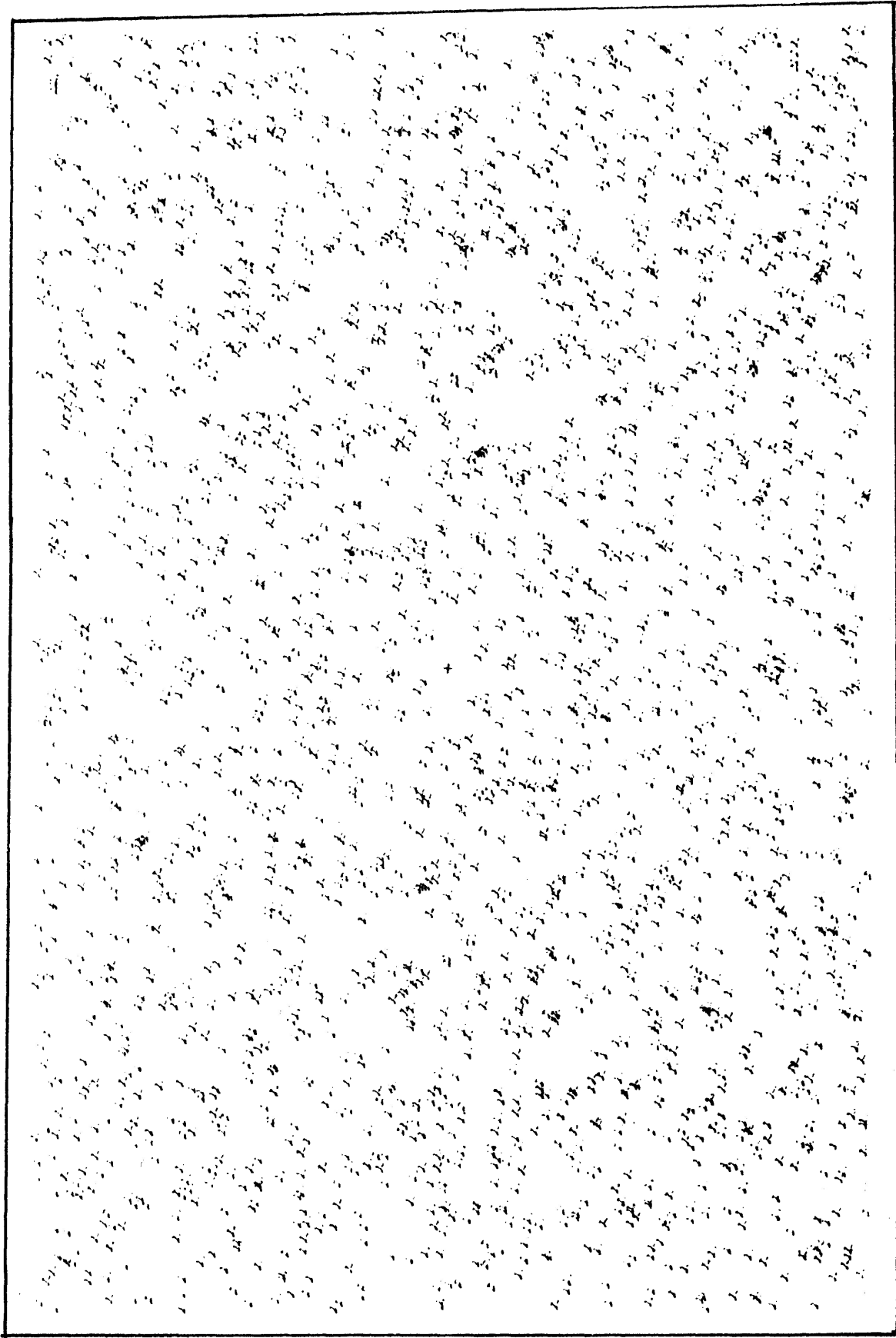
scale x4  
strain ratio 3.8:1

**FIG. 3-27**



—L-S, horizontal  
#7 CROWROCK INLET  
S ————— S  
scale x2  
strain ratio 2.5:1

**FIG. 3-28**



L-S, horizontal  
#8 CROWROCK INLET

S ————— S

scale x2  
strain ratio 3.1:1

**FIG. 3-29**

X/Z ratios are listed in Table 3-3. In all these samples but one (#2 Seagull Island) the strain ellipse long axis was parallel to the schistosity. Examining the plots reveals that the method provided clearer results (point free region) for some samples than others. The method appears to provide a superior means of obtaining a strain estimate than the centre to centre method. The eight plots above were derived from the same data which were used for the centre to centre method (Figs. 3-9 to 3-16). The centre to centre method did not provide satisfactory strain estimates from these data.

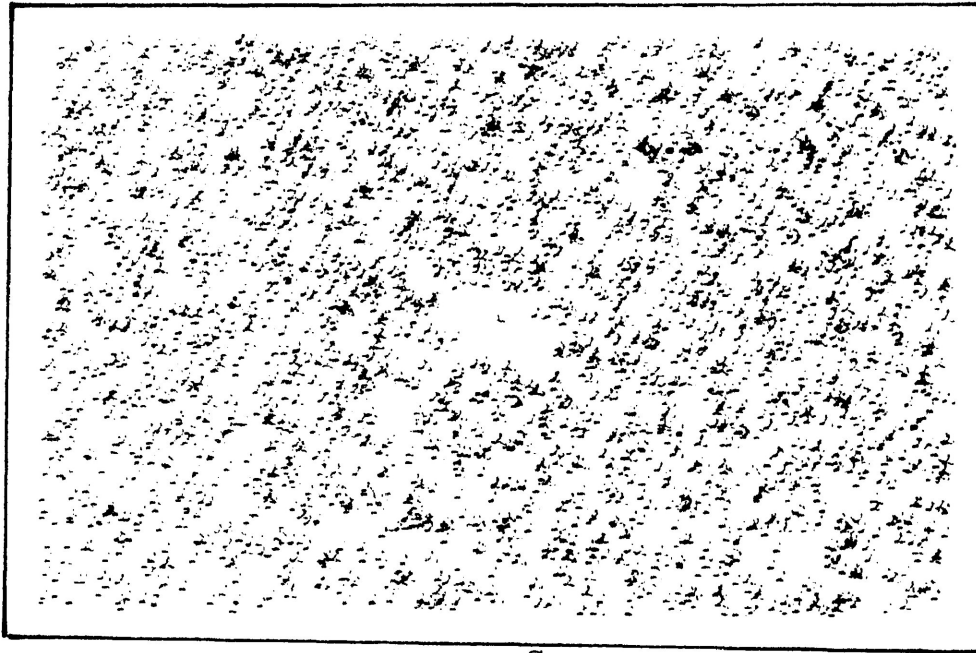
The method was also used to obtain three dimensional strain estimates from cut surfaces of oriented specimens and from thin sections. Pairs of cut surfaces (slabs) and thin sections were cut normal to the schistosity, perpendicular and parallel to a lineation where one was visible. Where a lineation was absent the sections were cut normal to the schistosity, normal and parallel to the dip direction of the schistosity as this generally approximates the orientation of the sections in samples where a lineation was present. These planes also tend to be relatively near the horizontal and vertical planes respectively and are referred to as such on the diagrams (Figures 3-30 to 3-55). The location of grain centres were recorded for the grains, feldspar or quartz, and coordinates of the points were determined. The plots produced comprise Figures 3-30 through 3-55. The results of

Table 3-3: Strain Analysis Results  
All Object-Object Separations Method  
Data from outcrops

Sample	X/Z	n
Seagull Island #1	1.6	199
Seagull Island #2	2.0	194
Dads Island #3	1.5	186
Dads Island #4	2.3	96
Raith #5	3.6	197
Raith #6	3.8	191
Crowrock Inlet #7	2.5	198
Crowrock Inlet #8	3.1	156

n = number of points in original plot





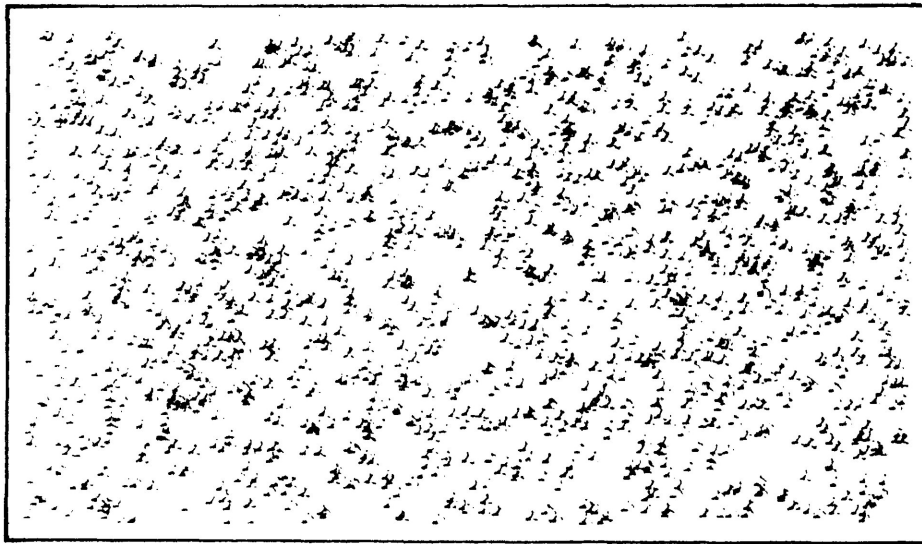
└ S, horizontal

Thin Section: Bor-80-M89A-2  
DANCE TOWNSHIP

S  
|  
S

scale x6  
strain ratio 3.1:1

**FIG. 3-30**



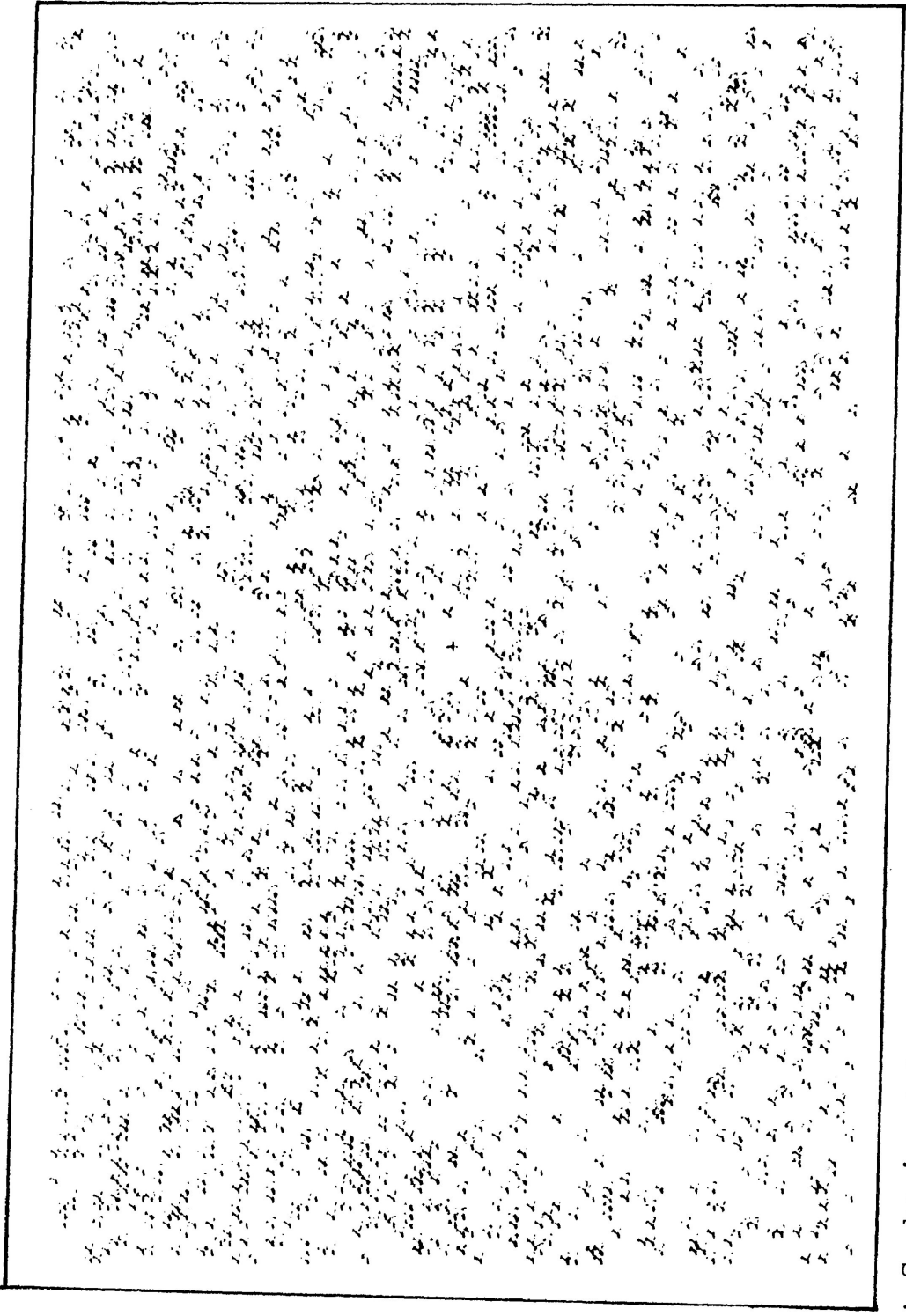
└ S, vertical

Thin Section: Bor-80-M89A-1  
DANCE TOWNSHIP

S  
|  
S

scale x6  
strain ratio 2.6:1

**FIG. 3-31**

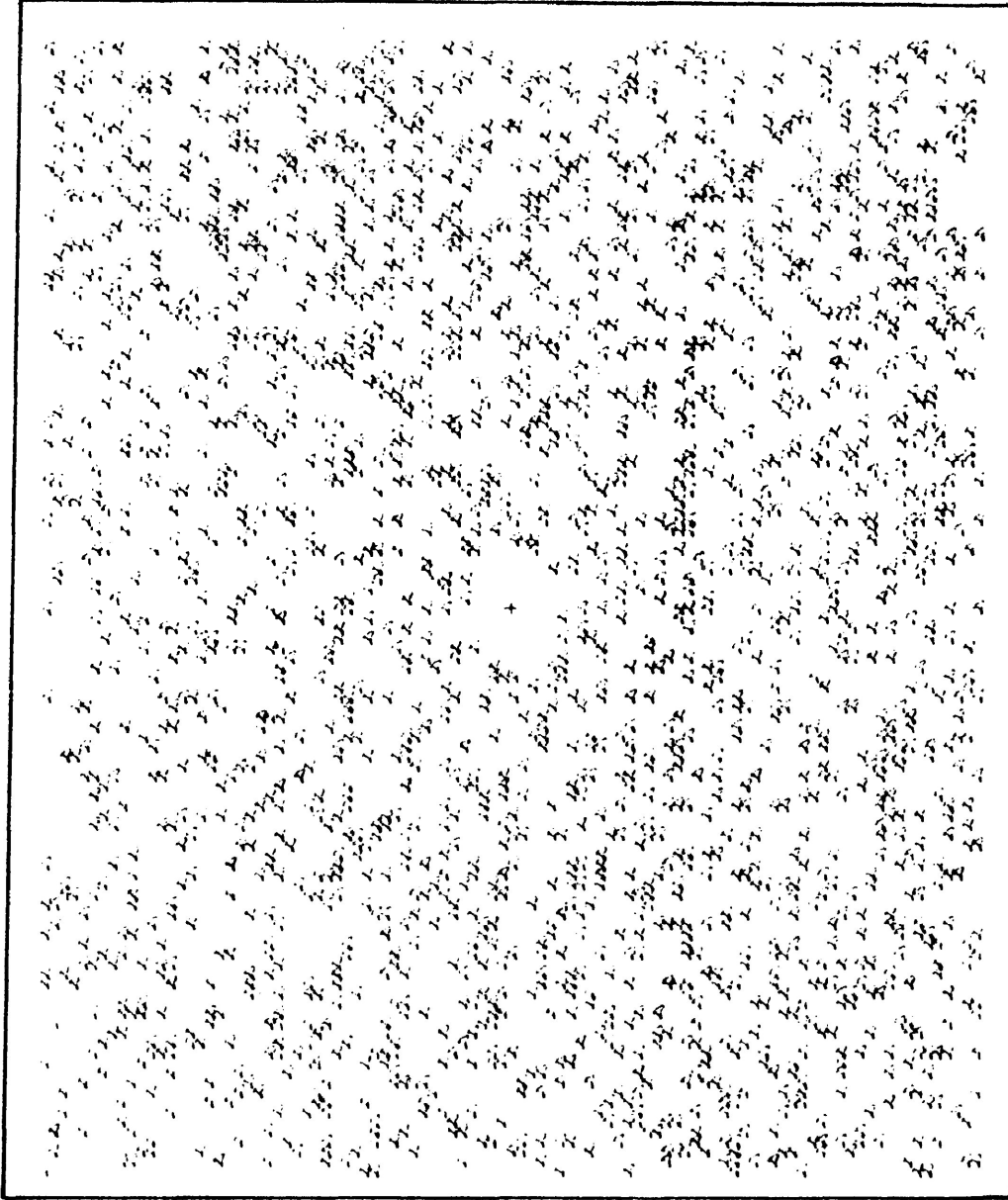


L-S, horizontal  
Bor-80-M89A-2  
DANCE TOWNSHIP

S ————— S

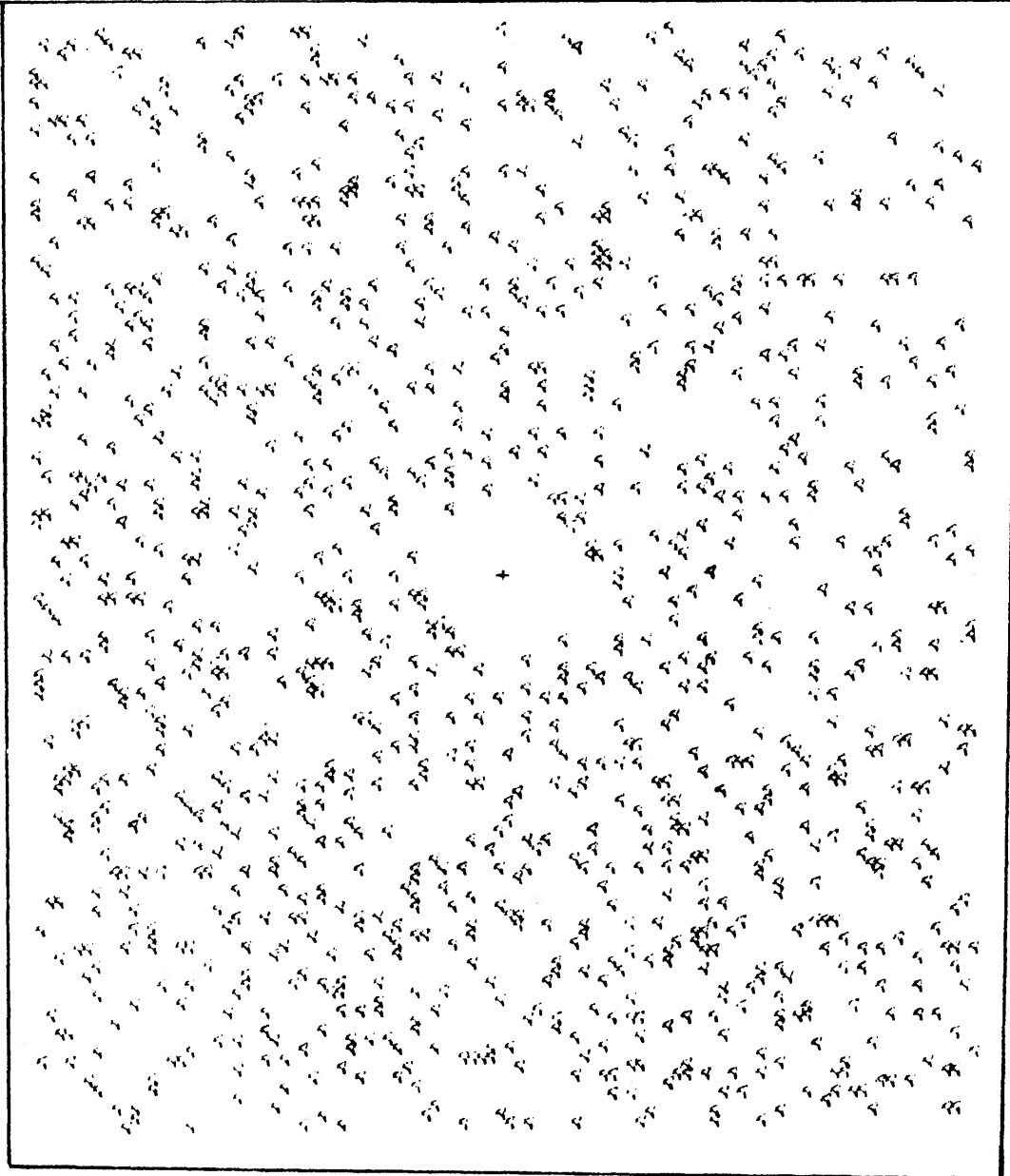
scale x5  
strain ratio 2.0:1

**FIG. 3-32**



L-S, vertical S ————— S scale x5  
Bor-80-M89A-1 strain ratio 1.9:1  
DANCE TOWNSHIP

**FIG. 3-33**

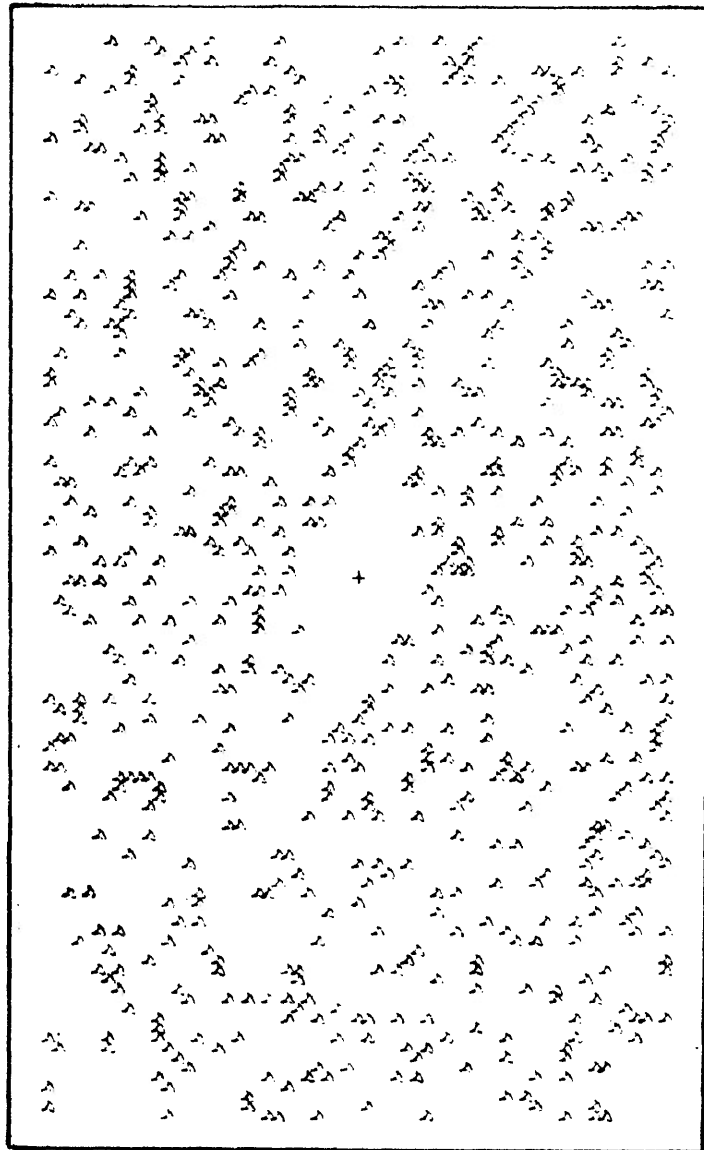


L-S, horizontal S — S scale x5

Bor-80-M123A strain ratio 1.3:1

LITTLE TURTLE LAKE

**FIG. 3-34**



⊥ S, vertical

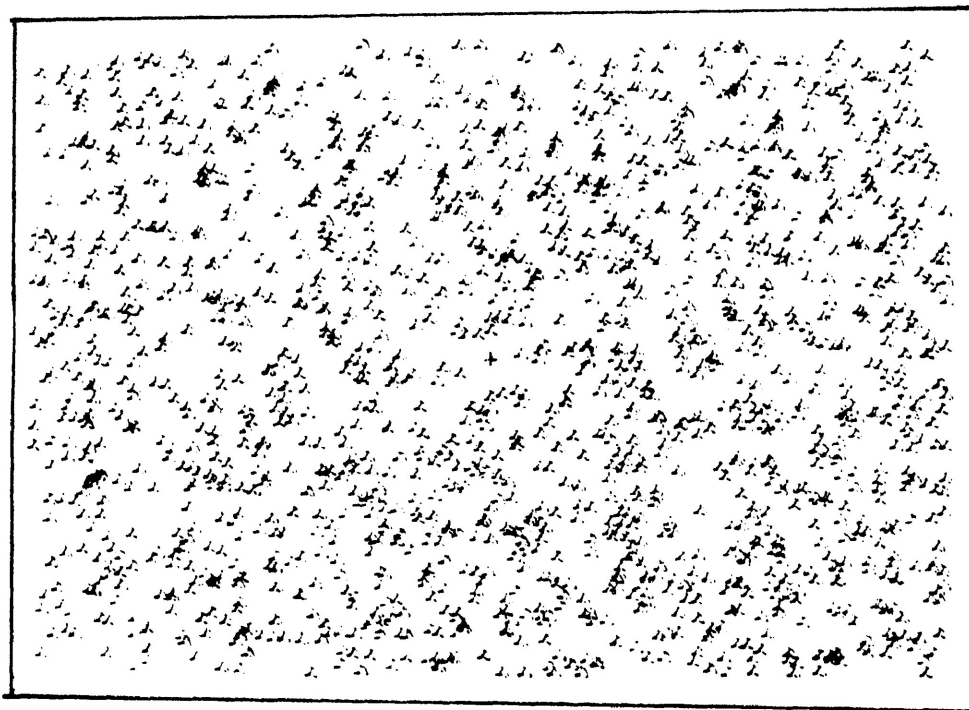
S ————— S

scale x5

Bor-80-M123B  
LITTLE TURTLE LAKE

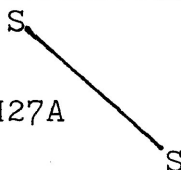
strain ratio 2.0:1

**FIG. 3-35**



⊥ S, horizontal

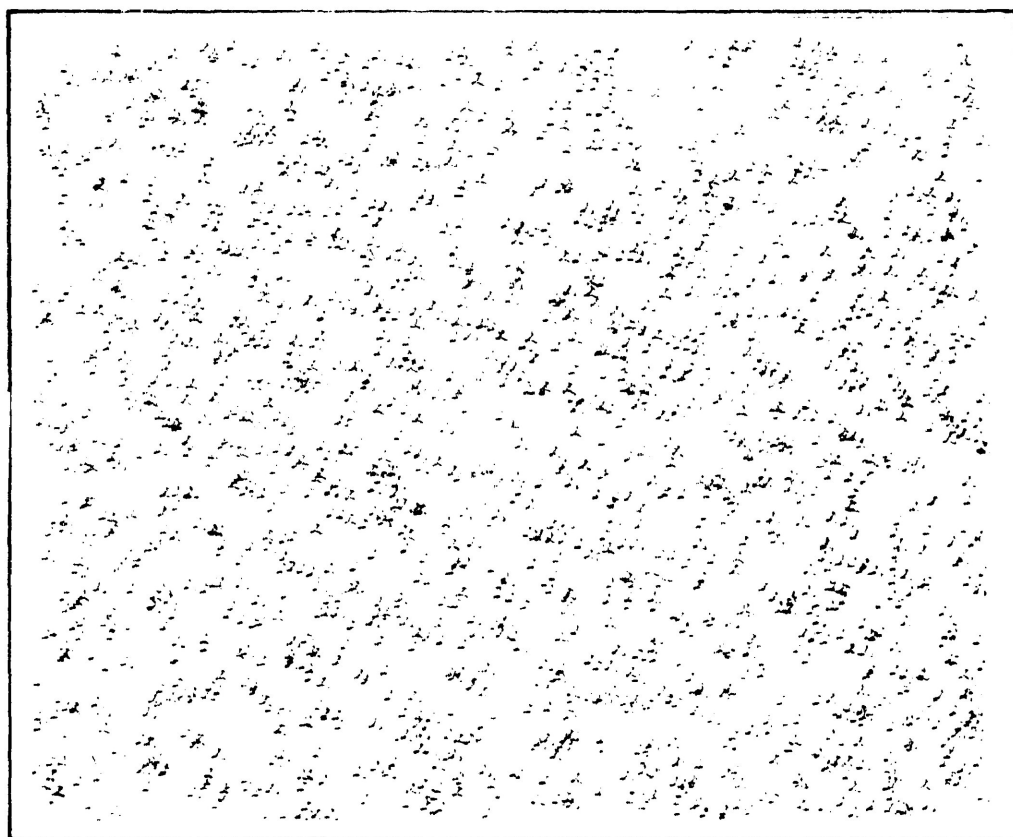
Thin Section: Bor-80-M27A  
KASHABOWIE LAKE



scale x9

strain ratio 4.8:1

**FIG. 3-36**



⊥ S, vertical

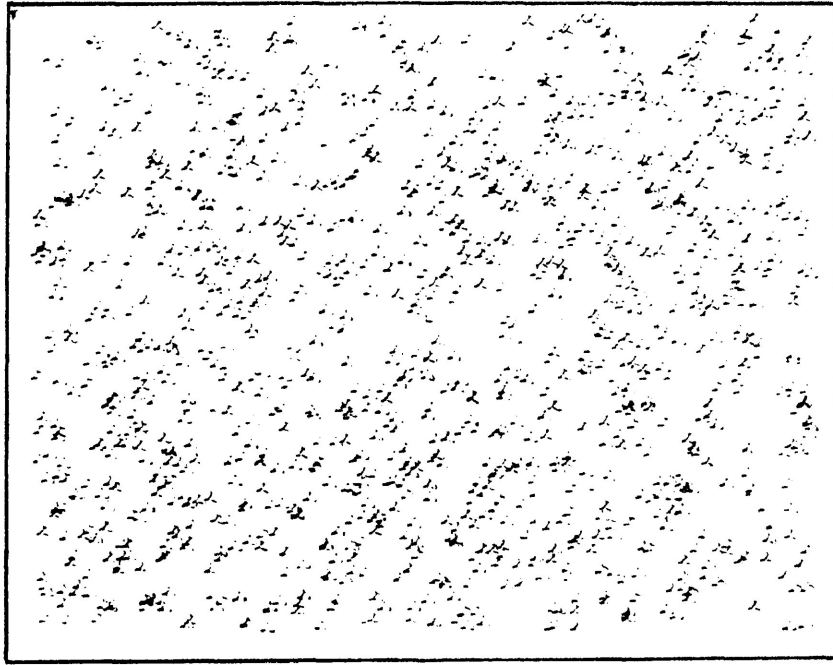
Thin Section: Bor-80-M27B  
KASHABOWIE LAKE



scale x17.5

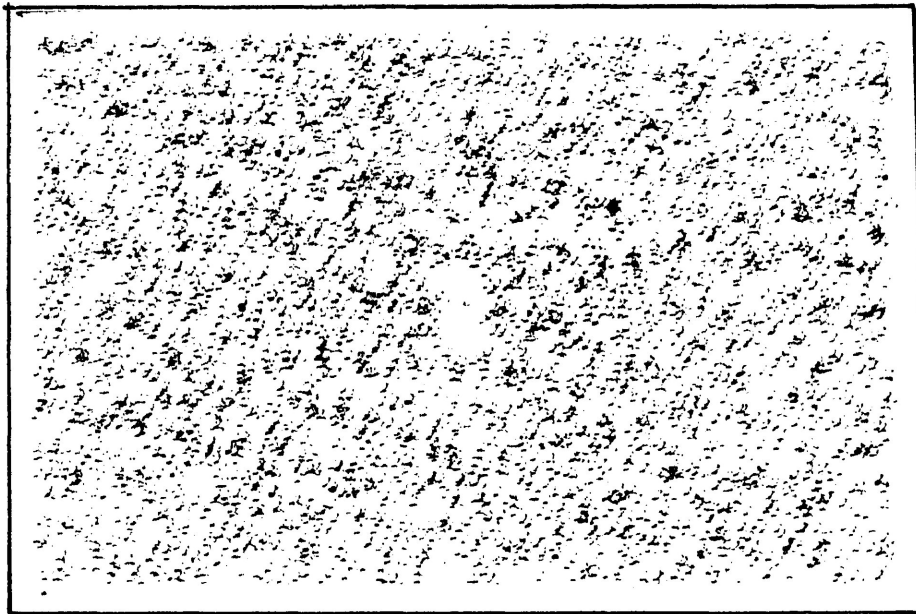
strain ratio 3.4:1

**FIG. 3-37**



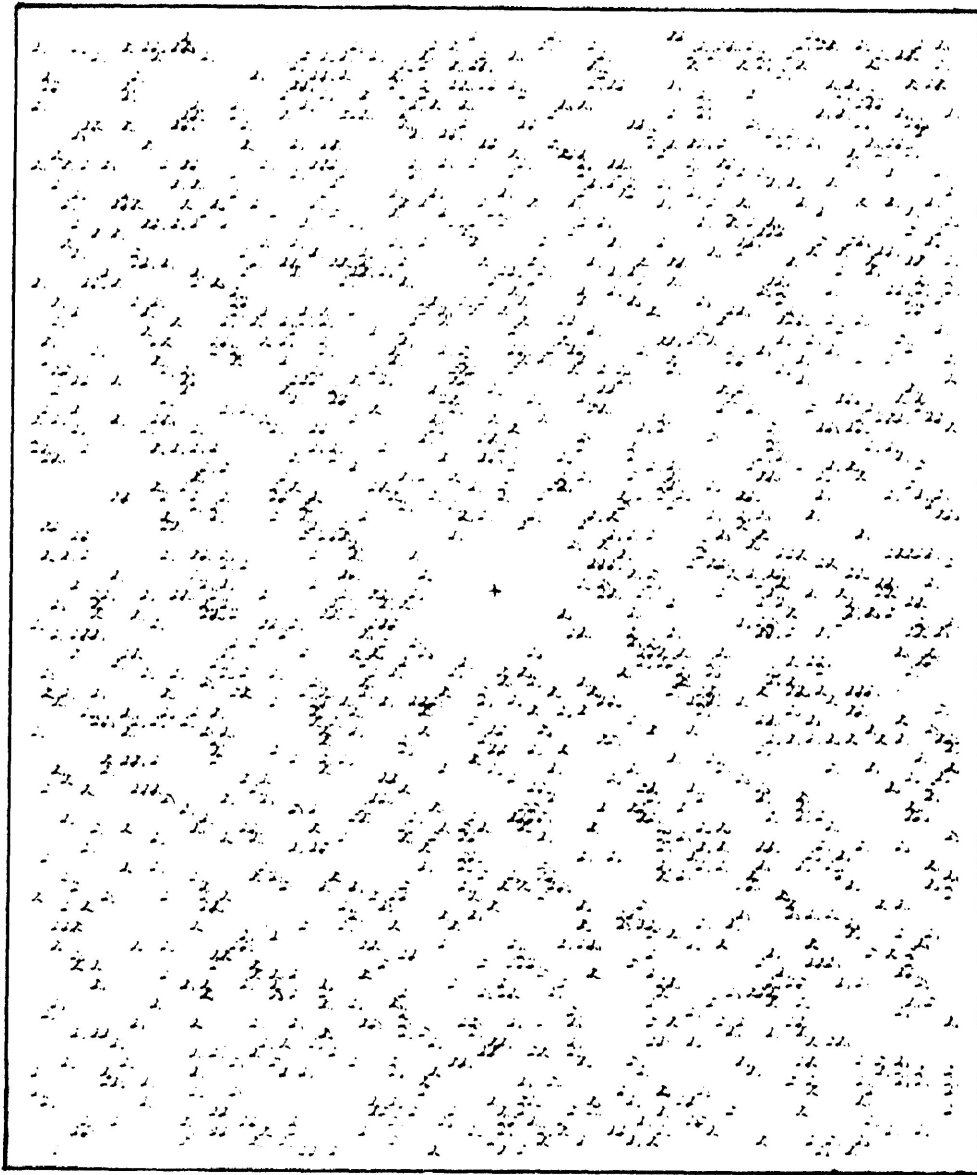
⊥ S, horizontal      S ————— S      scale x9  
 Thin Section: Bor-80-26A      strain ratio 5.3:1  
 ATHELSTANE LAKE

**FIG. 3-38**



⊥ S, vertical      S  
 Thin Section: Bor-80-26B      |      scale x9  
 ATHELSTANE LAKE      S      strain ratio 1.9:1

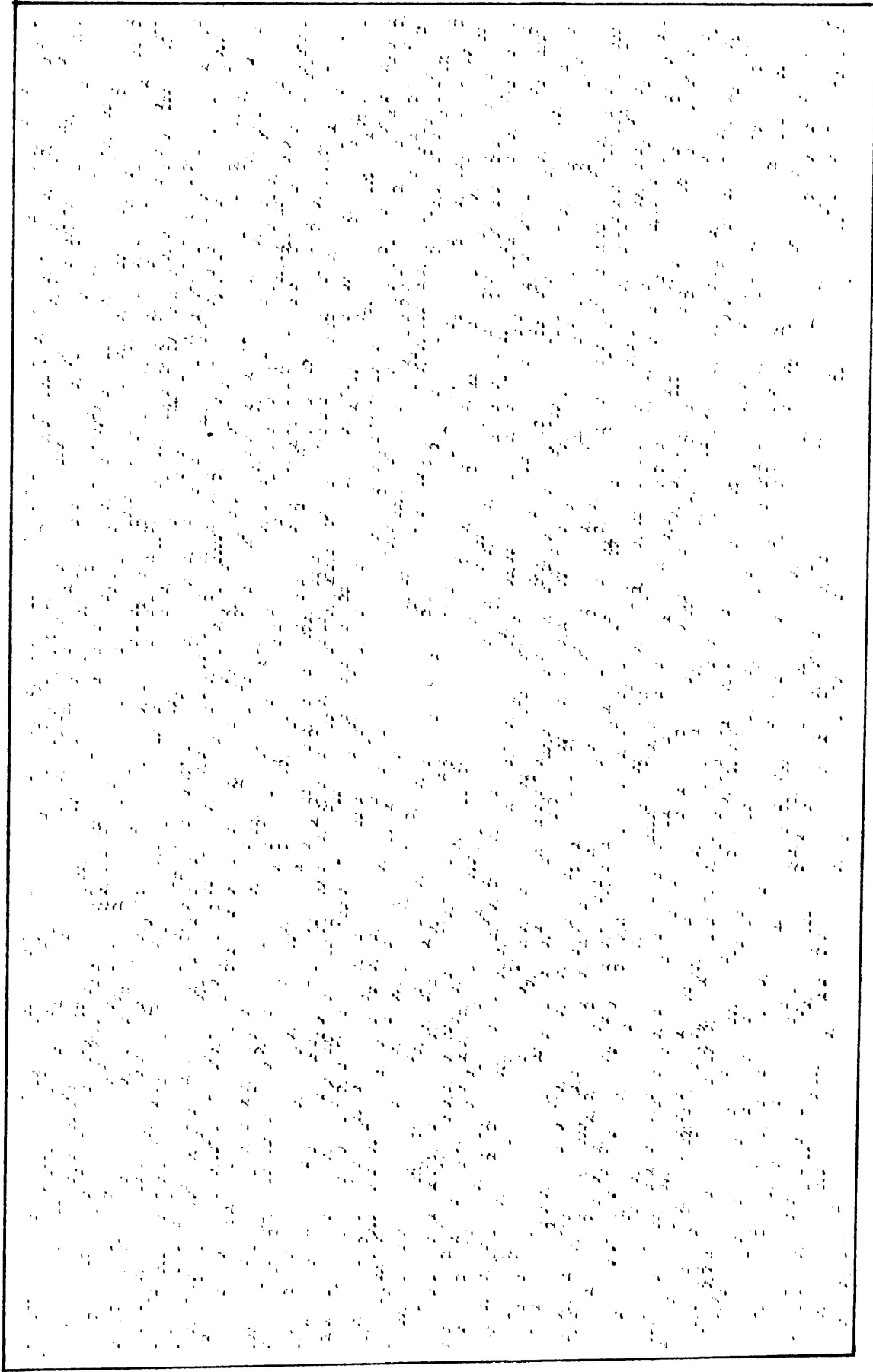
**FIG. 3-39**



└ S, horizontal S————S scale x5  
Bor-80-19A strain ratio 1.4:1  
ATHELSTANE LAKE

**FIG. 3-40**





— S, vertical

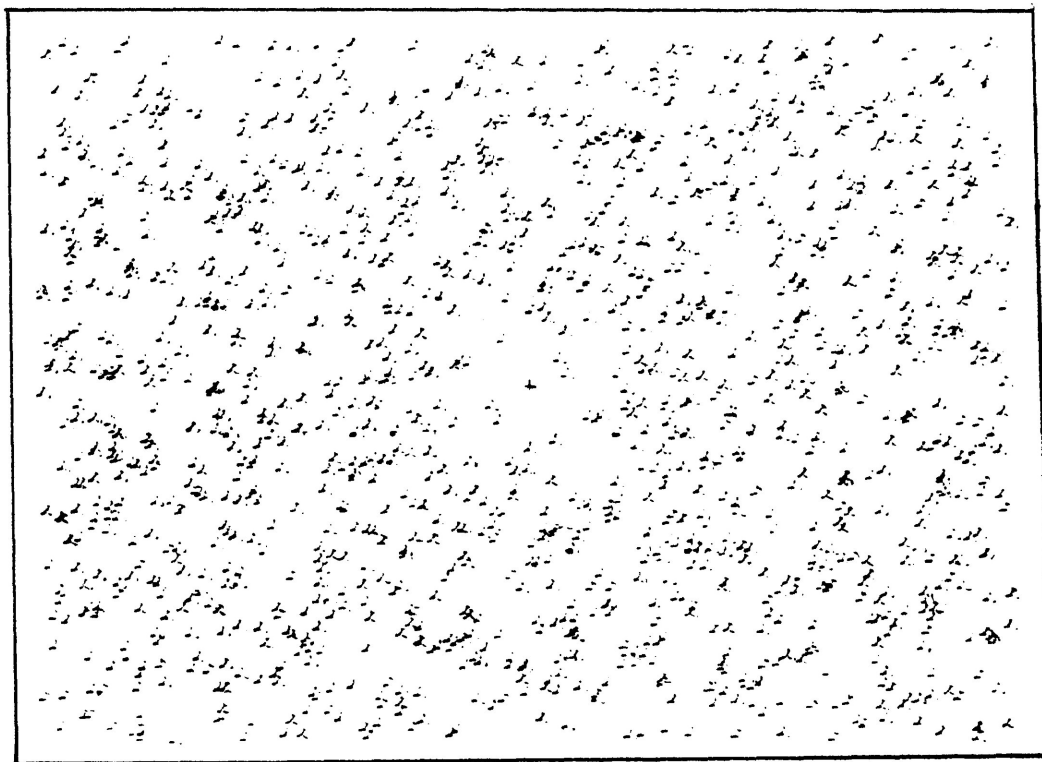
Bor-80-19B  
ATHELSTANE LAKE

— S —

scale x5

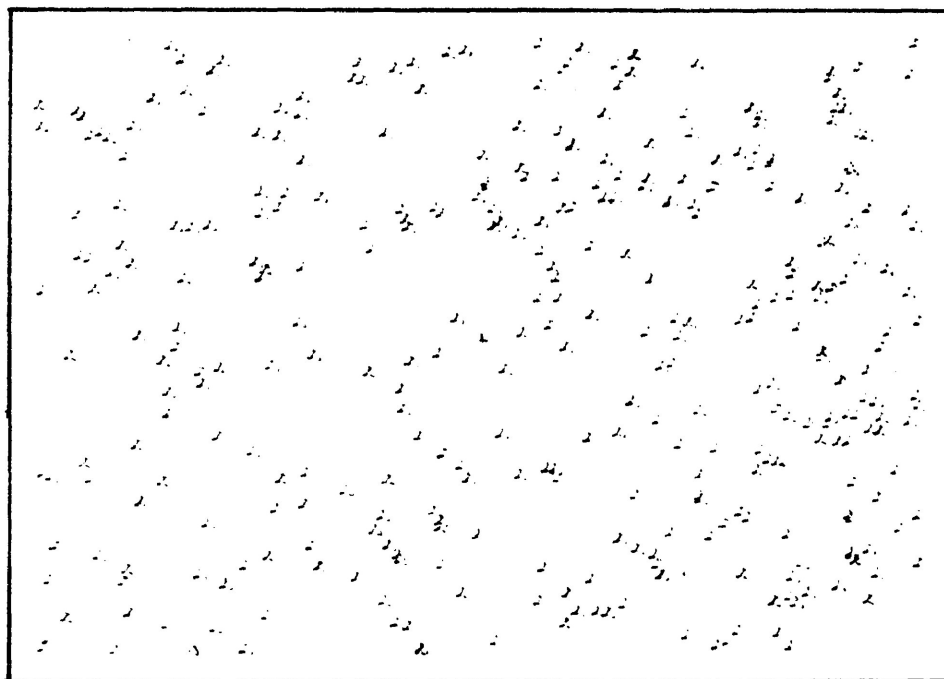
strain ratio 1.3:1

**FIG. 3-41**



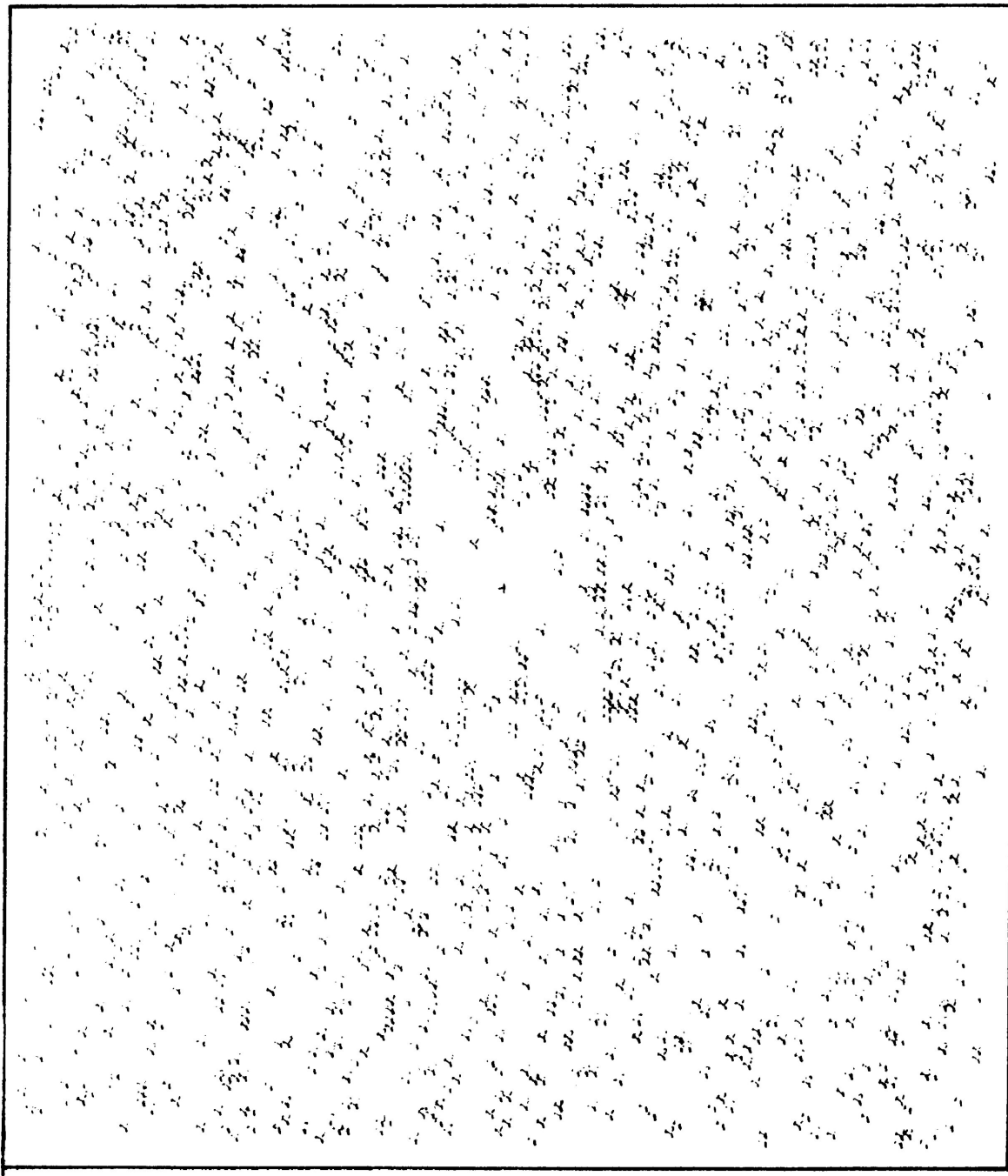
⊥ S, horizontal      S—————S      scale x9  
Thin Section: Bor-80-M11B      strain ratio 4.0:1  
RAITH

**FIG. 3-42**



⊥ S, vertical      S—————S      scale x9  
Thin Section: Bor-80-M11      strain ratio ?  
RAITH

**FIG. 3-43**

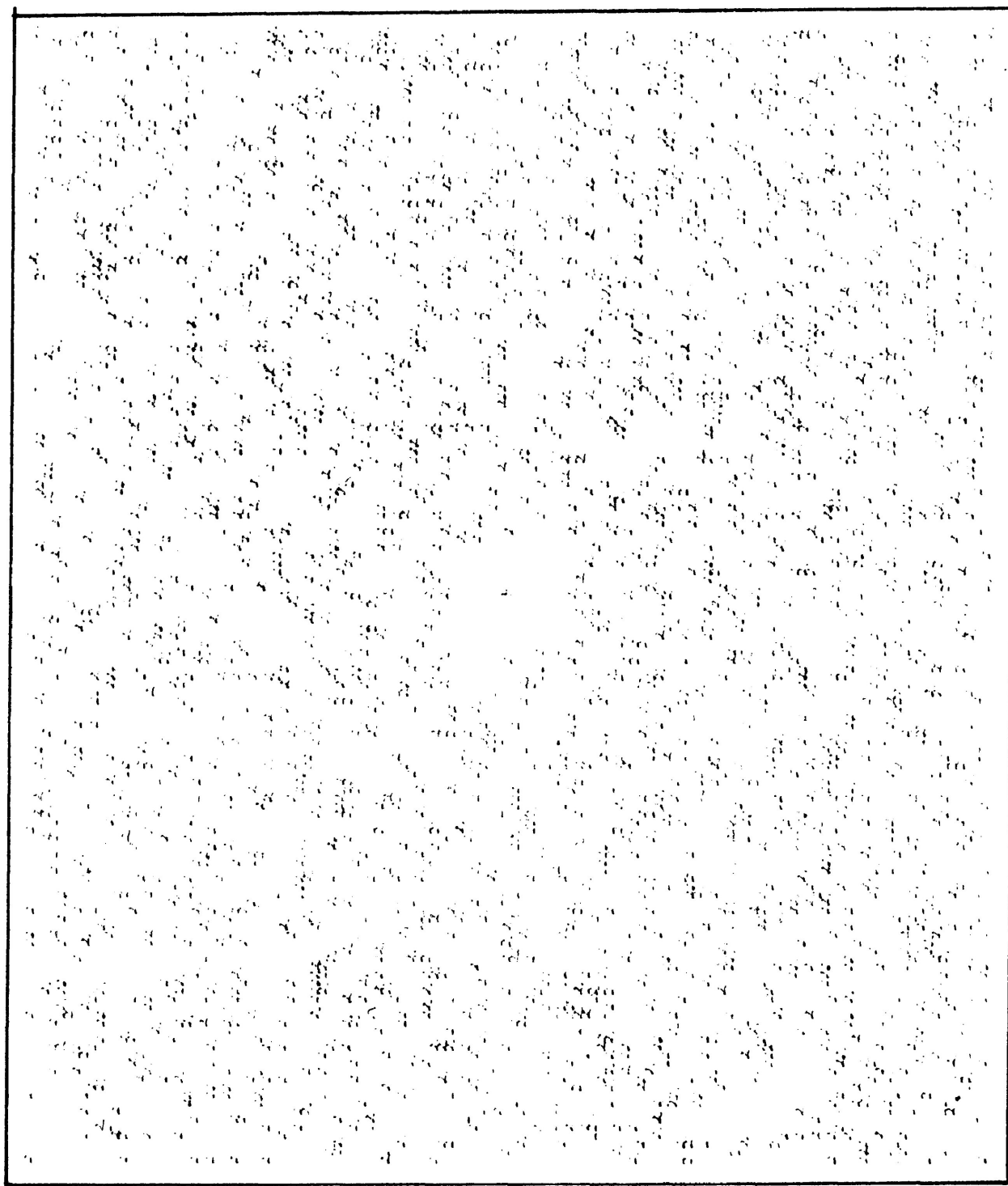


scale x5  
strain ratio 2.5:1

S  
S

—S, horizontal  
Bor-80-M19A  
DOG LAKE

**FIG. 3-44**



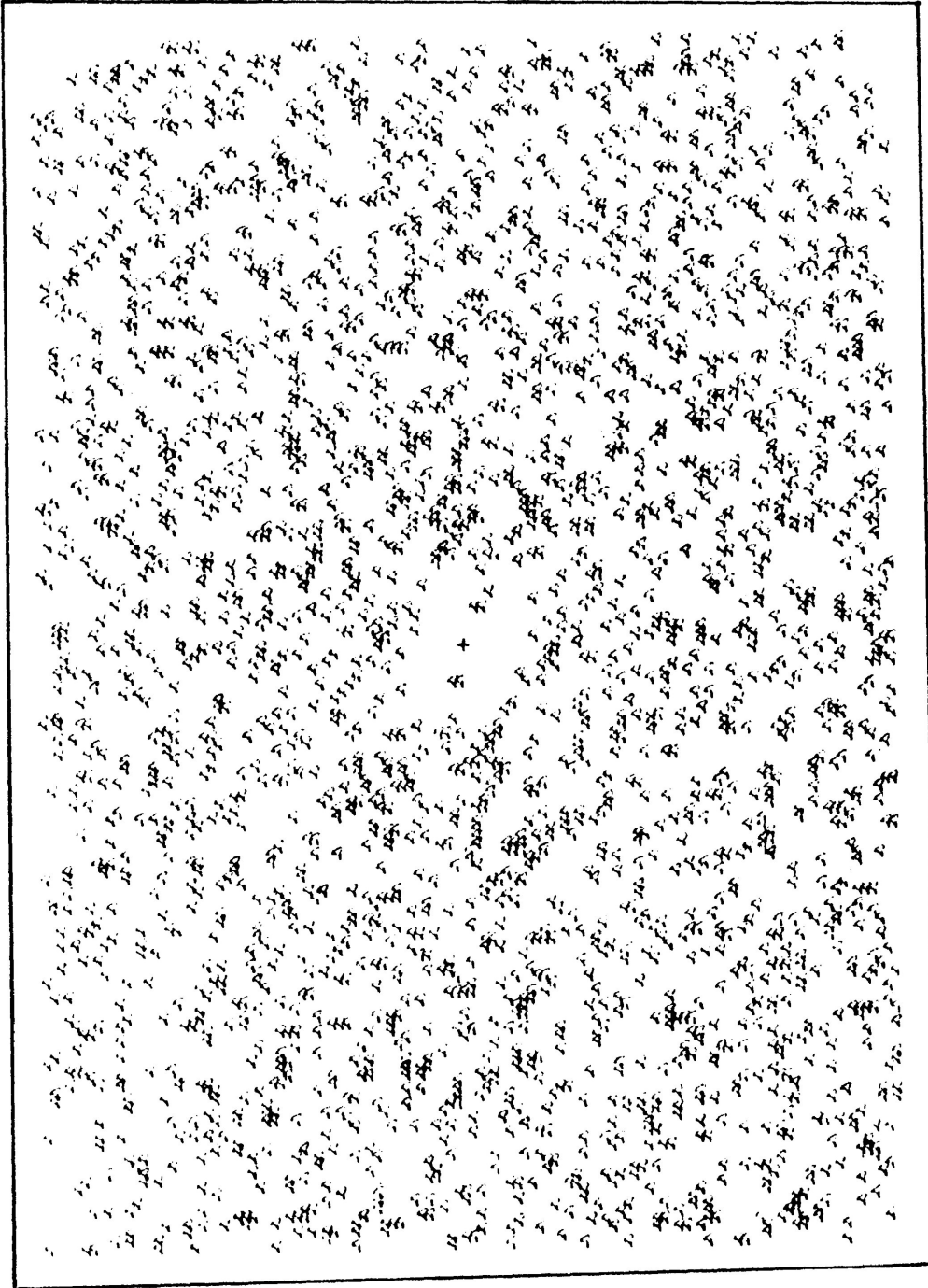
—LS, vertical

S — S

scale x5  
strain ratio 1.8:1

Bor-80-M19B  
DOG LAKE

**FIG. 3-45**

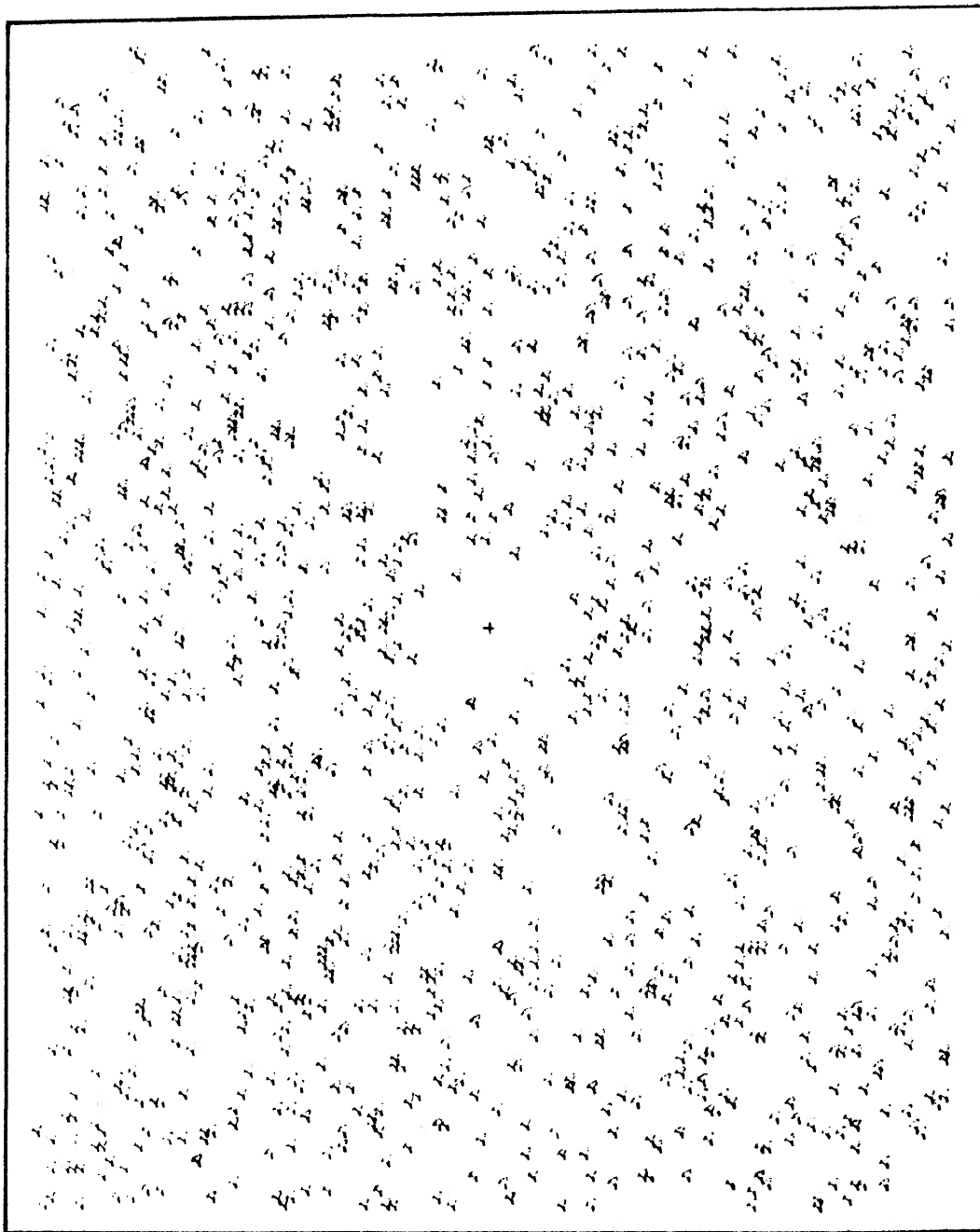


scale x4  
strain ratio 1.4:1



J-S, horizontal  
Bor-80-M20A  
DOG LAKE

**FIG. 3-46**



— S, vertical

— S

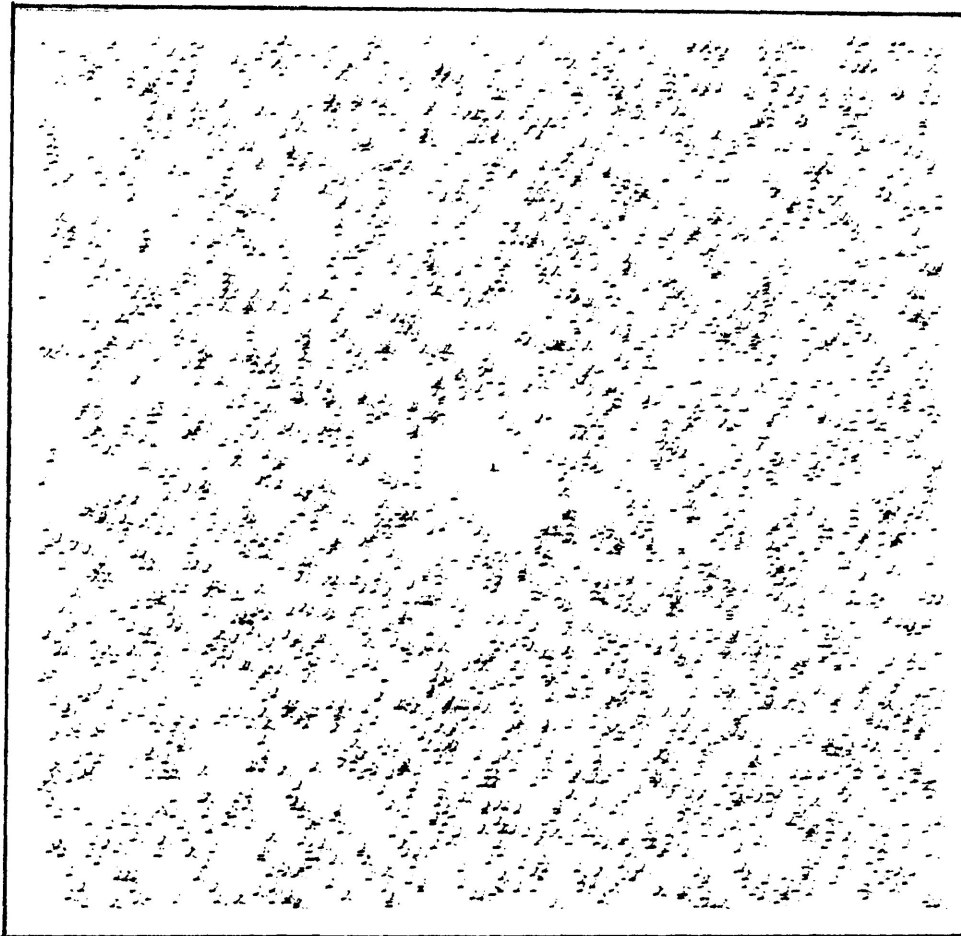
scale x4

S

Bor-80-M20B

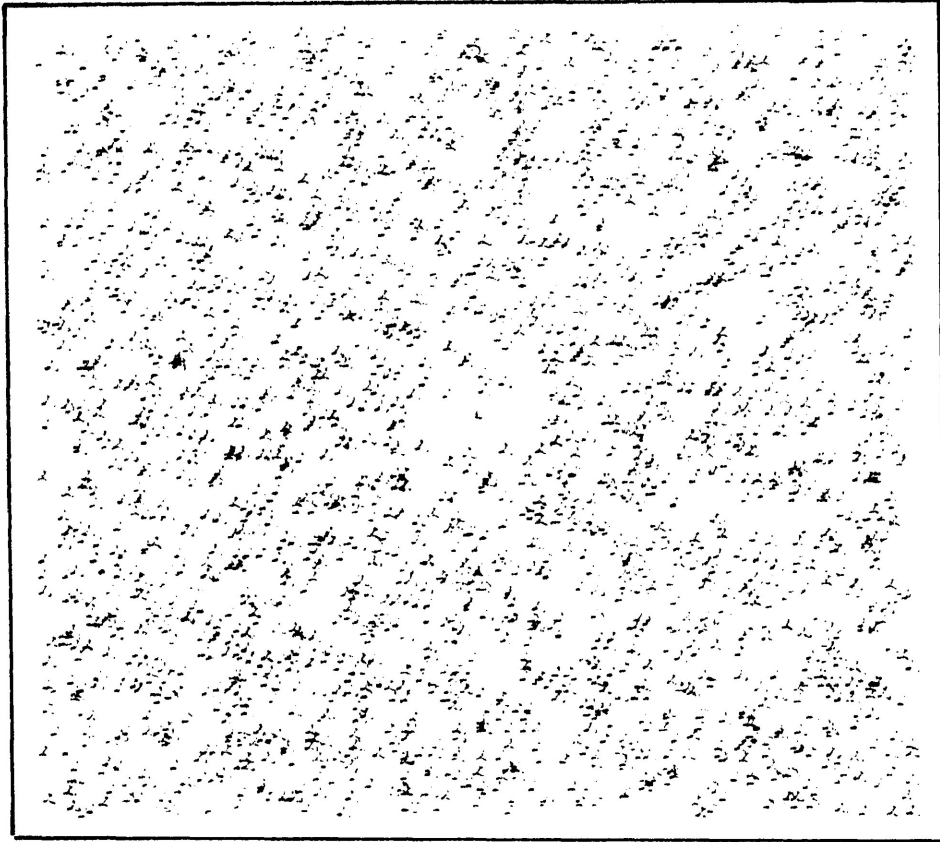
DOG LAKE

**FIG. 3-47**



—L.S, horizontal      S—————S      scale x35  
Thin Section: Bor-80-M22A      strain ratio 1.7:1  
DOG LAKE

**FIG. 3-48**



└ S, vertical      S—————S      scale x35  
Thin Section: Bor-80-M22B      strain ratio 2.7:1  
DOG LAKE

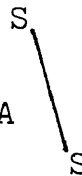
**FIG. 3-49**





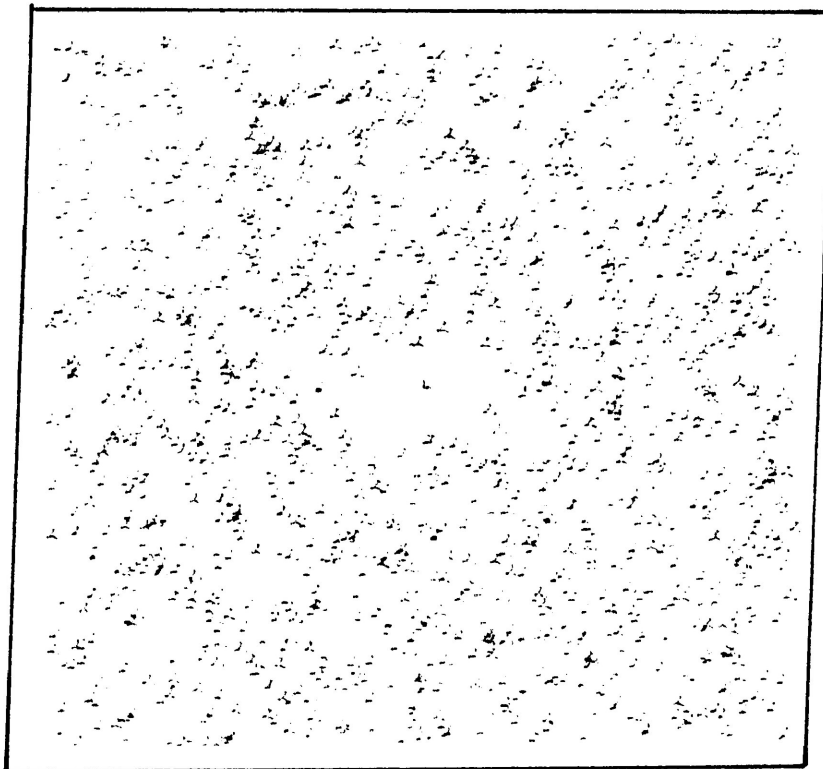
⊥ S, horizontal

Thin Section: Bor-80-M155A  
DOG LAKE



scale x9  
strain ratio 1.7:1

**FIG. 3-50**

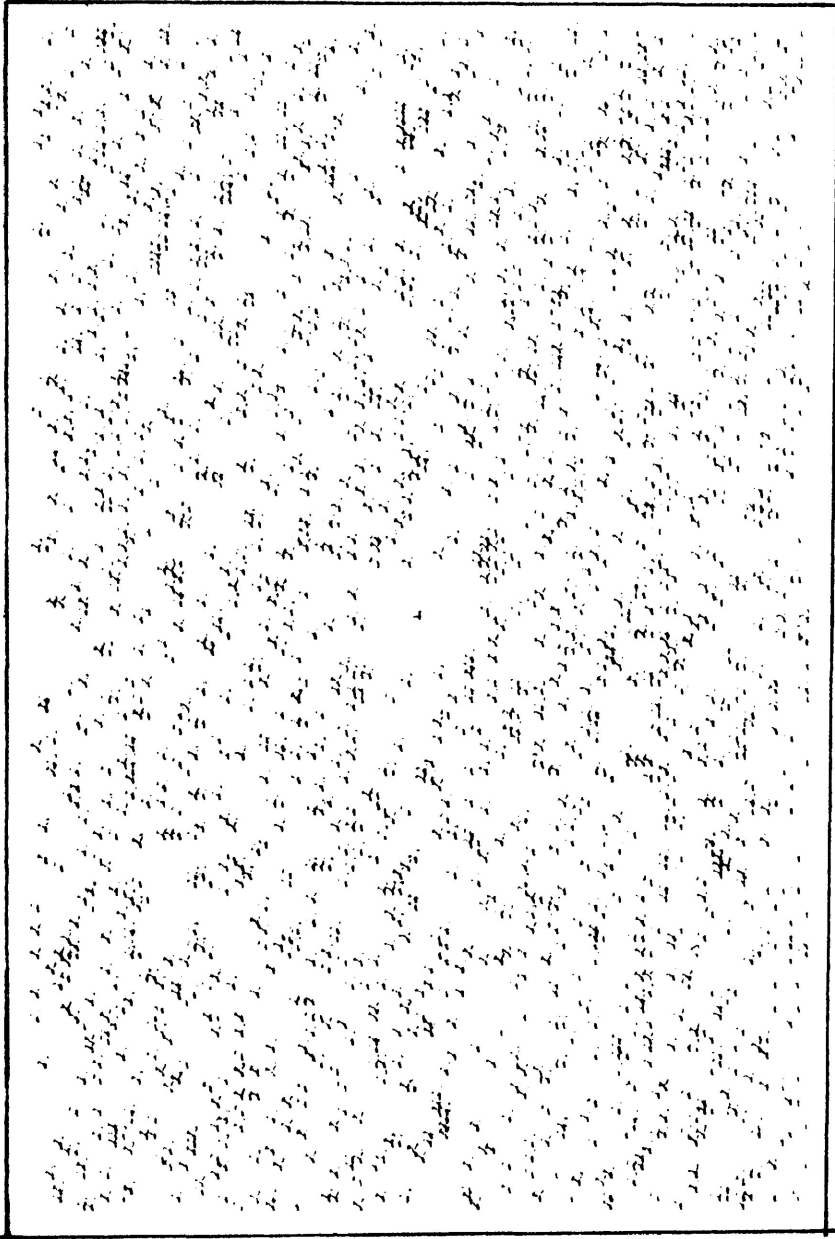


⊥ S, vertical

Thin Section: Bor-80-M155B strain ratio 1.7:1  
DOG LAKE

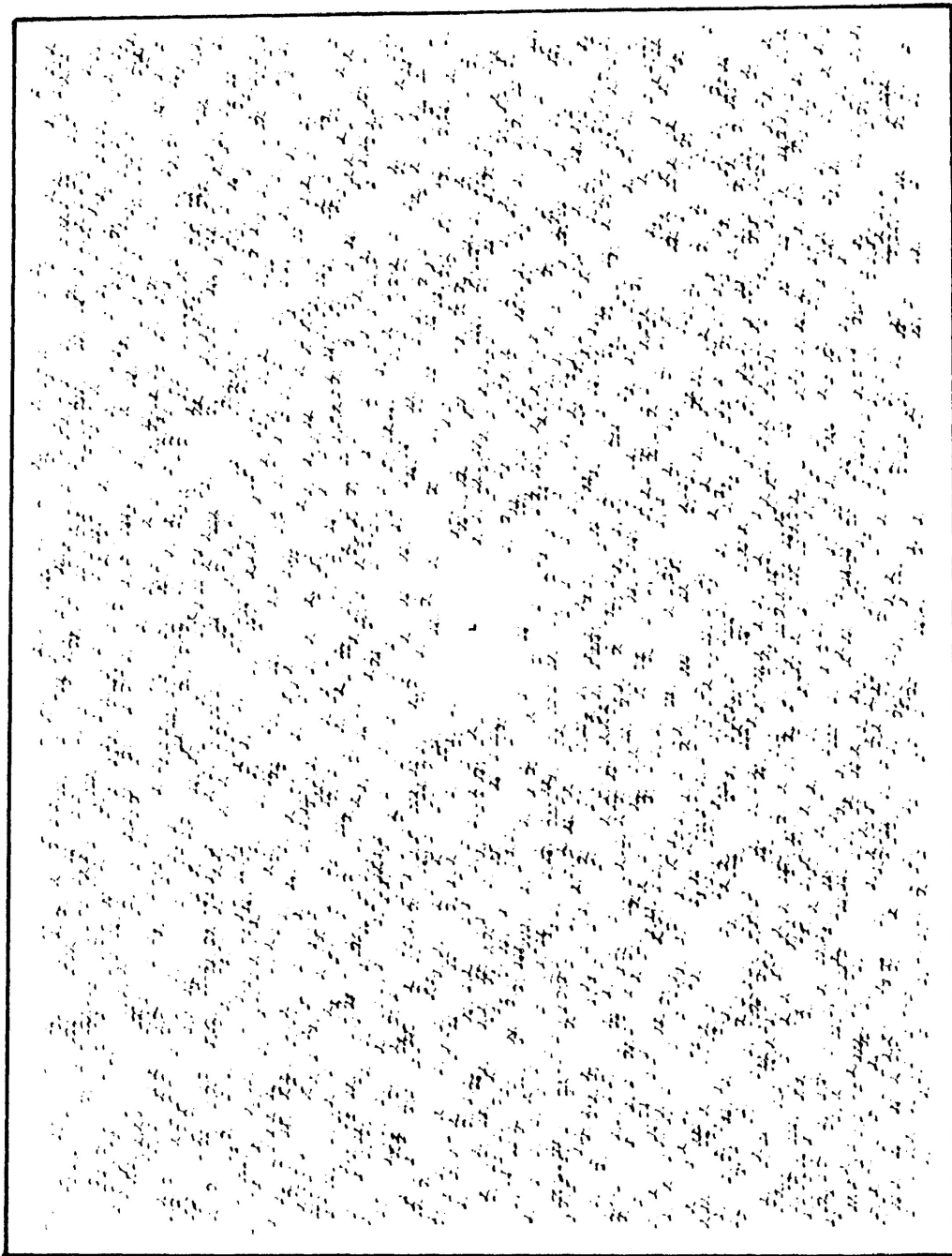
S ————— S scale x9

**FIG. 3-51**



—L—S, horizontal S———S scale x4 strain ratio 3.3:1  
Bor-80-15A  
HIGHWAY 527

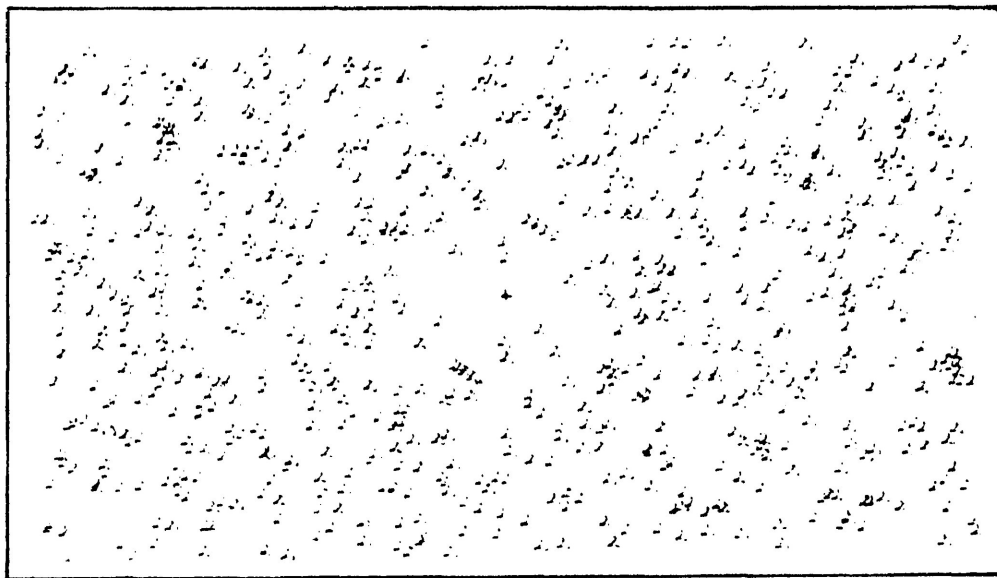
**FIG. 3-52**



└S, vertical  
Bor-80-15B  
HIGHWAY 527

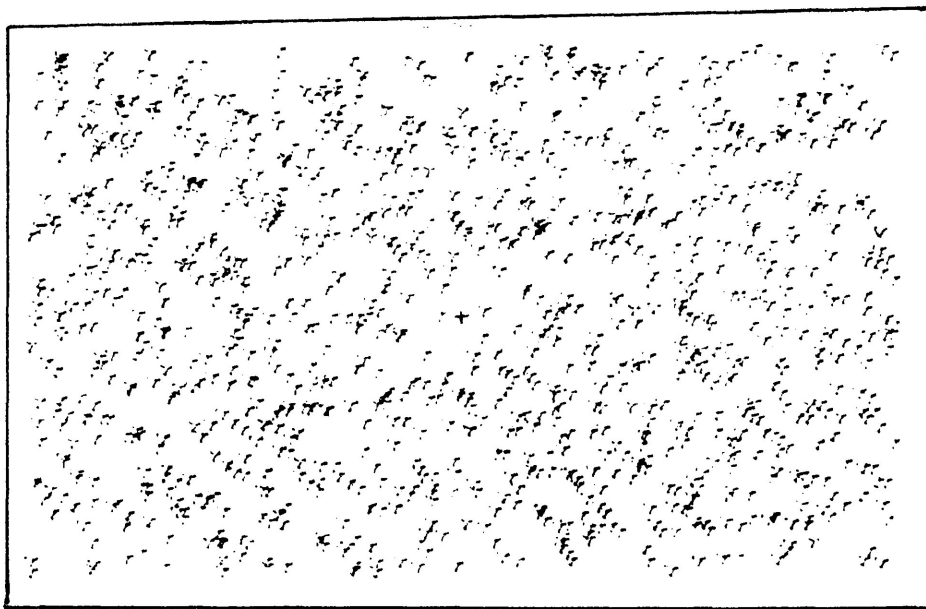
S ————— S scale x4  
strain ratio 2.3:1

**FIG. 3-53**



⊥ S, horizontal      S—————S      scale x6.5  
 Thin Section: Bor-80-15A      strain ratio 4.4:1  
 HIGHWAY 527

**FIG. 3-54**



⊥ S, vertical      S—————S      scale x6.5  
 Thin Section: Bor-80-15B      strain ratio 3.6:1  
 HIGHWAY 527

**FIG. 3-55**

the strain analysis are shown in Table 3-4. The table also indicates whether quartz or feldspar grain centres were used and the number of centres comprising the original plot. Some data were not used for determination of the shape of the strain ellipse as indicated on Table 3-4. Assuming that the measurements were made in the XZ (normal to schistosity, parallel to lineation) and YZ (normal to schistosity, normal to lineation) planes of the finite strain ellipsoid the values of  $a(=X/Y)$  and  $b(=Y/Z)$  were determined (Table 3-5). Assuming constant volume deformation the lengths of the principal axes of the strain ellipsoid were determined and are listed in Table 3-5. Figure 3-56 is a Flinn plot of the three dimensional strain analysis results.

All the specimens except one lie in the flattening field of Flinn's deformation plot. Strain determinations were made from both cut surfaces and thin sections for two samples (BOR-80-15, BOR-80-M89A). These measurements from each sample are joined by a line on Figure 3-56. The strain analysis gave similar, but not the same, results in each case. In the first case the strain measured in thin section was greater than that from the cut surface. The reverse was true of the second sample.

#### E) Results and Conclusions of the Strain Study

The results of all three dimensional strain analyses are summarized on the Flinn diagram, Figure 3-57. It appears that the

Table 3-4: All Object-Object Separations Method  
Data from cut surfaces and thin sections

Sample (Locality) Q-quartz F-feldspar		⊥ S    L (XZ) (L to S dip direction) ≈horizontal	n	⊥ S    L (YZ) (   to S dip direction) ≈vertical	n
BOR-80-M89A (slab)	F	2.0	200	1.9	200
BOR-80-M89A (t.s.) (Dance Township)	F	3.1	130	2.6	200
BOR-80-M123 (slab)* (Little Turtle Lake)	F	1.3	155	2.0	110
BOR-80-M27 (t.s.) (Kashabowie Lake)	Q	4.8	156	3.4	158
BOR-80-26 (t.s.) (Athelstane Lake)	Q	5.3	106	1.9	200
BOR-80-19 (t.s.) (Athelstane Lake)	F	1.4	136	1.3	144
BOR-80-M11 (t.s.)* (Raith)	F	4.0	124	?	87
BOR-80-M19 (slab)	F	2.5	146	1.8	175
BOR-80-M20 (slab)*	F	1.4	174	2.8	150
BOR-80-M22 (t.s.)*	F	1.7	156	2.7	200
BOR-80-M155 (t.s.) (Dog Lake)	F	1.7	107	1.7	152
BOR-80-15 (slab)	F	4.4	115	3.6	125
BOR-80-15 (t.s.) (Hwy. 527)	F	3.3	199	2.3	200

n = number of points in original plot

\*These samples were not used for 3-dimensional strain determinations.

M20, M123 - ellipses were not oriented parallel to the schistosity and  
Y/Z > X/Z

M11 - not able to determine Y/Z from plot

M22 - Y/Z > X/Z

Table 3-5: Strain Analysis Results  
 All Object-Object Separations Method  
 Data from cut surfaces and thin sections

Sample	a	b	X : Y : Z	X·Y·Z	$\frac{a-1}{K=b-1}$
BOR-80-M89A					
slab	1.1	1.9	1.3 : 1.2 : 0.6	0.94	0.11
thin section	1.2	2.6	1.6 : 1.3 : 0.5	1.04	0.13
BOR-80-M27	1.4	3.4	1.9 : 1.3 : 0.4	0.99	0.17
BOR-80-26	2.8	1.9	2.5 : 0.9 : 0.5	1.13	2.00
BOR-80-19	1.1	1.3	1.2 : 1.1 : 0.8	1.06	0.33
BOR-80-M19	1.4	1.8	1.5 : 1.1 : 0.6	0.99	0.50
BOR-80-M155	1.0	1.7	1.2 : 1.2 : 0.7	1.01	0.00
BOR-80-15					
slab	1.2	3.6	1.7 : 1.4 : 0.4	0.95	0.08
thin section	1.4	2.3	1.7 : 1.2 : 0.5	1.02	0.31

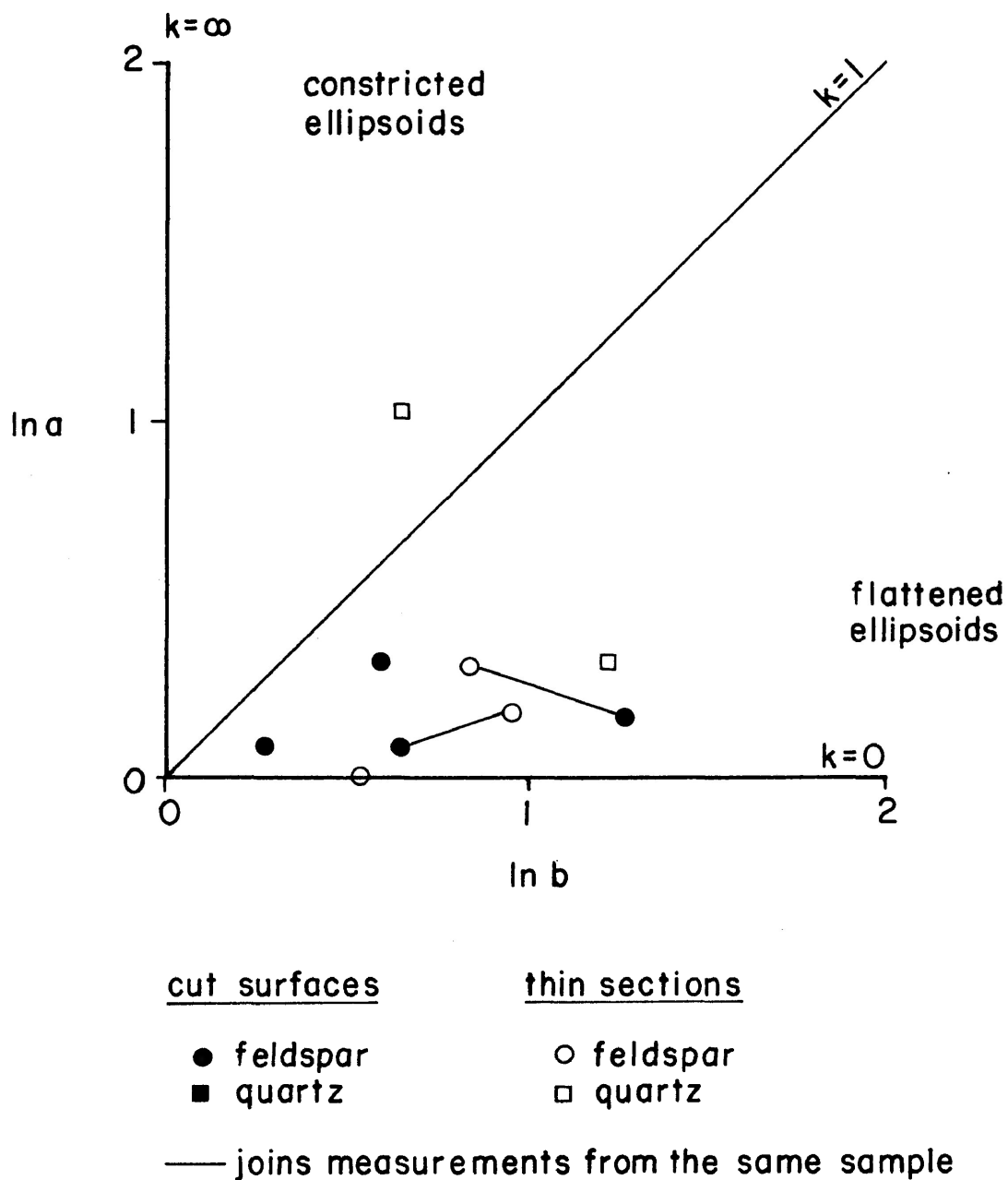
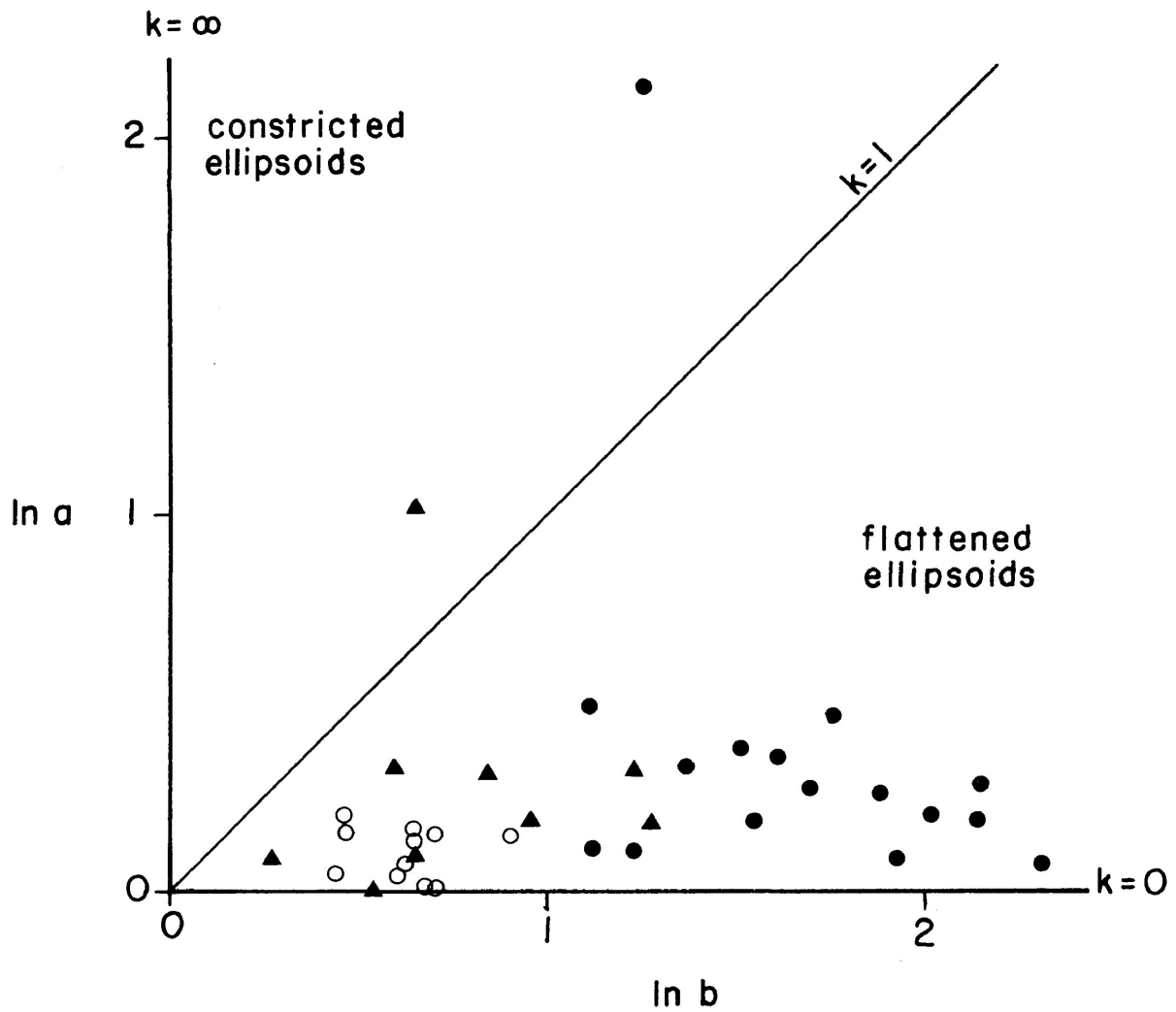


FIG. 3-56: Flinn Plot - Strain determined using the All Object-Object Separations method from cut surfaces and thin sections





- quartz grains - harmonic mean
- feldspar grains - harmonic mean
- ▲ all object-object separations

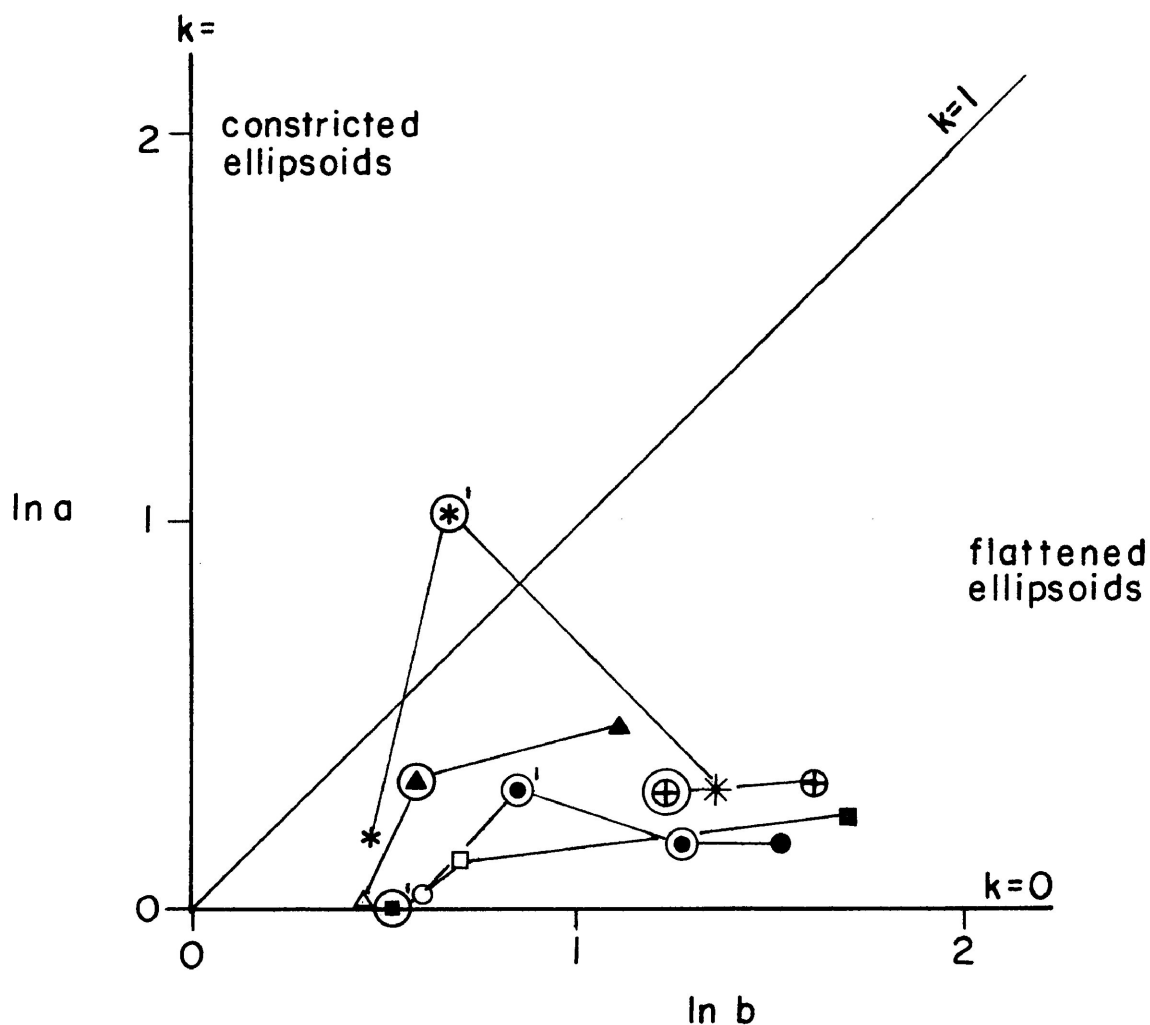
FIG. 3-57: Flinn Plot - Results of Strain Analysis

measurements of deformed shapes of quartz grains gave the largest strain values followed by the determinations using the all object-object separations method. The feldspar grain-shape analysis indicated the lowest strain values. Figure 3-58 further emphasizes this observation. Here strain determinations from the same samples obtained using the two different methods are compared. In each sample the grain-shape analysis of the quartz grains indicates the greatest amount of strain. In all the samples but one (BOR-80-M155) the all object-object separations give the next highest strain estimates followed by the estimates from feldspar grain shapes.

The quartz grain-shape analysis probably provides the closest approximation to the whole rock strain due to ductile deformation. The quartz grains appear to have strained homogeneously with their matrix and, as previously mentioned, generally comprise the matrix in which feldspar grains 'float'. The feldspar grains do not provide a good indication of strain magnitude as they have not deformed homogeneously with their matrix. The grain shape measurements do not take into account rock strain arising from particulate flow.

The centre to centre method was unsuitable for strain determinations in the fault zone as particulate flow made the identification of nearest neighbours before deformation impossible.

Although it should theoretically take into account the strain of matrix and grains the all object-object separations



<u>Sample</u>	<u>Harmonic Mean</u>		<u>All Object-Object</u>
	QUARTZ	FELDSPAR	<u>Separations</u>
	CUT SURFACES (THIN SECTIONS')		
BOR-80-15	●	○	⊙
BOR-80-M155	■	□	⊠
BOR-80-M19	▲	△	⊡
BOR-80-26	*	*	⊛
BOR-80-M27	⊕	⊕	⊕

FIG. 3-58: Flinn Plot - Comparison between results of strain analysis methods

method produced strain values lower than the results of quartz grain shape analysis. This may be due to particulate flow. The spatial distribution of the dispersed markers may have been altered which would affect the strain analysis results. The strain ellipse obtained could be a compromise between the strain arising from particulate flow and the strain due to ductile deformation if the principal axes of strain due to the two components were at an angle to one another. It is also highly possible that the strain within the fault zone is too high to be measured by this method and exceeds Fry's limit of a strain ratio of 6:1 for visual interpretation of the results of the all object-object separations method.

Strain determined from deformed quartz grains indicates an average extension in X of 130%, in Y of 58% and shortening in Z of 71%. This is a minimum strain estimate which does not include strain of rocks arising due to particulate flow.

Figure 3-57 illustrates that strain within the fault zone was predominantly flattening. Only two strain estimates indicate constrictive deformation. The quartz experienced more strain than the feldspar. Due to its ductile nature the quartz may have begun to deform before the feldspar.

The strain ellipse is flattened parallel to the schistosity within the fault zone. The X direction is generally near horizontal, parallel to a lineation which was sometimes

visible. Two samples (BOR-80-M95, BOR-80-M120) indicated that Y was horizontal.

The flattening deformation indicates that simple shear (sensu stricto) alone could not be responsible for the strain within the fault zone as simple shear results in plane strain ( $k=1$ ). Thus the deformation within the fault zone may comprise shear strains with flattening parallel to the shear plane. There is little evidence that volume change has occurred across the fault zone.

## F) Magnetic Susceptibility Anisotropy

The intensity of magnetization produced in a material (J) is related to the applied field (H) by the magnetic susceptibility (k) such that:

$$J=kH$$

Graham (1954) first suggested that the anisotropy of magnetic susceptibility might be a valuable method of petrofabric analysis. Anisotropic magnetic susceptibility in a rock may result from the alignment of magnetocrystalline axes of non-isometric magnetic minerals such as hematite or pyrrhotite or from the preferred orientation of elongate grains of isometric ferrimagnetic minerals such as magnetite. The bulk magnetic susceptibility of a rock may be controlled by small amounts of magnetite even when other magnetic minerals are present due to the higher intrinsic magnetic susceptibility of magnetite compared to hematite and pyrrhotite (Singh et al., 1975) (Rathore, 1979b).

The three dimensional variation in magnetic susceptibility of the magnetic fabric is characterized by the shape of the magnetic susceptibility anisotropy ellipsoid and by the orientation of the three principal susceptibilities  $K_{max}$ ,  $K_{int}$ ,  $K_{min}$ , the maximum, intermediate and minimum susceptibilities. The orientations of the principal susceptibilities may be plotted on a lower hemisphere equal area stereonet. The shape of the susceptibility ellipsoid is described in a similar manner to the strain ellipsoid.

$P_1 = k_{\max}/k_{\text{int}}$  describes the extent to which the fabric is linear  
(magnetic lineation)

$P_3 = k_{\text{int}}/k_{\min}$  describes the extent to which the fabric is planar  
(magnetic foliation)

A "susceptibility plot" of  $P_1$  vs  $P_3$  is comparable to the deformation plot of Flinn (1962) where  $a = X/Y$  is plotted against  $b=Y/Z$  where  $X, Y, Z$  are the principal strain axes ( $X>Y>Z$ ). A line of slope 1 separates ellipsoids which have been constricted from those which have been flattened.

In undeformed rocks the minimum susceptibility generally lies normal to the bedding plane of sedimentary rocks or normal to any flow plane of igneous rocks (Rathore, 1979a). The degree of anisotropy is generally higher in metamorphic rocks and deformed rocks. The minimum susceptibility is normal to cleavage/foliation planes. The magnetic susceptibility anisotropy ellipsoid of tectonites has been shown to equate with planar and linear macroscopic fabric elements where present and to correspond with the principal axes of the total strain ellipsoid (Singh et al., 1975, Wood et al., 1976, Kligfield et al., 1977, Rathore 1979a, b, 1980b, Goldstein, 1980, Rathore and Becke, 1980, Borradaile and Tarling, 1981). Borradaile and Tarling have shown that the depositional magnetic fabric may be retained at 30% shortening when particulate flow was the predominant mechanism of deformation. They propose the tectonic magnetic fabric and depositional magnetic fabric may

interact, where spaced cleavage is present, resulting in the maximum susceptibility lying parallel to the cleavage-bedding intersection.

*Method:* Ten cores, 2.5 cm. in diameter and 2.5 cm in length, were analysed by Dr. D.H. Tarling of the Dept. of Geophysics and Planetary Physics, University of Newcastle upon Tyne using the Complete Results Anisotropy Delineator (Molyneax, 1971). Each core is rotated within two mutually perpendicular coils. The exciting coil produces a 7 Oe magnetic field alternating at 10 kHz which induces a current in the pick up coil which is proportional to the magnetic susceptibility of the specimen in the plane of the instrument. The magnetic susceptibility is measured at regular, small intervals (128 per rotation) throughout each rotation. The sample is rotated about three orthogonal axes. The computer calculates the directions of the principal axes of magnetic susceptibility relative to a fiducial mark on the specimen and the magnitude of the principal axes of the magnetic susceptibility anisotropy ellipsoid (Borradaile and Tarling, 1981).

*Results:* The results of the analyses are presented in Table 3-6 and Figures 3-59 and 3-60. Figure 3-59 illustrates the orientation of the principal axes of the magnetic susceptibility anisotropy ellipsoid along with macroscopic planar and linear elements of

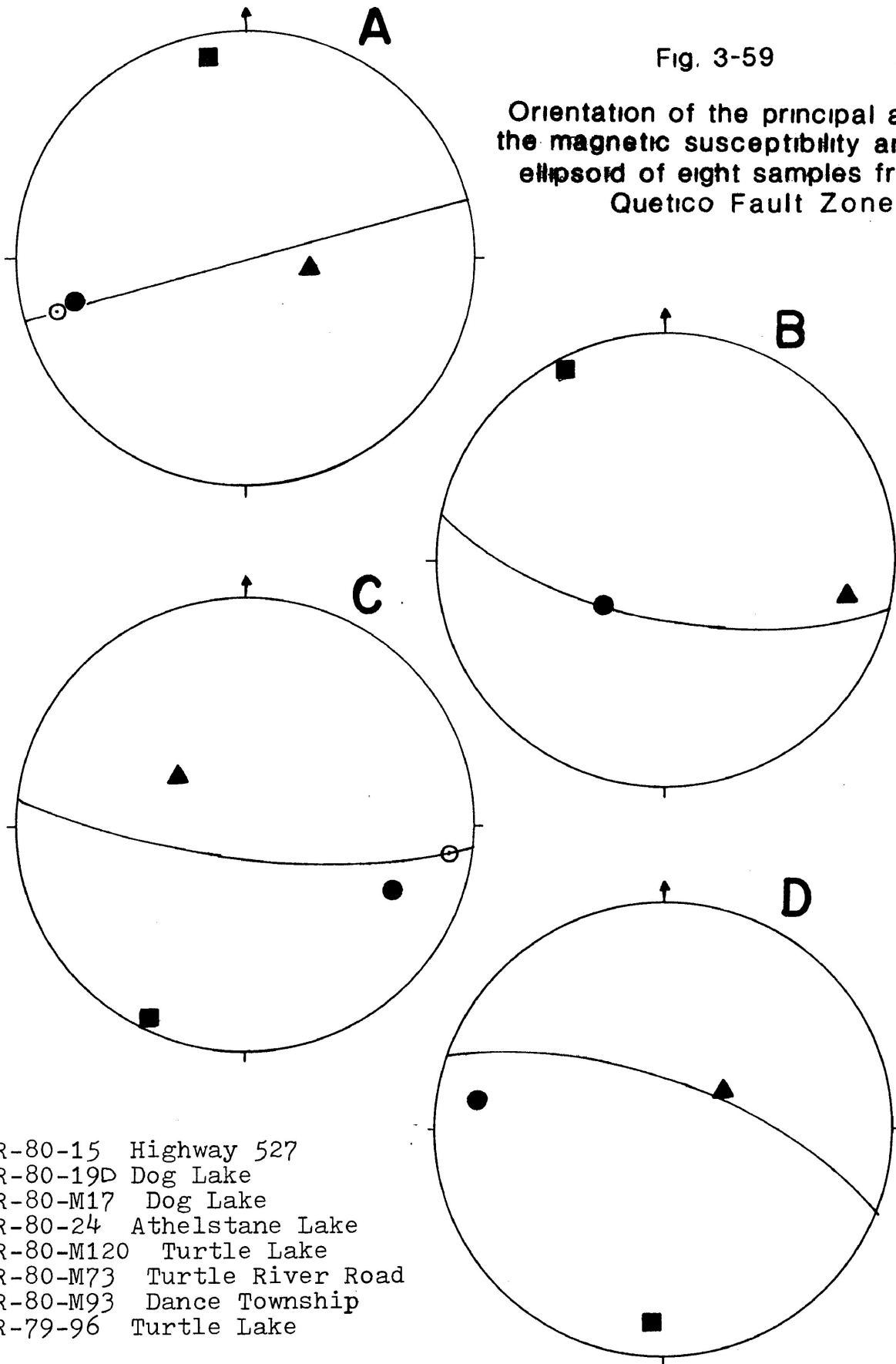


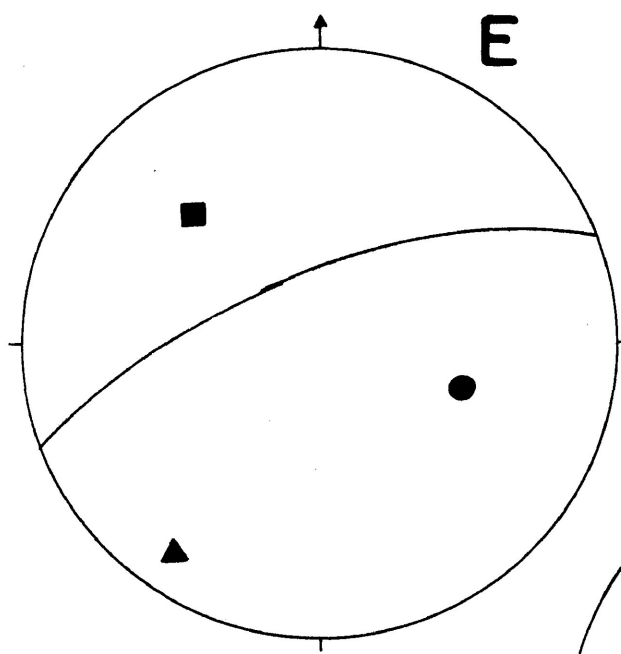
Table 3-6: Magnetic Susceptibility Anisotropy Data

Sample	$P_1 = \frac{k_{\max}}{k_{\text{int}}}$	$P_3 = \frac{k_{\text{int}}}{k_{\min}}$
A-BOR-80-15	1.0486	1.1532
B-BOR-80-19	1.1232	1.3162
C-BOR-80-M17	1.3076	1.4704
D-BOR-80-24	1.0544	1.3961
E-BOR-80-M120	1.0445	1.1505
F-BOR-80-M73	1.0325	1.0348
G-BOR-80-M93	1.0394	1.3146
H-BOR-79-96A (hinge)	1.0794	1.0872
96B (limb)	1.0359	1.1532
96C (limb)	1.0501	1.1831

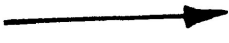
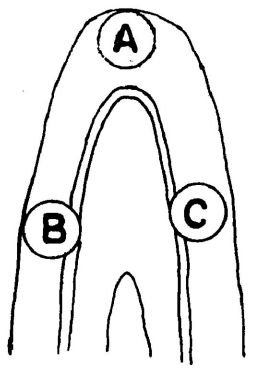
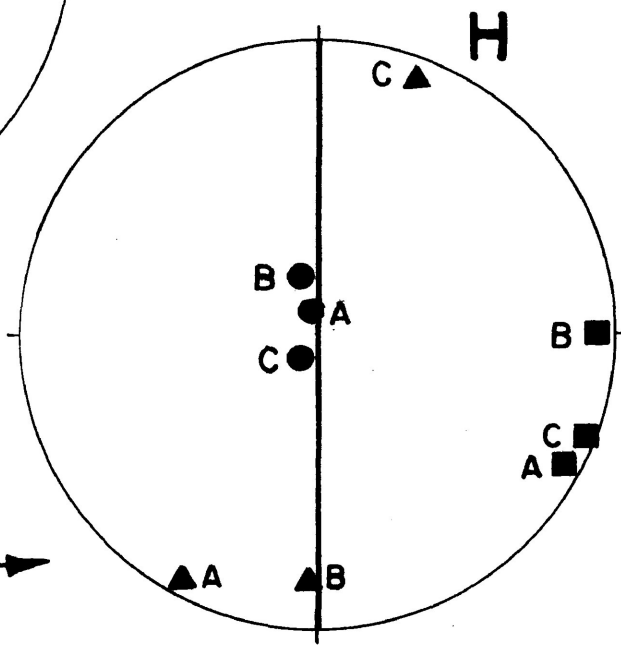
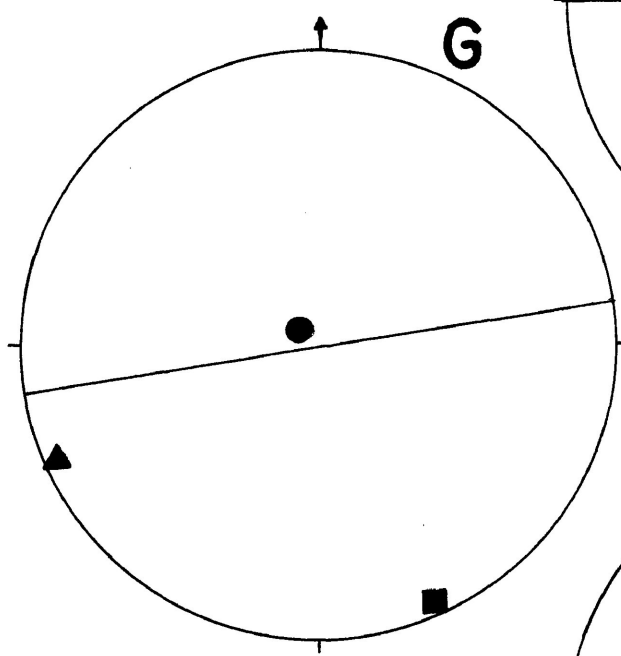
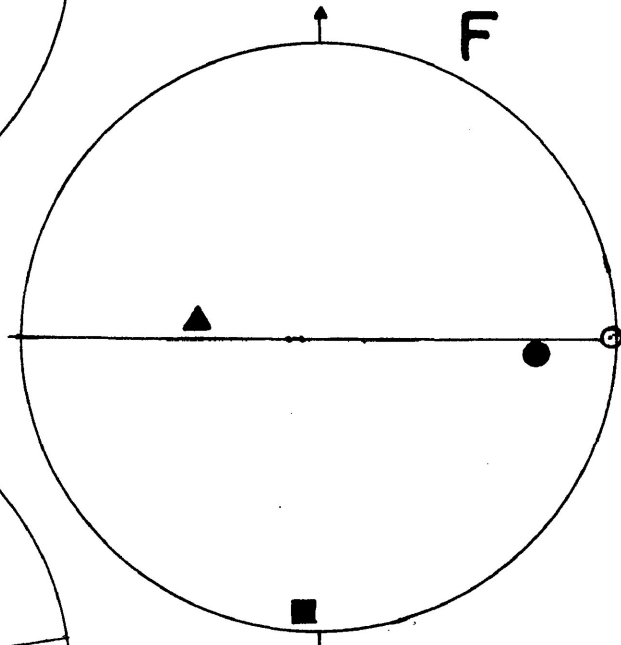
Fig. 3-59

Orientation of the principal axes of the magnetic susceptibility anisotropy ellipsoid of eight samples from the Quetico Fault Zone





- maximum susceptibility
- ▲ intermediate susceptibility
- minimum susceptibility
- lination
- schistosity
- axial plane of fold



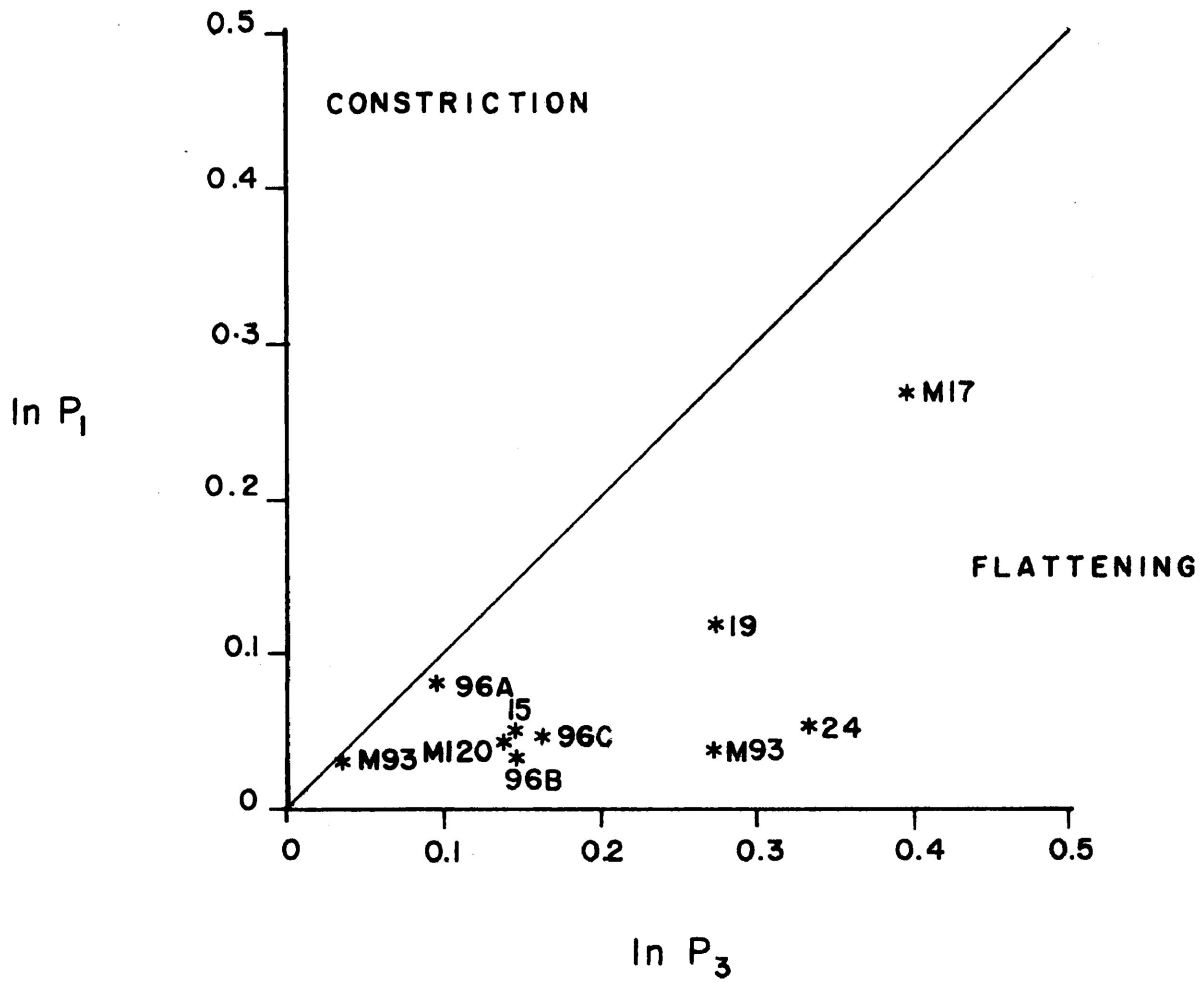


FIG. 3-60 : SUSCEPTIBILITY PLOT

each specimen. Figure 3-60 is a susceptibility plot of  $P_1$  vs  $P_3$  indicating the shape of the magnetic susceptibility ellipsoid for each specimen.

The specimens examined comprise seven individual cores (Fig. 3-59 A to G) and three cores from a fold - one core from the hinge of the fold and one from each limb (Fig. 3-59 H). There is generally good correlation between the magnetic fabric of the samples and observed macroscopic fabric elements. The maximum and intermediate susceptibility axes lie close to the schistosity and the maximum susceptibility lies close to the lineation where present. Amongst the samples the lineations comprise slickensides (Fig. 3-59 A, C), mineral lineation, (Fig. 3-59 F) and fold axis (Fig. 3-59 H). The magnetic susceptibility ellipsoid may, therefore, correspond with the strain ellipsoid. The orientation of the principal axes of the magnetic susceptibility ellipsoid of the sample in Fig. 3-59 E does not correspond well with the observed schistosity. This may have been due to interference between a pre-existing fabric and the mylonitic fabric (Borradaile and Tarling, 1981).

The susceptibility ellipsoids for all the specimens lie in the flattening field of the susceptibility plot. If the susceptibility ellipsoid can be taken to correlate with the strain ellipsoid, then flattening strain can be inferred from this data. This, in general, agrees with the findings of the strain analyses

elsewhere within the fault zone.

The three cores from the fold from Turtle Lake (Fig. 3-59 H) are particularly interesting. The principal susceptibilities of all three cores are similar in orientation. This suggests that the folds were flattened after they were formed or that the mylonitic fabric cuts across the folds parallel to the fold axial plane. Thus the susceptibility ellipsoid of the fold hinge has the same orientation as those from the limbs. The orientation of the ellipsoids resembles that of the strain ellipsoid of Ramsay's model of similar folds formed by a uniform homogeneous strain together with progressive inhomogeneous simple shear (Ramsay, 1967 p. 422, 423). The specimen from the fold hinge (BOR-79-96A) is also less flattened than the specimens from the limbs (BOR-79-96B,C) as in Ramsay's model and as shown on the susceptibility plot (Fig. 3-60). This suggests that flattening deformation following folding or homogeneous strain accompanying simple shear deformation may have been responsible for the formation of the fold.

4 - QUARTZ c-AXIS PETROFABRICS - THEORY

## A) Introduction

Crystallographic preferred orientations commonly develop in deformed rocks. Preferred orientation of the c-axis of quartz in rocks has been extensively studied because of the widespread occurrence of quartz and the relative ease with which the orientation of the quartz c-axis can be measured. These preferred orientations are generally attributed to intracrystalline slip and the accompanying rotation of crystallographic axes during deformation.

The quartz c-axis fabrics which are most commonly described in the literature in naturally deformed quartz bearing rocks are shown in Figure 4-1. They are:

- 1) point maxima
- 2) single girdle maxima
- 3a) Type I crossed girdle maxima
- 3b) Type II crossed girdle maxima

Type I crossed girdles comprise small circle girdles of c-axes distributed about the pole to the schistosity plane of the deformed rock. These small circle girdles are often connected by a girdle normal to the lineation as shown in Figure 4-1 and contain triangular maxima. Type II crossed girdles consist of two great circle girdles which intersect the schistosity normal to the lineation where a maximum is located. Note that many authors take

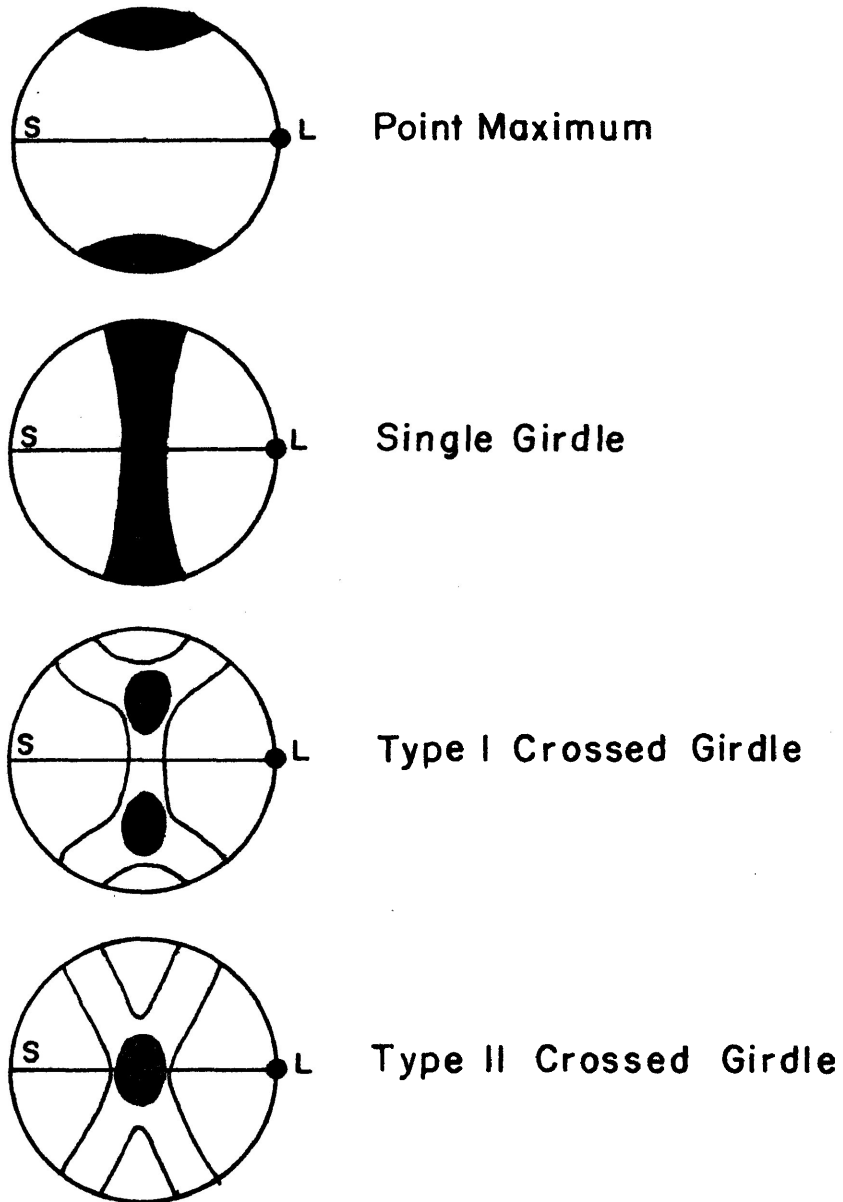


FIG. 4-1: COMMON NATURALLY OCCURRING QUARTZ C-AXIS FABRICS

(S and L indicate commonly observed schistosity and fabric lination orientations; by inference many authors take these to indicate the XY plane and X-direction of a strain ellipsoid.)



the schistosity and fabric lineation to indicate the XY plane and X direction of a strain ellipsoid.

Intracrystalline slip has been shown to be the predominant mechanism responsible for the development of preferred crystallographic orientations of quartz (Tullis et al, 1973). The intensity of preferred orientation of quartz c-axes increases with increased strain. Several factors influence the patterns of quartz c-axis preferred orientation which develop.

- 1) the slip systems operative in quartz during deformation
- 2) the shape and orientation of the finite strain ellipsoid
- 3) the strain history or deformation history (coaxial or non-coaxial)

Recrystallization, the relative proportion of quartz in a rock, and the presence of original preferred crystallographic orientations may influence quartz c-axis petrofabric patterns.

Quartz c-axis petrofabric studies may reveal much about the physical conditions at the time of deformation. The slip systems which operate in quartz during deformation by intracrystalline slip are determined by temperature, confining pressure, and presence or absence of water in the quartz. The general conditions underwhich the various slip systems in quartz operate are only partly known. Thus when particular c-axis

patterns known to result from slip on specific slip systems are identified, the physical conditions at the time of deformation may be inferred. Patterns of quartz c-axis preferred orientation may allow some conjecture about the shape of the finite strain ellipsoid as some petrofabric patterns have been related to the shape of the strain ellipsoid where strain studies have accompanied petrofabric studies. Some information about strain history may be derived from quartz c-axis fabrics. Symmetrical quartz c-axis petrofabrics develop during coaxial progressive deformation and asymmetric fabrics develop during non-coaxial progressive deformation. Means (1976) explained that the terms coaxial and non-coaxial refer to the orientation of the incremental principal strain directions with respect to material lines. Thus in coaxial deformation the incremental strain axes remain constant in orientation with respect to material lines and in non-coaxial deformation the orientation of the incremental principal strain directions is variable or may change with respect to material lines. Asymmetric fabrics, in particular quartz crystallographic fabrics, have been shown to reflect the sense of shear where simple shear is considered to be the mode of deformation in natural examples.

## B) Intracrystalline Slip and the Development of Crystallographic Preferred Orientations

Intracrystalline slip occurs by the glide of dislocations on planes of high atomic density. Dislocation glide occurs on specific crystallographic planes in specific crystallographic directions. Low index crystallographic planes are favoured as slip planes. Slip generally occurs on planes having atomic bonds which are most easily broken in the crystal allowing the glide of dislocations. Slip on crystallographic planes resembles homogeneous simple shear when considered on the scale of the whole grain. While a mineral grain is deformed by dislocation glide the crystallographic structure of the mineral is undistorted because slip occurs on rational crystallographic planes. Thus crystallographic axes may serve as a reference frame in intragranular deformation. Figure 4-2 illustrates how preferred dimensional orientation and preferred crystallographic orientation are produced simultaneously by intracrystalline slip. The simple model was constructed using a card deck to simulate slip on crystallographic planes. The cards represent slip planes. A circle drawn on the deck becomes progressively strained to an ellipse by slip on the "slip planes". The elliptical grain shape may be taken to define a preferred dimensional orientation schistosity. The diagrams in Figure 4-2 demonstrate that with increasing strain the angle between the slip plane and the

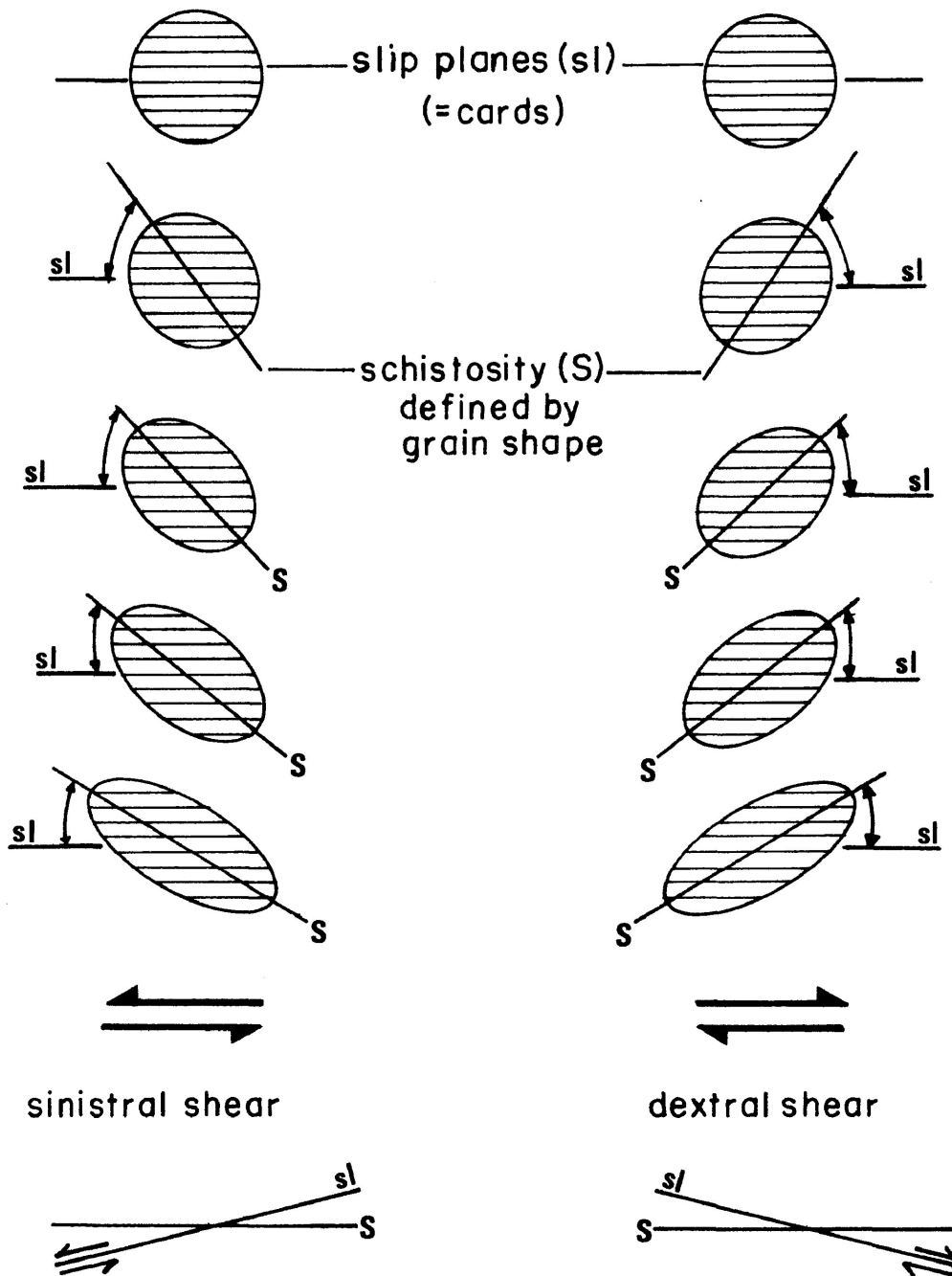


FIG. 4-2: INTRACRYSTALLINE SLIP

Card deck model simulates slip on crystallographic planes. With increasing strain the angle between the slip plane and the grain shape schistosity becomes progressively smaller. The orientation of the slip plane with respect to the schistosity depends on the sense of shear.

"schistosity" becomes progressively smaller. Thus the slip plane comes to lie close to the schistosity after large strains. Related crystallographic axes become reoriented at the same time. For instance if the slip plane in Figure 4-2 was the basal plane in quartz ((0001)), the  $\underline{c}$ -axis (which is normal to (0001)) would come to lie close to the normal to the schistosity (the principal shortening direction) after large strains. It should also be noted in Figure 4-2 that the orientation of the slip planes with respect to the schistosity depends on the sense of shear. The slip planes lie counterclockwise from the schistosity when slip on the planes is in a sinistral sense and clockwise when slip is dextral.

It is fairly well established that intracrystalline slip is often responsible for the development of preferred crystallographic orientations of quartz in deformed rocks. Tullis et al (1973) have shown that preferred orientations produced in experimentally deformed quartzites were the result of intracrystalline slip. Computer models in which "grains" have been strained by simulating intracrystalline slip have produced crystallographic preferred orientation patterns similar to those found in nature (Etchecopar, 1977, Lister et al, 1978). Electron microscope studies of naturally deformed quartz-rich rocks (for example Burg and Laurent, 1978, Carreras et al, 1977) have shown that  $\underline{c}$ -axis fabrics in quartz are the result of glide on one or more

preferential glide planes. Such studies have shown that the quartz c-axis preferred orientation patterns develop progressively with increasing shear strain and increasing grain deformation. The shear strain has been estimated in these studies using the variation in schistosity orientation in a shear zone as described by Ramsay and Graham (1970). Ramsay and Graham examined the special case of simple shear however not all workers using this method have shown that the constraints outlined by Ramsay and Graham are true of their examples.

#### C) Slip Systems in Quartz

An examination of the slip systems which are operative in quartz facilitates understanding the quartz fabrics which develop as a result of deformation by intracrystalline slip. Table 4-1 lists the slip systems which have been identified in quartz. A slip system is defined by a slip plane and a slip direction. Miller indices define the slip planes (hkl) and directions [uvw]. Equivalent planes of the same family have the symbol {hkl} and equivalent directions of the same family the symbol <uvw>.

The identification of these slip systems has involved studies by many workers. In early experimental studies which produced plastic deformation and recrystallization of quartz, Carter et al (1964) suggested that deformation was by slip on (0001)

TABLE 4-1: Slip Systems in Quartz

slip plane	slip direction		
basal	a	(0001)	$\langle 11\bar{2}0 \rangle$
1° prism	c	{10 $\bar{1}$ 0}	[0001]
	a	{10 $\bar{1}$ 0}	$\langle 11\bar{2}0 \rangle$
	c+a	{10 $\bar{1}$ 0}	$\langle 11\bar{2}3 \rangle$
2° prism	c	{11 $\bar{2}$ 0}	[0001]
rhombo	a	{1 $\bar{1}$ 01}	$\langle 11\bar{2}0 \rangle$
		{1 $\bar{1}$ 02}	$\langle 11\bar{2}0 \rangle$
		{1 $\bar{1}$ 03}	$\langle 11\bar{2}0 \rangle$
	c+a	{1 $\bar{1}$ 01}	$\langle 11\bar{2}3 \rangle$
		{11 $\bar{2}$ 1}	
pyramid	c+a	{11 $\bar{2}$ 2}	$\langle 11\bar{2}3 \rangle$

Carter et al (1964), Christie et al (1964), Christie and Green (1964), Heard and Carter (1968), Baeta and Ashbee (1969, 1970), McLaren and Retchford (1969), Avé Lallement and Carter (1971), Hobbs et al (1972), Ardel et al (1974), Twiss (1974), Morrison-Smith et al (1976) and Nicolas and Poirier (1976).

and by other mechanisms. Studies followed which attempted to identify quartz slip systems in order to understand the mechanism responsible for the deformation of quartz. Quartz slip systems have been described by Christie et al (1964), Christie and Green (1964), Heard and Carter (1968), Baeta and Ashbee (1969, 1970), McLaren and Retchford (1969), Avé Lallement and Carter (1971), Hobbs et al (1972), Ardel et al (1974), Twiss (1974) and Morrison-Smith et al (1976). Early studies identified slip systems by examining slip plane traces in deformed crystals and by studying the orientation of deformation lamellae which are believed to lie in slip planes. More recently, electron microscope studies have allowed examination of dislocations and the identification of burgers' vectors for slip.

A number of factors may affect the amount of slip which occurs on the various slip systems. They are:

- 1) critical resolved shear stress
- 2) temperature
- 3) confining pressure (this factor is not examined directly in the literature)
- 4) strain rate
- 5) H<sub>2</sub>O content of quartz

The onset of plastic deformation by slip depends on the orientation of a slip system with respect to the direction of the normal stress. Schmid and Boas (1950, in Nicolas and Poirier, 1976, p. 40-42) have shown that for any orientation of a slip



system in a crystal, slip begins for a given value of the shear stress resolved on the slip plane in the slip direction (Schmid's Law). This value ( $\sigma_c$ ) is known as the critical resolved shear stress (CRSS). Each group or family of slip systems in a crystal generally has its own CRSS. The CRSS varies with temperature and thus the relative ease with which slip occurs on a slip system varies with temperature. The slip system which is active under a given load for a given temperature and a given orientation is the one with the lowest CRSS and highest resolved shear stress. There are domains of temperature where one slip system is predominantly active.

Heard and Carter (1968) and Avé Lallement and Carter (1971) suggested that basal slip predominates at low temperatures (possibly equivalent to high confining pressure) and prism slip at high temperatures (low confining pressure) based on observations of the orientation of deformation lamellae in experimentally deformed quartzite. Tullis et al (1973) observed basal and prismatic deformation lamellae in experimentally deformed quartzites. Larger proportions of prismatic slip were observed in samples deformed at higher temperatures. Tullis et al also suggested that slip on first order prismatic planes ( $\{10\bar{1}0\}$ ) was replaced by slip on second order prismatic planes ( $\{11\bar{2}0\}$ ) at higher temperatures.

Strain rate appears to affect the operative slip systems differently. Tullis et al (1973) reported that with decreasing

strain rate the temperature at which prismatic slip becomes active is lowered. Blacic (1975) reported that the transition temperature of slip on (0001) (basal slip) in the  $\langle a \rangle$  direction to slip on (10 $\bar{1}$ 0) (prismatic slip) in the  $\langle c \rangle$  direction decreased with decreasing strain rate in accordance with the observations of Tullis et al. Thus the effects of high temperature on the operative slip systems in quartz are similar to the effects of low strain rates and vice versa.

Griggs and Blacic (1965) reported that dry natural quartz crystals retained high hardness and strength in experimental deformation to temperatures of 800°C to 1000°C at low confining pressure. This strength approaches the theoretical one. A synthetic quartz crystal containing water molecules, however, was deformed above 380°C (the critical temperature at which weakening occurred in their experiments) by stresses much lower than those required to deform the natural dry crystals. The process responsible for the weakening of the quartz was termed "hydrolytic weakening" (Griggs, 1967). Griggs attributed the hydrolytic weakening to enhanced mobility of dislocations by hydrolysis of the Si-O bonds. Hydrolytic weakening has proven to be an important factor in the deformation of quartz and other silicates (Blacic, 1971). Griggs (1967) showed that deformation in H<sub>2</sub>O bearing quartz crystals was thermally activated. The critical temperature at which weakening of the crystals occurs (weakening temperature)

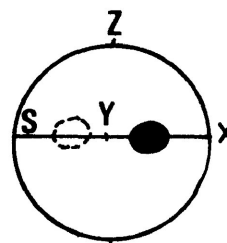
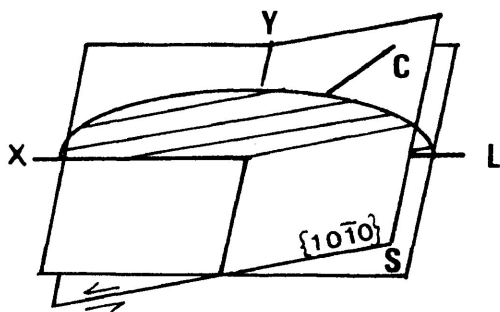
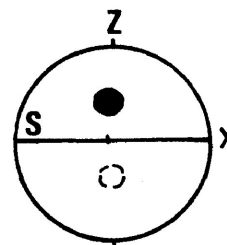
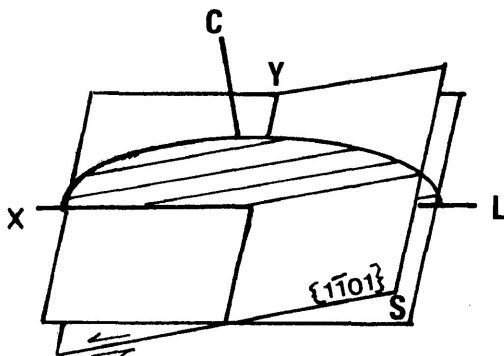
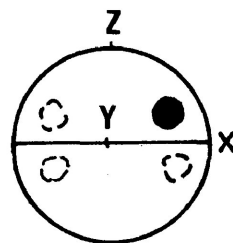
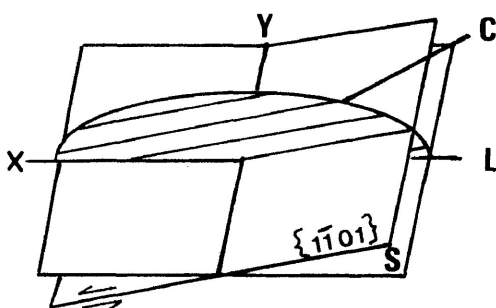
depends on the water content. Griggs (1974) noted that the weakening temperature of quartz decreases with increased water content and decreased strain rate. McLaren and Retchford (1969) suggested that water in the quartz lattice promotes the climb of dislocations as well as slip by dislocation glide. Blacic (1975) observed that the conversion from basal to prismatic slip seems to occur at the weakening temperature and thus this conversion takes place at lower temperatures with increased water content. Blacic noted, however, that basal slip is commonly dominant over prismatic slip in hydrolytically weakened natural crystals. Bell and Etheridge (1976) suggested that variations in total rock water content may produce variations in hydrolytic weakening behaviour in natural occurrences. They examined the effects of hydrolytic weakening in quartz from a mylonite zone separating rocks metamorphosed in the granulite facies (0.2% H<sub>2</sub>O) from rocks representative of the amphibolite facies (1.0 % H<sub>2</sub>O). Quartz c-axis preferred orientations developed more rapidly with respect to strain in the amphibolite facies rocks. Bell and Etheridge attributed this and other differences in the rocks of the two metamorphic facies to hydrolytic weakening of quartz in the rocks containing greater amounts of water although it was not known how much water was actually in the structure of the quartz grains. To support their statement that total rock water content may result in hydrolytic weakening of quartz, Bell and Etheridge cite the

experiments of Green et al (1970) and Tullis et al (1973). In these experiments external water became available from the confining medium of the samples during the deformation experiments and apparently resulted in hydrolytic weakening of the quartz in the samples being deformed.

D) Factors Influencing the Development of Quartz c-axis Preferred Orientations

i) *The Influence of Slip Systems on Quartz c-axis Fabrics*

The diagrams of Figure 4-3 are based on a single grain and were constructed in order to illustrate the general nature of the quartz c-axis fabrics which may develop during intracrystalline slip on some individual (common) slip systems. Note that in the "three-dimensional" diagrams the schistosity corresponds to the XY plane of the finite strain ellipsoid as defined by the deformed grain shape. The lineation corresponds to the X axis of the strain ellipsoid (where  $X \geq Y \geq Z$ ). The stereographic projection (lower hemisphere) illustrates the pattern of quartz c-axis preferred orientations which would develop if a number of individual grains were deformed by slip on the slip system and after large strains when the slip plane comes to lie very close to the schistosity. Each of the diagrams demonstrates slip on the slip planes in a sinistral sense.

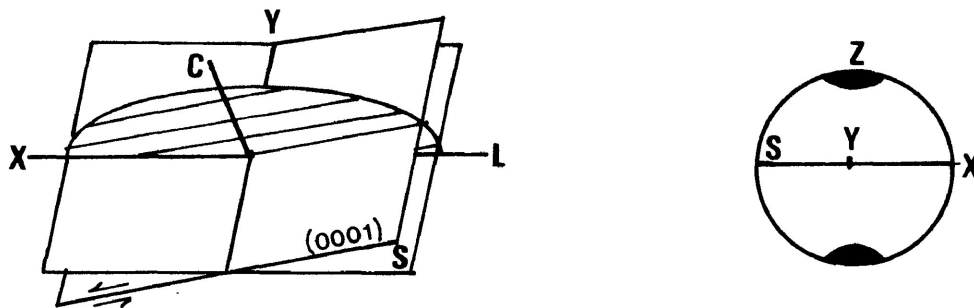
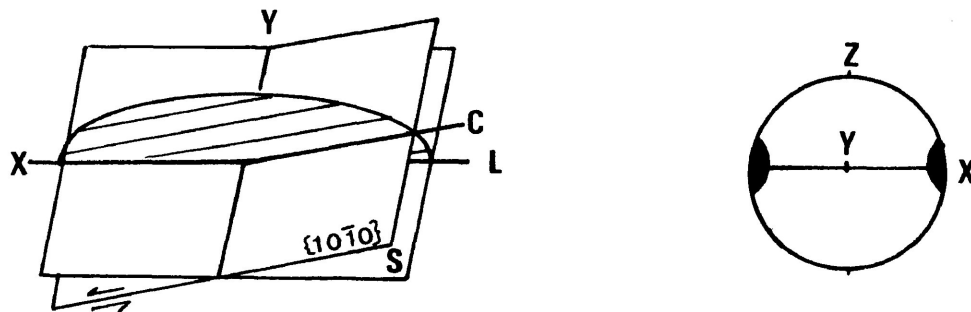
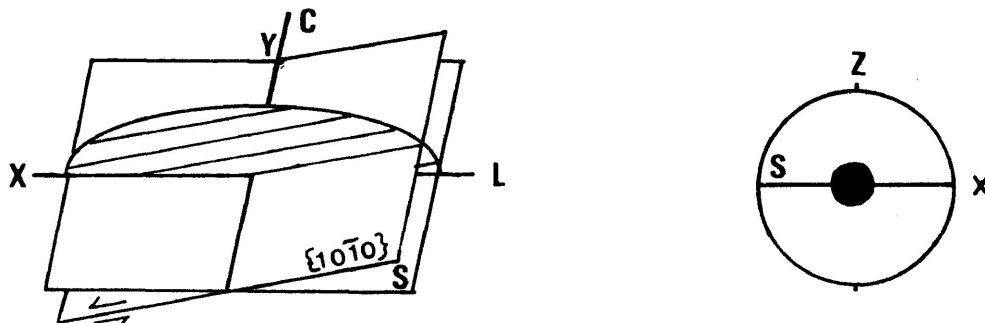
D - Prism  $\langle c+a \rangle$  SlipE - Rhomb  $\langle a \rangle$  SlipF - Rhomb  $\langle c+a \rangle$  SlipC -  $\underline{c}$ -axis

S - grain shape schistosity

L - mineral lineation

X, Y, Z - principal axes of the finite strain ellipsoid

○ - other possible  $\underline{c}$ -axis maxima which result when the geometry is such that one or both elements of the slip system (the slip plane and slip direction) have an acute angular relationship with the  $\underline{c}$ -axis.

A - Basal  $\langle a \rangle$  SlipB - Prism  $\langle c \rangle$  SlipC - Prism  $\langle a \rangle$  SlipFIG. 4-3: QUARTZ  $c$ -AXIS PETROFABRICS

The pairs of diagrams represent 6 different slip systems. The left-hand diagram comprises a single grain and indicates the orientation of the  $c$ -axis with respect to the slip plane. The right-hand diagram illustrates the resulting quartz  $c$ -axis petrofabric which would develop after large strains when the slip plane lies close in orientation to the schistosity.

Figure 4-3a illustrates slip on basal planes of quartz in an  $\langle a \rangle$  direction. As the  $\underline{c}$ -axis is perpendicular to the basal plane the resulting  $\underline{c}$ -axis fabric is characterized by a maximum normal to the schistosity and the lineation after large strains when the slip plane lies close in orientation to the schistosity. Figure 4-3b demonstrates slip on prism planes in the  $\langle c \rangle$  direction. In this case the  $\underline{c}$ -axis lies in the slip plane and parallel to the slip direction.  $\underline{c}$ -axis maxima parallel to the lineation and lying in the schistosity should develop for large strains. Figure 4-3c shows prismatic slip in an  $\langle a \rangle$  direction. Here the  $\underline{c}$ -axis lies in the slip plane but perpendicular to the slip direction of the quartz grain. The resulting maximum of  $\underline{c}$ -axes for large strains would lie in the schistosity parallel to the Y axis of the strain ellipsoid (normal to the lineation). Figure 4-3d illustrates prismatic slip in a direction between  $\underline{c}$  and  $\underline{a}$  ( $\langle c + a \rangle$ ). Again the  $\underline{c}$ -axis lies in the slip plane but is intermediate between X and Y. The resulting maximum might appear as shown. Figure 4-3e demonstrates slip on a rhomb plane in an  $\langle a \rangle$  direction. The orientation of the  $\underline{c}$ -axis with respect to the slip plane is shown. The resulting maximum at large strains would lie in the plane normal to the schistosity (YZ) at an angle to Y and Z. Figure 4-3f illustrates slip on rhomb planes in a direction between  $\underline{c}$  and  $\underline{a}$  ( $\langle c + a \rangle$ ). The orientation of the  $\underline{c}$ -axis compared to the slip plane is shown. A  $\underline{c}$ -axis maximum would form at an angle to the

schistosity and the lineation as shown.

These are rather simple models demonstrating how different preferred orientations of quartz c-axes develop by intragranular slip. The preferred orientations produced are point maxima. In general, rock deformation requires that more than one slip system be active in the constituent minerals. Grains are constrained by their neighbours and are not free to deform "ideally" as shown in the model (Fig. 4-3). The maintainance of grain-grain continuity in an aggregate requires the operation of more than one slip system. The common occurrence of girdle distributions of c-axes in nature suggests that many fabrics are largely the result of slip on more than one slip system.

*Number of slip systems required for deformation:* Von Mises' ductility criterion (Nicolas and Poirier, 1976) states that a polycrystal (many grains of one mineral) can deform coherently to large strains by dislocation glide alone only if the grains can slip on five independent slip systems simultaneously. An independent slip system is one whose movement cannot be duplicated by a combination of slip on the other operative slip systems. In other words, for all the individual grains to be deformed homogeneously the five independent slip systems must be able to operate. This criterion may be somewhat restrictive for rock deformation. Ashby and Verrall (1977) suggest that if non-homogeneous deformation



is allowed, so that grains deform compatibly but not uniformly, the Von Mises' criterion may be relaxed and four slip systems may be sufficient. The number of slip systems required for coherent deformation may be further reduced if conditions permit the operation of recovery processes. Dislocation climb allows dislocations to "climb" over and glide past obstacles. Fewer slip systems may also be required within grains if particulate flow (Borradaile, 1981) occurs allowing sliding on grain boundaries, multigrain boundaries (such as microfaults), and newly created grain boundaries as well as rolling of grains at their points of contact.

The deformation of an aggregate or polycrystal may also be affected by the fact that most rocks are polymineralic polycrystals (as opposed to monomineralic polycrystals described by Von Mises, and Ashby and Verrall). The different plastic properties of each constituent mineral contribute to the overall deformation of the rock and thus the required slip systems for coherent deformation may be affected. The behaviour of one mineral may be influenced by the characteristics of neighbouring minerals.

*Computer model simulating quartz c-axis petrofabrics resulting from slip on several slip systems:* A model of coaxial deformation by intracrystalline slip in a hypothetical "aggregate" of quartz grains was described by Lister et al (1978). The computer model success-

fully reproduced some preferred crystallographic orientations which have been produced experimentally and some which are found in nature. The model, called the Taylor-Bishop-Hill model, is named for the workers who originally proposed it. The computer model simulates the deformation of quartz grains by glide on various combinations of dislocation slip systems and produces the preferred crystallographic orientation patterns of c-axes which result from rotation of the crystal axes during the simulated deformation. The input for the model includes the initial orientation distribution (generally random), the set of possible glide systems and their relative CRSS values and details of the deformation and its path. The slip systems are assigned relative values of CRSS which determine the relative ease with which the slip systems operate and thus the amount of slip which occurs on each slip system. The simulated deformation of the model "aggregate" takes place grain by grain. At various stages throughout the incremental deformation the orientation of the grains is stored for construction of diagrams. Lister et al enumerate the following assumptions:

- 1 - Deformation is by dislocation glide only and occurs by the simultaneous operation of a number of discrete glide systems each of which approximates simple shear relative to the glide plane.
- 2 - Deformation is uniform throughout the polycrystalline mass at all stages, i.e.) strain is homogeneous. The strain in each grain of the aggregate is identical to the overall strain.
- 3 - The material behaves according to a rigid-plastic flow law,

i.e.) the material behaves rigidly under increasing deviatoric stress until yield occurs at sharply defined stresses. Each glide system is characterized by a critical resolved shear stress for yield which is assigned as part of the input for the model.

These assumptions place a number of limitations on the model. For the "aggregate" to deform homogeneously by dislocation glide five independent slip systems must operate (Von Mises' criterion). In nature grains do not all strain equally. Favourably oriented grains for slip will deform more than less favourably oriented grains. The model requires the "grains" which are unfavourably oriented for slip on one slip system (i.e. the most active slip system) to deform by slip on a combination of the other systems.

The most important drawback of the model is that it does not seem to take into account the actual framework of the aggregate i.e.) the position of grain boundaries and constraints imposed on the deformation of a grain by its neighbours in an aggregate. Although Lister et al. describe the strain in the grain aggregate as homogeneous, nowhere are the grains themselves actually described. The input for the model only includes grain orientation. Each grain is deformed increment by increment in isolation so it seems that intergranular interactions and the requirement that the aggregate comprise a coherent body before and after deformation have been overlooked.

The results of the simulated model must be viewed with this in mind. The patterns of preferred orientation which develop

are only limited by the model input which defines the material properties: the set of glide systems and their relative CRSS. Lister et al (1978) explained that the set of glide systems determines the total possible variation in fabrics that can develop and that the relative CRSS values which determine which glide systems and combinations of glide systems will be responsible for the glide deformation determine the primary characteristics of any pattern of preferred orientation. The patterns are also influenced by the strain history. This influence will be discussed later.

Lister et al (1978) utilized basal, prism and rhomb slip systems in their deformation simulations. Four model quartz grain "collections" (called quartzites by Lister et al) were deformed each having a different combination of slip systems and CRSS values as shown in Table 4-2. Note that the slip systems assigned the lowest CRSS are those on which slip will occur most easily. Each model "quartzite" was subjected to deformation approximating axial symmetric shortening (flattening), plane strain, and axial symmetric extension (constriction). Figure 4-4 comprises the distributions of quartz  $\underline{c}$ -axes which resulted. With increasing simulated strain the intensity of preferred crystallographic orientation increased. As noted the slip systems which operated determined the general nature of the  $\underline{c}$ -axis fabrics but the shape of the strain ellipsoid also strongly influenced the patterns

FIG. 4-4

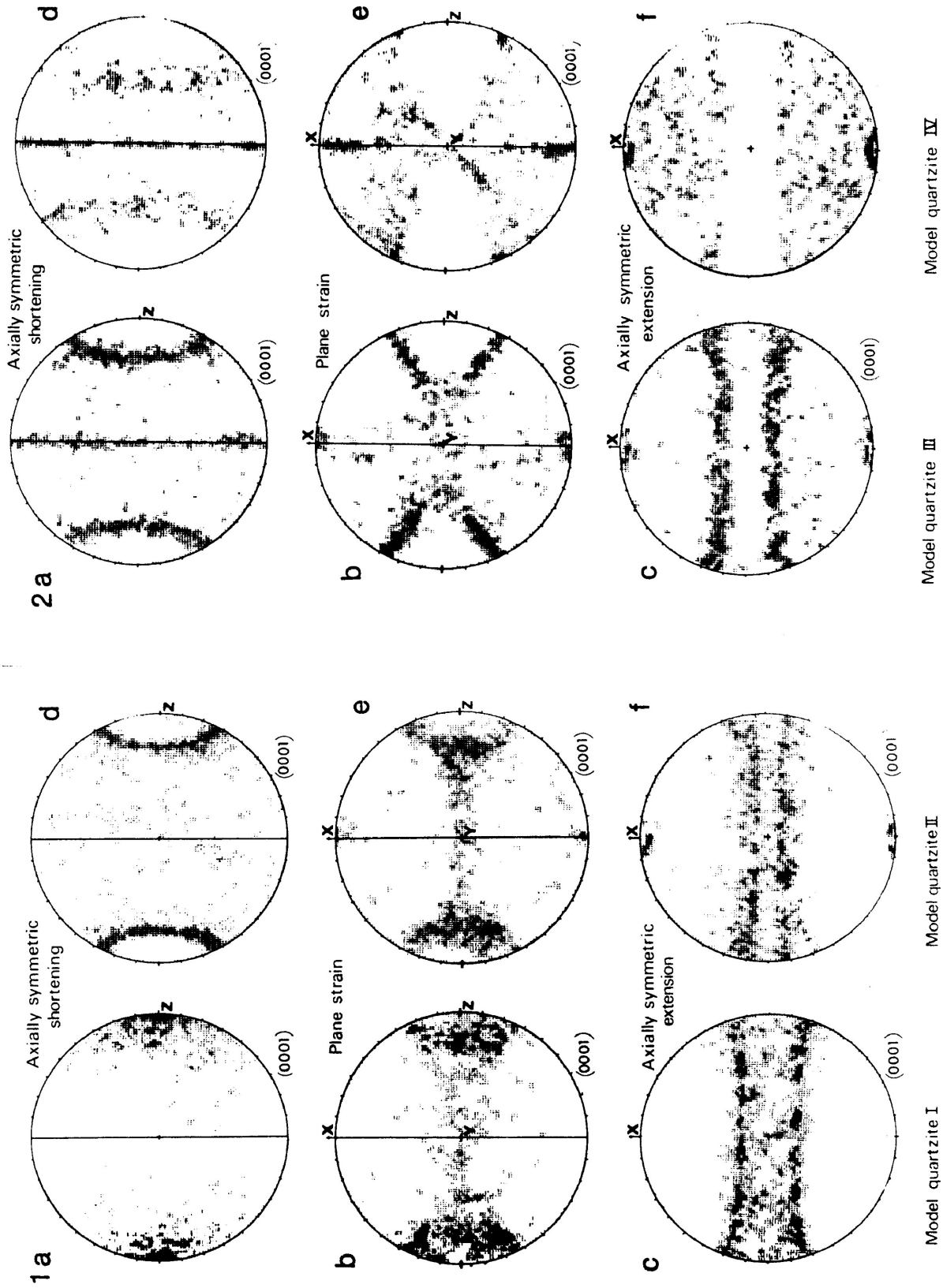


TABLE 4-2: Slip systems and relative CRSS for simulated deformation of four model quartz grain aggregates by intracrystalline slip. (Lister et al., 1978).

Glide Plane	Glide Direction	Relative CRSS for models			
		I	II	III	IV
c{0001} basal	a $\langle \bar{1}2\bar{1}0 \rangle$	1.00	1.00	1.00	1.00
m{10 $\bar{1}$ 0} prism	a $\langle \bar{1}2\bar{1}0 \rangle$	-	-	0.01	0.60
	c $\langle 0001 \rangle$	-	-	-	1.00
	c+a $\langle \bar{1}2\bar{1}3 \rangle$	-	-	-	2.00
n{10 $\bar{1}$ 1} (+) rhomb	a $\langle \bar{1}2\bar{1}0 \rangle$	4.00	2.00	-	1.50
	c+a $\langle \bar{1}1\bar{2}3 \rangle$	5.00	2.00	2.00	2.00
z{01 $\bar{1}$ 1} (-) rhomb	a $\langle \bar{1}2\bar{1}0 \rangle$	-	2.05	-	1.55
	c+a $\langle \bar{1}1\bar{2}3 \rangle$	-	2.05	-	2.05

FIG. 4-4; (facing page)

Quartz c-axis fabrics resulting from simulated deformation of four model quartz grain aggregates by intracrystalline slip. Note that each model comprises a different combination of slip systems and relative CRSS values (Table 4-2) and each model is subjected to axial symmetric shortening, plane strain, and axial symmetric extension.

which resulted. From Figure 4-4 it can be seen that in general predominantly basal slip in an  $\langle a \rangle$  direction resulted in a maximum near the Z direction (Fig. 4-4 - Model Quartzite I) where  $X > Y > Z$  are the principal strain axes. This is in accordance with predictions made in the earlier sketches (Figure 4-3a). In the simulations the introduction of rhomb and prism slip (Figure 4-4 - Model Quartzites II, III, IV) resulted in maxima in the form of small or great circle girdles about Z with low density of  $\underline{c}$ -axes at Z. Many of the fabrics formed by the Taylor-Bishop-Hill model are similar to those produced experimentally and found in nature i.e.) point maxima, small circle girdles (type I crossed girdles) and great circle girdles (type II crossed girdles). The experimentally derived fabrics of Tullis et al (1973) are similar to those predicted by Lister et al. At low temperatures or high strain rates ( $< 600^\circ\text{C}$  at  $10^{-6} \text{ sec}^{-1}$ ) a maximum of  $\underline{c}$ -axes developed parallel to the principal compressive stress direction ( $\sigma_1 > \sigma_2 = \sigma_3$ ). At higher temperatures  $\underline{c}$ -axes lie in small circle girdles about  $\sigma_1$ . The opening angle of the small circle girdle increases with increasing temperature corresponding to an increase in the proportion of prism slip as compared to basal slip.

ii) *The Influence of Recovery and Recrystallization on Quartz  $\underline{c}$ -axis Fabrics*

Dynamic recovery and syntectonic or dynamic recrystallization

may contribute to preferred crystallographic orientations and must, therefore be considered in this discussion. Dynamic recovery involves dislocation climb and polygonization. Polygonization is the development of subgrains, slightly misoriented portions of the grain with low angle grain boundaries (less than  $7^\circ$  misorientation between subgrain and host) (Nicolas and Poirier, 1976). These are thermally activated processes. Dislocation climb is an important process in preferred orientation development as dislocation movement, which is impaired by obstacles such as dislocation networks and tangles in lower temperature work hardening conditions, is allowed to continue when dislocations can climb over obstacles. Dislocation climb thus enhances deformation by intracrystalline slip by allowing continued operation of dislocation glide. Recovery may reduce the number of required slip systems for homogeneous strain for this reason. Dynamic recrystallization may occur by 1) the progressive misorientation of subgrains and by 2) the migration of grain boundaries (Guillope and Poirier, 1979). Regardless of how the recrystallized grains are formed, dislocation glide continues within subgrains and recrystallized grains produced during deformation and thus preferred orientations of these grains would be similar to those of the original grains. Green et al (1970) observed that syntectonically recrystallized grains were elongate as a result of continuing strain.



Quartz c-axis fabrics produced experimentally by Green et al (1970) and Tullis et al (1973) were very similar. In Green's experiments recrystallization was predominant. Tullis et al determined that deformation was by intracrystalline slip with little or no recrystallization. Tullis et al suggested that intracrystalline slip may have been important in producing the c-axis fabrics in the dynamic recrystallization experiments of Green et al or that another orienting mechanism was responsible for producing fabrics so similar to those which occurred as a result of intracrystalline slip. In naturally deformed rocks, fabrics in rocks which have undergone extensive recrystallization are described by Sylvester and Christie (1968) and have the form of two, crossed, great circle girdles (type II crossed girdles). These are very similar to fabrics demonstrated by Bouchez (1977) where intracrystalline slip was shown to be the predominant deformation mechanism.

Lister and Price (1978) suggested that fabrics developing during dynamic recrystallization are a result of the operation of dislocation glide processes. Although the regimes in which dislocation glide and recrystallization processes predominate are different they must overlap and the simultaneous operation of the processes is possible and may be related. Based on studies by Hobbs (1968) and by Bell and Etheridge (1976) which show that new grain orientations are related to host grain orientations, Lister

and Price (1978) suggested that the effect of dynamic recrystallization would be to diffuse or scatter the developing crystallographic fabric. They also suggested that dynamic recrystallization may not prevent fabrics reflecting dislocation processes as the recrystallized grains are subjected to the same processes as soon as they are formed. Bouchez and Pecher (1981) noted that where recrystallization has occurred and growth of grains is observed, the orientations of quartz c-axes have been scattered to result in more diffuse patterns than those observed in specimens where growth of grains did not occur.

*iii) The Influence of the Shape and Orientation of the Finite Strain Ellipsoid on Quartz c-axis Fabrics*

Figure 4-4 (model "quartzites" of Lister et al (1978)) indicated that the shape and orientation of the strain ellipsoid have a strong influence on the preferred orientation patterns of quartz c-axes which develop during deformation. In general, axial symmetric shortening (flattening) of the model quartz grain aggregates resulted in point maxima at Z (the minimum principal strain axis) or in small circle girdles around Z with or without some concentration of c-axes in the XY plane (Fig. 4-4, 1a, 1d, 2a, 2d). Plane strain resulted in girdle distributions. Some girdles were similar to type I crossed girdles comprising small circle girdles of c-axes around Z, connected through Y, and containing

triangular maxima (Fig. 4-4, 1b, 1e). Others more closely resembled crossed great circle girdles (type II crossed girdles) without the Y maximum (Fig. 4-4, 2b, 2e). Axial symmetric extension produced cleft girdles at high angles to X with low density of  $\underline{c}$ -axes along the YZ plane (Fig. 4-4, 1c, 1f, 2c, 2f). Lister and Hobbs (1980) using the Taylor-Bishop-Hill model produced  $\underline{c}$ -axis fabrics for three different model "quartzites" (Table 4-3). Similar patterns resulted for axial extension, plane strain and axial shortening as those produced by Lister et al (1978). The quartz  $\underline{c}$ -axis fabric patterns produced for general constriction and general flattening were transitional between the patterns produced by pure axial extension and plane strain, and by pure axial shortening and plane strain respectively.

In general the patterns of preferred orientation associated with strain ellipse shapes predicted by the Taylor-Bishop-Hill model are similar to those produced in experimental deformation by Tullis et al (1973) and Tullis (1977). Tullis et al (1973) described the quartz  $\underline{c}$ -axis fabrics which resulted from axial compression experiments using apparatus with a solid confining medium (Griggs, 1967). The axial compression experiments approximate flattening strain. At low temperatures a single maximum developed around the compression direction. At higher temperatures a small circle girdle developed around the compression direction. Tullis' (1977) plane strain experiments were performed in a similar

TABLE 4-3: Slip systems and relative CRSS for simulated deformation of three model quartz grain aggregates by intracrystalline slip (Lister and Hobbs, 1980).

Slip System plane <direction>	Relative CRSS for models		
	Model A	Model B	Model C
Basal <a>	1.00	1.00	1.00
Prism <a>	4.00		1.00
+ Rhomb <a>		3.00	
- Rhomb <a>	3.00	3.00	
+ Rhomb <c+a>		3.00	
- Rhomb <c+a>		3.00	
Steep dipyrarnid <c+a <sub>2</sub> >			3.00
Steep dipyrarnid <c+a <sub>3</sub> >			2.50

manner to the axial compression experiments except that the cylindrical sample was jacketed on two sides by a rigid material preventing deformation in one direction normal to the piston which compressed the sample. The sample was allowed to bulge out into glass which formed the confining medium on the other two sides of the sample. The quartz  $\underline{c}$ -axis fabrics resulting from the experiments simulating plane strain were similar to those produced in axial compression except a girdle of  $\underline{c}$ -axes connected the maxima through the intermediate "stress" direction (the direction of no strain in Tullis' experiment).

A number of studies have attempted to relate naturally occurring quartz fabrics to total strain. Marjoribanks (1976) measured the strain of grains in a quartzite using Ramsay's (1967)  $R_f - \phi$  method. The schistosity and lineation in the quartzite samples were defined by the flattening and elongation of the constituent quartz grains. Thus, the schistosity was considered the XY plane of the strain ellipsoid and the lineation, the X direction (where  $X \geq Y \geq Z$ ). Samples which had undergone flattening strain developed quartz  $\underline{c}$ -axis fabrics comprising small circle girdles about Z. With increasing constrictive strain Marjoribanks noted that the  $\underline{c}$ -axes became distributed along a great circle girdle intersecting the schistosity at Y but still resembling type I crossed-girdles. Bouchez (1977) determined the strain of a quartzite from the average axial ratio (presumably the arithmetic

mean) of quartz porphyroclasts and of ferruginous spots in the quartzite. The markers showed little fluctuation in orientation about the lineation direction. Although the arithmetic mean may not have provided the best estimation of the strain of the sample, the shape of the strain ellipsoid, close to plane strain and slightly into the constriction field as defined by Flinn (1962), was probably accurately indicated. The corresponding quartz c-axis preferred orientation patterns were type II crossed girdles. Miller and Christie (1981) also noted type II crossed girdles in rocks in which plane strain and moderate extension were measured. The fabrics were determined from the matrix (and pebbles) of a pebbly metaquartzite. The strain was measured using the method of Oertel (1978) and Miller and Oertel (1979) from the average pebble shapes on each of three mutually perpendicular planes. One sample in the study which indicated flattening strain had a c-axis fabric comprising several maxima clustered about the direction of maximum shortening with a weak connecting girdle through Y (i.e.) type I crossed girdle).

Table 4-4 summarizes and allows comparison between the quartz c-axis fabrics associated with strain ellipsoid shape for the models, experimentally deformed quartzites and naturally deformed rocks.

TABLE 4-4: Quartz c-axis preferred orientation patterns related with strain ellipse shape for various studies.

<u>Study</u>	Quartz <u>c</u> -axis fabric associated with strain ellipsoid shape		
	Constricted	Plain Strain	Flattened
<u>Model</u>			
Lister et al (1978)	cleft girdles (small circles $\bar{c}$ 75° opening angle)	type I (small circles around z) type II	type I (point maxima at z and small circles around z)
Lister and Hobbs (1980)	cleft girdles	type I (small circles around z) type II	type I (point maxima at z and small circles around z)
<u>Experimental</u>			
Tullis et al (1973)			type I (point maxima at z, small circles around z)
Tullis (1977)		type I (girdle connects small circles through Y)	
<u>Natural</u>			
Marjoribanks (1976)		type I (connecting girdle)	type I (small circles)
Bouchez (1977)		type II	
Miller and Christie (1980)		type II	type I (connecting girdle)

iv) *The Influence of Strain History on Quartz c-axis Fabrics:  
Coaxial versus Non-coaxial Deformation*

Etchecopar (1977) investigated and compared pure shear (coaxial) and simple shear (non-coaxial) deformation by simulating intracrystalline slip of grains of a hypothetical aggregate using a two dimensional computer model. The model comprised polygonal cells (=grains) each having one slip direction. The initial distribution of the slip directions of the grains was random. The cells were deformed by finite increments, independent of their neighbours, and then the best fit between the cells was obtained by determining the rotation, translation and amount of slip which would be necessary to minimize gaps and overlaps between cells and to minimize grain boundary sliding. The aggregate had an initial given shape. A final shape of the aggregate corresponding to the chosen strain was imposed as a boundary condition. The initial area was maintained after deformation. Limitations on the model, as described by Etchecopar, are:

- 1) the model is two dimensional and cells have only one slip direction
- 2) the model requires homogeneous slip in the slip direction, no bending of grains is allowed
- 3) the cells are assumed to be perfectly deformable in the slip direction and undeformable in other directions
- 4) gaps and overlaps appear between cells

The model is realistic however in as much as one predominantly



active slip system is often observed in nature. The grains most suitably oriented for slip will deform significantly more than those which are unsuitably oriented. Intergranular movements accompany the deformation and the grains are considered within the context of the aggregate (i.e.) the constraints imposed by the aggregate are not overlooked.

Etchecopar examined the preferred orientations of slip lines and grain shapes which developed. With increasing strain the following patterns of preferred orientation of slip directions developed. In pure shear the orientations of slip lines developed two peaks which were symmetrically inclined to the average elongation of the cells as shown in Figure 4-5. With increasing strain the peaks converged to become concentrated towards the elongation direction. In simple shear for weak to moderate strains ( $30^{\circ}$ - $60^{\circ}$  of shear) concentrations of slip lines are similar to the ones for pure shear. At higher strain ( $>60^{\circ}$  shear angle) in simple shear deformation the peak closer to the shear direction becomes larger than the other peak (Figure 4-5). The slip lines of this model would equate with slip planes in three dimensions. The elongation direction of "grains" in the aggregate would equate with the schistosity. The orientation of the slip plane with respect to the schistosity (defined by grain elongation) was characteristic of the sense of shear as slip on the slip planes resembles simple shear. In pure shear deformation of an aggregate

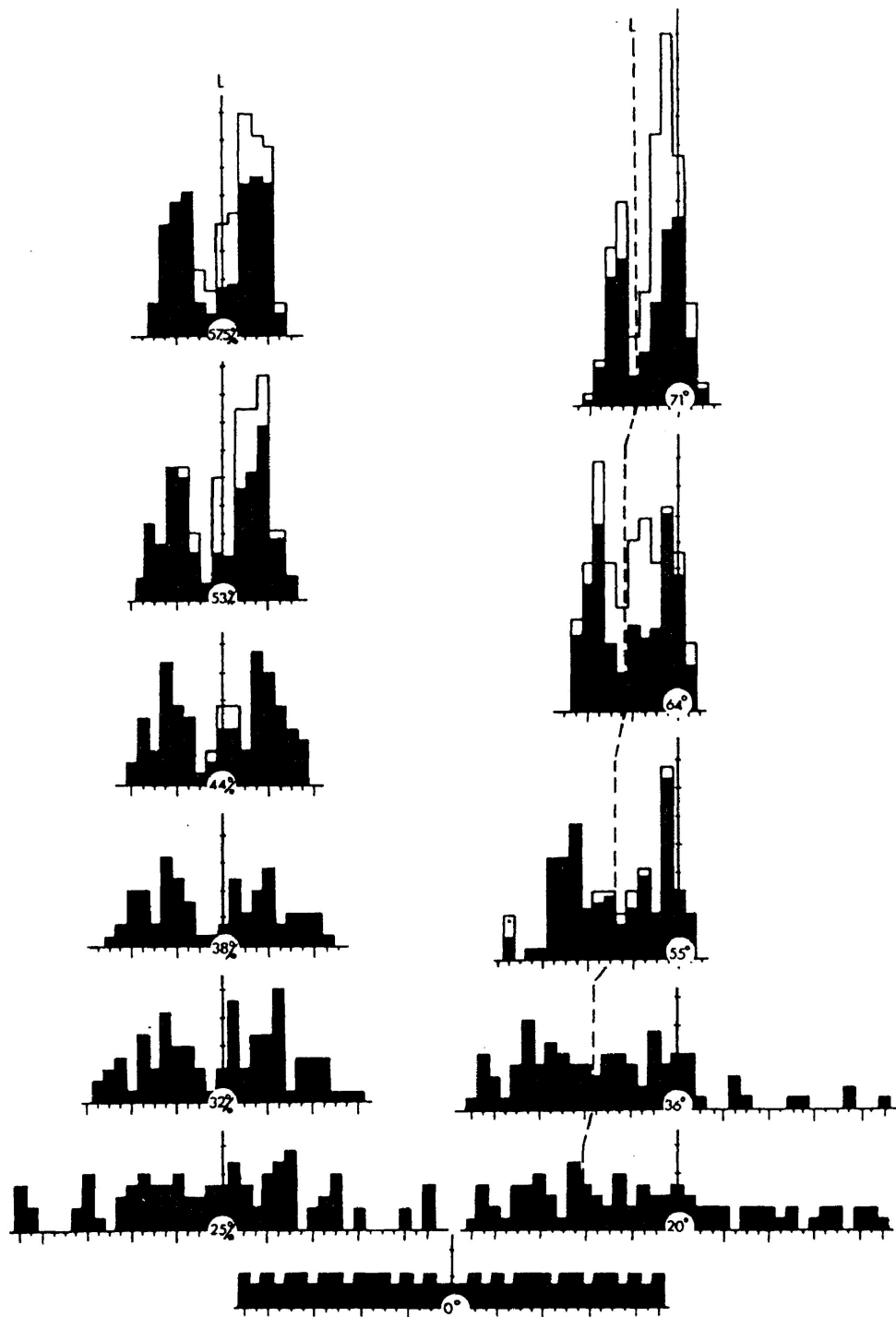


FIG. 4-5: Etchecopar's 2-dimensional model. Preferred orientations of slip lines with increasing pure shear (left) and increasing simple shear (right). Shaded: unfractured cells; unshaded: fractured cells. The graduated zero line at left is normal to the shortening direction; at right it is the shear direction. The dashed line L at right is the mean elongation direction in the deformed aggregate.

(Etchecopar, 1977)  
(diagram from Nicolas and Poirier, 1976)

the symmetrical and equal development of concentrations of slip directions around the elongation direction suggests slip occurred equally in both dextral and sinistral senses. In simple shear deformation the asymmetry of the preferred orientations of slip directions suggests the slip did not occur equally in both senses. The strongest preferred orientation would represent syn-thetic slip (reflecting the overall or total sense of shear (see Voll, 1960)). The weaker peak would thus represent antithetic slip (opposite sense of slip than the whole aggregate). Etchecopar described the behaviour of grains of various orientations during progressive deformation of the model and in fact the slip in cells of some initial orientations was antithetic. However, in simple shear deformation, as deformation proceeded the grains rotated so that slip became syn-thetic. This was expressed by the development of the stronger peak at the expense of the other peak at high strains.

Lister and Hobbs (1980) examined the quartz c-axis fabrics which developed when three model "quartzites" (see table 4-3) were subjected to simulated progressive simple shear using the Taylor-Bishop-Hill model. Quartz c-axis fabrics developed which were asymmetric with respect to the finite principal strain axes at high shear strains. At low strains the asymmetry was not marked. Figure 4-6 illustrates the c-axis fabrics which resulted for one of the model quartz grain aggregates. The

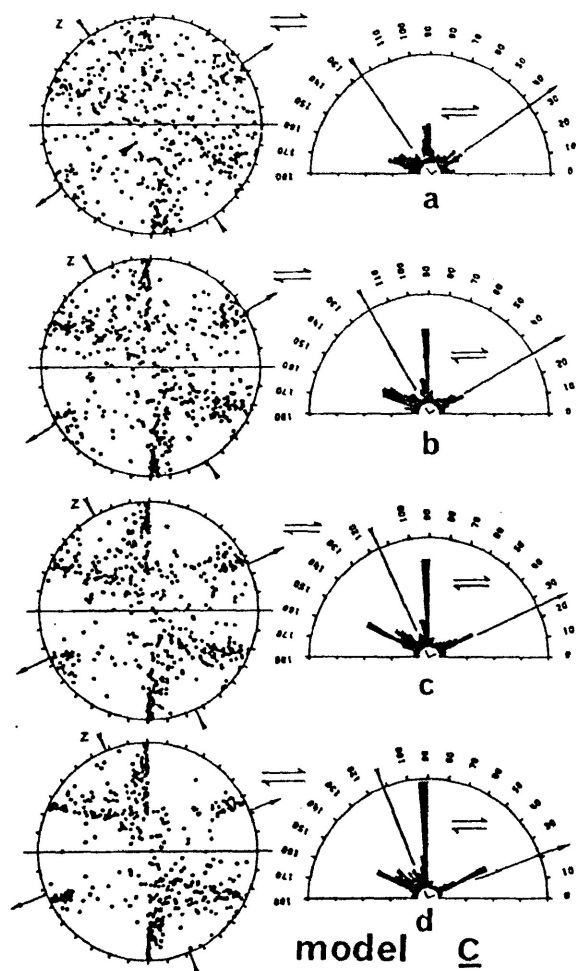


FIG. 4-6:  $\underline{c}$ -axis fabrics resulting from a model 'quartzite' subjected to progressive simple shear. The  $\underline{c}$ -axis pattern is asymmetric with the sharpest and most distinct girdle of  $\underline{c}$ -axes perpendicular to the slip plane and slip direction. The rose diagrams show the angular distribution of the trend of the  $\underline{c}$ -axes in the XZ plane of the finite strain ellipsoid.

(from Lister and Hobbs, 1980)

fabrics produced resembled type I crossed girdles, with the connecting girdle through Y, which were asymmetric with respect to the XY plane of the finite strain ellipsoid (=schistosity). The fabric was in each case related to the slip plane and the slip direction. A girdle of  $\underline{c}$ -axes developed which was orthogonal to both the slip plane and the slip direction. Although in Figure 4-6 the strongest maximum of quartz  $\underline{c}$ -axes lay in the girdle orthogonal to the shear plane this was not always the case. However, a distinct girdle of  $\underline{c}$ -axes was always produced which was orthogonal to the shear plane.

#### E) Sense of Shear Determined from Quartz $\underline{c}$ -Axis Fabric Asymmetry

Asymmetric quartz  $\underline{c}$ -axis fabrics may be useful for determining the sense of shear of an aggregate having undergone shear strains. Essentially, the sense of shear can be determined when the orientation of the slip or shear plane with respect to the schistosity can be established from the quartz  $\underline{c}$ -axis petrofabrics. The relationship shown in Figure 4-2 may be applied (considered here on the scale of the whole rock) (i.e.) the slip plane lies counterclockwise from the schistosity trace in sinistral shear and clockwise when shear is in the dextral sense.

Asymmetric fabrics which might develop from slip in predominantly one sense on a single slip system in quartz are

fairly easy to envisage. Figure 4-7 illustrates the quartz c-axis fabrics which would develop from predominantly sinistral or dextral slip on a number of individual slip systems. The diagrams are derived from Figure 4-3 which demonstrates the general case (coaxial strain history) of slip on one slip system. The asymmetric quartz c-axis fabrics which develop from slip on some slip systems appear to be useful for determining the sense of shear. In particular Figure 4-7a, basal slip in an  $\langle a \rangle$  direction. Also prism slip in the  $\langle c \rangle$  direction (Figure 4-7b) may be useful. In these examples the active slip system can be easily inferred from the orientation of c-axis maxima. Note that no asymmetry of c-axis fabric develops in the case of prism slip in the  $\langle a \rangle$  direction and therefore this slip system has been omitted from Figure 4-7. No asymmetry develops because the c-axis lies in the slip plane normal to the slip direction at the intersection of the traces of the slip plane and the schistosity. In some cases (Figure 4-7c, d, e) inferring the attitude of the slip plane from the asymmetry of the fabric with respect to the schistosity would be difficult unless the active slip system was actually known. The c-axis petrofabric diagrams for these systems look very similar and the slip plane orientation could not be accurately defined if the slip system was not known.

The determination of the sense of shear from asymmetric girdle distributions of quartz c-axes which are commonly found in

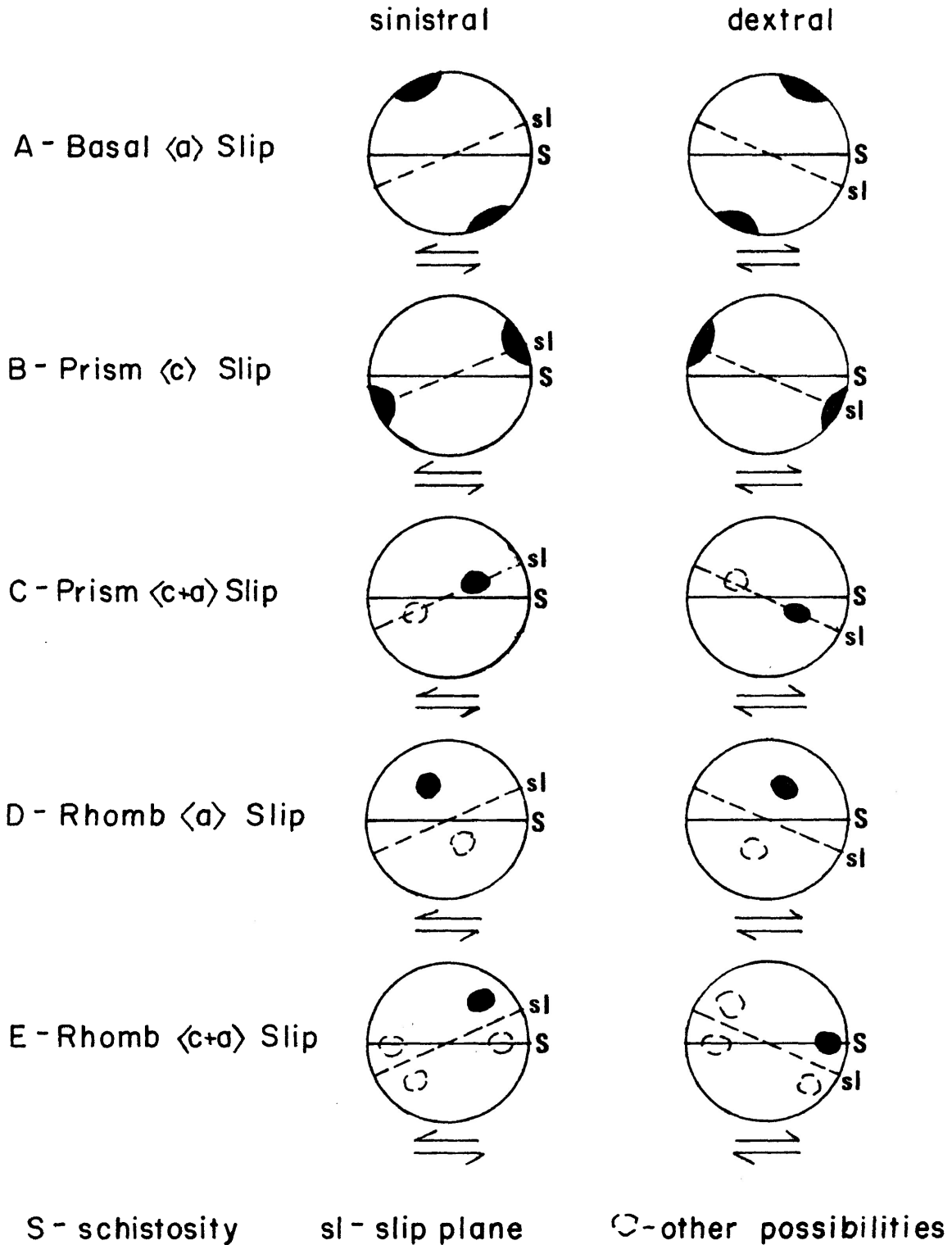


FIG. 4-7: Asymmetric quartz  $c$ -axis fabrics which develop from slip in predominantly one sense on individual slip systems.

Note: Prism  $\langle a \rangle$  slip is not shown as no asymmetry develops.

nature has been described by Bouchez (1978) and Bouchez and Pêcher (1981). They demonstrated that great circle girdles of quartz c-axes in the quartzites they studied lay normal to the slip direction and that the slip direction lay close to but distinct from the mineral lineation when the girdles of c-axes were asymmetric with respect to the schistosity. This was established based on studies of the orientation of subgrain boundaries and quartz a-axes.

In earlier studies Bouchez and Pêcher (1976) and Bouchez (1977) examined the preferred orientation of poles to subgrain boundaries. Subgrain boundaries are supposed to be tilt walls (of dislocations) resulting from slip. These tilt walls lie normal to the slip direction. Thus the poles to the subgrain boundaries should indicate the slip direction. The poles to the subgrain boundaries lay normal to the girdles of c-axes. Since many of the subgrain boundaries were found to be prismatic in orientation the basal plane was thought to be the dominant slip plane. Bouchez and Pêcher (1976) and Bouchez (1977) constructed rose diagrams of "basal plane traces" inferred from the orientation of the subgrain boundaries. The predominant maxima of basal plane traces in the rose diagram was taken to represent the slip direction and to infer the sense of shear. Bouchez (1978) examined quartz a-axis preferred orientations determined with the X-ray texture goniometer. The a-axes clustered normal to the girdles of quartz c-axes. A



single maxima of a-axes formed normal to single girdles of c-axes. Crossed girdles of c-axes had two corresponding a-axis maxima. The strongest a-axis maxima lay normal to the strongest c-axis girdle. The preferred orientations of the a-axes suggested  $\langle a \rangle$  was the prominent slip direction. The a-axis maxima were similar in orientation to the poles to the subgrain boundaries.

The sense of shear may be determined by defining the orientation of the slip or shear plane with respect to the schistosity. According to Pêcher (1981) the shear plane associated with single great circle girdles contains the slip direction (located normal to the girdle) and is supposed to contain the Y-axis of the finite strain ellipsoid (assuming XY corresponds to the schistosity and X to the quartz grain lineation where  $X \geq Y \geq Z$ ) as shown in Figure 4-8A. In the case of crossed great circle girdles the slip plane is supposed to contain Y and the slip direction which lies normal to the predominant girdle of c-axes (Figure 4-8B). The minor girdle of c-axes is thought to represent shear in the opposite sense as described by Etchecopar (1977) (antithetic slip). Bouchez and Pêcher found that the sense of shear determined from quartz c-axis fabric asymmetry indicated the correct sense of shear (known in the quartzites studies) in most cases.

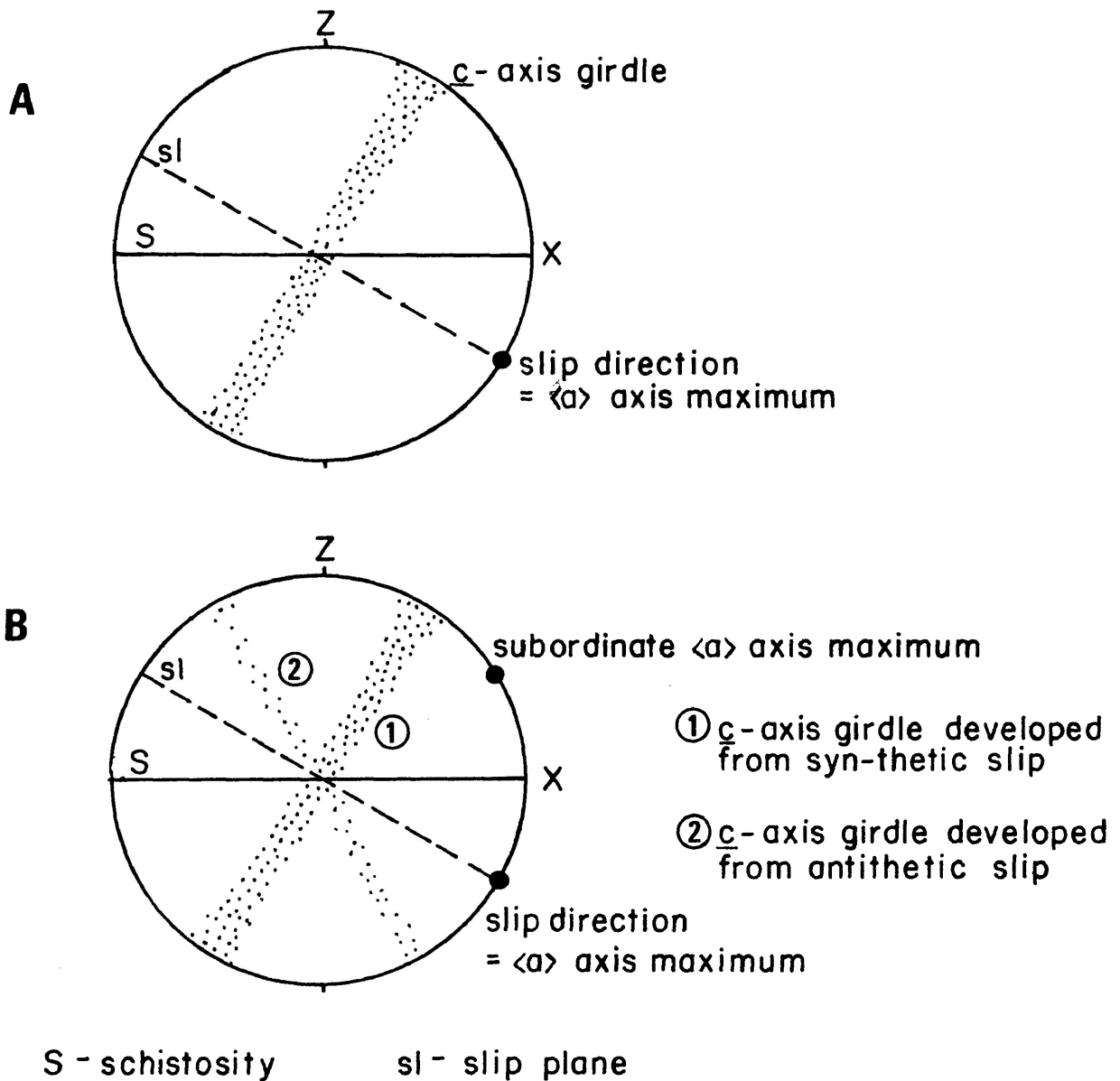


FIG. 4-8: Determination of the orientation of the slip plane from great circle girdle and crossed girdle distributions of quartz  $\underline{c}$ -axes as described by Bouchez and Pêcher (1981).

A-Single Great Circle Girdle - The slip direction lies normal to the girdle. The slip plane contains the slip direction and the Y-axis.

B-Crossed Great Circle Girdle - The slip direction lies normal to the strongest girdle. The slip plane contains the slip direction and the Y-axis.

5 - QUARTZ c-AXIS PETROFABRICS IN THE QUETICO FAULT ZONE

## A) Method

Oriented specimens were collected in the field from the selected localities (see Figure 1-4). Quartz-rich samples were chosen where possible, for quartz c-axis fabric determinations. Specimens ranging from essentially unstrained rocks to extremely strained rocks were included in the sampling. Oriented thin sections, commonly cut normal to the schistosity, were prepared from the samples collected.

The orientation of quartz c-axes was measured in these sections using a four-axis universal stage. The individual c-axis orientation of quartz was measured as described by Kerr (1977, p. 141-142) and Turner and Weiss (1968, p. 230-231). Quartz c-axis orientations were measured in the thin sections along traverses trending normal to the schistosity of the rock. Each quartz grain along the traverses was measured until 100 grains had been measured per thin section. The orientations of the quartz c-axes were plotted on an equal area stereographic projection (lower hemisphere)

## B) Petrofabric Diagrams

A rotation was applied to the data to bring the schistosity into a vertical attitude. The c-axes rotate because

the schistosity is rotated into the vertical. In samples in which a lineation was observed, the data were rotated to bring the lineation to the horizontal. In cases in which a lineation was not observed a rotation was applied to the data to bring the dip direction of the schistosity into the vertical. By performing these rotations a comparison of individual examples is more meaningful. In some samples the north-south axis is no longer located on the primitive of the stereonet (i.e. it is not horizontal in orientation) however the east-west axis still lies at or very close to the primitive of the stereonet.

Each petrofabric diagram constructed represents the orientation of 100 quartz c-axes. The diagrams were contoured using a one percent area counter by the free-counter method. The diagrams are all contoured at 1, 2, 3.5, 5 and 8 percent per one percent area and are ornamented as shown in the legend. Where a lineation has been indicated on a diagram the type of lineation is noted with the diagram.

#### C) Data

Figures 5-1 to 5-13 represent the quartz c-axis petrofabrics measured in samples from the selected localities of the Quetico fault zone. The figures are arranged geographically by locality from west to east and within the figures the petrofabric diagrams are arranged in order from north to south. The

## LEGEND

QUARTZ C-AXIS PETROFABRIC DIAGRAMS

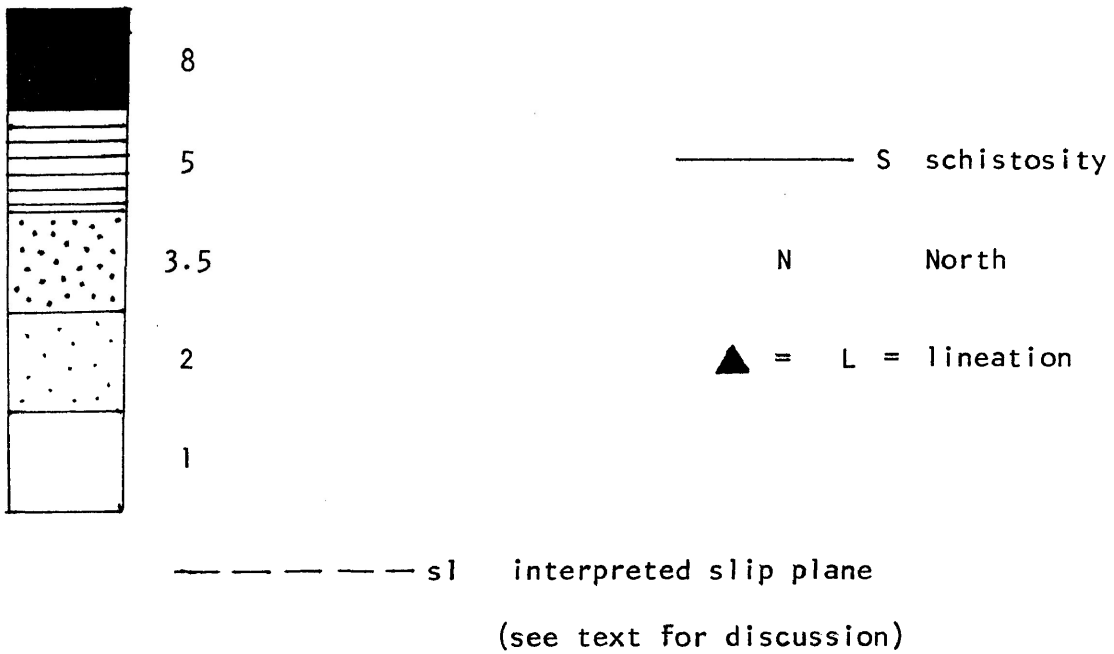
Figures 5-1 to 5-13

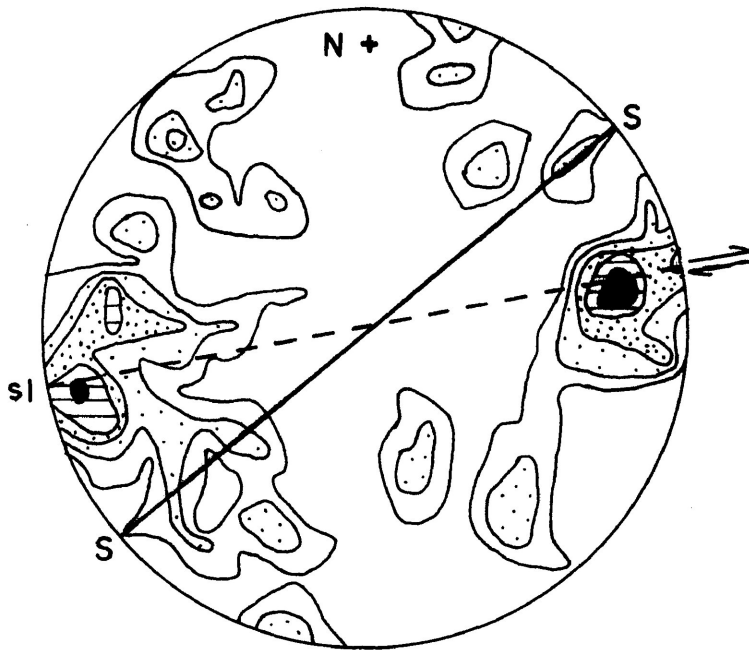
Equal area projection, lower hemisphere

Each diagram represents 100 measurements

Contoured at 1-2-3.5-5-8 percent per one percent area

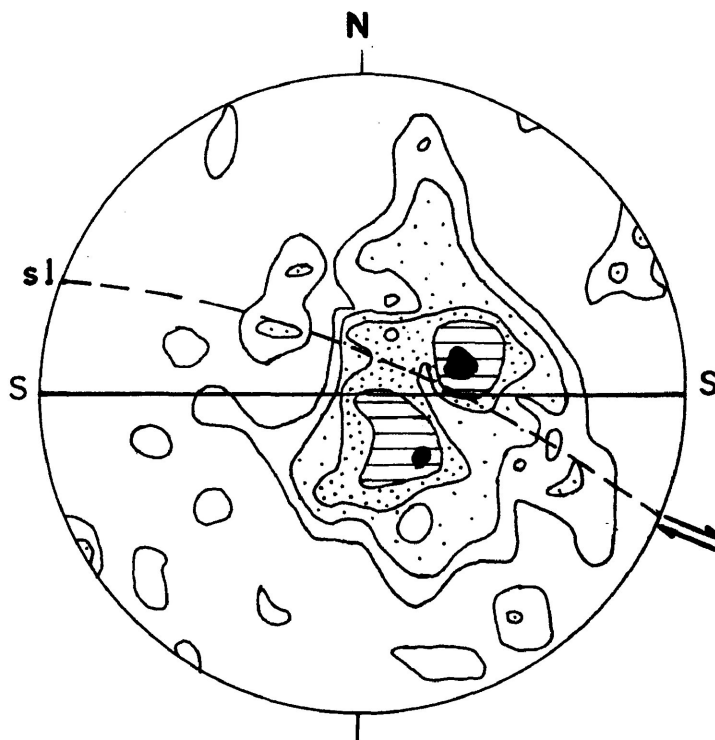
## Ornamentation





**FIG. 5-1A**

**BOR-80-M89**




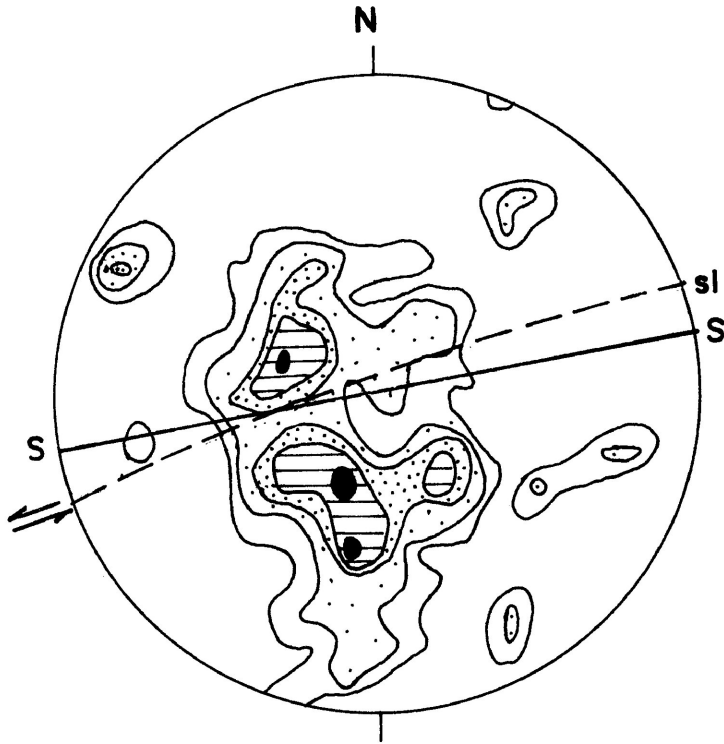
**FIG. 5-1B**

**BOR-80-M91**

LOCALITY - DANCE TOWNSHIP

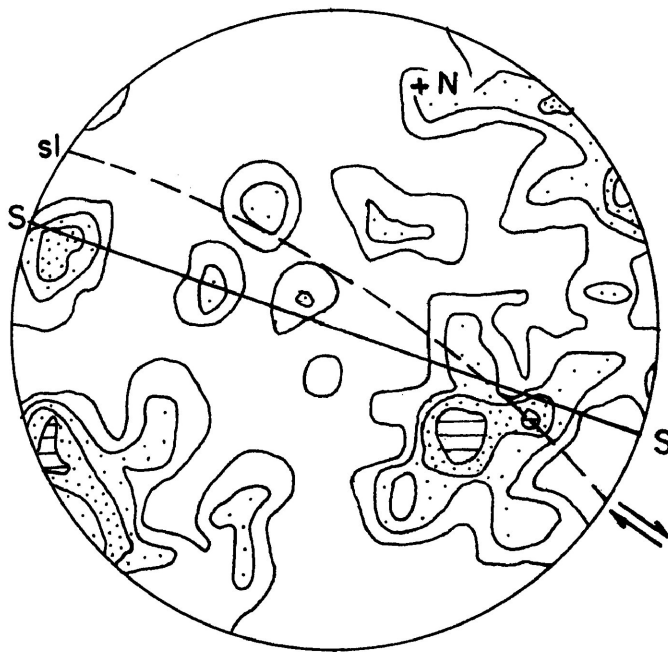
TABLE 5-1

SPECIMEN	SAMPLE DESCRIPTION	DESCRIPTION OF QUARTZ GRAINS
BOR-80-M89 (Figure 1A)	<ul style="list-style-type: none"> <li>- medium grained intrusive rock appears rather undeformed</li> <li>- schistosity very poorly defined (weak preferred orientation of mica).</li> <li>- approximately 40% quartz</li> </ul>	<ul style="list-style-type: none"> <li>- quartz grains somewhat elongate</li> <li>- most "grains" are composed of several fairly equant grains</li> <li>- some grains exhibit core-and-mantle texture</li> <li>- larger grains exhibit undulose extinction.</li> </ul>
BOR-80-M91 (Figure 1B)	<ul style="list-style-type: none"> <li>- fine grained laminated mylonite</li> <li>- light and dark coloured layers well defined</li> <li>- contains a few remnant feldspar porphyroclasts</li> <li>- approximately 20% quartz</li> </ul>	<ul style="list-style-type: none"> <li>- fine recrystallized grains</li> <li>- grains are elongate</li> <li>- grains exhibit undulose extinction, deformation lamellae</li> <li>- subgrains commonly at ends of grains (some with high angle boundaries)</li> </ul>
BOR-80-M93 (Figure 1C)	<ul style="list-style-type: none"> <li>- finely laminated fine grained mylonite</li> <li>- dark streaks occur in the light coloured material</li> <li>- contains numerous feldspar porphyroclasts (remnants)</li> <li>- approximately 20% quartz</li> </ul>	<ul style="list-style-type: none"> <li>- as BOR-80-M91</li> <li>- contains some bands of quartz composed of elongate grains</li> </ul> 
BOR-80-M95 (Figure 1D)	<ul style="list-style-type: none"> <li>- fine to medium grained intrusive (similar to BOR-80-M89)</li> <li>- undeformed appearance</li> <li>- weakly developed schistosity</li> <li>- approximately 40% quartz</li> </ul>	<ul style="list-style-type: none"> <li>- elongate grains having well developed undulose extinction</li> <li>- subgrains commonly developed (some with high angle grain boundaries)</li> </ul>



**FIG. 5-1C**

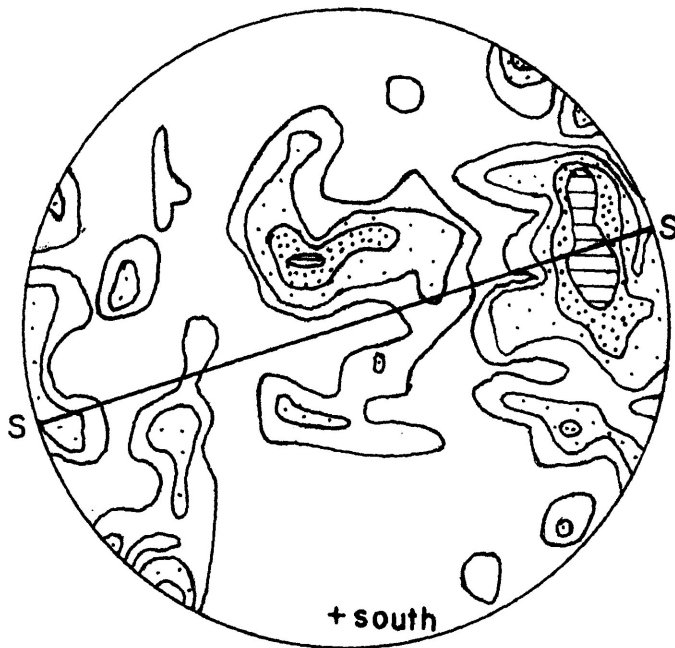
**BOR-80-M93**



**FIG. 5-1D**

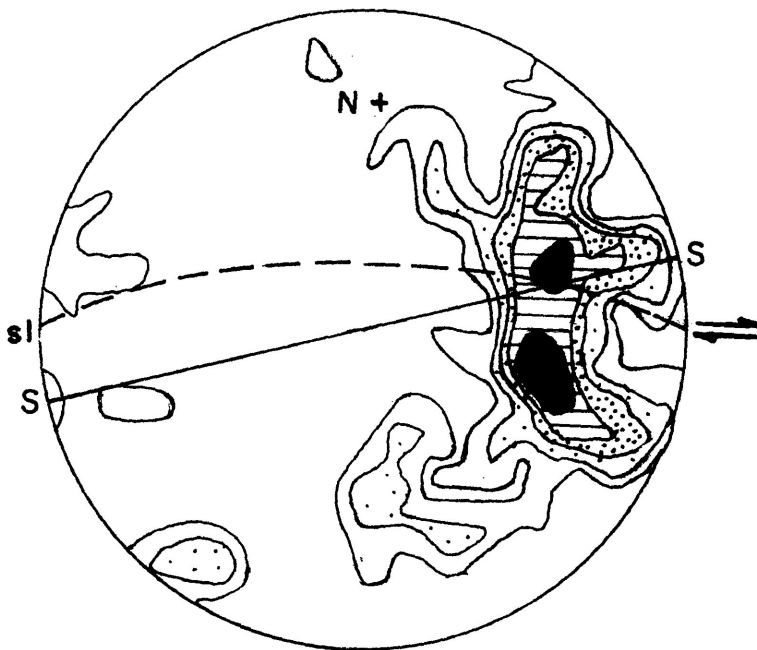
**BOR-80-M95**





**FIG. 5-2A**

**BOR-80-MI40**




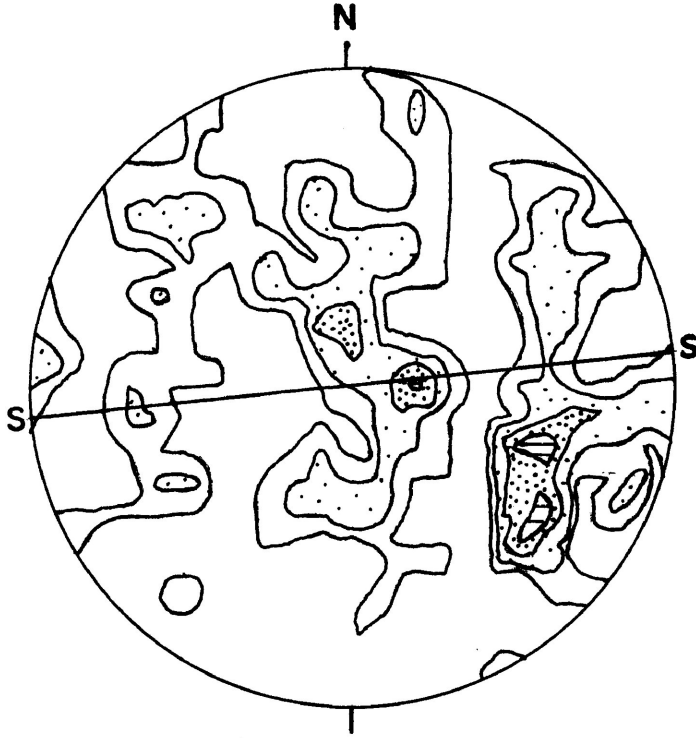
**FIG. 5-2B**

**BOR-80-MI37**

LOCALITY - MACDONALD INLET, RAINY LAKE

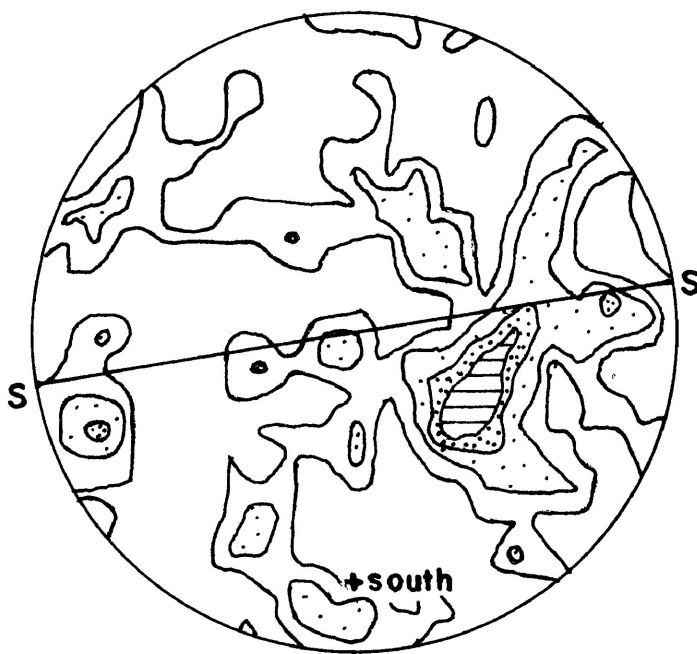
TABLE 5-2

SPECIMEN	SAMPLE DESCRIPTION	DESCRIPTION OF QUARTZ GRAINS
BOR-80-M140  (Figure 2A)	<ul style="list-style-type: none"> <li>- fine grained layered mylonite (pink and dark layers)</li> <li>- abundant porphyroclasts of feldspar-ovoid shape (<math>\approx 4</math> mm length)</li> <li>- approximately 30-40% quartz</li> </ul>	<ul style="list-style-type: none"> <li>- very elongate quartz grains</li> <li>- grains are composed of elongate sub-grains often rectangular in shape</li> </ul>  <ul style="list-style-type: none"> <li>- subgrains exhibit undulose extinction</li> </ul>
BOR-80-M137  (Figure 2B)	<ul style="list-style-type: none"> <li>- fine grained light/dark layered mylonitic rock</li> <li>- small (<math>\approx 1</math> mm diameter) feldspar porphyroclasts</li> <li>- approximately 40% quartz</li> </ul>	<ul style="list-style-type: none"> <li>- as BOR-80-M140</li> </ul>
BOR-80-M134  (Figure 2C)	<ul style="list-style-type: none"> <li>- layered mylonite similar to above samples</li> <li>- dark and light layers</li> <li>- contains ovoid feldspar porphyroclasts</li> <li>- approximately 30% quartz</li> </ul>	<ul style="list-style-type: none"> <li>- very elongate grains as above</li> </ul>



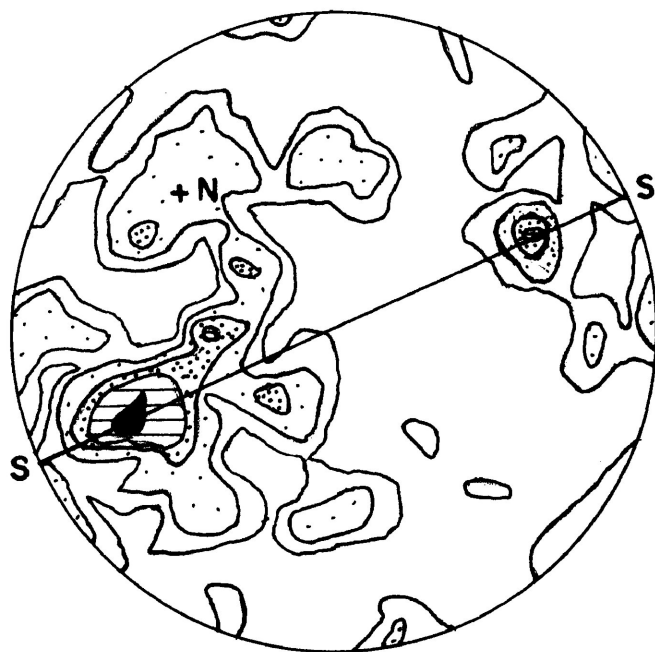
**FIG. 5-2C**

**BOR-80-M134**



**FIG. 5-3A**

**BOR - 80 - M101**

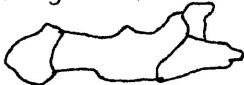


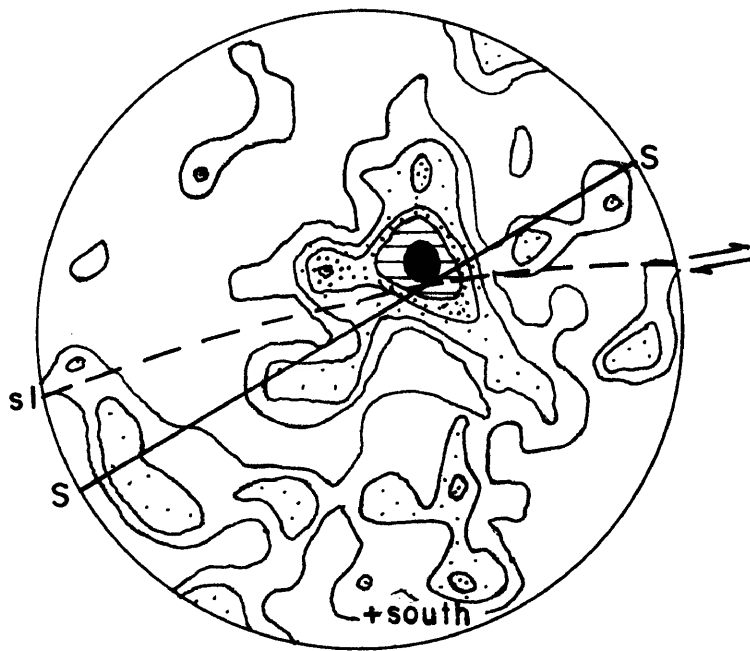
**FIG. 5-3B**

**BOR - 80 - M99**

LOCALITY - CROWROCK INLET, RAINY LAKE

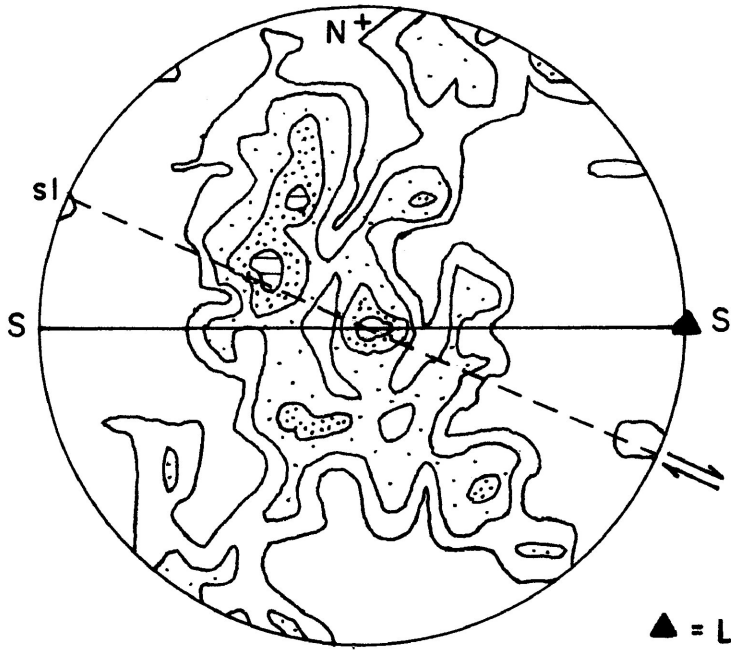
TABLE 5-3

SPECIMEN	SAMPLE DESCRIPTION	DESCRIPTION OF QUARTZ GRAINS
BOR-80-M101  (Figure 3A)	<ul style="list-style-type: none"> <li>- fine to medium grained mylonitic rock - well developed schistosity</li> <li>- mostly dark green with light coloured layers</li> <li>- small porphyroclasts of feldspar</li> <li>- approximately 40% quartz</li> </ul>	<ul style="list-style-type: none"> <li>- elongate quartz grains exhibiting undulose extinction</li> <li>- development of subgrains (with high angle grain boundaries) in larger grains</li> </ul> 
BOR-80-M99  (Figure 3B)	<ul style="list-style-type: none"> <li>- portion of a light coloured layer in dark/light layered rock</li> <li>- pink layer is very fine grained</li> <li>- layer composed entirely of quartz</li> </ul>	<ul style="list-style-type: none"> <li>- very fine grained quartz</li> <li>- mosaic of slightly elongate quartz grains</li> <li>- grains exhibit undulose extinction</li> <li>- subgrains are common-many have high angle grain boundaries</li> </ul>
BOR-80-M78  (Figure 3C)	<ul style="list-style-type: none"> <li>- pink rock composed of feldspar with ribbons of quartz</li> <li>- elongate quartz grains define the schistosity</li> <li>- approximately 60% quartz</li> </ul>	<ul style="list-style-type: none"> <li>- primarily very elongate grains exhibiting undulose extinction-subgrains common</li> <li>- some ribbons of quartz</li> <li>- some fairly equant grains</li> <li>- large grains with strong undulose extinction have deformation bands</li> </ul>



**FIG. 5-3C**

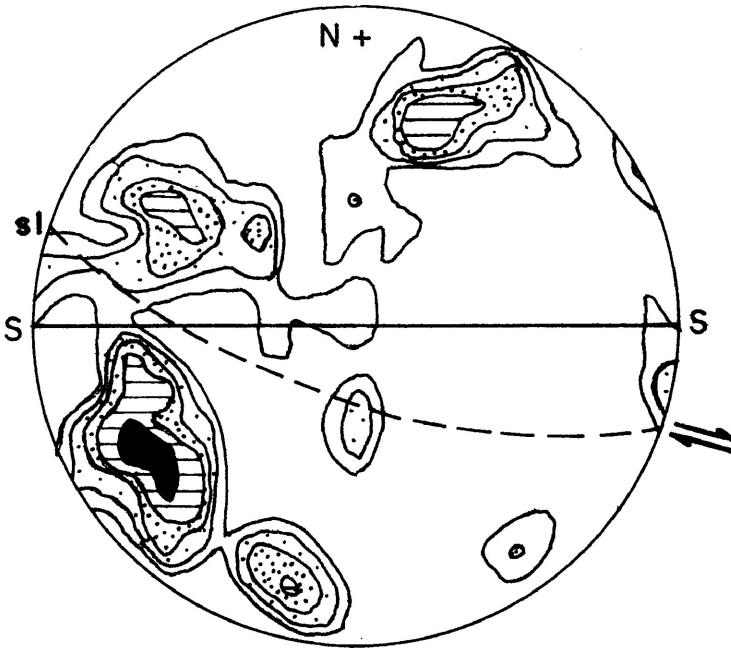
**BOR-80-M78**



**FIG. 5-4A**

**BOR-80-M73**

**▲ = L = quartz p. d. o.**



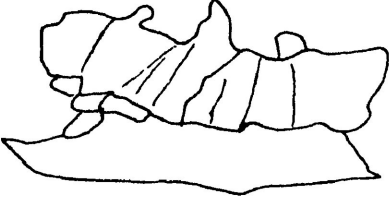
**FIG. 5-4B**

**BOR-80-M75**

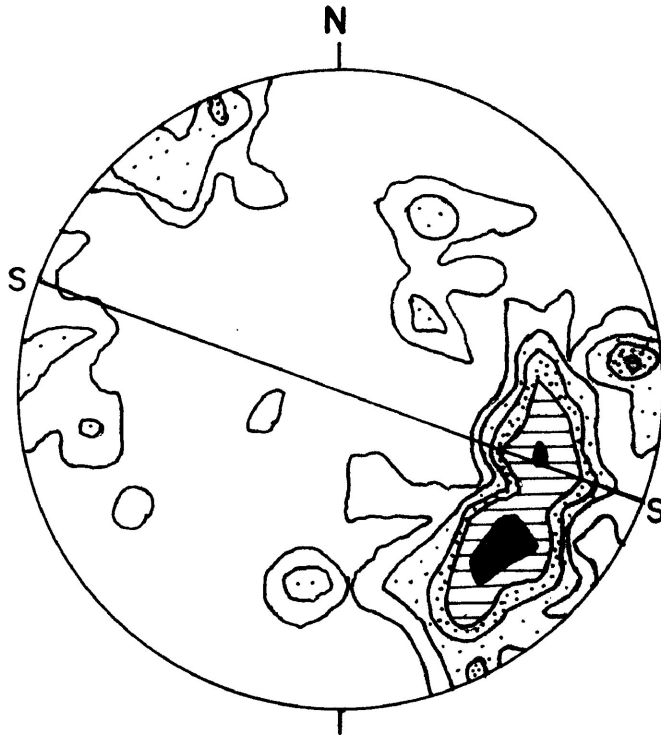
**▲ = L = quartz p. d. o.**

LOCALITY - TURTLE RIVER ROAD

TABLE 5-4

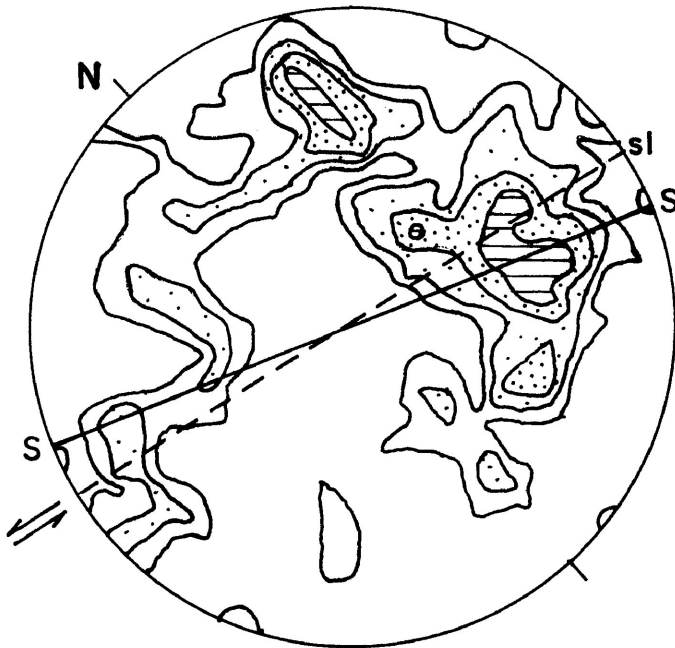
SPECIMEN	SAMPLE DESCRIPTION	DESCRIPTION OF QUARTZ GRAINS
BOR-80-M73 (Figure 4A)	<ul style="list-style-type: none"> <li>- pink mylonite with very fine dark layers in light coloured rock</li> <li>- contains very elongate quartz grains in feldspar rich matrix</li> <li>- ovoid feldspar porphyroclasts</li> </ul>	<ul style="list-style-type: none"> <li>- quartz grains rod-like</li> <li>- composed of elongate grains (somewhat rectangular in shape)</li> <li>- subgrains are common</li> <li>- larger grains exhibit strong undulose extinction and deformation bands</li> </ul>
BOR-80-M75 (Figure 4B)	<ul style="list-style-type: none"> <li>- quartz vein in quartz-feldspar-biotite gneiss</li> <li>- weakly deformed</li> </ul>	<ul style="list-style-type: none"> <li>- vein material composed of fairly large quartz grains which exhibit strong undulose extinction and deformation bands</li> <li>- grains are elongate, have serrated grain boundaries</li> <li>- a few subgrains observed</li> </ul> 





**FIG. 5-5A**

**BOR-80-M126**




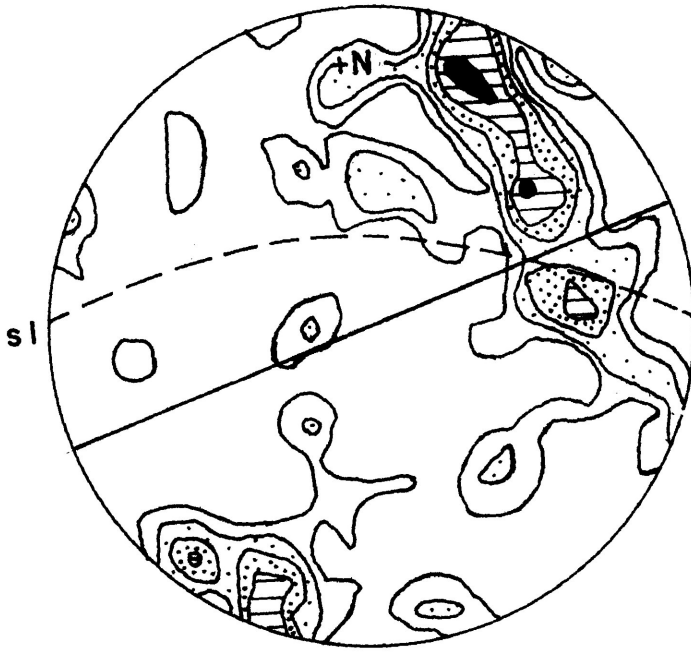
**FIG. 5-5B**

**BOR-80-M115**

LOCALITY - LITTLE TURTLE LAKE

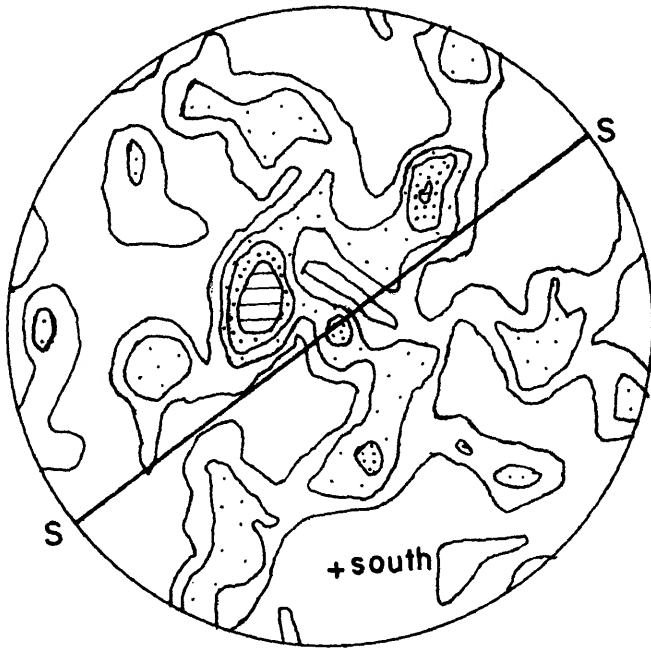
TABLE 5-5

SPECIMEN	SAMPLE DESCRIPTION	DESCRIPTION OF QUARTZ GRAINS
BOR-80-M126  (Figure 5A)	<ul style="list-style-type: none"> <li>- quartz vein material</li> </ul>	<ul style="list-style-type: none"> <li>- large elongate grains have undulose extinction, core and mantle texture</li> <li>- most grains are smaller, more equant</li> <li>- exhibit undulose extinction, serrated grain boundaries, have subgrains</li> </ul>
BOR-80-M115  (Figure 5B)	<ul style="list-style-type: none"> <li>- fine grained pink mylonitic/cataclastic rock</li> <li>- Irregular dark streaky layering defines schistosity</li> <li>- some feldspar porphyroclasts</li> <li>- approximately 30% quartz</li> </ul>	<ul style="list-style-type: none"> <li>- mostly elongate grains with undulose extinction</li> <li>- some very elongate grains contain deformation bands</li> <li>- subgrains with high angle boundaries common-more equant</li> </ul>
BOR-80-M120  (Figure 5C)	<ul style="list-style-type: none"> <li>- fine to medium grained layered gneissic rock</li> <li>- light coloured layers fine grained, porphyroclastic</li> <li>- approximately 50% quartz</li> </ul>	<ul style="list-style-type: none"> <li>- elongate quartz grains exhibit undulose extinction and some deformation bands</li> <li>- most grains are composed of a mosaic of several grains with roughly rectangular shape</li> <li>- some subgrains observed.</li> </ul> 



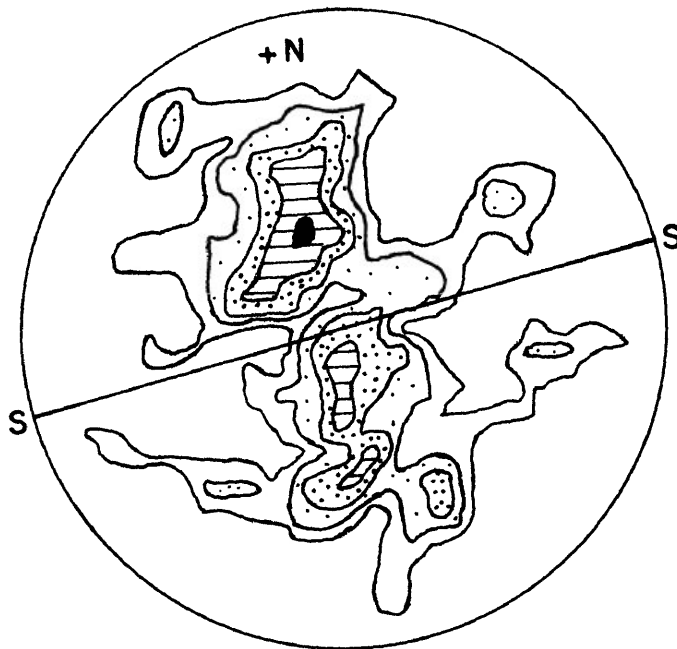
**FIG. 5-5C**

**BOR-80-M120**



**FIG. 5-6A**

**BOR-80-M53**


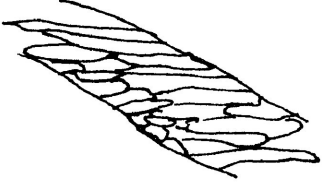


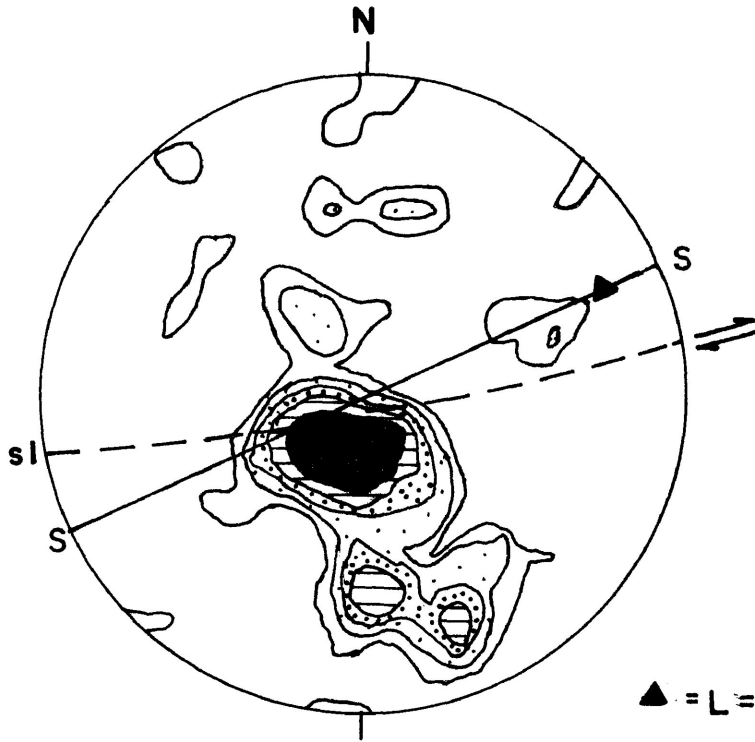
**FIG. 5-6B**

**BOR-80-M54**

LOCALITY - LAC DES MILLE LACS

TABLE 5-6

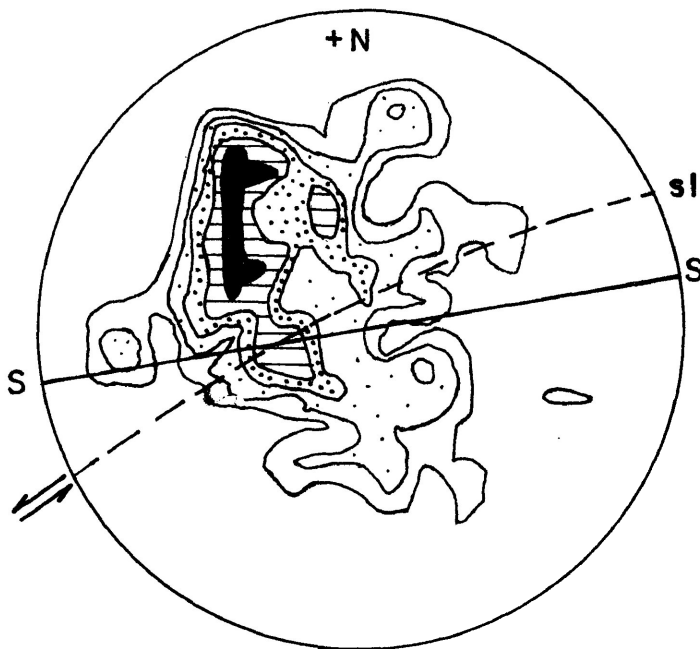
SPECIMEN	SAMPLE DESCRIPTION	DESCRIPTION OF QUARTZ GRAINS
BOR-80-M53 (Figure 6A)	<ul style="list-style-type: none"> <li>- feldspar rich gneissic rock</li> <li>- fine grained dark layers</li> <li>- porphyroclastic texture</li> <li>- weakly developed-approximately 50% quartz</li> </ul>	<ul style="list-style-type: none"> <li>- mostly elongate grains with undulose extinction, some deformation bands, core-and-mantle texture</li> <li>- some ribbons and some more equant grains</li> <li>- some subgrains, many with high angle grain boundaries</li> </ul> 
BOR-80-M54 (Figure 6B)	<ul style="list-style-type: none"> <li>- dark coloured mylonitic rock with thin light coloured layers</li> <li>- well defined schistosity</li> <li>- common feldspar porphyroclasts</li> <li>- approximately 40% quartz</li> </ul>	<ul style="list-style-type: none"> <li>- very elongate quartz grains with subgrains developing</li> <li>- exhibit undulose extinction</li> <li>- some ribbons</li> </ul> 



**FIG. 5-7A**

**BOR-80-M27**

▲ = L = amphibole p. d. o.




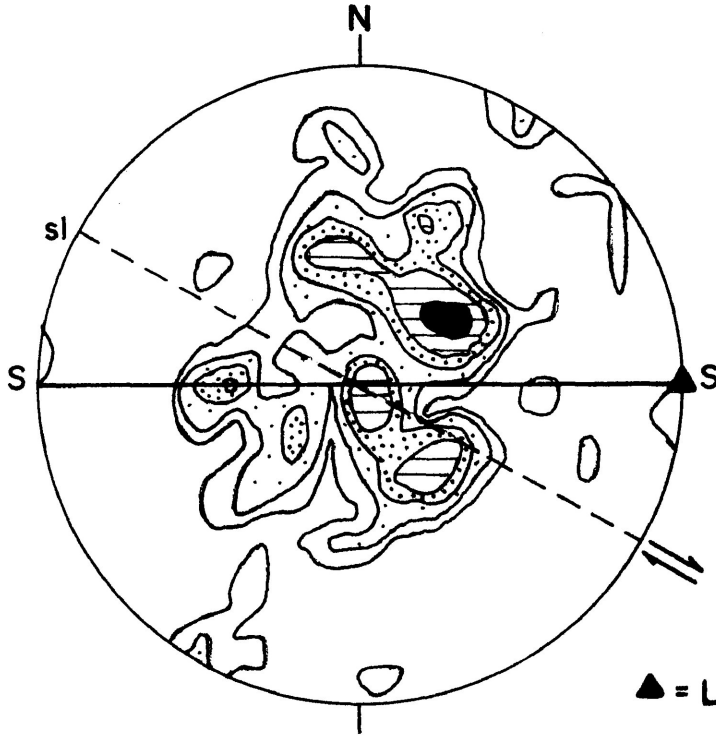
**FIG. 5-7B**

**BOR-80-M37**

LOCALITY - KASHABOWIE LAKE

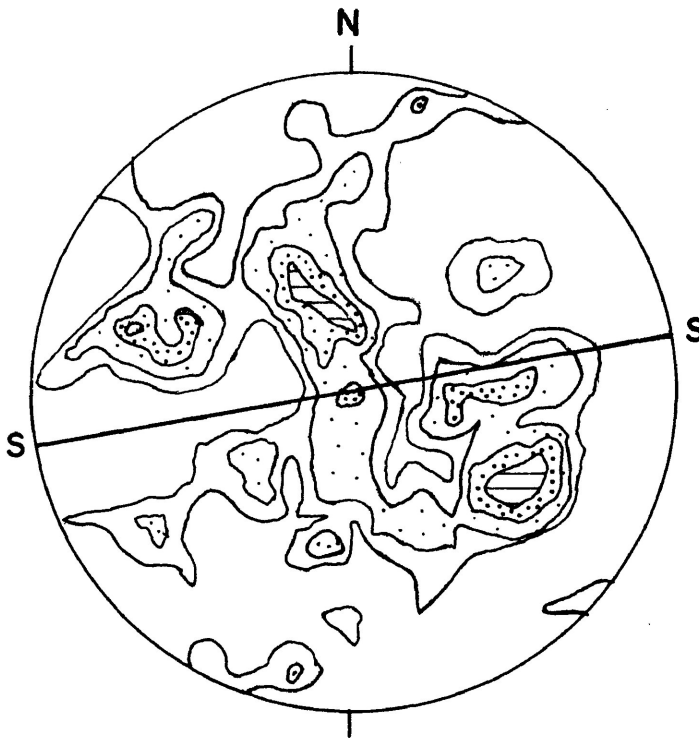
TABLE 5-7

SPECIMEN	SAMPLE DESCRIPTION	DESCRIPTION OF QUARTZ GRAINS
BOR-80-M27 (Figure 7A)	<ul style="list-style-type: none"> <li>- medium grained pink intrusive rock</li> <li>- black amphibole grains define the schistosity</li> <li>- matrix of fine grained quartz and feldspar</li> <li>- approximately 30% quartz</li> </ul>	<ul style="list-style-type: none"> <li>- highly elongate grains and ribbons</li> <li>- exhibit undulose extinction, have some deformation bands</li> <li>- some subgrain development</li> </ul>
BOR-80-M37 (Figure 7B)	<ul style="list-style-type: none"> <li>- similar to BOR-80-M27A</li> <li>- quartz more abundant (40%)</li> <li>- schistosity less well defined</li> </ul>	<ul style="list-style-type: none"> <li>- less deformed than BOR-80-M27A</li> <li>- also comprises elongate grains and ribbons with strong undulose extinction and deformation bands</li> </ul> 



**FIG. 5-8A**

**BOR-80-26**



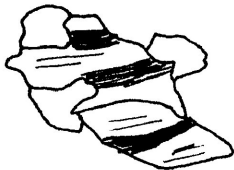
**FIG. 5-8B**

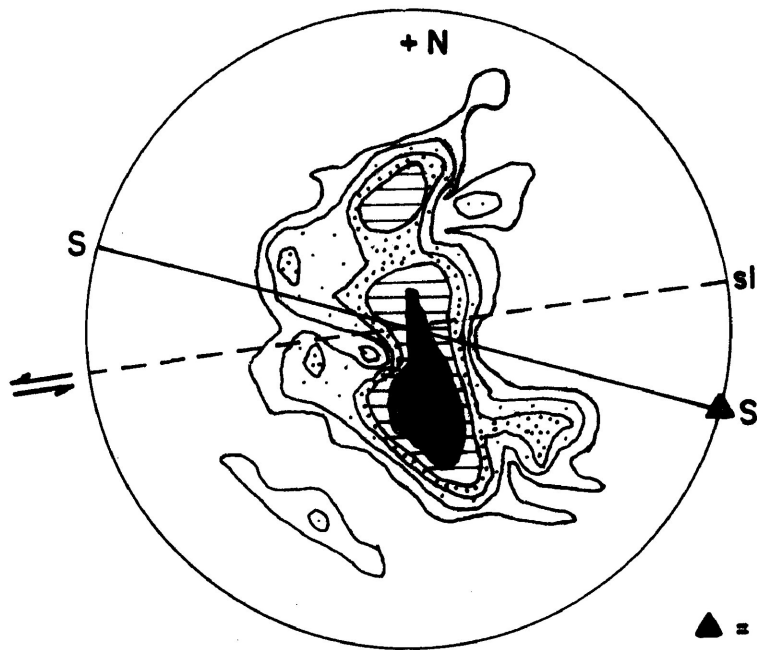
**BOR-80-19**



LOCALITY - ATHELSTANE LAKE

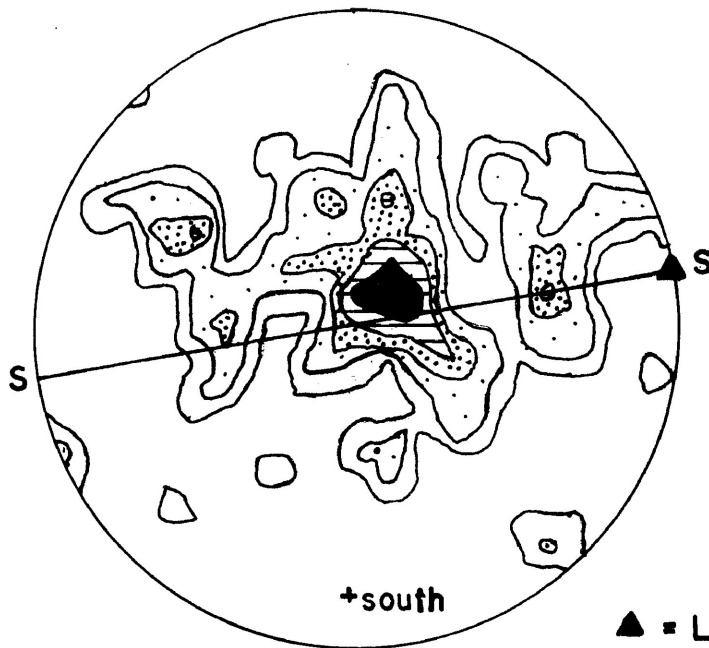
TABLE 5-8

SPECIMEN	SAMPLE DESCRIPTION	DESCRIPTION OF QUARTZ GRAINS
BOR-80-26  (Figure 8A)	<ul style="list-style-type: none"> <li>- fine to medium grained pink granitic rock rich in feldspar</li> <li>- weakly developed porphyroclastic texture</li> <li>- schistosity defined by biotite flakes and feldspar p.d.o.</li> <li>- approximately 30% quartz</li> </ul>	<ul style="list-style-type: none"> <li>- grains composed of a mosaic of smaller elongate grains</li> <li>- strong undulatory extinction in most grains</li> <li>- serrated grain boundaries, some subgrains developed</li> </ul>
BOR-80-19  (Figure 8B)	<ul style="list-style-type: none"> <li>- medium grained grey granitic rock - undeformed appearance</li> <li>- poorly defined schistosity</li> <li>- approximately 40% quartz</li> </ul>	<ul style="list-style-type: none"> <li>- mostly very elongate grains with strong undulose extinction and deformation bands</li> <li>- serrated grain boundaries</li> <li>- large, elongate, subgrains (with high angle grain boundaries) observed</li> </ul> 



**FIG. 5-9A**

**BOR-80-M11**



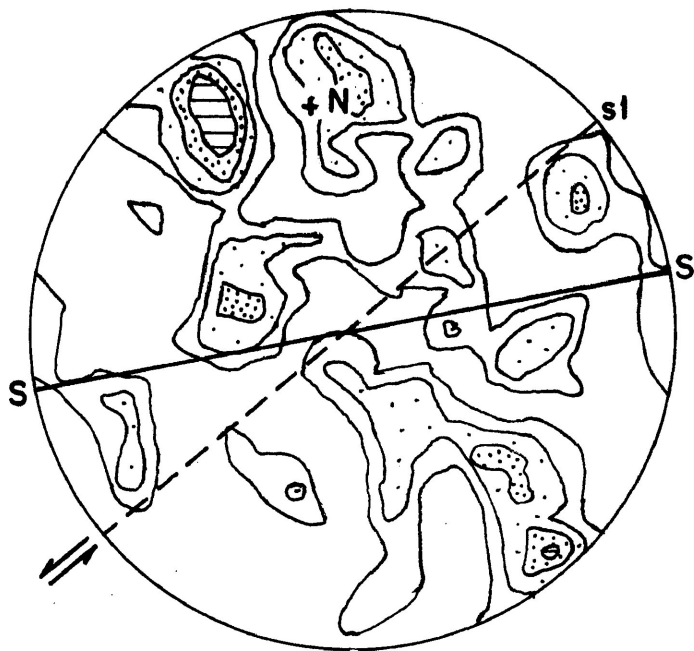
**FIG. 5-9B**

**BOR-80-M5**

LOCALITY - RAITH

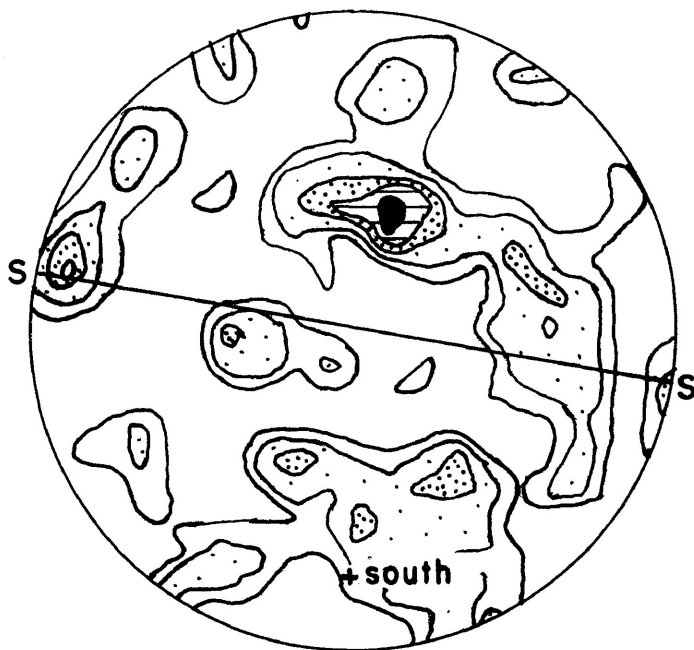
TABLE 5-9

SPECIMEN	SAMPLE DESCRIPTION	DESCRIPTION OF QUARTZ GRAINS
BOR-80-M11 (Figure 9A)	<ul style="list-style-type: none"> <li>- medium grained granitic rock with feldspar porphyroclasts (protomylonite)</li> <li>- finer grained quartz and biotite between large feldspars</li> <li>- approximately 40% quartz</li> </ul>	<ul style="list-style-type: none"> <li>- quartz 'grains' composed of mosaic of elongate grains</li> <li>- grains exhibit weak undulose extinctions</li> <li>- some small subgrains occur at the edges of grains</li> <li>- some ribbons</li> <li>- some very fine grained recrystallized portions</li> </ul>
BOR-80-M5 (Figure 9B)	<ul style="list-style-type: none"> <li>- medium grained porphyroclastic protomylonite (granitic)</li> <li>- well defined p.d.o. schistosity</li> <li>- approximately 50% quartz</li> </ul>	<ul style="list-style-type: none"> <li>- most grains comprise a mosaic of weakly elongate subgrains</li> <li>- some elongate grains exhibit undulose extinction</li> <li>- a few ribbon grains</li> </ul>



**FIG. 5-10A**

**BOR-80-M68**



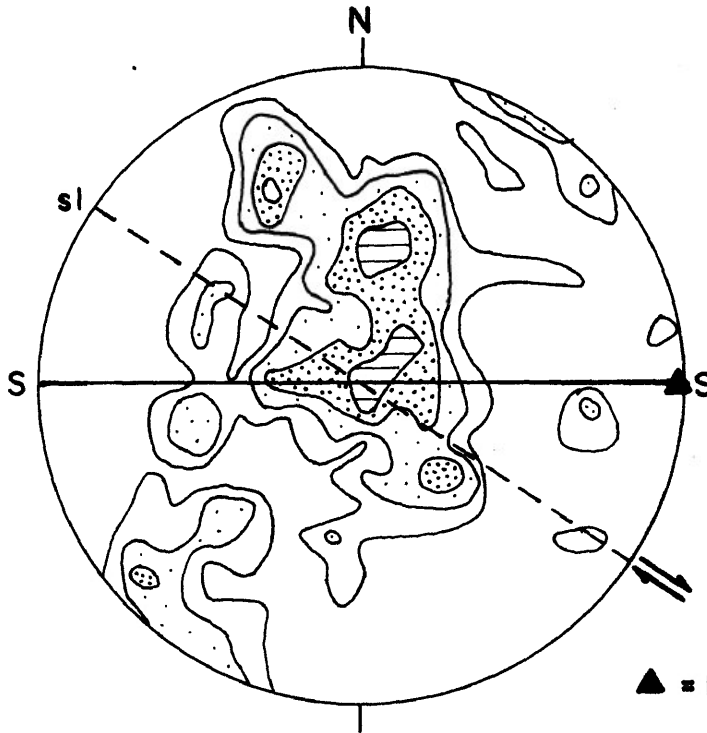
**FIG. 5-10B**

**BOR-80-19D**

LOCALITY - BUDA BAY, DOG LAKE

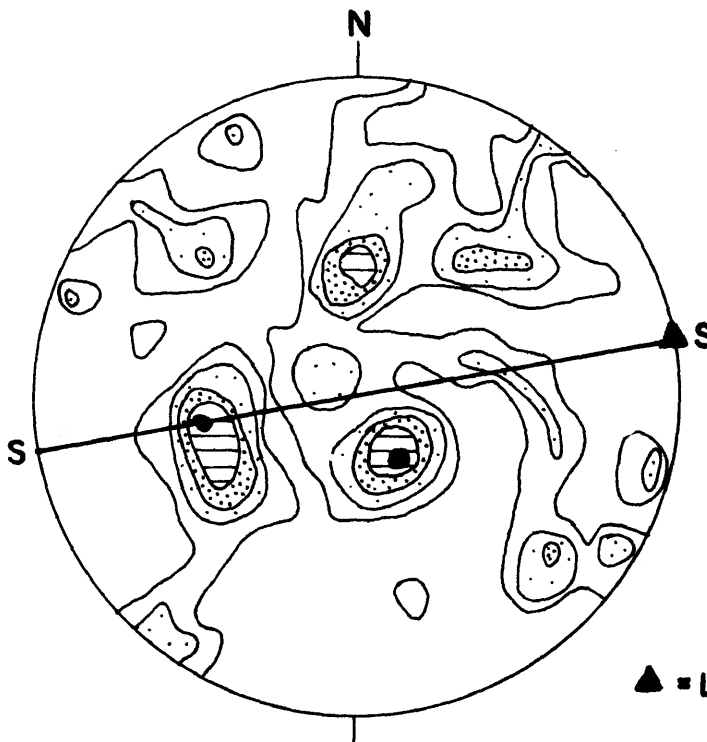
TABLE 5-10

SPECIMEN	SAMPLE DESCRIPTION	DESCRIPTION OF QUARTZ GRAINS
BOR-80-M68 (Figure 10A)	<ul style="list-style-type: none"> <li>- quartzo feldspathic protomylonite (granitic)</li> <li>- ovoid feldspar porphyroclasts of varying size</li> <li>- well defined p.d.o. schistosity</li> <li>- approximately 40% quartz</li> </ul>	<ul style="list-style-type: none"> <li>- elongate quartz 'grains' are composed of a mosaic of elongate grains with some ribbon grains</li> <li>- grains exhibit strong undulose extinction and deformation bands</li> <li>- some small subgrains around larger grains</li> </ul>
BOR-80-19D (Figure 10B)	<ul style="list-style-type: none"> <li>- fine grained quartz-feldspar-biotite schist</li> <li>- a few coarser layers</li> <li>- approximately 50% quartz</li> </ul>	<ul style="list-style-type: none"> <li>- quartz grains almost undeformed</li> <li>- equant grains with weak undulose extinction</li> </ul>



**FIG. 5-11A**

**BOR-80-M23**



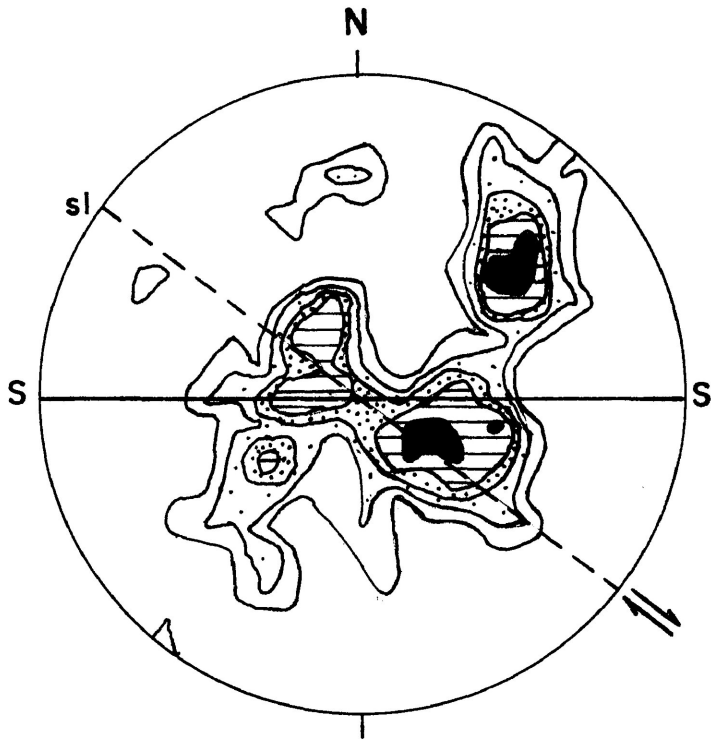
**FIG. 5-11B**

**BOR-80-M56b**

LOCALITY - CENTRAL DOG LAKE (WEST SHORE, CENTRAL ISLANDS)

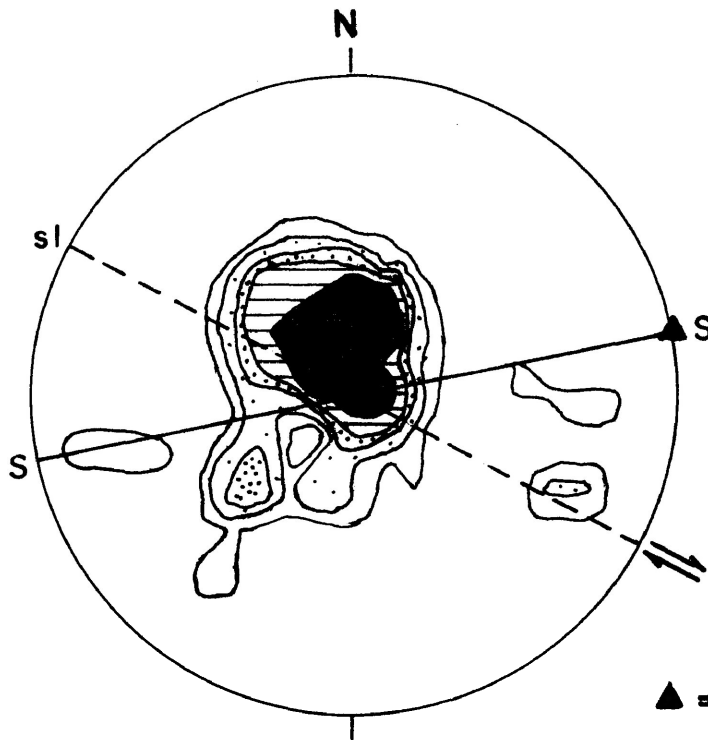
TABLE 5-11

SPECIMEN	SAMPLE DESCRIPTION	DESCRIPTION OF QUARTZ GRAINS
BOR-80-M23 West Shore (Figure 11A)	<ul style="list-style-type: none"> <li>- porphyroclastic mylonitic rock</li> <li>- ovoid feldspar porphyroclasts in a chloritic matrix</li> <li>- well defined p.d.o. schistosity</li> <li>- approximately 50% quartz</li> </ul>	<ul style="list-style-type: none"> <li>- generally mosaics of elongate grains and ribbons occur</li> <li>- serrated grain boundaries</li> <li>- many small grains are formed at grain boundaries and inside grains</li> </ul>
BOR-89-M56b Big Island (Figure 11B)	<ul style="list-style-type: none"> <li>- fine to medium grained granitic rock-weakly deformed</li> <li>- biotite flakes define schistosity</li> <li>- approximately 30% quartz</li> </ul>	<ul style="list-style-type: none"> <li>- grains exhibit strong undulose extinction, serrated grain boundaries</li> <li>- some grains composed of a mosaic of elongate subgrains</li> </ul> 
BOR-80-M60 Big Island (Figure 11C)	<ul style="list-style-type: none"> <li>- quartz vein</li> <li>- regional schistosity</li> </ul>	<ul style="list-style-type: none"> <li>- fine grained mosaic of elongate grains with undulose extinction</li> <li>- many subgrains at grain boundaries</li> </ul>
BOR-80-M13 Seagull Island (Figure 11D)	<ul style="list-style-type: none"> <li>- quartz vein containing a few small feldspar grains</li> </ul>	<ul style="list-style-type: none"> <li>- as above</li> </ul> 
BOR-80-M4 Seagull Island (Figure 11E)	<ul style="list-style-type: none"> <li>- quartz vein (ribbon-like) in biotite schist</li> </ul>	<ul style="list-style-type: none"> <li>- as above but some grains are composed of all subgrains</li> </ul>
BOR-80-M2 Seagull Island (Figure 11F)	<ul style="list-style-type: none"> <li>- quartz vein (ribbon-like)</li> </ul>	<ul style="list-style-type: none"> <li>- as above with serrated grain boundaries</li> <li>- some deformation bands in more deformed grains</li> <li>- some ribbon grains</li> </ul>
BOR-80-M19 Dad's Island (Figure 11G)	<ul style="list-style-type: none"> <li>- medium to coarse grained gneissic rock (proto-mylonite)</li> <li>- fairly undeformed appearance</li> <li>- approximately 30% quartz</li> </ul>	<ul style="list-style-type: none"> <li>- mosaics of elongate quartz grains</li> <li>- some grains very elongate-ribbons</li> <li>- all exhibit undulose extinction</li> <li>- serrated grain boundaries</li> </ul>
BOR-80-M17 Dad's Island (Figure 11H)	<ul style="list-style-type: none"> <li>- similar to BOR-80-M19 but finer grained</li> <li>- appears to be slightly more deformed</li> <li>- approximately 40% quartz</li> </ul>	<ul style="list-style-type: none"> <li>- mosaic of very elongate grains/subgrains</li> <li>- grains exhibit undulose extinction</li> <li>- some exhibit deformation bands</li> <li>- some ribbon grains</li> </ul>



**FIG. 5-11C**

**BOR-80-M60**

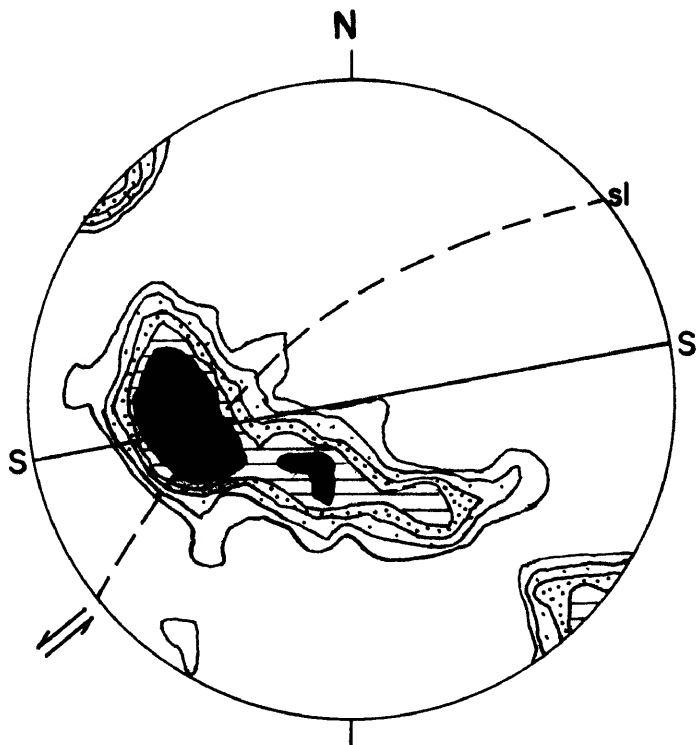


**FIG.5-11D**

**BOR-80-M13**

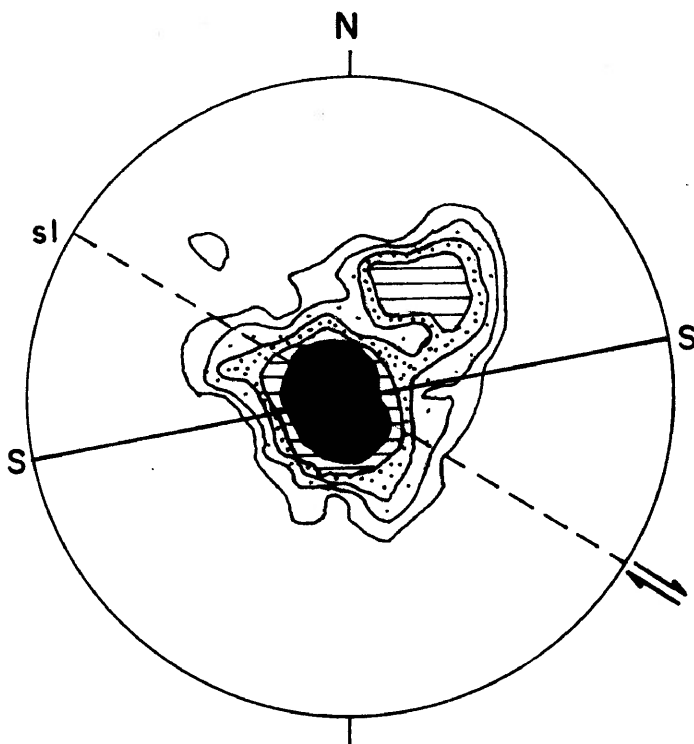
**▲ = L = slickensides**





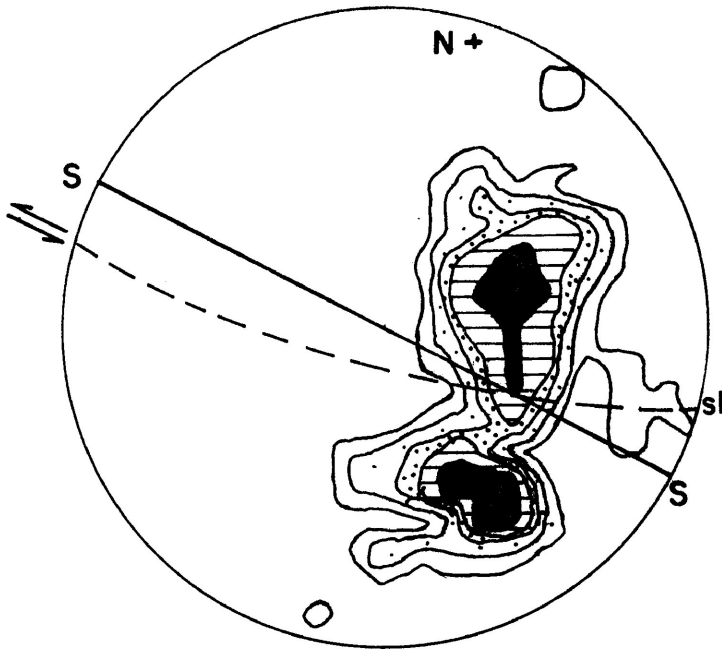
**FIG. 5-11E**

**BOR-80-M4**



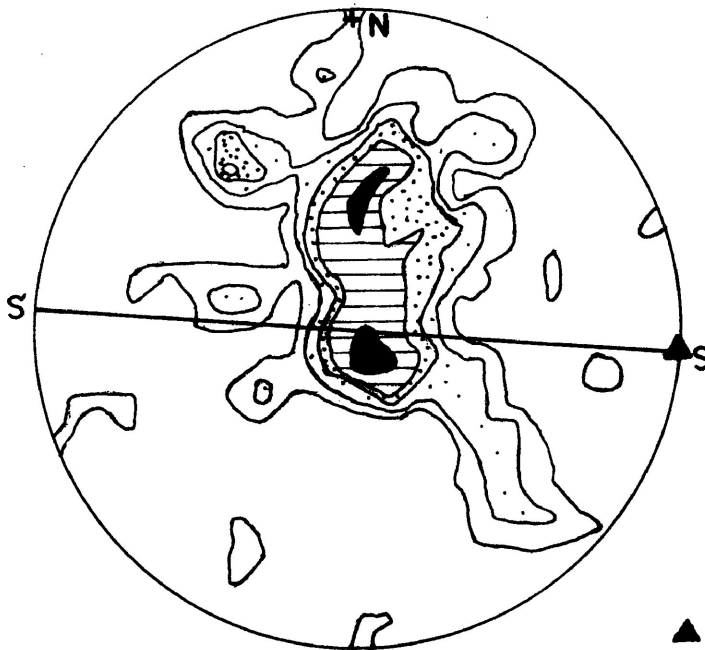
**FIG. 5-11F**

**BOR-80-M2**



**FIG. 5-11G**

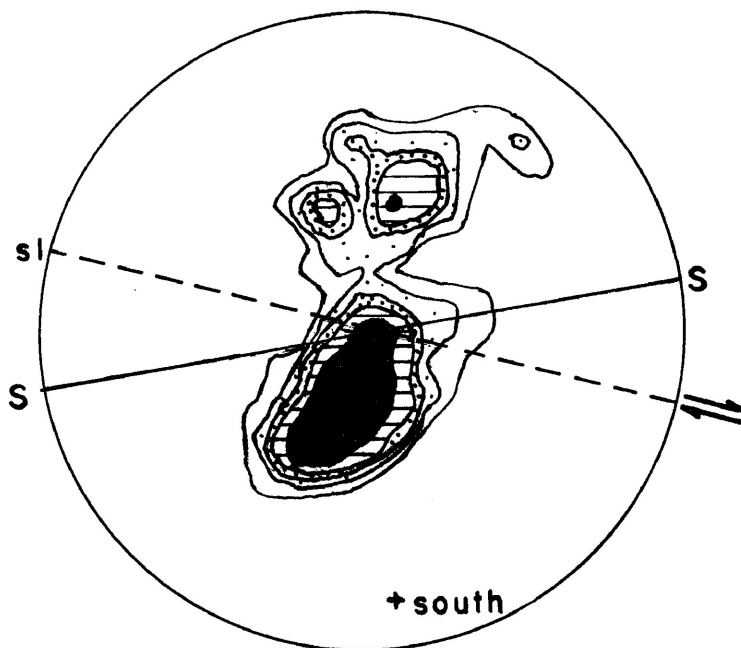
**BOR-80-MI9**



**FIG. 5-11H**

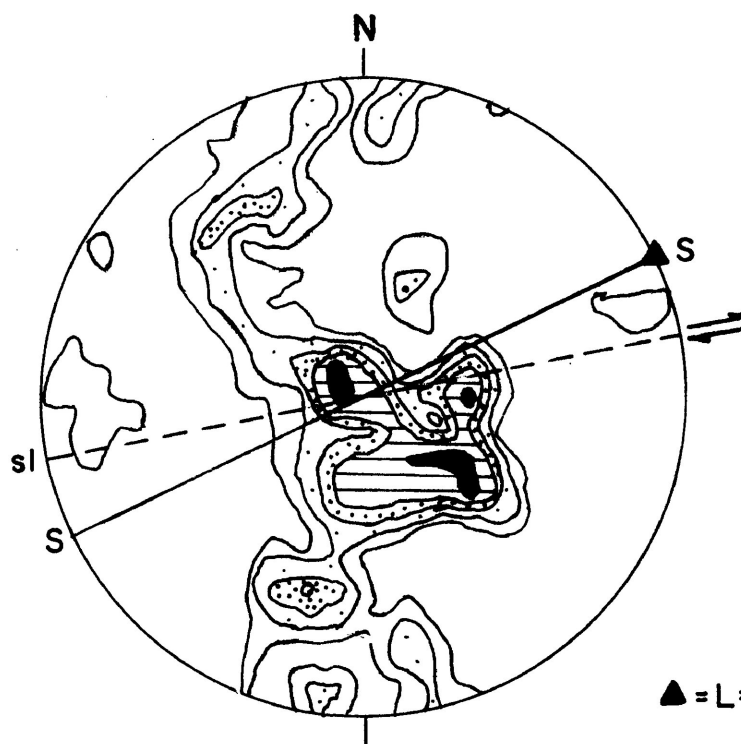
**BOR-80-MI7**

**▲ = L = slickensides (dextral)**



**FIG. 5-12A**

**BOR-80-MI48**





**FIG. 5-12B**

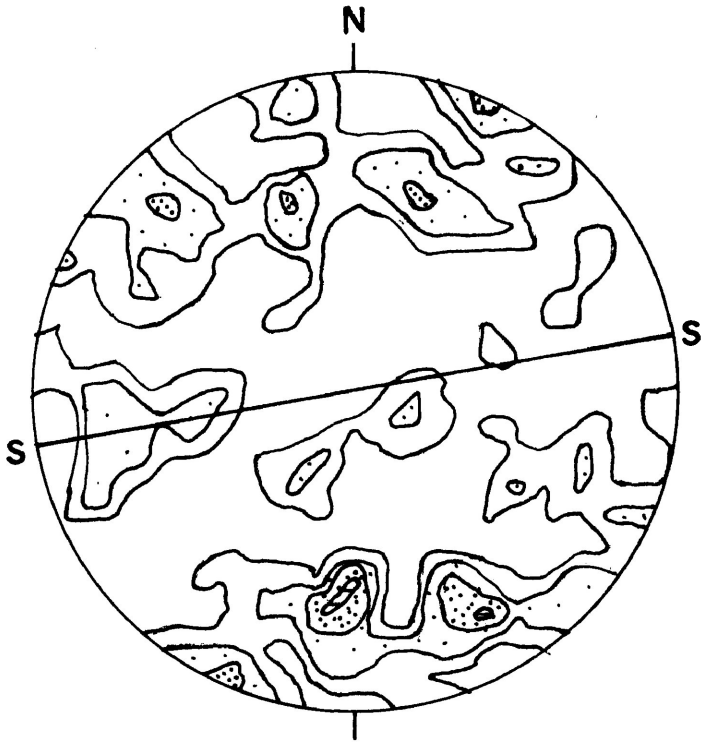
**BOR-80-MI55**

▲ = L = quartz and feldspar p.d.o.

LOCALITY - STIRRETT BAY, DOG LAKE

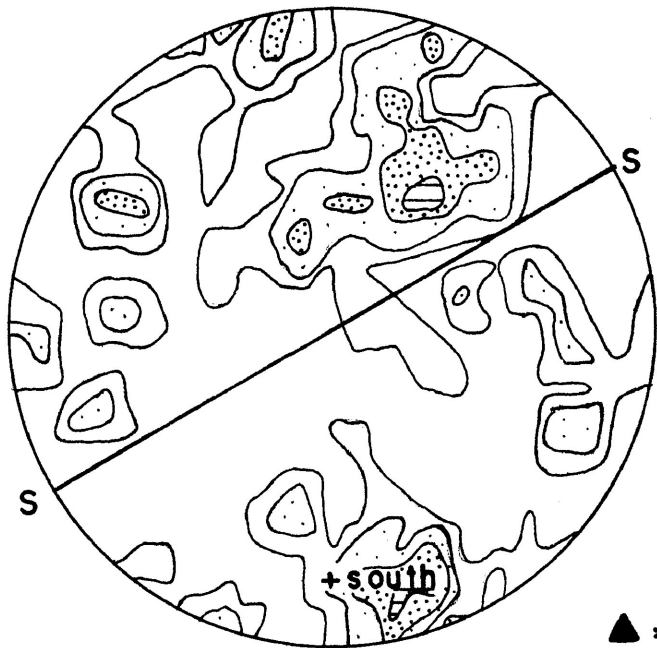
TABLE 5-12

SPECIMEN	SAMPLE DESCRIPTION	DESCRIPTION OF QUARTZ GRAINS
BOR-80-M148 (Figure 12A)	- quartz vein	- mosaic of very elongate grains exhibiting strong undulose extinction and deformation bands - abundant subgrains have developed around edges 
BOR-80-M155 (Figure 12B)	- porphyroclastic mylonitic rock - ovoid shaped feldspar porphyroclasts - quartz ribbon grains - approximately 40% quartz	- very elongate quartz grains with strong undulose extinction - some subgrains have developed around grain edges 
BOR-80-M160 (Figure 12C)	- fine grained granitic rock - undeformed appearance - approximately 40% quartz	- weak undulose extinction in quartz grains - equant grains with a few subgrains



**FIG. 5-12C**

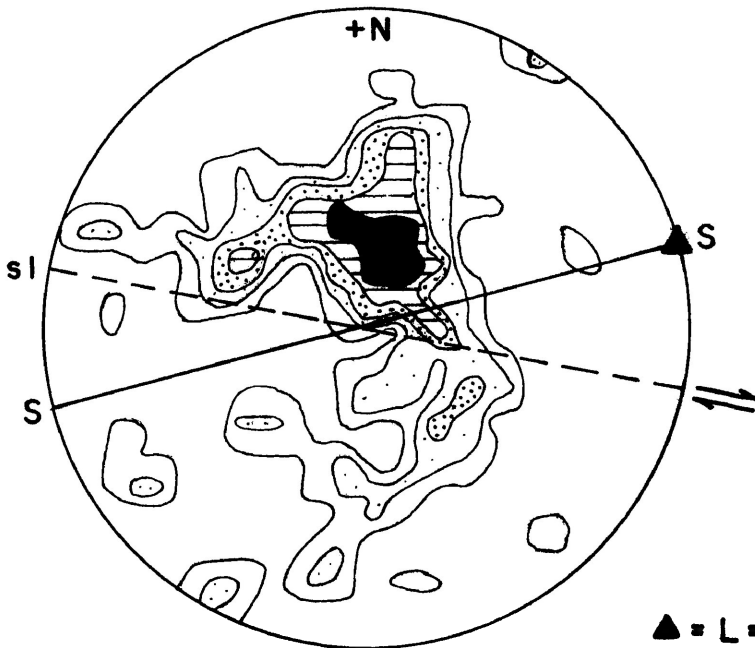
**BOR-80-M160**



**FIG. 5-13A**

**BOR-80-10**

▲ = L = slickensides (dextral)




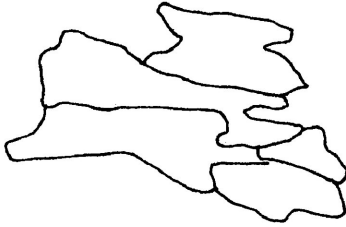
**FIG. 5-13B**

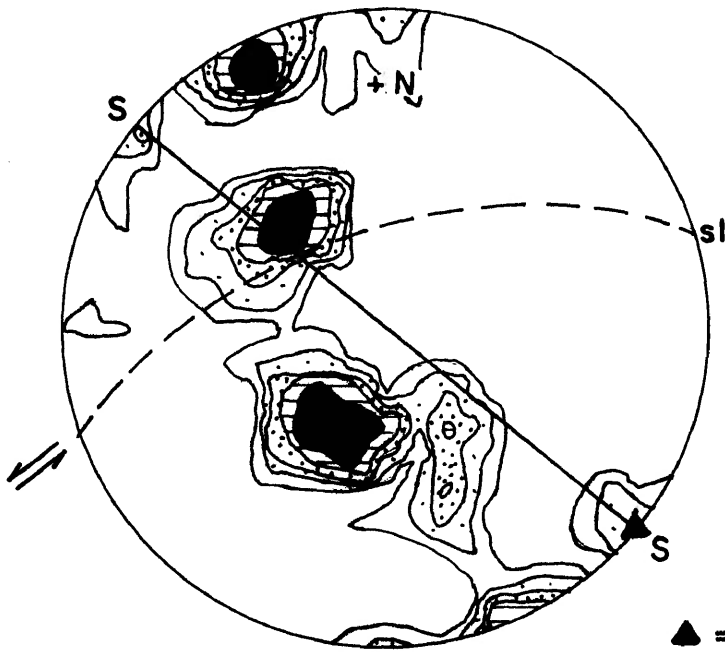
**BOR-80-15**

▲ = L = slickensides (dextral)

LOCALITY - HIGHWAY 527

TABLE 5-13

SPECIMEN	SAMPLE DESCRIPTION	DESCRIPTION OF QUARTZ GRAINS
BOR-80-10 (Figure 13A)	<ul style="list-style-type: none"> <li>- fairly undeformed feldspar-quartz-biotite gneissic rock</li> <li>- approximately 30% quartz</li> </ul>	<ul style="list-style-type: none"> <li>- grains have undulose extinction</li> <li>- some subgrains have developed</li> </ul>
BOR-80-15 (Figure 13B)	<ul style="list-style-type: none"> <li>- porphyroclastic protomylonite</li> <li>- feldspar-quartz-biotite-gneissic rock</li> <li>- approximately 30% quartz</li> </ul>	<ul style="list-style-type: none"> <li>- grains comprise a mosaic of elongate grains with undulose extinction</li> <li>- many subgrains</li> <li>- serrated grain boundaries</li> </ul> 
BOR-80-M169 (Figure 13C)	<ul style="list-style-type: none"> <li>- quartz vein</li> </ul>	<ul style="list-style-type: none"> <li>- mosaic of elongate grains (some very large)</li> <li>- grains have undulose extinction</li> <li>- grains comprise fairly equant subgrains</li> </ul> 



**FIG. 5-13C**

**BOR-80-M169**

**▲ = L = slickensides**



accompanying tables (Tables 5-1 to 5-13) provide some petrographic information about the samples and some microstructural characteristics of the quartz grains measured in the samples.

#### D) Observations

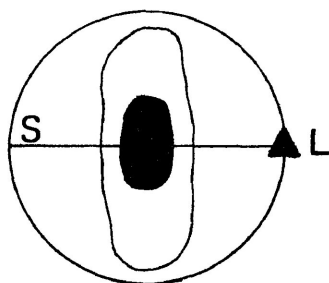
The definition and strength of the preferred orientation patterns of the quartz c-axis petrofabrics appears to correspond to the intensity of strain of the samples. The intensity of strain was inferred from the elongation of the quartz grains and the deformation structures within the quartz. It is suggested that grains become more and more elongate with increasing strain and that they also exhibit an increase in textural evidence of internal deformation, dynamic recovery, and recrystallization. The samples comprising equant grains yield quartz c-axis petrofabrics typified by diffuse maxima lacking a definite or clearly recognizable pattern of preferred orientation. For examples of this see BOR-80-10 (Fig. 5-13A), BOR-80-19D (Fig. 5-10B) and BOR-80-M160 (Fig. 5-12C). Samples in which the quartz grains are somewhat elongate show weak fabric development. Patterns are recognizable but indistinct as in BOR-80-M89 (Fig. 5-1A), BOR-80-M95 (Fig. 5-1D), BOR-80-M101 (Fig. 5-3A), BOR-80-19 (Fig. 5-8B) and BOR-80-M68 (Fig. 5-10A). The samples comprising very elongate grains, including those which exhibit abundant dynamic recovery and dynamic recrystallization, have well developed, distinct

preferred orientation patterns. Some examples are BOR-80-M91 (Fig. 5-1B), BOR-80-M93 (Fig. 5-1C), BOR-80-M137 (Fig. 5-2B), BOR-80-M54 (Fig. 5-6B), BOR-80-M27 (Fig. 5-7A), BOR-80-M37 (Fig. 5-7B), BOR-80-M11 (Fig. 5-9A), BOR-80-M23 (Fig. 5-11A), BOR-80-M19 (Fig. 5-11G) and BOR-80-M17 (Fig. 5-11H). A few samples in which the elongation of quartz grains is pronounced yield rather indistinct fabric patterns. They are: BOR-80-M140 (Fig. 5-2A), BOR-80-M134 (Fig. 5-2C), BOR-80-M78 (Fig. 5-3C), BOR-80-M53 (Fig. 5-6A) and BOR-80-M56b (Fig. 5-11B). It should also be noted that in samples where quartz is very abundant a strong, although somewhat variable, preferred orientation of c-axes exists. The deformation structures of the quartz suggest that the samples were exposed to different intensities of deformation. These samples are: BOR-80-M13 (Fig. 5-11D), BOR-80-M60 (Fig. 5-11C), BOR-80-M4 (Fig. 5-11E), BOR-80-M2 (Fig. 5-11F), BOR-80-M148 (Fig. 5-12A) and BOR-80-M169 (Fig. 5-13C).

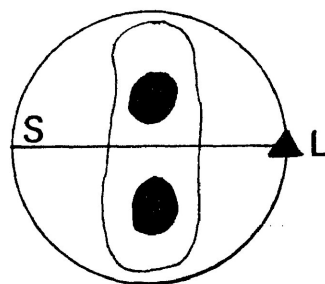
In the present study a variety of patterns of preferred orientation have been established. Despite the diversity of patterns certain characteristics appear to be shared. The most prevalent patterns of quartz c-axis preferred orientation are expressed by partial or complete great circle girdles oriented normal to or at high angles to the grain-shape schistosity, and by maxima located close to the schistosity trace. These maxima are normal to the lineation (L) where this element is present. In cases where L was not present the maxima commonly lie close to

a line  $90^\circ$  from the pole to the schistosity and parallel to the dip direction of the schistosity. Two types of maxima are associated with great circle girdles: a) single maxima located at or very near to the trace of S and b) double maxima, two maxima lying in the great circle girdle at small angles to and on either side of the S trace. Examples of these patterns are listed below:

Single Maximum



Double Maxima



BOR-80-M95 (Fig. 5-1D)  
 BOR-80-M78 (Fig. 5-3C)  
 BOR-80-M115 (Fig. 5-5B)  
 BOR-80-M27 (Fig. 5-7A)  
 BOR-80-M37 (Fig. 5-7B)  
 BOR-80-M11 (Fig. 5-9A)  
 BOR-80-M13 (Fig. 5-11D)  
 BOR-80-M2 (Fig. 5-11F)  
 BOR-80-M4 (Fig. 5-11E)  
 BOR-80-M148 (Fig. 5-12A)  
 BOR-80-15 (Fig. 5-13B)

BOR-80-M89 (Fig. 5-1A)  
 BOR-80-M91 (Fig. 5-1B)  
 BOR-80-M93 (Fig. 5-1C)  
 BOR-80-M137 (Fig. 5-2B)  
 BOR-80-M126 (Fig. 5-5A)  
 BOR-80-M54 (Fig. 5-6B)  
 BOR-80-26 (Fig. 5-8A)  
 BOR-80-M23 (Fig. 5-11A)  
 BOR-80-M60 (Fig. 5-11C)  
 BOR-80-M19 (Fig. 5-11G)  
 BOR-80-M17 (Fig. 5-11H)  
 BOR-80-M155 (Fig. 5-12B)

In other great circle distributions of the data maxima occur which do not follow either of the patterns described above. Examples are BOR-80-M75 (Fig. 5-4B), BOR-89-M120 (Fig. 5-5C), BOR-80-M68 (Fig. 5-10A) and BOR-80-M169 (Fig. 5-13C).

In two samples point maxima or clusters occur. Examples are BOR-89-M13 (Fig. 5-11D) and BOR-80-M2 (Fig. 5-11F).

Several examples appear to represent crossed great circle girdles. The girdles intersect in S with a maximum near the S trace and normal to the lineation when this is present. BOR-80-M73 (Fig. 5-4A) is the most characteristic example of type II crossed girdles. Other samples which may comprise type II crossed girdles but which are not as well defined are: BOR-80-M101 (Fig. 5-3A), BOR-80-M53 (Fig. 5-6A), BOR-80-19 (Fig. 5-8B) and BOR-80-M56b (Fig. 5-11B). Three samples may represent small circle distributions (type I crossed girdles). BOR-80-M160 (Fig. 5-12C) is the best example. The others are BOR-80-19D (Fig. 5-10B) and BOR-80-10 (Fig. 5-13A). Note that the last two groups (the crossed girdles) are generally observed where the fabrics are not well defined and in rocks which are inferred to be weakly strained.

Four samples, BOR-80-M140 (Fig. 5-2A), BOR-80-M134 (Fig. 5-2C), BOR-80-M99 (Fig. 5-3B) and BOR-80-M5 (Fig. 5-9B) do not fit any of the above patterns of preferred orientation. The distribution of data in these samples are dispersed however in each case maxima near the S trace appear along girdles vaguely parallelling S.

The patterns of quartz c-axis preferred orientation may be compared to the shape of the strain ellipsoid as determined in Chapter 3. Table 5-14 lists the samples which were used in the strain analysis and from which quartz c-axis fabrics were derived.

Table 5-14: Comparison between the shape of the strain ellipsoid and quartz c-axis petrofabric patterns developed in rocks from the Quetico fault zone.

Sample	$k \left( = \frac{a-1}{b-1} \right)$	Strain Ellipsoid Shape	Quartz <u>c</u> -axis petrofabric pattern
BOR-80-M89	0.13	flattening	great circle girdle
BOR-80-M95	0.042*	flattening	great circle girdle
BOR-80-M140	0.007*	flattening	great circle girdle
BOR-80-M137	0.034*	flattening	great circle girdle
BOR-80-M73	2.964*	constrictive	crossed great circle girdles
BOR-80-M120	0.053*	flattening	great circle girdle
BOR-80-M54	0.040*	flattening	great circle girdle
BOR-80-M27	0.103*/0.17	flattening	great circle girdle
BOR-80-26	0.125*/2.00	flattening/ constrictive	great circle girdle
BOR-80-19	0.33	flattening	possible crossed great circle girdles
BOR-80-M11	0.130*	flattening	great circle girdle
BOR-80-M68	0.024*	flattening	great circle girdle
BOR-80-M19	0.313*	flattening	great circle girdle
BOR-80-M155	0.07*/0.0	flattening	great circle girdle
BOR-80-15	0.052*/0.08	flattening	great circle girdle

\*strain analysis based on quartz grain shape (Harmonic mean)

other-strain analysis by All object-object separations method.

The table lists the  $k$ -values derived from the strain analysis. This value describes the shape of the strain ellipsoid.  $k=1$  for plane strain,  $k<1$  for flattened strain ellipsoids ( $k=0$  for pure flattening) and  $k>1$  for constrictive strain ellipsoids ( $k=\infty$  for pure constriction). The  $\underline{c}$ -axis fabric type for each sample is listed. The strain ellipsoid for most of the samples is flattened ( $k<1$ ) and the quartz  $\underline{c}$ -axis petrofabrics are great circle girdles normal to or at a high angle to the schistosity (perhaps the XY plane of the finite strain ellipsoid by transposition if not origin) and at a high angle to L (possibly equal to X) where measured. Exceptions to this can be found in sample BOR-80-M140 in which the girdle of  $\underline{c}$ -axes is roughly parallel to the schistosity and in sample BOR-80-19 which shows a poorly defined crossed great circle girdle pattern. The strain ellipsoid for two samples is constrictive ( $k>1$ ). The first, BOR-80-M73 clearly exhibits constrictive strain and is characterized by type II crossed girdles of quartz  $\underline{c}$ -axes (crossed great circle girdles intersecting in the schistosity). The second sample, BOR-80-26, exhibits a single great circle girdle pattern of  $\underline{c}$ -axes and is characterized by constrictive strain or by flattening strain depending on the method employed to measure the strain.

## E) Axial Distribution Analysis

Axial distribution analysis or A.V.A. (Achsenverteilungsanalysen) was developed by Ramsauer (1941) and Sander (1950) (in Turner and Weiss (1968) p. 247-253). In their study they attempted to delineate the distribution of grains with different orientations in a rock.

Current interpretation of quartz c-axis fabrics in terms of:

- a) slip systems active
- b) deformation history experienced
- c) sense of shear

relies on the assumption that the quartz was deformed by intracrystalline slip. If quartz c-axis fabrics developed as a result of progressive intracrystalline slip it would seem likely that the most strained grains (those which have undergone the most slip) would be the most strongly oriented in the preferred orientation pattern. In an attempt to determine whether there is a relationship between grain shape or elongation, and grain orientation in the rocks of this study, diagrams similar to those given by Turner and Weiss (1968, p. 247-253) were constructed.

*Method:* Samples were chosen which exhibited different microstructures and varying amounts of dynamic recovery and dynamic recrystallization. The analysis was carried out as follows:

- 1) The quartz c-axis petrofabric diagrams of the samples chosen for this analysis were divided into domains of different orientation, each domain representing a restricted range of

grain orientation. The domains for each sample were based on the samples' preferred orientation pattern. The maxima of the contoured petrofabric diagrams were taken to represent the grains having the greatest preferred orientation and thus domains of lesser preferred orientation were defined around the predominant maximum. Each domain was assigned a different ornamentation.

- 2) A tracing of an area of a thin section of the sample was prepared including every quartz grain and subgrain and grain of other species than quartz.
- 3) The orientation of each quartz grain in the sketch was measured and plotted on a stereonet. The grain was then stippled according to the orientation domain in which it fell.

*Results:* The resulting axial distribution diagrams and their corresponding orientation domain diagrams are shown in Figure 5-14 through 5-19. A brief description of each sample accompanies the A.V.A. diagram.

*Results of the Axial Distribution Analysis:* The A.V.A. diagrams seem to indicate that intracrystalline slip was responsible for the strain of those quartz crystals for which c-axis measurements were made. Within each sample the most elongate grains appear to correspond to the domain of strongest preferred orientation and the least elongate grains to the domain of least preferred orientation. This is true regardless of selection of quartz grains for measurements and regardless of strain, dynamic recovery or dynamic recrystallization which may have affected the quartz.



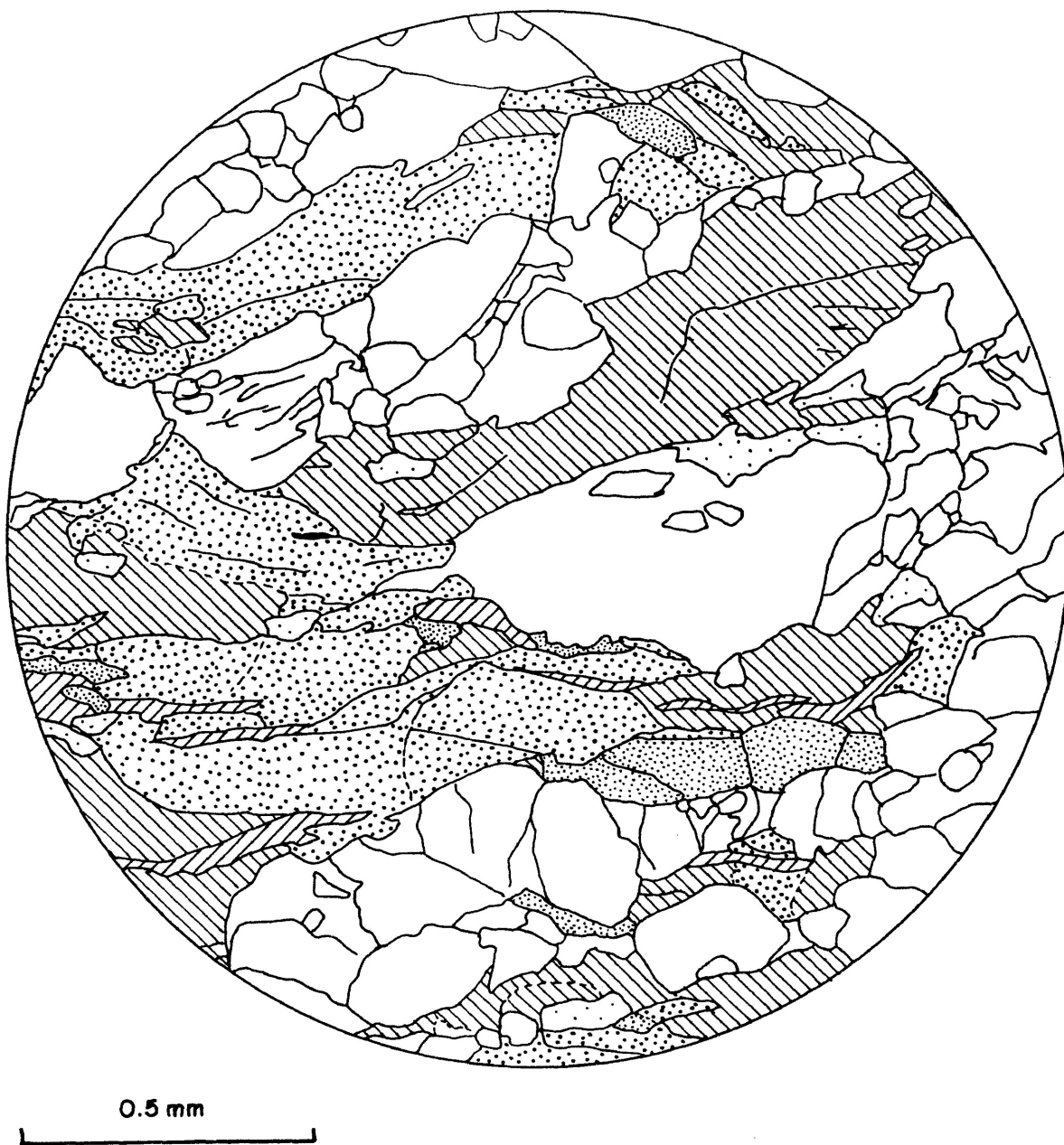
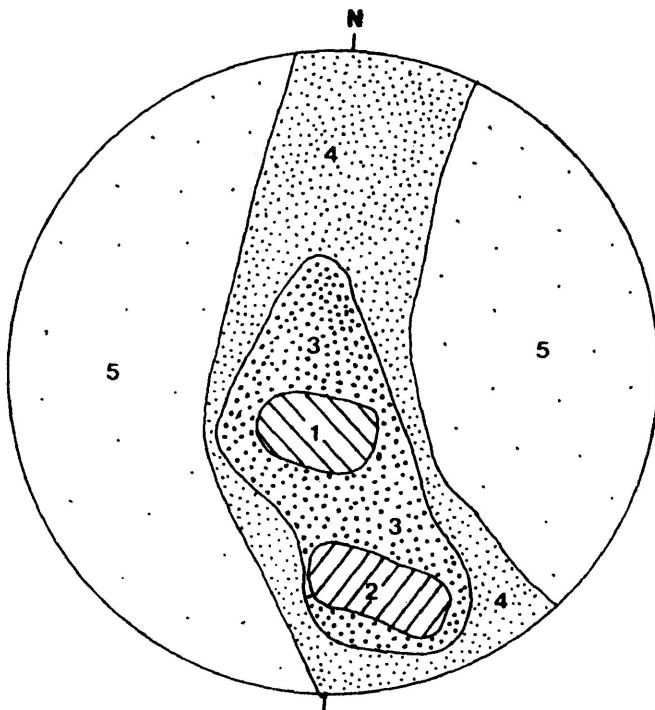


FIG. 5-14 Axial Distribution Diagram

- Ornamentation of quartz grains corresponds to orientation domain diagram.
- Unornamented grains represent mineral grains other than quartz.
- Black grains represent mica or micaceous bands.

Figure 5-14 - BOR-80-M27

The quartz in this sample appears to be very strained. It consists of very elongate grains and some ribbon grains. The quartz exhibits strong undulose extinction and contains deformation bands. There is little textural evidence of dynamic recovery and dynamic recrystallization in the sample. In the axial distribution diagram the most elongate grains are those with the strongest preferred orientation i.e.) those from domains 1 and 2 of the orientation domain diagram. The grains from domain 2, at least in this part of the thin section, are all very narrow elongate grains. Grains from domain 1 are larger, very elongate grains. The grains from domains 3 and 4 are also very elongate but somewhat less than those from domains 1 and 2. The grains from domain 5 are the least elongate.



Orientation Domain Diagram

Derived from Fig. 5-7A

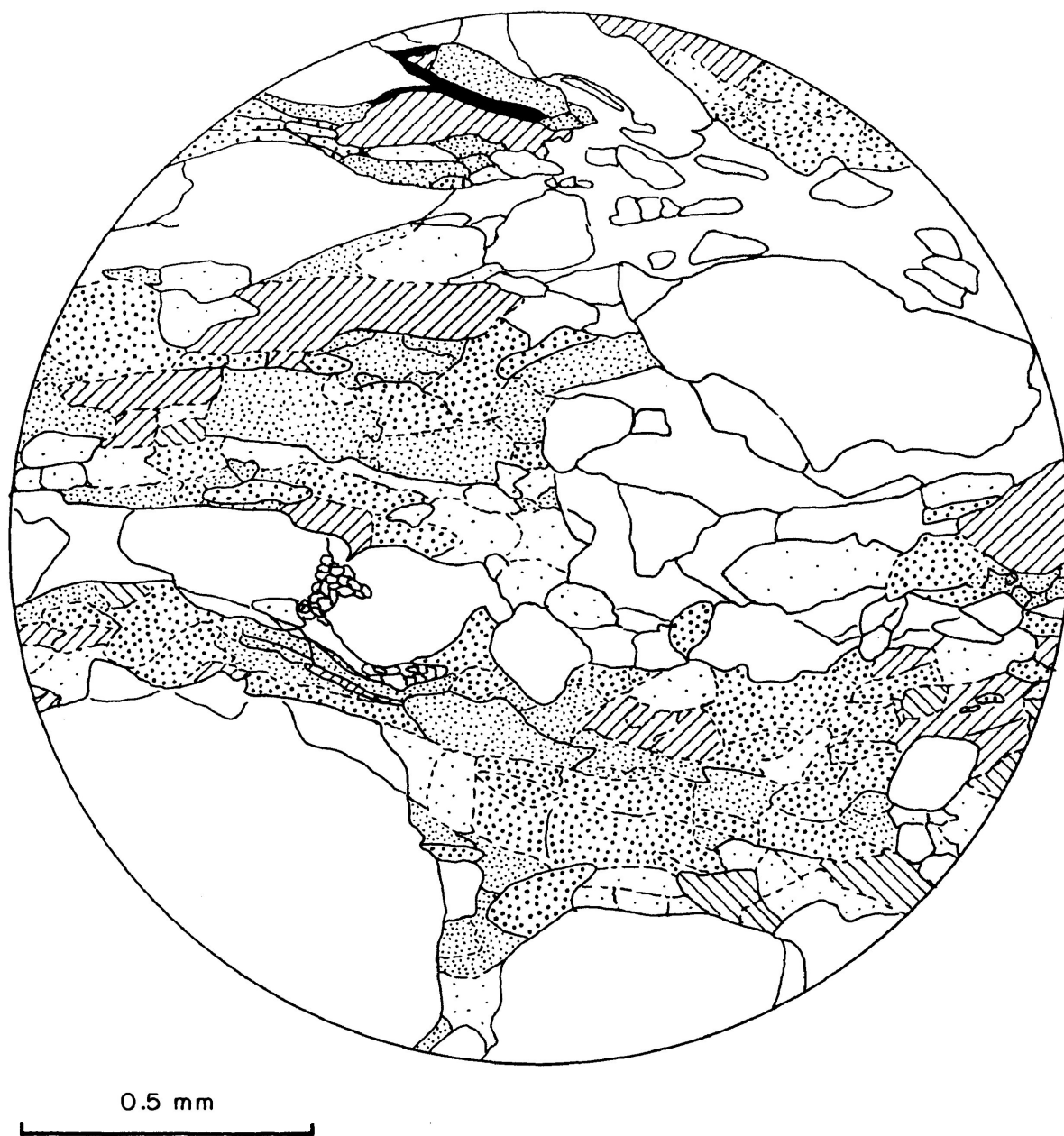
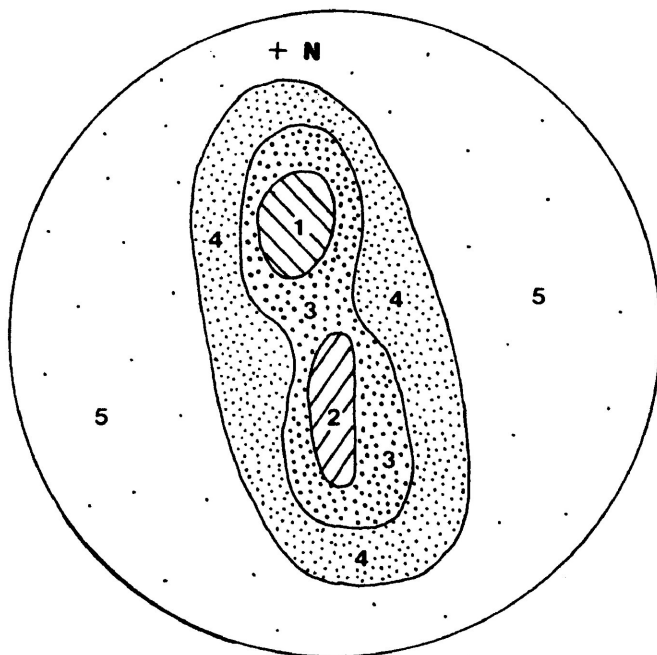


FIG. 5-15 Axial Distribution Diagram

- Ornamentation of quartz grains corresponds to orientation domain diagram.
- Unornamented grains represent mineral grains other than quartz.
- Black grains represent mica or micaceous bands.

Figure 5-15 - BOR-80-M54

The very elongate grains of quartz in this sample comprise numerous elongate subgrains. (Subgrain boundaries on the diagram are indicated by broken lines.) The subgrains suggest that recovery processes have been operative in the sample. In this sample the relationship between grain shape and orientation is not as clear as in the first example. The subgrains comprising the large quartz "grains" have different orientations and thus the original grains are divided into the smaller subgrains. However even amongst the subgrains it is clear that the most elongate grains are from domains 1 and 2. The least elongate grains are those from domain 5.



Orientation Domain Diagram

Derived from Fig. 5-6B

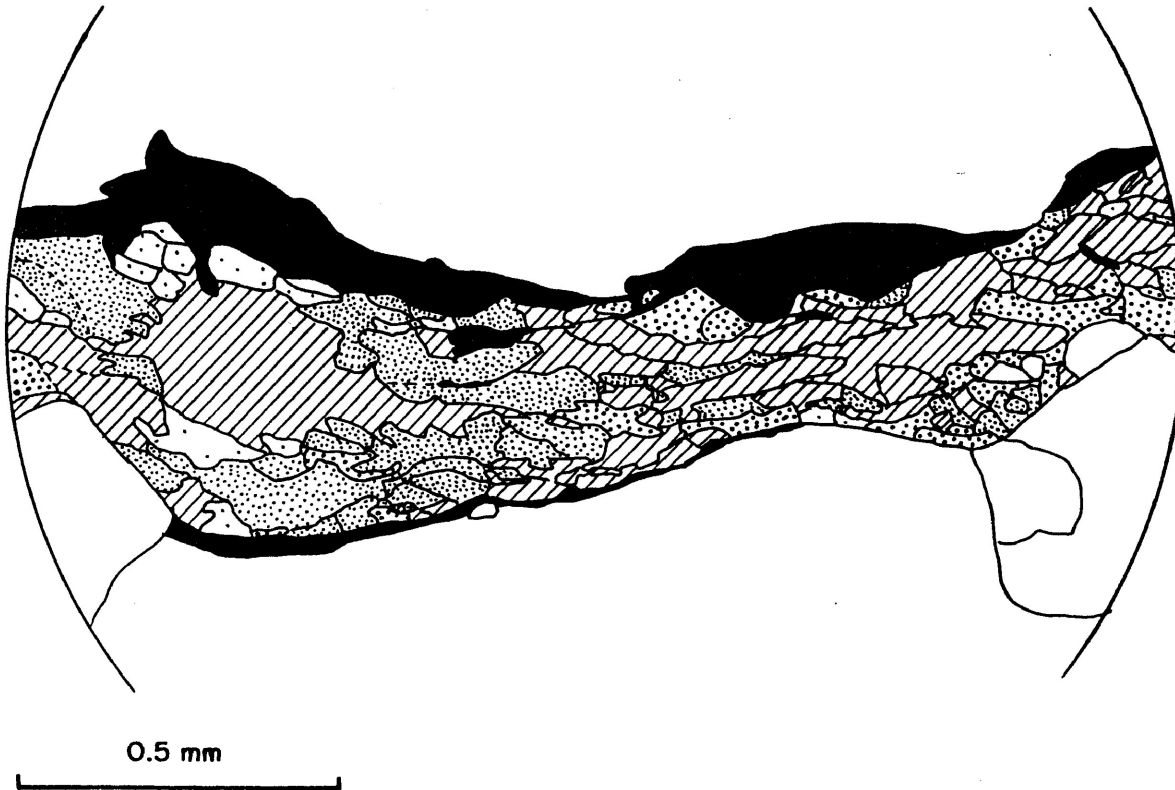
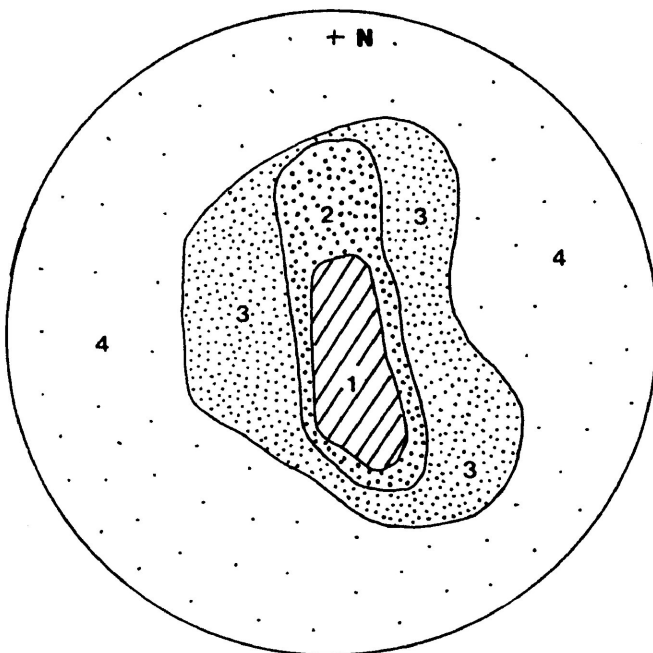


FIG. 5-16 Axial Distribution Diagram

- Ornamentation of quartz grains corresponds to orientation domain diagram.
- Unornamented grains represent mineral grains other than quartz.
- Black grains represent mica or micaceous bands.

Figure 5-16 - BOR-80-M11

The original quartz grains of this sample cannot be clearly identified. The quartz comprises elongate mosaics of very elongate subgrains. Some small recrystallized grains occur at subgrain boundaries. This area of the thin section was deliberately chosen as the subgrains on the left are less elongate than those on the right. In many parts of the thin section the quartz appears much more strained than in the diagram and comprises extremely elongate subgrains. The more elongate grains on the right side of the A.V.A. diagram are mostly from domains 1 and 2. The less elongate grains on the left are more variable in orientation. The elongate grains are from domains 1 and 2. The more equant grains are from domain 4.



Orientation Domain Diagram

Derived from Fig. 5-9A

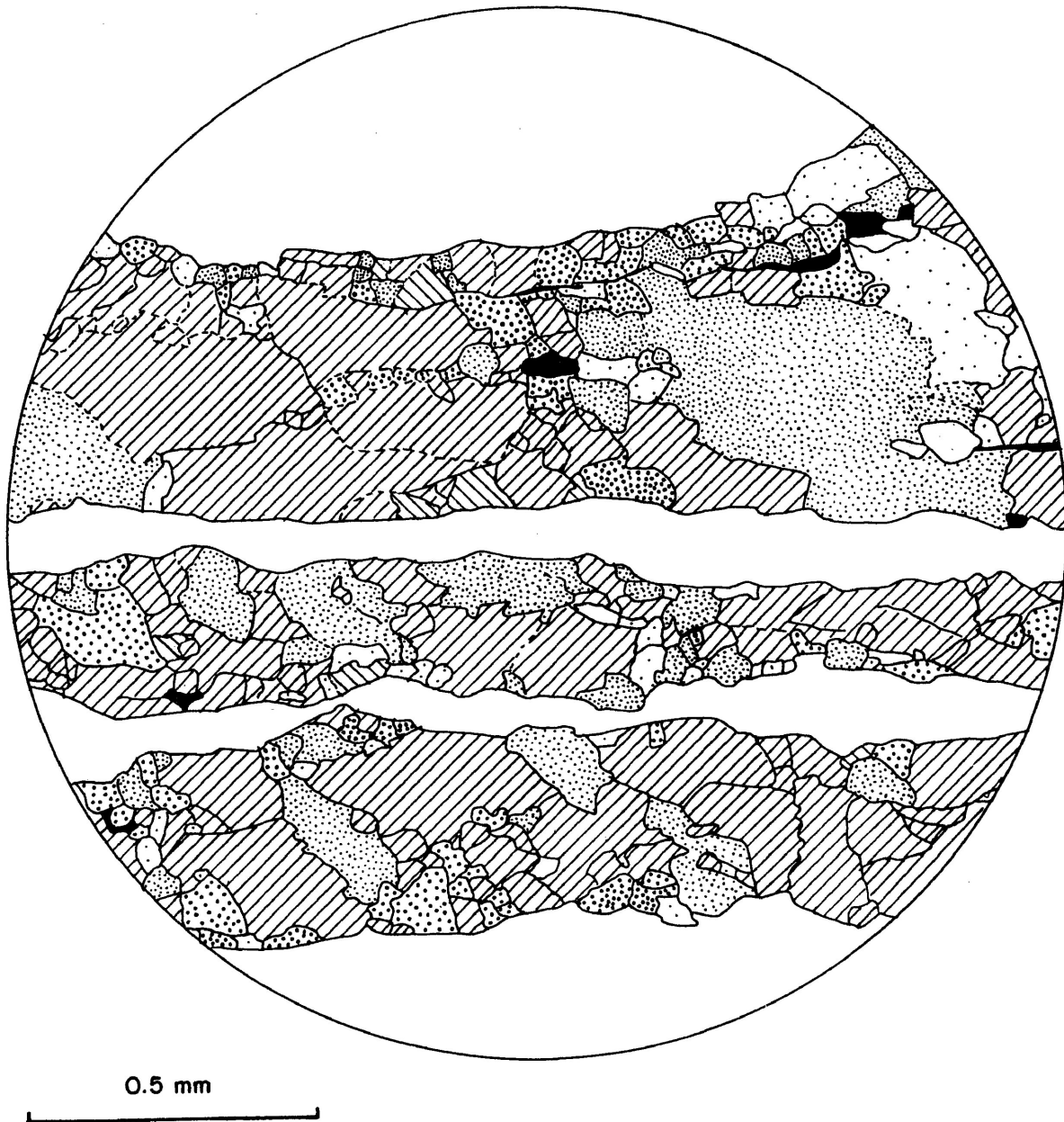
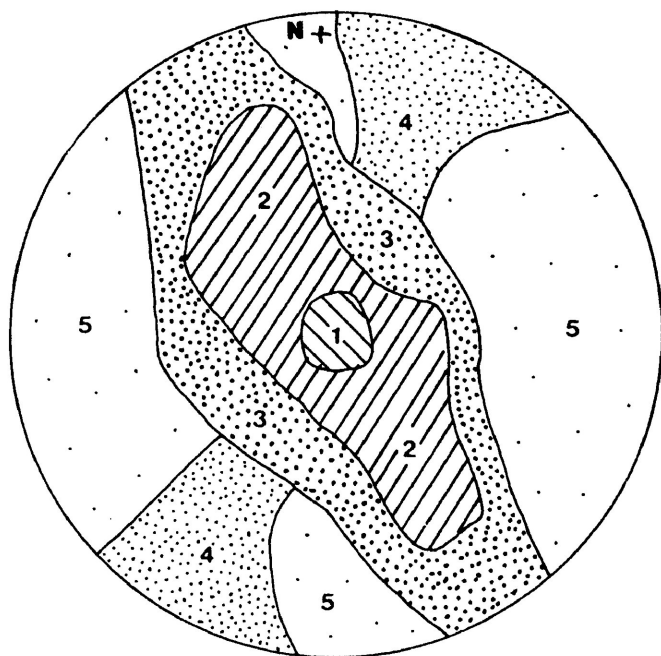


FIG. 5-17 Axial Distribution Diagram

- Ornamentation of quartz grains corresponds to orientation domain diagram.
- Unornamented grains represent mineral grains other than quartz.
- Black grains represent mica or micaceous bands.

Figure 5-17 - BOR-80-M73

Dynamic recovery and dynamic recrystallization are quite evident in this sample. The polycrystalline quartz rods, three of which cross the sketch, are composed of elongate grains and subgrains. The larger grains exhibit undulose extinction and some contain deformation bands. The smaller more equant grains are fairly strain free. The relationship between grain shape and orientation is not as distinct here as in earlier examples. There appears to be a tendency for the most elongate grains to be from domains 3 and 5. Although few grains from domain 1 were measured, they all appear to be quite equant. The grains from domain 4 are those of the weaker girdle of the crossed girdle preferred orientation pattern. These grains all appear to lie at a similar angle to the length of the quartz rods within the diagram.



Orientation Domain Diagram

Derived from Fig. 5-4A



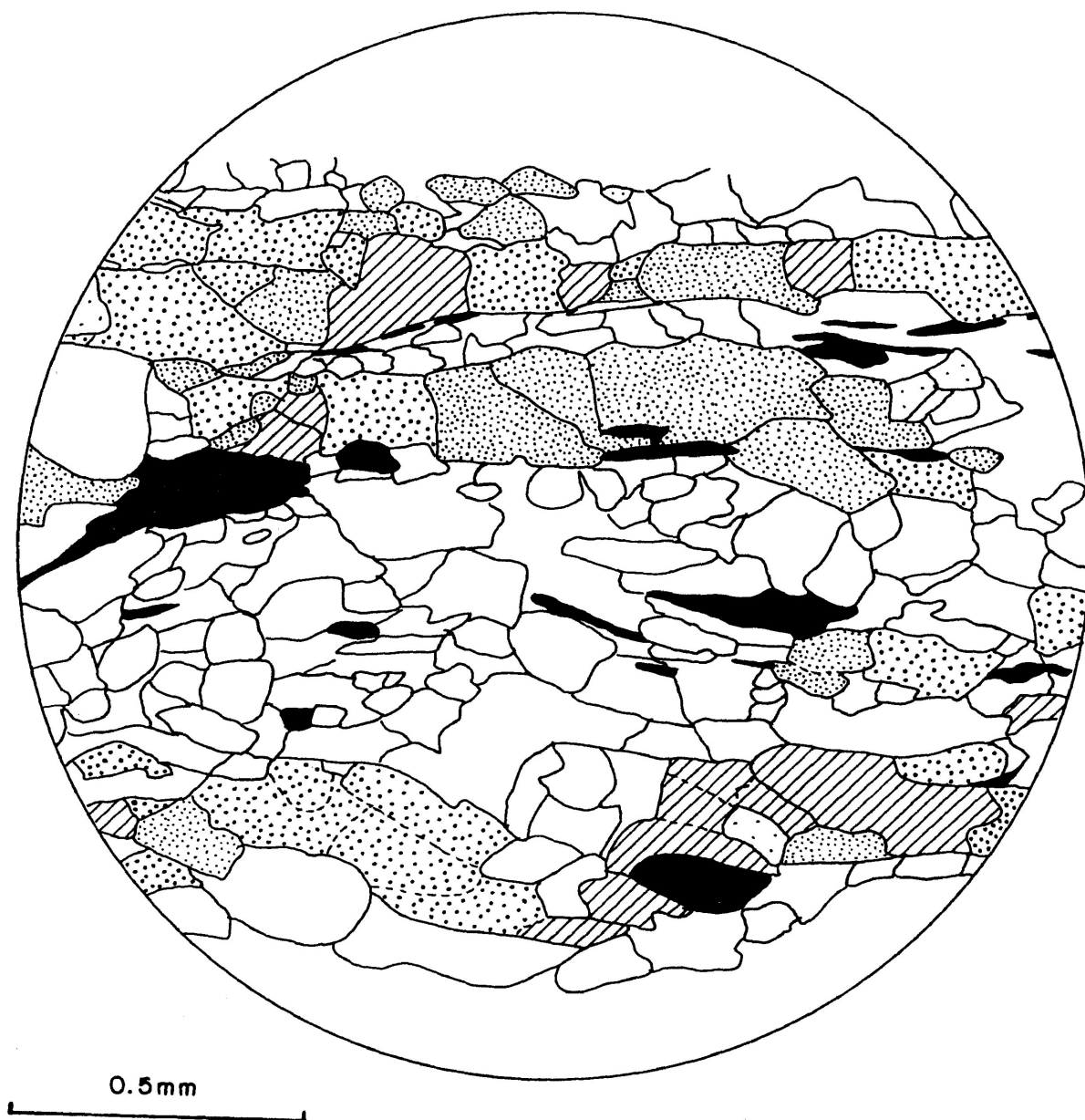
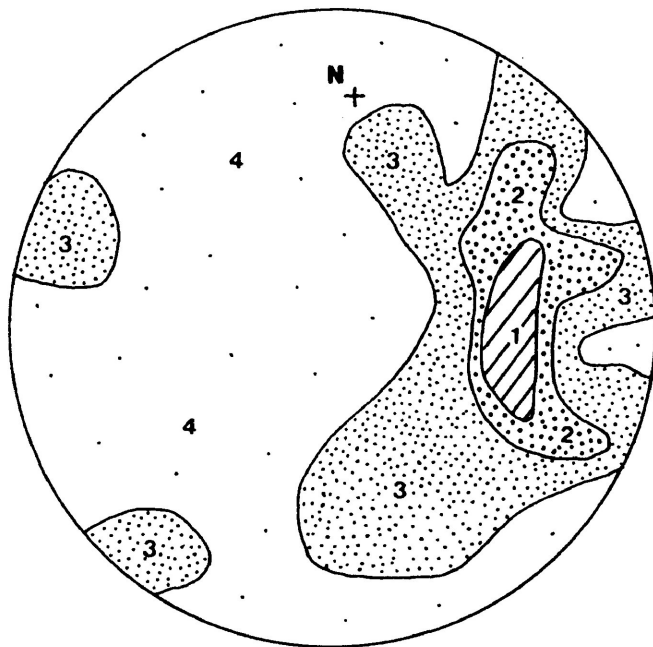


FIG. 5-18 Axial Distribution Diagram

- Ornamentation of quartz grains corresponds to orientation domain diagram.
- Unornamented grains represent mineral grains other than quartz.
- Black grains represent mica or micaceous bands.

Figure 5-18 - BOR-80-M137

The quartz in this sample comprises very elongate aggregates of dynamically recrystallized grains. Several of these aggregates are depicted in the A.V.A. diagram. The recrystallized grains themselves are not very elongate and have a rectangular appearance. The grains from domains 1 and 2 may be more elongate than those from domain 3. The grains of domain 4 are quite equant.



Orientation Domain Diagram

Derived from Fig. 5-2B

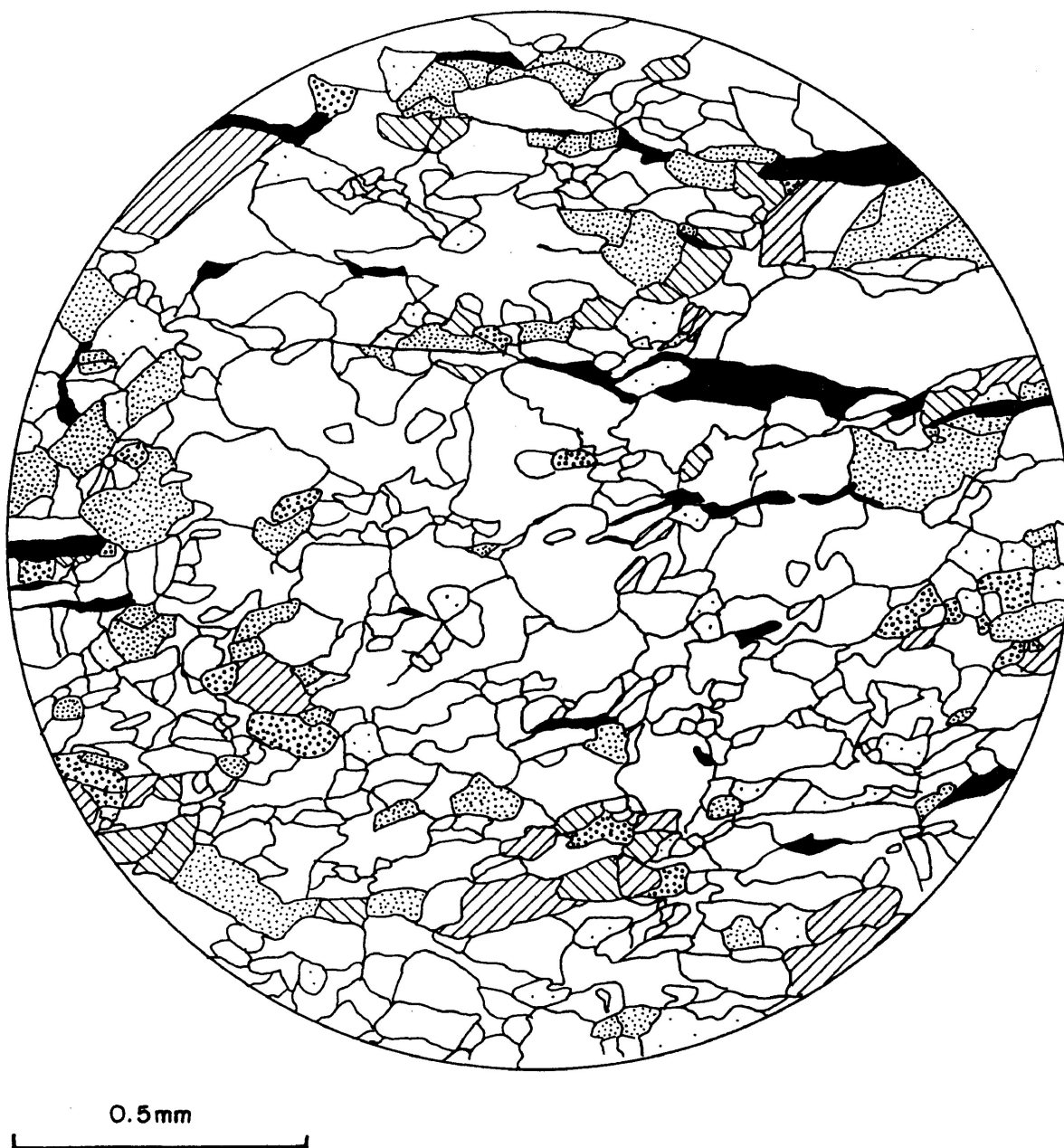
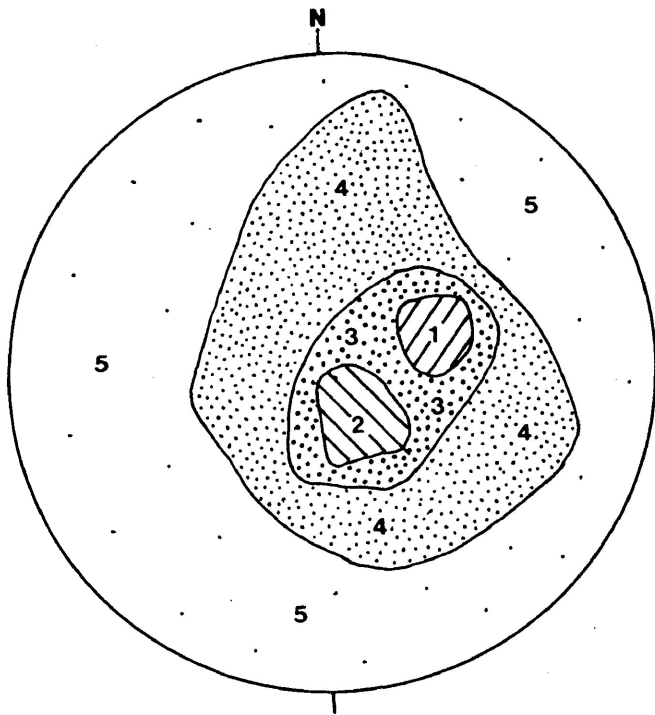


FIG. 5-19 Axial Distribution Diagram

- Ornamentation of quartz grains corresponds to orientation domain diagram.
- Unornamented grains represent mineral grains other than quartz.
- Black grains represent mica or micaceous bands.

Figure 5-19 - BOR-80-M91

This sample is a fine grained mylonite which has undergone extensive recrystallization. The grains are somewhat elongate. The quartz exhibits weak undulose extinction. It is possible to recognize, even in these recrystallized grains, that those from domain 5 are quite equant and that the more elongate grains are from domains 1 and 2. Some quite elongate grains are from domains 3 and 4.



Orientation Domain Diagram

Derived from Fig. 5-1B

F) Interpretation of Quartz c-axis Petrofabric Diagrams

Some preliminary interpretation of the petrofabric diagrams can be made since it appears that intracrystalline slip is responsible for the strain of quartz grains and the preferred orientation of quartz in the samples from the Quetico fault zone. Table 5-15 presents the interpretation of the diagrams. The slip systems which may have been responsible for the preferred orientation patterns observed are listed. These are determined from the distribution of maxima on the fabric diagrams using the principles discussed in the preceding chapter. The strain history is given as coaxial or non-coaxial based on whether the quartz fabric pattern is symmetrical with respect to the schistosity or asymmetrical. In the case of asymmetric fabrics the sense of shear may be determined as described in the previous chapter. The slip plane orientation may be determined in most cases since the slip plane contains the slip direction (the normal to the girdle of c-axes) and the Y axis of the strain ellipsoid which is presumed to correspond to the intersection of the great circle girdle with the schistosity. In cases where interpretation of the diagrams was not possible the columns have been left blank.

Table 5-15: Interpretation of Quartz c-axis Petrofabric Diagrams from the Quetico Fault Zone

Sample (Figure number)	Slip Systems Active (possible)	Coaxial (C) or Non-Coaxial (N-C) Strain History	Sense of Shear (in plan view)
BOR-80-M89* (Fig. 5-1A)	Prism <a>	N-C	dextral
BOR-80-M91 (Fig. 5-1B)	Rhomb <a> Prism <a>	N-C	dextral
BOR-80-M93 (Fig. 5-1C)	Rhomb <a> Prism <a>	N-C	sinistral
BOR-80-M95 (Fig. 5-1D)	Prism <a> Basal <a>	N-C	dextral
BOR-80-M140 (Fig. 5-2A)	(Prism <a> Prism <c>)		
BOR-80-M137 (Fig. 5-2B)	Rhomb <a> Prism <a> (Basal <a>)	N-C	dextral
BOR-80-M134 (Fig. 5-2C)			
BOR-80-M101 (Fig. 5-3A)	Prism <a> (Rhomb <a> Basal <a>)		
BOR-80-M99 (Fig. 5-3B)	Prism <a> (Rhomb <a>)		
BOR-80-M78 (Fig. 5-3C)	Prism <a> (Rhomb <a> Basal <a>)	N-C	dextral
BOR-80-M73 (Fig. 5-4A)	Prism <a> (Basal <a> Rhomb <a>)	N-C	dextral
BOR-80-M75 (Fig. 5-4B)	Prism <a> Rhomb <a> (Basal <a>)	N-C	dextral
BOR-80-M126 (Fig. 5-5A)	Rhomb <a> Prism <a>	C	

Table 5-15: Continued

Sample (Figure number)	Slip Systems Active (possible)	Coaxial (C) or Non-Coaxial (N-C) Strain History	Sense of Shear (In plan view)
BOR-80-M115 (Fig. 5-5B)	Prism <a> Rhomb <a>	N-C	sinistral
BOR-80-M120 (Fig. 5-5C)	Rhomb <a> Prism <a> (Basal <a>)	N-C	dextral
BOR-80-M53 (Fig. 5-6A)	Prism <a> Basal <a> (Rhomb <a>)		
BOR-80-M54 (Fig. 5-6B)	Rhomb <a> Prism <a> (Basal <a>)	C	
BOR-80-M27 (Fig. 5-7A)	Prism <a> Rhomb <a>	N-C	dextral
BOR-80-M37 (Fig. 5-7B)	Rhomb <a> Prism <a>	N-C	sinistral
BOR-80-26 (Fig. 5-8A)	Rhomb <a> Prism <a> (Basal <a>)	N-C	dextral
BOR-80-19 (Fig. 5-8B)	Rhomb <a> Prism <a> Basal <a>		
BOR-80-M11 (Fig. 5-9A)	Prism <a> Rhomb <a>	N-C	sinistral
BOR-80-M5 (Fig. 5-9B)	Prism <a> (Prism <c>) (Rhomb <a>)		
BOR-80-M68 (Fig. 5-10A)	Basal <a> Rhomb <a>	N-C	sinistral
BOR-80-19D (Fig. 5-10B)	Basal <a> Rhomb <a>		
BOR-80-M23 (Fig. 5-11A)	Rhomb <a> Prism <a> (Basal <a>)	N-C	dextral

TABLE 5-15: Continued

Sample (Figure number)	Slip Systems Active (possible)	Coaxial (C) or Non-Coaxial (N-C) Strain History	Sense of Shear (in plan view)
BOR-80-M56b (Fig. 5-11B)	Rhomb <a> (Basal <a>)		
BOR-80-M60 (Fig. 5-11C)	Prism <a> Rhomb <a>	N-C	dextral
BOR-80-M13 (Fig. 5-11D)	Prism <a> (Rhomb <a>)	N-C	dextral
BOR-80-M4 (Fig. 5-11E)	Prism <a> Rhomb <a> Basal <a>	N-C	sinistral
BOR-80-M2 (Fig. 5-11F)	Prism <a> (Rhomb <a>)	N-C	dextral
BOR-80-M19 (Fig. 5-11G)	Rhomb <a> Prism <a>	N-C	sinistral
BOR-80-M17 (Fig. 5-11H)	Rhomb <a> Prism <a>		
BOR-80-M148 (Fig. 5-12A)	Prism <a> Rhomb <a>	N-C	dextral
BOR-80-M155 (Fig. 5-12B)	Rhomb <a> Prism <a> Basal <a>	N-C	dextral
BOR-80-M160 (Fig. 5-12C)	Basal <a>	C	
BOR-80-10 (Fig. 5-13A)	Rhomb <a> Basal <a>		
BOR-80-15 (Fig. 5-13B)	Prism <a> Rhomb <a>	N-C	dextral
BOR-80-M169 (Fig. 5-13C)	Prism <a> Rhomb <a> Basal <a>	N-C	sinistral

\* S poorly defined.



## G) Discussion

The patterns of c-axis preferred orientation suggest that slip on prism planes in the  $\langle a \rangle$  direction and slip on rhombohedral planes in the  $\langle a \rangle$  direction are primarily responsible for the deformation of quartz grains of rocks within the Quetico fault zone. A number of samples exhibit basal slip in the  $\langle a \rangle$  direction. In one case prism slip in the  $\langle c \rangle$  direction seems to have been responsible for the deformation and may have contributed to the fabric development of other examples. Prism  $\langle a \rangle$  slip is characterized by a maximum of c-axes lying in the schistosity normal to the lineation (the maximum is regarded to closely approximate to the Y-axis of the finite strain ellipsoid) (see Fig. 4-3c). The rhomb  $\langle a \rangle$  slip is represented by pairs of maxima at an angle to the schistosity in a plane approximately normal to the lineation (see Fig. 4-3e). Basal  $\langle a \rangle$  slip is defined by c-axis maxima at a high angle to the schistosity and the lineation (near the Z axis of the finite strain ellipsoid) (see Fig. 4-3a). Prism  $\langle c \rangle$  slip is characterized by c-axis maxima near the schistosity and approximately parallel to the lineation (see Fig. 4-3b).

Tullis et al (1973) demonstrated experimentally that at high temperatures ( $>600^{\circ}\text{C}$ ) and low strain rates the proportion of prism slip increased with respect to basal slip. The preponderance of rhombohedral and prism slip suggests that the deformation

of the quartz in samples from this study occurred at high temperatures. The strain rates within the fault zone may be considered fairly high. Sibson (1977) suggested aseismic strain rates at depth of  $10^{-10}$  to  $10^{-11}$   $\text{sec}^{-1}$ . These are relatively high strain rates although experimental strain rates were of the order of  $10^{-6}$   $\text{sec}^{-1}$  (Tullis et al, 1973).

It is interesting to note that the samples, collected from widely separated localities, which appear to involve significant basal slip as a deformation mechanism are generally also samples with poor fabric development. These include samples BOR-80-M95 (Fig. 5-1D), BOR-80-19D (Fig. 5-10B), BOR-80-M160 (Fig. 5-12C) and BOR-80-10 (Fig. 5-13A). This suggests that basal slip may have been associated with small total strains (where determined) and rhombohedral and prism slip with greater total strains. The dependence of intracrystalline deformation mechanisms on total strain of the rock is here tentatively suggested although its investigation is beyond this study. Tullis et al (1973) have shown, however, that in experimental deformation the fabrics developed do not change their form with increasing deformation but become more defined. As noted, fabric pattern changes accompanying changes of slip plane preference are related to increasing temperature. It may be that the phenomenon observed here is due to poor definition of the fabrics in the weakly deformed rocks or to other factors not accounted for or measureable

in the samples. For example no data are available on the water content of the quartz from these samples and consequently the effect of the water content cannot be considered here.

The fabric patterns of the quartz c-axes appear to be related to the shape and orientation of the total strain ellipsoid. The girdles of c-axes generally appear to lie normal to the schistosity and the lineation. The schistosity is regarded to closely approximate the flattening plane (XY) of the total strain ellipsoid and the lineation is regarded to approximate the elongation axis (X). In the samples examined, great circle girdles of c-axes were associated with flattening strain and crossed great circle girdles with constrictive strain. If this association can be extended to other samples from the study area, it would indicate that flattening strain was predominant along the length of the fault zone.

A non-coaxial deformation history appears to be indicated by the large number of fabrics from the study area which are asymmetric with respect to the schistosity. This may suggest that deformation was accompanied by large shear strains. It is not implied here that the shear strain was simple shear s.s. A few samples of symmetrical fabrics suggest coaxial deformation occurred.

The degree of reliability in determination of shear sense based on asymmetric fabrics requires the assumption that the deformation included large shear strains. The asymmetric fabrics

indicate that shear sense was primarily dextral but that significant sinistral slip occurred as well. Seventeen samples indicated dextral shear, eight indicated sinistral shear.

Quartz c-axis fabrics, however, may be affected by late stages in the deformation and these may obliterate earlier stages by overprinting. Lister and Williams (1979) examined the effect on quartz c-axis petrofabrics of changing deformation during the closing stages of deformation by varying the relative importance of the components of deformation during the advanced stages in the process using the Taylor-Bishop-Hill model simulations. The simulation assumes that the same slip systems operate throughout the deformation. The grains of the model grain aggregate were subjected to non-coaxial deformation (truly simple shear) and then coaxial deformation with the shortening axis normal to the foliation developed early in the deformation and the extension axis parallel to the lineation. The results of the simulation are shown in Figure 5-20. Lister and Williams determined that the asymmetry of the intensity distribution (distribution of maxima) was preserved and serves as an indicator of early shear movements. However, the shape of the fabric changes to reflect the orientation of the axes of the later deformation and appears symmetrical with respect to the schistosity. Thus the effect of the closing stages of deformation may be important in the study of quartz c-axis petrofabrics. Brunel (1980) examined natural)

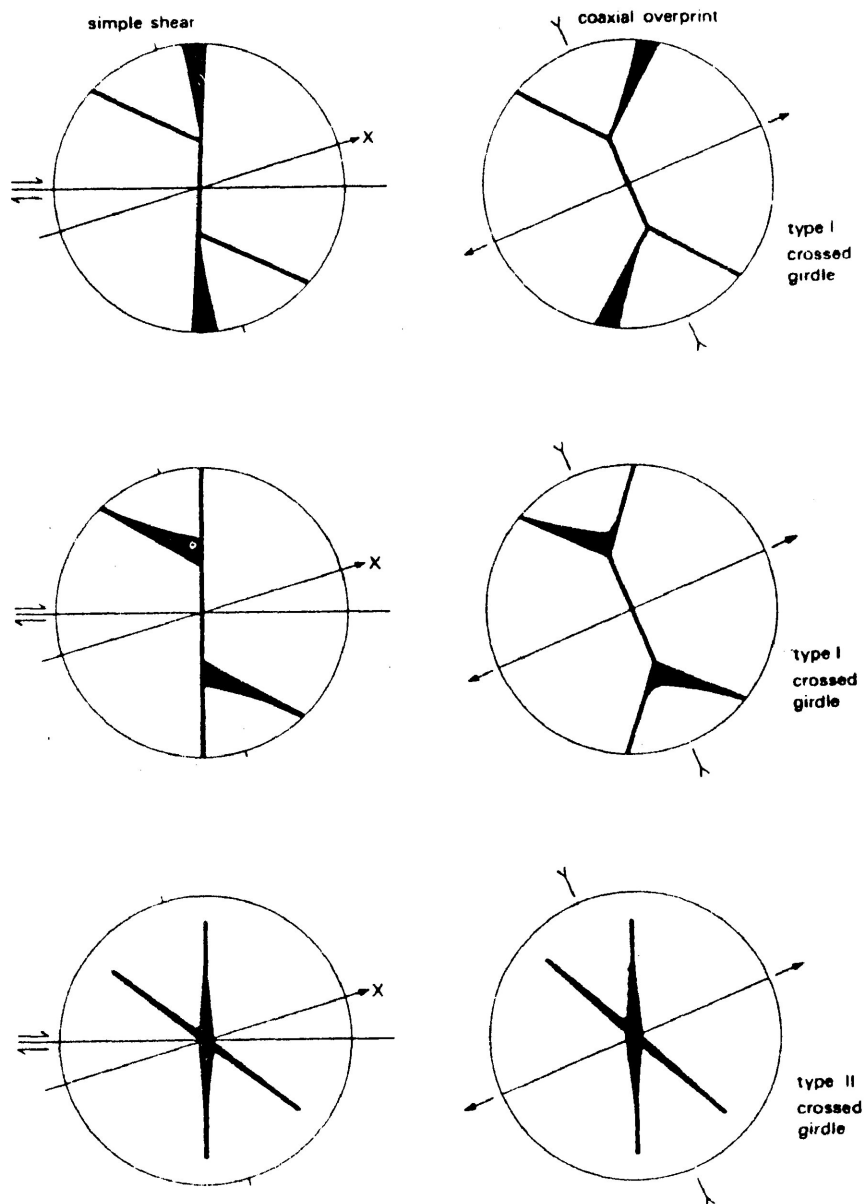


FIG. 5-20: The effect of coaxial deformation following progressive simple shear on three fabric patterns. The shape of the fabric is altered but the asymmetry of the distribution of maxima is preserved.

(from Lister and Williams, 1979)

examples of quartzites and also suggested that the quartz c-axis fabrics reflect late strain increments. One example he studied, in particular, reflected the late stages of deformation which had been defined by microtextural and microstructural studies. The distribution of maxima in the great circle girdles of c-axes in the samples Brunel examined were determined by the early deformation stages whereas the fabric shape, textures, and grain shapes reflected mainly late deformation stages. Examples in this study which suggest that late stage or later deformation may have affected the fabrics are: BOR-80-M93 (Fig. 5-1C), BOR-80-M54 (Fig. 5-6B) and BOR-80-M17 (Fig. 5-11H). These fabrics exhibit an asymmetric distribution of intensity of quartz c-axis preferred orientation while the overall shape of the fabric remains symmetrical or nearly symmetrical with respect to the schistosity. The c-axis fabrics in the Quetico fault zone may only reflect the sense of shear in the latest stages of deformation and not that of the overall displacement.

## 6 - SUMMATION

This thesis has dealt specifically with structures, textures and fault rocks of the Quetico fault zone. The following summarizes the findings of the study in terms of the original objectives.

*The brittle-ductile nature of deformation in the fault zone:*

- 1 - Ductile deformation was predominant in the fault zone as indicated by the prevalence of mylonitic rocks and the prominent mylonitic schistosity.
- 2 - Brittle deformation was subordinate since cataclastic textures are less common.
- 3 - Ductile deformation was followed by brittle deformation. Brittle textures and structures overprint ductile textures and structures.
- 4 - Microfaults are brittle-ductile structures, which may indicate the onset of, or transition to brittle deformation.

*Deformation mechanisms:*

- 1 - Microstructures indicate that quartz within the fault rocks deformed by crystal-plastic processes accompanied by dynamic recovery and syntectonic recrystallization.
- 2 - The predominant slip systems active in quartz were slip on prism planes in the a-direction and slip on rhomb planes in the a-direction as determined from quartz c-axis petrofabric patterns.
- 3 - Microstructures indicate that feldspar grains were often

deformed by fracture and less commonly by crystal-plastic processes and dynamic recovery and dynamic recrystallization.

- 4 - Microfaults indicate that particulate flow may have made a significant contribution to deformation within the fault zone rocks.

*Sense of motion:*

- 1 - The sense of motion on the Quetico fault was dextral as indicated by:
  - predominant dextral microfaults which reflect the overall sense of motion.
  - asymmetry of quartz c-axis petrofabrics.

*Nature of strain within the fault zone:*

- 1 - Predominantly flattening strain within the fault zone was determined from the harmonic mean of deformed grain axial ratios and strain analysis by the all object-object separations method.
- 2 - The flattening plane is roughly parallel to the plane of the fault zone and the mylonitic schistosity.
- 3 - The magnetic susceptibility anisotropy ellipsoid for mylonitic rocks is also flat-shaped.
- 4 - Asymmetric quartz c-axis fabrics indicate a non-coaxial deformation history.
- 5 - The microfaults indicate that shearing accompanied or was later than the flattening. Their formation depends on a pre-existing foliation.
- 6 - The folds within the fault zone may also form as a result of flattening and shearing.



*Strain estimate:*

- 1 - A minimum strain estimate derived from the harmonic mean of deformed quartz grains axial ratios indicates extension in X of 130%, in Y of 58% and shortening parallel to Z of 71%.

*Original structural level of the presently exposed fault rocks:*

- 1 - The mylonitic rocks of the fault zone formed in Sibson's (1977) quasi-plastic regime - depths greater than 10-15 km.
- 2 - The rocks of the cataclasite series and pseudotachylite formed under conditions similar to Sibson's elasto-frictional regime-depths less than 10-15 km.

*Discussion:* The transition from predominantly ductile deformation to brittle deformation during the time the fault was active suggests a change in physical conditions during this same period such as a decrease in temperature. Cooling might indicate that the fault was being progressively exhumed and that the presently exposed fault rocks moved relatively upward in the crust from the Q-P regime into the E-F regime of Sibson (1977). The author suggests that in actual fact a drastic change from well below the EF-QP transition to above it would not really be necessary for the embrittlement of the fault rocks. It has been shown that slip on prism  $\langle a \rangle$  and rhomb  $\langle a \rangle$  slip systems was predominant in quartz in the fault zone rocks. A decrease in temperature sufficient to disallow prism and rhomb slip and make basal  $\langle a \rangle$  slip the predominant slip system could easily result in the

embrittlement of the fault rocks. The basal crystallographic planes would be unsuitably oriented for slip and plastic deformation would not continue.

It must be noted that an increase in strain-rate could also produce this transition from ductile to brittle deformation. An increase in strain rate great enough that plastic deformation could no longer accommodate the large strains required to maintain continuity of the rock would result in failure, fracture and the production of cataclastic textures. A similar change from ductile to brittle deformation has been noted in a number of large shear and fault zones in different parts of the world. Some are described by Sibson (1977), McMahon Moore (1979), Watts and Williams (1979), Jégouzo (1980) and Stone (1981).

The Quetico fault is one of a number of large faults in the southern Superior province. The Sydney Lake fault zone is the only other fault zone which has been studied to any extent (Stone, 1981). It is located approximately 250 km northwest of the Quetico fault zone in northwestern Ontario and Manitoba. The two faults are quite similar in a number of characteristics. The Sydney Lake fault also forms the boundary between two subprovinces - the English River subprovince and the Uchi subprovince. Stone documents 30 km of dextral, strike-slip motion on the fault. The Sydney Lake fault zone follows the boundary through an 80 degree change in orientation while the Quetico fault remains relatively straight

and is only parallel to its adjacent subprovince boundaries for part of its length. The Quetico fault seems to follow the pre-existing rock fabric of the Quetico and Wabigoon subprovinces. In both fault zones flattening strain is characteristic and ductile textures are overprinted by brittle textures.

Stone notes that the numerous strike-slip faults in the Superior Province appear to have initiated at the end of the Archean. He proposed that their initiation may mark the beginning of large scale mantle convections such as are believed to drive modern crustal plates.

## REFERENCES

- Ardell, A.J., Christie, J.M. and McCormick, J.W., 1974: Dislocation images in quartz and the determination of the Burgers vectors; *Philosophical Magazine*, Vol. 29, 1399-1411.
- Ashby, M.F. and Verall, R.A., 1973: Diffusion - accommodated flow and super-plasticity; *Acta Metalurgica*, Vol. 21, p. 149-163.
- Ashby, M.F. and Verall, R.A., 1977: Micromechanisms of flow and fracture, and their relevance to the rheology of the upper mantle; in Kelly, A., Cook, A.H. and Greenwood, G.W., editors, *Creep of Engineering Materials and of the Earth*, *Philosophical Transactions of the Royal Society of London, Series A.*, Vol. 288; p. 59-95.
- Avé Lallemant, H. and Carter, N.L., 1971: Pressure dependence of quartz deformation lamellae orientations; *American Journal of Science*, Vol. 270, p. 218-235.
- Ayres, L.D., Lumbers, S.B., Milne, V.G. and Robeson, D.W., 1970: Ontario Geological Map. West Central Sheet, Map 2199, scale 1 inch to 16 miles.
- Baeta, R.D. and Ashbee, K.H.G., 1969: Slip systems in quartz: I. Experiments; II. Interpretation. *American Mineralogist*, Vol. 54; p. 1551-1582.

- Baeta, R.D. and Ashbee, K.H.G., 1970: Mechanical deformation of quartz: 1. Constant strain-rate compression experiments: Philosophical Magazine, Vol. 22, p. 601-624.
- Bau, A.F.S., 1979: History of regional deformation of Archean rocks in the Kashabowie Lake - Lac des Mille Lacs area, northwestern Ontario; unpublished Ph.D. thesis, University of Toronto.
- Bell, T.H. and Etheridge, M.A., 1973: Microstructure of mylonites and their descriptive terminology; Lithos, Vol. 6, p. 337-348.
- Bell, T.H. and Etheridge, M.A., 1976: The deformation and recrystallization of quartz in a mylonite zone, central Australia; Tectonophysics, Vol. 32, p. 238-267.
- Blacic, J.D., 1971: Hydrolytic weakening of quartz and olivine; Thesis, University of California, Los Angeles, 205 pages.
- Blacic, J.D., 1975: Plastic deformation mechanisms in quartz: the effect of water; Tectonophysics, Vol. 27, p. 271-294.
- Borg, I., Friedman, M., Handin, J. and Higgs, D.V., 1960: Experimental deformation of St. Peter sand: a study of cataclastic flow; in Griggs, D. and Handin, J., editors, Geological Society of America Memoir, Vol. 79, p. 133-192.
- Borradaile, G.J., 1981: Particulate flow of rock and the formation of cleavage; Tectonophysics, Vol. 72, p. 305-321.

- Borradaile, G.J., 1982: Comparison of Archean structural styles in two belts of the Canadian Superior Province; *Pre-cambrian Research*, Vol. 19, p. 179-189.
- Borradaile, G.J., 1982: Microfaults and Mylonitic Schistosity; in *Atlas of Deformation and Metamorphic Rock Fabrics*, Borradaile, G.J., Bayly, M.B. and Powell, C. McA., editors, Springer-Verlag, Berlin, Heidelberg, New York, p. 196-197.
- Borradaile, G.J. and Kennedy, M.C., 1982: Pseudotachylite; in *Atlas of Deformation and Metamorphic Rock Fabrics*, Borradaile, G.J., Bayly, M.B. and Powell, C. McA., editors, Springer-Verlag, Berlin, Heidelberg, New York, p. 366-367.
- Borradaile, G.J. and Tarling, D.H., 1981: The influence of deformation mechanisms on magnetic fabrics in weakly deformed rocks; *Tectonophysics*, Vol. 77, p. 151-168.
- Bouchez, J.L., 1977: Plastic deformation of quartzites at low temperature in an area of natural strain gradient; *Tectonophysics*, Vol. 39, p. 25-50.
- Bouchez, J.L., 1978: Preferred orientations of quartz 'a' axes in some tectonites: Kinematic inferences; *Tectonophysics*, Vol. 49, p. T25-T30.
- Bouchez, J.L. and Pêcher, A., 1976: Plasticité du quartz et sens de cisaillement dans des quartzites du Grand chevauche-

- ment Central Himalayen; Bulletin de la Société Géologique de France, Vol. 18, p. 1377-1385.
- Bouchez, J.L. and Pêcher, A., 1981: The Himalayan Main Central Thrust pile and its quartz-rich tectonites in central Nepal; Tectonophysics, Vol. 78, p. 28-50.
- Bouillier, A.M. and Gueguen, Y., 1975: SP-mylonites: origin of some mylonite by superplastic flow; Contributions to Mineralogy Petrology; Vol. 50, p. 93-104.
- Brunel, M., 1980: Quartz fabrics in shear-zone mylonites; evidence for a major imprint due to late strain increments; Tectonophysics, Vol. 74, p. T33-T44.
- Burg, J.P. and Laurent, P., 1978: Strain analysis of a shear zone in a granodiorite; Tectonophysics, Vol. 47, p. 15-42.
- Carreras, J., Estrada, A. and White, S., 1977: The effect of folding on the c-axis fabrics of a quartz mylonite; Tectonophysics, Vol. 39, p. 3-24.
- Carter, M.W., 1983: Geology of the Greenwich Lake area, District of Thunder Bay; Ontario Geological Survey, Open File Report 5437, 49 pages.
- Carter, N.L., Christie, J.M. and Griggs, D.T., 1964: Experimental deformation and recrystallization of quartz; Journal of Geology, Vol. 72, p. 687-733.
- Christie, J.M., 1960: Mylonitic rocks of the Moine thrust-zone in the Assynt Region, N.W. Scotland; Edinburgh Geological

- Society Transactions, Vol. 18, p. 79-93.
- Christie, J.M. and Green, H.W., 1964: Several new slip mechanisms in quartz; (Abstract), Transactions of the American Geophysical Union, Vol. 45, p. 103.
- Christie, J.M., Griggs, D.T. and Carter, N.L., 1964: Experimental evidence of basal slip in quartz; Journal of Geology, Vol. 72, p. 734-756.
- Cloos, E., 1947: Oolite deformation in the South Mountain fold, Maryland; Geological Society of America Bulletin, Vol. 58, p. 843-918.
- Davies, J.C., 1973a: Geology of the Fort Frances Area, District of Rainy River; Ontario Division of Mines Geological Report 107, 35 pages. Accompanied by Map 2263, scale 1 inch to 1/2 mile.
- Davies, J.C. and Pryslak, A.P., 1967: Kenora-Fort Frances Sheet, Districts of Kenora and Rainy River; Ontario Department of Mines, Geological Compilation Series, Map 2115, scale 1 inch to 4 miles.
- Dunnet, D., 1969: A technique of finite strain analysis using elliptical particles; Tectonophysics, Vol. 7, p. 117-136.
- Dunnet, D. and Siddans, A.W.B., 1971: Non-random sedimentary fabrics and their modification by strain; Tectonophysics, Vol. 12, p. 307-325.
- Etchecopar, A., 1977: A plane kinematic model of progressive



- deformation in a polycrystalline aggregate; *Tectonophysics*, Vol. 39, p. 121-139.
- Fletcher, G.L. and Irvine, T.N., 1954: *Geology of the Emo Area, District of Rainy River; Ontario Department of Mines, Annual Report, Vol. 63, part 5. Accompanied by Map 1954-2, scale 1 inch to 1 mile.*
- Flinn, D., 1962: *On folding during three-dimensional progressive deformation; Quarterly Journal of the Geological Society of London, Vol. 118, p. 385-433.*
- Fry, N., 1979: *Random point distributions and strain measurement in rocks; Tectonophysics, Vol. 60, p. 89-105.*
- Fumerton, S.L., 1980: *Calm Lake area, District of Rainy River. In Summary of Field work, 1980 by the Ontario Geological Survey, Report No. 8, Milne, V.G., White, O., Barlow, R. and Colvine, S., editors, p. 32-35.*
- Fumerton, S.L., 1982: *Redefinition of the Quetico Fault near Atikokan, Ontario. Canadian Journal of Earth Sciences, Vol. 19, p. 222-224.*
- Fumerton, S.L. and Bumgarner, E.L., 1980: *Calm Lake Area, District of Rainy River; Ontario Geological Survey Preliminary Map P. 2405, Geological Series, scale 1 inch to 1/4 mile.*
- Goldstein, A.G., 1980: *Magnetic susceptibility anisotropy of mylonites from the Lake Char mylonite zone, southeastern New England; in Analytical Studies in Structural Geology,*

- Schwerdtner, W.M., Huddleston, P.J. and Dixon, J.M.,  
editors, Tectonophysics, Vol. 66, p. 197-211.
- Graham, J.W., 1954: Magnetic susceptibility anisotropy, an un-  
exploited petrofabric element; Geological Society of  
America Bulletin, Vol. 65, p. 1257-1258.
- Green, H.W., Griggs, D.T. and Christie, J.M., 1970: Syntectonic  
and annealing recrystallization of fine-grained quartz  
aggregates in Experimental and Natural Rock Deformation,  
P. Paulitsch, Editor, Springer-Verlag, N.Y., p. 272-335.
- Griggs, D.T., 1967: Hydrolytic weakening of quartz and other  
silicates; Geophysical Journal of the Royal Astronomical  
Society, Vol. 14, p. 19-31.
- Griggs, D.T., 1974: A model of hydrolytic weakening in quartz;  
Journal of Geophysical Research, Vol. 79, p. 1653-1661.
- Griggs, D.T. and Blacic, J.D., 1965: Quartz: anomalous weakness  
of synthetic crystals; Science, Vol. 147, p. 292-295.
- Guillope, M. and Porier, J.P., 1979: Dynamic recrystallization  
during creep of single crystalline halite: an experimental  
study; Journal of Geophysical Research, Vol. 84, p. 5557-  
5567.
- Harris, F.R., 1974: Geology of the Rainy Lake Area, District of  
Rainy River; Ontario Division of Mines Geological Report  
115, 94 pages. Accompanied by Maps 2278 and 2279, scale  
1 inch to 1/2 mile.

- Hawley, J.E., 1929: Geology of the Sapawe Lake Area, with notes on some iron and gold deposits of Rainy River District; Ontario Department of Mines Annual Report, Vol. 38, part 6, p. 1-58. Accompanied by Map No. 38e, scale 1 inch to 3/4 mile.
- Heard, H.C. and Carter, N.L., 1968: Experimentally induced "natural" intragranular flow in quartz and quartzite; American Journal of Science, Vol. 266, p. 1-42.
- Higgins, M.W., 1971: Cataclastic Rocks; United States Geological Survey Professional Paper 687.
- Hobbs, B.E., 1968: Recrystallization of single crystal of quartz; Tectonophysics, Vol. 6, p. 353-401.
- Hobbs, B.E., McLaren, A.C. and Paterson, M.S., 1972: Plasticity of Single Crystals of Synthetic Quartz in Flow and Fracture of Rocks, Geophysical Monograph 16, H.D. Heard et al, Editors, American Geophysical Union, Washington, D.C., p. 29-55.
- Hobbs, B.E., Means, W.D. and Williams, P.F., 1976: An Outline of Structural Geology; John Wiley and Sons, Inc., Toronto, 571 pages.
- Irvine, T.N., 1963: Geology of Western Lac des Mille Lacs Area, District of Thunder Bay; Ontario Department of Mines, Geological Report 12, 24 pages. Accompanied by Map 2022, scale 1 inch to 1 mile.

- Jégouzo, P., 1980: The South Armorican shear zone; *Journal of Structural Geology*, Vol. 2, p. 39-47.
- Kaye, L., 1967: *Geology of Eastern Lac des Mille Lacs Area, District of Thunder Bay*; Ontario Department of Mines Geological Report 48, 30 pages. Accompanied by Maps 2104 and 2105, scale 1 inch to 1/2 mile.
- Kehlenbeck, M.M., 1976: Nature of the Quetico-Wabigoon boundary in the de Courcey-Smiley Lakes area, northwestern Ontario; *Canadian Journal of Earth Sciences*, Vol. 13, p. 737-748.
- Kelly, A. and Groves, G.W., 1970: *Crystallography and Crystal Defects*; Longmans, London, 428 pages.
- Kennedy, M.C., 1980: *Metamorphism and Structure across the Quetico structural subprovince, Raith, Ontario*; unpublished B.Sc. thesis, Lakehead University.
- Kerr, P.F., 1977: *Optical Mineralogy*; McGraw-Hill, Toronto, Ont., 492 pages.
- Kligfield, R., Lowrie, W. and Dalziel, I.W.D., 1977: Magnetic susceptibility anisotropy as a strain indicator in the Sudbury Basin, Ontario; *Tectonophysics*, Vol. 40, p. 287-308.
- Lapworth, C., 1885: The Highland controversy in British geology: its causes, course and consequences; *Nature*, Vol. 32, p. 558-559.

- Lawson, A.C., 1888: Report on the Geology of the Rainy Lake Region; Geological Natural History Survey of Canada Annual Report, Vol. 3, part 1, Report F, 183 pages. Accompanied by map, scale 1 inch to 2 miles.
- Lawson, A.C., 1913: The Archean Geology of Rainy Lake Restudied; Geological Survey of Canada, Memoir 40, 115 pages. Accompanied by Map 98A, scale 1 inch to 1 mile.
- Lisle, R.J., 1977: Estimation of the tectonic strain ratio from the mean shape of deformed elliptical markers; *Geologie en Mijnbouw*, Vol. 56, p. 140-144.
- Lister, G.S. and Hobbs, B.E., 1980: The simulation of fabric development during plastic deformation and its application to quartzite: The influence of deformation history, *Journal of Structural Geology*, Vol. 2, p. 355-387.
- Lister, G.S. and Price, G.P., 1978. Fabric development in a quartz-feldspar mylonite; *Tectonophysics*, Vol. 49, p. 37-78.
- Lister, G.S. and Williams, P.F., 1979: Fabric development in shear zones: theoretical controls and observed phenomena; *Journal of Structural Geology*, Vol. 1, p. 283-297.
- MacKasey, W.O., Blackburn, C.E. and Trowell, N.F., 1974: A regional approach to the Wabigoon-Quetico belts and its bearing on exploration in northwestern Ontario; Ontario Division of Mines, Misc. Paper 58, 29 pages.
- Majoribanks, R.W., 1976: The relation between microfabric and

- strain in a progressively deformed quartzite sequence from Central Australia; *Tectonophysics*, Vol. 32, p. 269-293.
- McLaren, A.C. and Retchford, J.A., 1969: Transmission electron microscopy study of the dislocations in plastically deformed synthetic quartz; *Physica Status Solidi*, Vol. 33, p. 657-668.
- McMahon Moore, J., 1979: Tectonics of the Najd transcurrent fault system, Saudi Arabia; *Journal of the Geological Society of London*, Vol. 136, p. 441-454.
- Means, W.D., 1976: *Stress and Strain*, Springer-Verlag, New York, N.Y., 399 pages.
- Miller, D.M. and Christie, J.M., 1981: Comparison of quartz microfabric with strain in recrystallized quartzite; *Journal of Structural Geology*, Vol. 3, p. 129-141.
- Miller, D.M. and Oertel, G., 1979: Strain determination from the measurement of pebble shapes: a modification; *Tectonophysics*, Vol. 55, p. T11 to T13.
- Molyneux, L., 1971: A complete result magnetometer for measuring the remnant magnetization of rocks; *Geophysical Journal*, Vol. 24, p. 115-131.
- Moody, J.D. and Hill, M.J., 1956: Wrench fault tectonics; *Geological Society of America Bulletin*, Vol. 67, p. 1207-1246.

- Moore, E.S., 1939: Geology and Ore Deposits of the Atikokan Area; Ontario Department of Mines, Vol. 47, part 2, p. 1-34.
- Morrison-Smith, D.J., Paterson, M.S. and Hobbs, B.E., 1976: An electron microscope study of plastic deformation in single crystals of synthetic quartz; Tectonophysics, Vol. 33, p. 43-79.
- McKinstry, H.C., 1953: Shears of second order; American Journal of Science, Vol. 251, p. 401-414.
- Nicolas, A. and Poirier, J.P., 1976: Crystalline plasticity and solid state flow in metamorphic rocks, John Wiley and Sons, N.Y., 444 pages.
- Oertel, G., 1978: Strain determination from the measurement of pebble shapes; Tectonophysics, Vol. 50, p. 71-77.
- Parkinson, R.N., 1962: Operation Overthrust; p. 90-101 in The Tectonics of the Canadian Shield; Royal Society of Canada, Special Publication No. 4.
- Paterson, M.S., 1976: Some aspects of experimental rock deformation; Philosophical Transactions of the Royal Society of London, Series A., Vol. 283, p. 163-172.
- Paterson, M.S., 1978. Experimental Rock Deformation - the Brittle Field; Springer, Berlin, 254 pages.
- Pecher, A., 1981: Experimental decrepitation and re-equilibration in fluid inclusions in synthetic quartz; in Lister, G.S.,

- Behr, H.J., Weber, K. and Zwart, H.J., editors, The Effect of Deformation on Rocks, Tectonophysics, Vol. 78, p. 567-583.
- Pirie, J., 1978: Geology of the Crooked Pine Lake Area, District of Rainy River; Ontario Geological Survey Report 179, 73 pages. Accompanied by Map 2405, scale 1 inch to 1/2 mile.
- Platt, J.P. and Vissers, R.L.M., 1980: Extensional structures in anisotropic rocks; Journal of Structural Geology, Vol. 2, 397-410.
- Price, N.J., 1966: Fault and joint development in brittle and semi-brittle rock; Pergamon Press, London, Eng., 176 pages.
- Pye, E.G. and Fenwick, K.G., 1965: Atikokan-Lakehead Sheet, Districts of Kenora, Rainy River and Thunder Bay; Ontario Department of Mines, Geological Compilation Series Map 2065, scale 1 inch to 4 miles.
- Raj, R. and Ashby, M.F., 1971: On grain boundary sliding and diffusional creep; Metallurgical Transactions, Vol. 2, p. 1113-1127.
- Ramsay, J.G., 1967: Folding and fracturing of rocks; McGraw-Hill, New York, N.Y., 568 pages.
- Ramsay, J.G. and Graham, R.H., 1970: Strain variation in shear belts; Canadian Journal of Earth Sciences, Vol. 7, p.



scale 1 inch to 1/2 mile.

- Sibson, R.H., 1975: Generation of pseudotachylite by ancient seismic faulting; *Geophysical Journal of the Royal Astronomical Society*; Vol. 43, 775-794.
- Sibson, R.H., 1977: Fault rocks and fault mechanisms; *Journal of the Geological Society of London*, Vol. 133, p. 191-213.
- Sibson, R.H., 1980: Transient discontinuities in ductile shear zones; *Journal of Structural Geology*, Vol. 2, 165-171.
- Singh, J. (now Rathore, J.S.), Sanderson, D.J. and Tarling, D.H., 1975: The magnetic susceptibility anisotropy of deformed rocks from North Cornwall, England; *Tectonophysics*, Vol. 27, p. 141-153.
- Spry, A., 1969: *Metamorphic Textures*; Pergamon Press, Oxford, 350 pages.
- Stockwell, C.H., 1964: Fourth report on structural provinces, orogenies and time-classification of rocks of the Canadian Precambrian shield; *Geological Survey of Canada, Paper 64-17*, p. 1-21.
- Stone, D., 1981: The Sydney Lake fault zone in Ontario and Manitoba, Canada; Unpublished Ph.D. thesis, University of Toronto.
- Sylvester, A.G. and Christie, J.M., 1968: The origin of crossed-girdle orientations of optic axes in deformed quartzites; *Journal of Geology*, Vol. 76, p. 571-580.

786-813.

- Rathore, J.S., 1979a: Magnetic susceptibility anisotropy in the Cambrian Slate belt of North Wales and correlation with strain; *Tectonophysics*, Vol. 53, p. 83-97.
- Rathore, J.S., 1979b: Application of magnetic susceptibility technique to the study of geological structures in the Armorican Massif, France; *Tectonophysics*, Vol. 60, p. 207-216.
- Rathore, J.S., 1980b: Evidence of sinistral movements along the Judicarian Line drawn from a study of magnetic fabrics in the regions of Mount Croce and Asten (South Tyrol); *Geologische Rundschau*, Vol. 69, p. 678-694.
- Rathore, J.S. and Becke, M., 1980: Magnetic fabric analyses in the Gail Valley (Carinthia, Austria) for the determination of the sense of movements along this region of the Periadriatic Line; *Tectonophysics*, Vol. 69, p. 349-368.
- Schwerdtner, W.M., Stone, D., Osadetz, K., Morgan, J. and Stott, G.M., 1979: Granitoid complexes and the Archean tectonic record in the southern part of Northwestern Ontario; *Canadian Journal of Earth Sciences*, Vol. 16, p. 1965-1977.
- Shklanka, R., 1972: Geology of the Steep Rock Lake Area, District of Rainy River; Ontario Department of Mines, Geological Report 93 pt. 1, 114 pages. Accompanied by Map 2217,

- Tullis, J., 1977: Preferred orientation of quartz produced by slip during plane strain; *Tectonophysics*, Vol. 39, p. 87-102.
- Tullis, J., 1978: Processes and conditions of mylonite formation as inferred from experimental deformation studies; *Geological Society of America Short Course, Mylonites natural and experimental*, Boston, March 7 and 8, 1978.
- Tullis, J., Christie, J.M. and Griggs, D.T., 1973: Microstructures and preferred orientations in experimentally deformed quartzites; *Geological Society of America Bulletin*, Vol. 84, p. 297-314.
- Tullis, J., Snoke, A.W. and Todd, V.R., 1982: Significance and petrogenesis of mylonitic rocks; *Geology*, Vol. 10, p. 227-230.
- Turner, F.J. and Weiss, L.E., 1963: *Structural Analysis of Metamorphic Tectonites*; McGraw-Hill, Toronto, Ont. 545 pages.
- Twiss, R.J., 1974: Structure and significance of planar deformation features in synthetic quartz; *Geology*, Vol. 2, p. 329-332.
- Vernon, R.H., 1974: Controls of mylonitic compositional layering during non-cataclastic ductile deformation; *Geological Magazine*, Vol. 3, p. 121-123.
- Voll, G., 1960: *New work on petrofabrics*, Liverpool and Manchester

Geological Journal (continued as Geological Journal),  
Vol. 2, p. 503-567.

- Watts, M.J. and Williams, G.D., 1979: Fault rocks as indicators of progressive shear deformation in the Guincamp region, Brittany; *Journal of Structural Geology*, Vol. 1, p. 323-332.
- White, S., 1973: The dislocation structures responsible for the optical effects in some naturally deformed quartzes; *Journal of Material Science*, Vol. 8, 490-499.
- White, S., 1977: Geological significance of recovery and recrystallization processes in quartz; *Tectonophysics*, Vol. 39, p. 143-170.
- White, S.H., Burrows, S.E., Carreras, J., Shaw, N.D. and Humphreys, F.J., 1980: On mylonites in ductile shear zones; *Journal of Structural Geology*, Vol. 2, 175-187.
- Wood, D.S., Oertal, G., Singh, J. (now Rathore, J.S.) and Bennet, H.F., 1976: Strain and anisotropy in rocks; *Philosophical Transaction of the Royal Society of London, Series A283*, p. 27-42.
- Wood, J., Dekker, J., Jansen, J.G., Keay, J.P. and Panagapko, D., 1980: Mine Centre Area, District of Rainy River; Ontario Geological Survey Preliminary Maps, Eastern Half P. 2202, Western Half P. 2201, Geological Series, scale 1 inch to 1/4 mile.

Zeck, H.P., 1979: Cataclastites, Hemiclastites, Holoclastites,  
Blasto-ditto and Myloblastites - Cataclastic Rocks;  
American Journal of Science, Vol. 274, p. 1064-1073.

C M.C.KENNEDY M.SC. THESIS (1984) APPENDIX I  
C ALL-OBJECT MUTUAL SEPARATIONS METHOD OF STRAIN ANALYSIS  
C PORRADALE & KENNEDY (1982-3), GEOLOGY DEPT, LAKEHEAD UNIVERSITY,  
C THUNDER BAY, ONTARIO P7B 5E1, CANADA. TEL. 1-(807)-345-2121

```
DIMENSION XX(40000),YY(40000)
DIMENSION X(200),Y(200)
CALL INITIAL (8)
C..DEFINE THE COORDINATE AXES FOR THE GRAPH PLOTTER OUTPUT
  XC=0.0
  YC=0.0
  AMIN=0.0
  AMAX=20.0
  TIC=1.0
C..LABEL Y-AXIS
  ITYP=4
  ALEN=20.0
  CALL PAXIS(XC,YC,AMIN,AMAX,TIC,ITYP,IDEC,ALEN)
C..LABEL X-AXIS
  ITYP=3
  CALL PAXIS(XC,YC,AMIN,AMAX,TIC,ITYP,IDEC,ALEN)
C
C..DEFINE THE ARRAY OF POINTS WHICH COMPRISE THE ORIGINAL PLOT
C..N IS THE NUMBER OF DATA POINTS (X AND Y COORDINATES)
  1 READ (5,1) N
  1 FORMAT(I3)
C..A SCALE FACTOR IS GIVEN SO THE FINAL PLOT WILL BE AN APPROPRIATE
C..SIZE FOR OUTPUT
  4 READ (5,4) SCALE
  4 FORMAT(F6,2)
  DO 3 I=1,N
C..X(I) AND Y(I) ARE THE X AND Y COORDINATES OF THE POINTS OF THE
C..ORIGINAL PLOT
    READ (5,2) X(I),Y(I)
  2 FORMAT(2F6,2)
C..ENLARGE/REDUCE SCALE FOR OUTPUT
  3 Y(I)=X(I)*SCALE
  3 Y(I)=Y(I)*SCALE
C..DETERMINE THE MIN AND MAX VALUES OF X AND Y
  CALL SMALL(N,X,SMALLX,MX)
  CALL SMALL(N,Y,SMALLY,MY)
  CALL BIG(N,X,BIGX,MPX)
  CALL BIG(N,Y,BIGY,MPY)
  WRITE(6,21) SMALLX,SMALLY,BIGX,BIGY,N
  21 FORMAT(1H1,4F10.3,16/)
  8 WRITE(6,8) MX,MPX,MY,MPY
  8 FORMAT(1H,4I4)
C..DEFINE A LIMITED AREA NEAR THE CENTRE OF THE PLOT IN WHICH A
C..POINT MAY BE CHOSEN AS THE CENTRE
C..RULX IS THE LOWER LIMIT OF X VALUES
C..RULY IS THE LOWER LIMIT OF Y VALUES
C..RULX IS THE LOWER LIMIT OF X VALUES
C..RULY IS THE LOWER LIMIT OF Y VALUES
  STEPX=(BIGX-SMALLX)/1000.
  STEPY=(BIGY-SMALLY)/1000.
  PLUX=SMALLX+400.*STEPX
```

```

RULX=SMALX+600.*STEPX
RULY=SMALY+400.*STEPLY
RULY=SMALY+600.*STEPLY
WRITE(6,91) RULX,RULY,RULY,RULY
91 FORMAT(1H, 4F10.4/)

C.. CHOOSE A DATA POINT IN THE MIDDLE OF THE RANGE AS A REFERENCE
C.. K IS A COUNTER TO N
K=0
N1=N+1
100 K=K+1
IF (K.FO.M1) WRITE(6,101)
101 FORMAT(1H1,'STOP')
IF (X(K).GT.RULX.AND.X(K).LE.RULX.AND.Y(K).GT.RULY.AND.Y(K).LE.
1RULY) GO TO 110
GO TO 100
110 NREF=K
C.. REFERENCE POINT HAS BEEN CHOSEN ABOUT IN MIDDLE OF RANGE
C.. WRITE THE X AND Y COORDINATES OF THE REFERENCE POINT (X(NREF),Y(NREF))
C.. AND THE NUMBER OF THE INPUT DATA POINT WHICH WAS CHOSEN AS NREF
22 FORMAT(1H, 2F10.3, I6/)

C.. PLOT REFERENCE POINT
CALL PLOT (X(NREF),Y(NREF),1)
CALL PENDN
CALL MARKER (1)
CALL PENUP

C.. DEFINE THE LIMITS OF THE DERIVED PLOT (THE LIMITS ARE DEFINED AS ONE
C.. QUARTER OF THE RANGE OF X AND Y VALUES AROUND THE REFERENCE POINT)
C.. DPPX IS THE DERIVED PLOT POSITIVE X VALUES
C.. DPPY IS THE DERIVED PLOT POSITIVE Y VALUES
C.. DPMX IS THE DERIVED PLOT MINUS X VALUES
C.. DPMY IS THE DERIVED PLOT MINUS Y VALUES
DPPX=(RIGX-SMALX)/4
DPPY=(RIGY-SMALY)/4
DPMX=(SMALX-BIGX)/4
DPMY=(SMALY-RIGY)/4
J=1

C.. TRANSFORM THE ARRAY SO THAT EACH DATA POINT WITHIN THE DERIVED
C.. PLOT IN TURN LIES AT NREF
DO 30 K=1, N
TX= (X(NREF)-X(K))
TY= (Y(NREF)-Y(K))
C.. DETERMINE IF THE POINT LIES WITHIN THE DERIVED PLOT (IF NOT IT IS
C.. DISCARDED)
IF (TX.GT.DPPX) GO TO 30
IF (TX.LT.DPMX) GO TO 30
IF (TY.GT.DPPY) GO TO 30
IF (TY.LT.DPMY) GO TO 30
C.. IF THE POINT LIES WITHIN THE DERIVED PLOT THE TRANSFORMED POSITIONS OF
C.. ALL OTHER POINTS IN THE ARRAY ARE RETAINED
C.. COORDINATES OF THE NEW ARRAY ARE (XX,YY)
DO 10 I=1, N
XX(I)= X(I)+TX
YY(I)= Y(I)+TY
J=J+1
10 CONTINUE

```

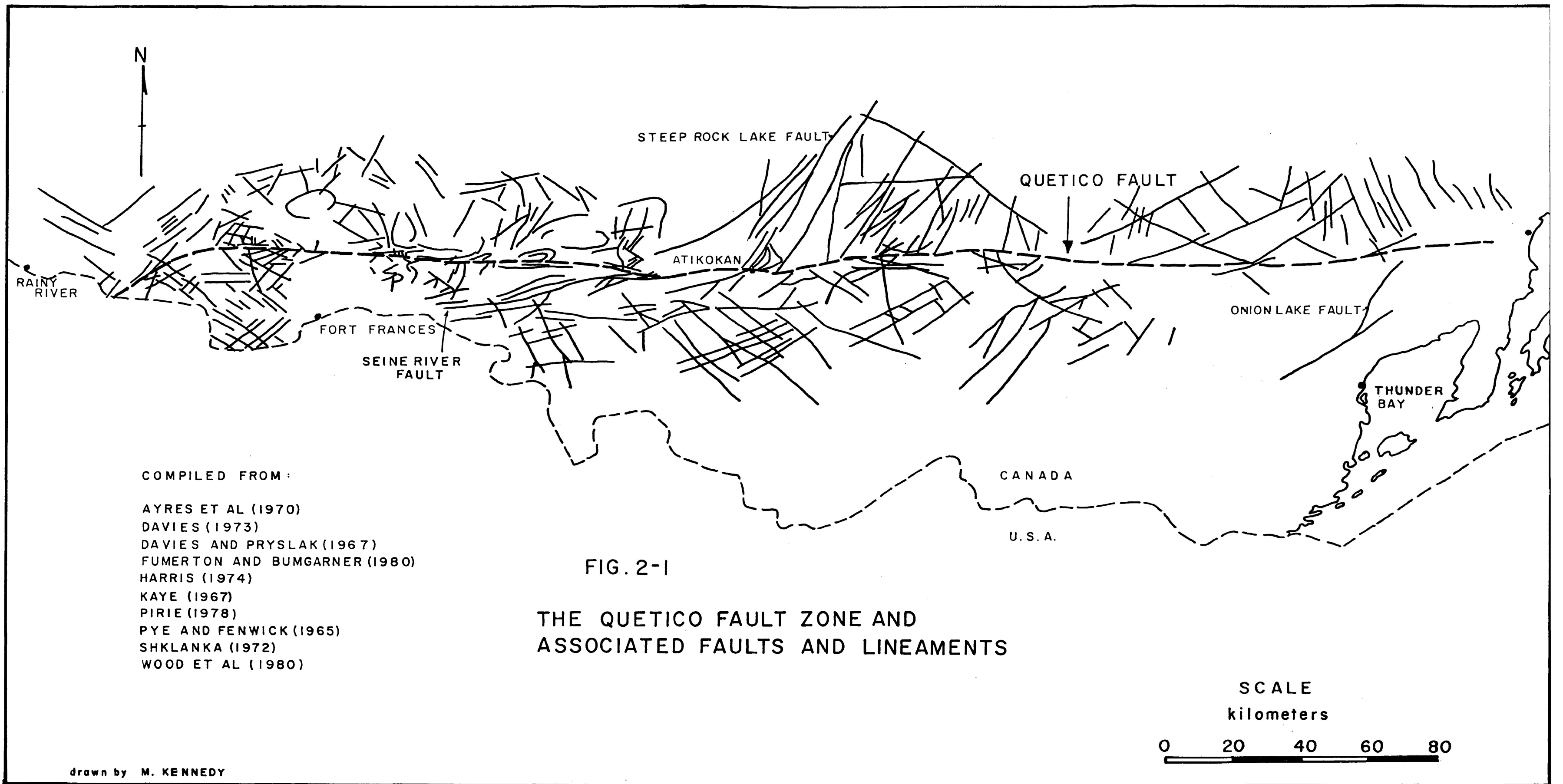
```

30 CONTINUE
JJ=J
C.. PLOT THE ARRAY (XX,YY) WITHIN THE LIMITS OF THE DERIVED PLOT TO AVOID
C.. EDGE EFFECTS
DO 27 J=1, JJ
XA=XX(J)
YA=YY(J)
TPEN=1
C.. DULX IS THE DERIVED PLOT UPPER LIMIT OF X
C.. DULY IS THE DERIVED PLOT LOWER LIMIT OF X
C.. DULY IS THE DERIVED PLOT UPPER LIMIT OF Y
C.. DULY IS THE DERIVED PLOT LOWER LIMIT OF Y
DULX=X(NREF)+DDPX
DULY=Y(NREF)-DDPY
DULY=Y(NREF)+DDPY
IF (XA.GT.DULX) GO TO 27
IF (XA.LT.DULX) GO TO 27
IF (YA.GT.DULY) GO TO 27
IF (YA.LT.DULY) GO TO 27
IF (XA.EQ.X(NREF).AND.YA.EQ.Y(NREF)) GO TO 27
CALL PLOT (XA, YA, IPEN)
CALL PENDM
CALL MARKER (3)
CALL PENUP
CONTINUE
CALL RSTR
STOP
END
27 CONTINUE
C
C
C.. SUBROUTINE SMALL FINDS THE SMALLEST VALUE OF X (SMALX)
C.. MX INDICATES WHICH PIECE OF THE INPUT DATA CONTAINS SMALX
C.. MX SUBROUTINE SMALL(N,X,SMALX,MX)
DIMENSION X(N)
SMALX=X(1)
MX=1
DO 10 I=2, N
IF (X(I).GE.SMALX) GO TO 10
IF (X(I).LT.SMALX) GO TO 11
11 MX=I
10 CONTINUE
RETURN
END
C
C
C.. SUBROUTINE BIG FINDS THE BIGGEST VALUE OF X (BIGX)
C.. MPX INDICATES WHICH PIECE OF INPUT DATA CONTAINS BIGX
C.. MPX SUBROUTINE BIG(N,X,BIGX,MPX)
DIMENSION X(N)
BIGX=X(1)
MPX=1
DO 10 I=2, N
IF (X(I).LE.BIGX) GO TO 10
IF (X(I).GT.BIGX) GO TO 11
11 MPX=I
10 CONTINUE
RETURN
END

```







COMPILED FROM :

AYRES ET AL (1970)  
 DAVIES (1973)  
 DAVIES AND PRYSLAK (1967)  
 FUMERTON AND BUMGARNER (1980)  
 HARRIS (1974)  
 KAYE (1967)  
 PIRIE (1978)  
 PYE AND FENWICK (1965)  
 SHKLANKA (1972)  
 WOOD ET AL (1980)

FIG. 2-1

THE QUETICO FAULT ZONE AND  
 ASSOCIATED FAULTS AND LINEAMENTS

SCALE  
 kilometers

0 20 40 60 80

drawn by M. KENNEDY

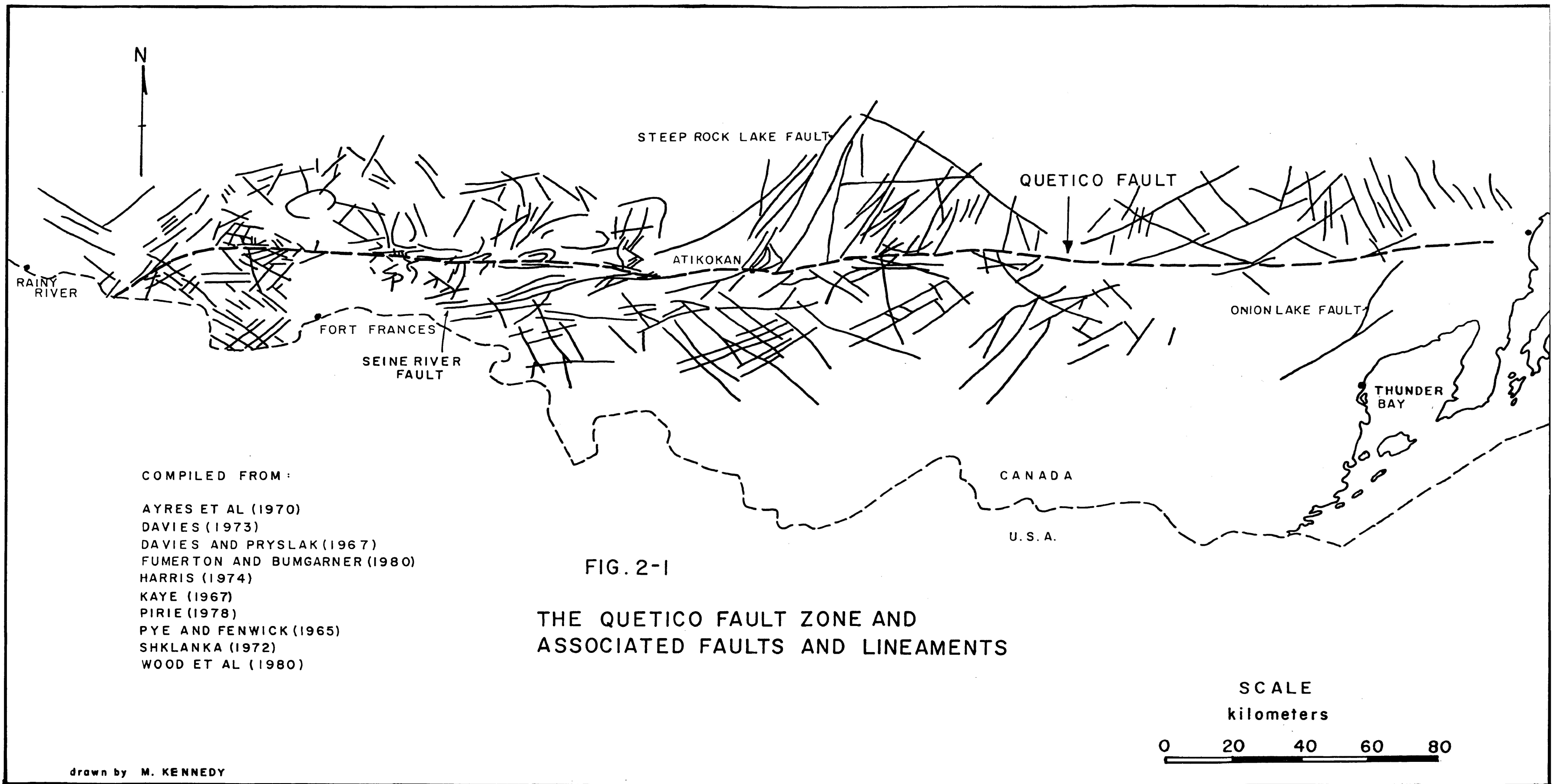


FIG. 2-1  
THE QUETICO FAULT ZONE AND  
ASSOCIATED FAULTS AND LINEAMENTS